THE UNIVERSITY *of* EDINBURGH

Evaluation of spectrally efficient indoor optical wireless transmission techniques

Thilo Christian Martin Fath

A thesis submitted for the degree of Doctor of Philosophy.
The University of Edinburgh.
October 2013

Lay summary

In recent years, the deployment of wireless communication systems has increased steadily. Current and future multimedia services such as web browsing, music and video downloads, video telephony and television on demand require higher data rates, and thus enlarged transmission capacity. This increase in data traffic largely affects the wireless data transfer in home and office environments as the major amount of wireless data traffic is generated in indoor environments due to home-based Internet access for instance.

The major bottleneck in coping with this growth is the available radio frequency (RF) spectrum. Nowadays, nearly the entire RF spectrum is allocated by diverse wireless services. As a result, RF spectrum gets a precious commodity and becomes scarce. The available bandwidth constitutes a limiting factor for achieving higher transmission rates and for providing wireless services to more and more users. Therefore, the enhancement of spectral efficiency, *i.e.* the usage of the available bandwidth in a more efficient way, and the utilisation of currently unused frequency ranges for wireless communications are in the spotlight of ongoing research activities.

Optical wireless communications (OWC) has the potential to become a remedy for the shortage of the RF spectrum. With the advent of high luminance light emitting diodes (LEDs), efficient and inexpensive illumination devices are available which will progressively replace existing light bulbs and fluorescent lamps paving the way for OWC. LEDs, being electronic devices, represent appropriate optical transmitters which can be used in home and office environments. However, off-the-shelf LEDs have a limited modulation capability, *i.e.* they can only be switched on/off up to a certain speed. Therefore, there is limited bandwidth for practical OWC systems. Consequently, achieving large spectral efficiencies, and thus high data rates, is of great concern for OWC systems.

The aim of this thesis is the evaluation of spectrally efficient optical wireless transmission techniques in indoor environments. The contribution of this research work is threefold: Firstly, the potential of the parallel usage of several optical transmitters is analysed. It is found that the usage of multiple optical transmitters and receivers can substantially improve the performance of OWC. Secondly, a novel transmitter concept for OWC is proposed. This concept enables a low-complex and power-efficient optical transmitter design compared to conventional optical wireless transmitters which are subject to complex system implementations. Transmission experiments prove the functionality of the implemented optical wireless transmitter. Finally, a novel approach for wireless data transmission within an aircraft cabin is presented. The proposed application uses visual codes for data transmission. For proof of concept, the system is evaluated in an aircraft cabin mock-up under realistic conditions.

Abstract

Optical wireless communications (OWC) has the potential to become a remedy for the shortage of the radio frequency (RF) spectrum. Especially in indoor environments, OWC could enable wireless home networking systems which offload data traffic from existing RF systems. In OWC, data is transmitted by modulating the intensity of light sources, typically incoherent light emitting diodes (LEDs). Thus, OWC systems employ intensity modulation (IM) and direct detection (DD) of the optical carrier. Since off-the-shelf LEDs have a limited modulation capability, the transmission bandwidth of practical OWC systems is restricted. Consequently, the available bandwidth has to be used efficiently.

In this thesis, spectrally efficient optical wireless transmission techniques are evaluated. Firstly, multiple transmitter-receiver techniques are investigated. These multiple-input-multiple-output (MIMO) techniques provide high spectral efficiency, and therefore high data rates. Specifically, the MIMO techniques repetition coding (RC), spatial multiplexing (SMP) and spatial modulation (SM) are analysed for indoor OWC. The performance of these techniques is evaluated analytically and by means of computer simulations. It is shown that inducing power imbalance between the multiple optical transmitters can substantially improve the performance of optical MIMO techniques as the power imbalance improves the differentiability of the multiple channels. In addition, it is found that link blockage and the utilisation of transmitters having different optical wavelengths enhance channel differentiability as well. These methods enable the utilisation of optical MIMO techniques under conditions which typically disallow the application of MIMO schemes due to little differences between the multiple links.

Secondly, a novel optical wireless transmitter concept is developed. This concept uses discrete power level stepping to generate intensity modulated optical signals, such as orthogonal frequency division multiplexing (OFDM) waveforms. The transmitter consists of several on-off-switchable LED groups which are individually controlled to emit scaled optical intensities. As a result, the digital-to-analogue conversion of the signals to be sent is done in the optical domain. This method enables the implementation of low-complex and power-efficient optical transmitter front-ends – the major shortcoming of conventional optical OFDM transmitters.

Thirdly, a novel approach for wireless data transmission within an aircraft cabin is presented. The data is transferred by 2-dimensional visual code sequences. These sequences are displayed on the in-flight entertainment (IFE) screen and are captured by the built-in camera of a user device which acts as receiver. Transmission experiments within an aircraft cabin mock-up demonstrate the functionality of the implemented system under realistic conditions, such as ambient illumination and geometric configuration.

Altogether, this thesis has analysed the potential of spectrally efficient optical wireless transmission techniques. It is shown that OWC systems can greatly benefit from these techniques.

Declaration of originality

I hereby declare that the research recorded in this thesis and the thesis itself was composed and originated entirely by myself at EADS Innovation Works Germany and in the Institute for Digital Communications at The University of Edinburgh, with the following exceptions:

The schematics and the circuit board layout of the optical wireless transmitter presented in Chapter 4 have been done by Dr Christoph Heller.

The visual code application presented in Chapter 5 uses code segments of the open source *libqrencode library* and of the image processing implementation *ZXing* which have been adapted by Dr Falk Schubert.

Thilo Christian Martin Fath

Acknowledgements

First and foremost, I would like to thank my supervisor Prof. Harald Haas for his guidance and support throughout my PhD studies. His encouraging and unfailing comments lighted me the way for my research work and helped me stay on track over the years. In particular, his constructive feedback and high attention to detail were invaluable for the successful completion of my PhD.

In addition, I would like to thank my external examiner Prof. Dominic O'Brien from The University of Oxford and my internal examiner Dr Majid Safari for kindly agreeing to review this thesis.

Moreover, I would like to express my gratitude to my former colleagues at EADS Innovation Works in Munich for providing me the chance to do my research work in industry and for the enjoyable working atmosphere. Special thanks and acknowledgements go to Dr Christoph Heller, Jirka Klaue and Dr Falk Schubert for their support and assistance in my research work. Thanks are also due to my fellow PhD students Johannes Blanckenstein, Christian Blümm, Prof. Alexander von Bodisco, Stefan Burger, Dr Emanuel Heidinger, Dr Frank Leipold, Dr Johannes Schels, Dimitri Tassetto and Dr Sebastian Voss for the fruitful discussions, for the leisure-time activities as well as for sharing joy and sorrow of our doctoral studies. Additionally, I appreciate my fellow PhD students from the Institute for Digital Communications at The University of Edinburgh for their support concerning formal and academic matters.

Finally and most of all: Möchte ich meinen tiefsten und herzlichsten Dank meiner Familie widmen für alles, was sie mir ermöglicht hat. Insbesondere gebührt mein Dank meiner Partnerin Lisa für ihre tatkräftige und unermüdliche Unterstützung im gemeinsamen Alltag, die es mir ermöglichte, mich auf meine Dissertation zu konzentrieren. Vor allem danke ich ihr, dass sie trotz der vielen Überstunden und der gemeinsamen Entbehrungen so viel Geduld und Verständnis für mich hatte und noch immer hat. Danke!

Contents

List of figures

List of tables

Acronyms and abbreviations

3G	third-generation
4G	fourth-generation
ACO-OFDM	asymmetrically clipped optical orthogonal frequency division multiplexing
ADC	analogue-to-digital converter
AEL	accessible emission limit
AWGN	additive white Gaussian noise
BER	bit error ratio
BLAST	Bell Laboratories layered space-time
CSI	channel state information
CSK	colour-shift-keying
DAC	digital-to-analogue converter
DC	direct-current
DCO-OFDM	direct-current-biased optical orthogonal frequency division multiplexing
DD	direct detection
EGC	equal gain combining
EMC	electromagnetic compatibility
EU	European Union
EVM	error vector magnitude
FEC	forward error correction
FFT	fast Fourier transformation

FOV	field-of-view
FPGA	field programmable gate array
fps	frames per second
FSO	free-space optical
GPRS	general packet radio service
ICI	inter-channel interference
IEEE	Institute of Electrical and Electronics Engineers
IFE	in-flight entertainment
IFFT	inverse fast Fourier transformation
iid	independent identically distributed
IM	intensity modulation
IR	infra-red
IrDA	Infrared Data Association
ISDN	integrated services digital network
ISI	inter-symbol interference
ISM	industrial, scientific and medical
LCD	liquid crystal display
LED	light emitting diode
LLR	log-likelihood ratio
LOS	line-of-sight
MIMO	multiple-input-multiple-output
MISO	multiple-input-single-output
ML	maximum-likelihood

MOSFET	metal-oxide-semiconductor field-effect transistor
MRC	maximum ratio combining
Msps	mega-samples per second
NLOS	non-line-of-sight
OFDM	orthogonal frequency division multiplexing
OOK	on-off-keying
OSTBC	orthogonal space-time block code
OWC	optical wireless communications
PAM	pulse amplitude modulation
PAM-DMT	pulse-amplitude-modulated discrete multitone modulation
PEP	pairwise error probability
PIN	positive intrinsic negative
PLC	power line communications
PPM	pulse position modulation
QAM	quadrature amplitude modulation
QR	quick response
RC	repetition coding
RF	radio frequency
RGB	red, green and blue
RX	receiver
SC	selection combining
SIC	successive interference cancellation
SIMO	single-input-multiple-output

SINR	signal-to-interference-plus-noise ratio
SISO	single-input-single-output
SM	spatial modulation
SMP	spatial multiplexing
SNR	signal-to-noise ratio
SSK	space shift keying
STBC	space-time block code
STC	space-time code
TCA	transconductance amplifier
TCSM	Trellis coded spatial modulation
TX	transmitter
URL	uniform resource locator
VLC	visible light communications
VLCC	Visible Light Communications Consortium
WLAN	wireless local area network
ZF	zero-forcing

List of principal symbols

α	optical power imbalance factor in linear scale defined as $\alpha = 10^{\frac{\delta}{10}}$.
δ	optical power imbalance factor in dB.
$\Delta_{d_{\mathrm{TX}}=x}^{E_{\mathrm{RX}}}$	impairment in received energy for transmitter separation distance $d_{\mathrm{TX}} = x$ m.
$\widehat{\Delta}_{d_{\mathrm{TX}}=x}^{E_{\mathrm{RX}}}$	impairment in received energy for transmitter separation distance $d_{\mathrm{TX}} = x$ m with induced link blockage.
Δ_{n_t}	relative difference defined as $\Delta_{n_t} = \frac{\lvert\overline{h_{n_t}} - h_{n_t}\rvert}{h_{n_t}}$.
Γ	reflectivity.
γ_{n_t}	induced power imbalance factor for transmitter n_t.
λ	wavelength.
ϕ	angle of emergence with respect to transmitter axis.
$\Phi_{\frac{1}{2}}$	transmitter semiangle (at half power).
ψ	angle of incidence with respect to receiver axis.
$\Psi_{\frac{1}{2}}$	field-of-view (FOV) semiangle of receiver.
ρ	optical-to-electrical conversion coefficient.
σ^2	variance of additive white Gaussian noise (AWGN).
σ^2_{shot}	shot noise variance.
$\sigma^2_{\text{thermal}}$	thermal noise variance.
A	detector area of receiver.
b	bit rate.
B	signal bandwidth.
b_m	bit assignment of signal vector $\mathbf{s}_m$.
b_{mn_t}	bit assignment which is conveyed when intensity I_m^{SM} is emitted by transmitter n_t.
c	coding rate of forward error correction (FEC) code.
d	transmitter-receiver separation distance.
d_{free}	free distance of forward error correction (FEC) code.
D_i	i^{th} light emitting diode (LED) group.
d_{TX}	transmitter separation distance.

e	number of erasures.
E_{RX}	average received electrical energy.
$E_{\mathrm{RX}_{d_{\mathrm{TX}}=x}}$	average received electrical energy for transmitter separation distance $d_{\mathrm{TX}} = x$ m.
E_s	average emitted electrical energy.
f	frequency of optical signal.
f_{s}	sampling frequency.
g	diversity gain.
h	channel coefficient of optical link.
$\overline{h}$	average measured channel gain.
$\widehat{h}$	estimated channel gain.
$h(t)$	channel impulse response.
$\mathbf{H}$	$N_r \times N_t$ channel matrix.
$\mathbf{H}_{d_{\mathrm{TX}}=x}$	channel matrix for transmitter separation distance $d_{\mathrm{TX}} = x$ m.
$\widehat{\mathbf{H}}_{d_{\mathrm{TX}}=x}$	channel matrix for transmitter separation distance $d_{\mathrm{TX}} = x$ m with induced link blockage.
h_l	channel coefficient of $l^{\,\mathrm{th}}$ sub-carrier.
$h_{n_r n_t}$	channel coefficient of wireless link between transmitter n_t and receiver n_r.
h_{Planck}	Planck constant.
$\mathbf{H}_{x_{\mathrm{RX}}=x,\, y_{\mathrm{RX}}=y}$	channel matrix for position offset of receiver array relative to room centre (x m offset on the x-axis and y m offset on the y-axis).
I	average emitted optical power.
I_i	electrical current which powers $i^{\,\mathrm{th}}$ light emitting diode (LED) group.
$\tilde{I}_{n_t}$	average optical power emitted by transmitter n_t.
I_{RX}	average received optical power.
$I_{\mathrm{RX}_{n_r}}$	average received optical power at receiver n_r.
I^{OOK}	intensity level of optical signal employing on-off-keying (OOK).
I^{PAM}	intensity level of optical signal employing pulse amplitude modulation (PAM).
I^{PPM}	intensity level of optical signal employing pulse position modulation (PPM).
I^{SM}	intensity level of optical signal employing spatial modulation (SM).

j	unit imaginary number.
k	substitution for: $\frac{-\ln(2)}{\ln\left(\cos(\Phi_{\frac{1}{2}})\right)}$.
l	constraint length of forward error correction (FEC) code.
L	size of fast Fourier transformation (FFT) / inverse fast Fourier transformation (IFFT).
$L(\mathbf{s}^i)$	log-likelihood ratio (LLR) for i^{th} bit conveyed in signal vector $\mathbf{s}$.
L_{cp}	length of cyclic prefix.
m	error correction capacity (number of erroneous codewords which can be corrected by forward error correction (FEC)).
M	signal constellation size.
$\mathbf{n}$	N_r-dimensional noise vector.
$n(t)$	noise.
N_0	noise power spectral density.
n_r	receiver index.
N_r	number of receivers.
n_t	transmitter index.
N_t	number of transmitters.
p	number of error detection codewords.
P_{elec}	maximum electrical power consumption of optical transmitter.
$\overline{P}_{\text{elec}}$	average electrical power consumption of optical transmitter.
P_i	optical power level emitted by i^{th} light emitting diode (LED) group.
P_{LED}	electrical power consumption of all light emitting diode (LED) groups.
$P_{\max}$	maximum power level of light emitting diode (LED).
P_{opt}	maximum optical output power of optical transmitter.
$\overline{P}_{\text{opt}}$	average optical output power of optical transmitter.
q	number of error correction codewords.
q_{e}	electron charge.
r	detector responsivity.
R	spectral efficiency in bit/s/Hz.
R_i	series resistor of i^{th} light emitting diode (LED) group.
R_{load}	load resistance.
$\mathbf{s}$	N_t-dimensional transmitted signal vector.
$\widehat{\mathbf{s}}$	decoded signal vector.

$s(t)$	transmitted waveform.
$\mathbf{S}_0^i$	set of signal vectors which have "0" at the i^{th} bit position.
$\mathbf{S}_1^i$	set of signal vectors which have "1" at the i^{th} bit position.
S_i	switching stage that digitally controls i^{th} light emitting diode (LED) group.
s_{n_t}	signal emitted by transmitter n_t.
t	number of errors.
T_s	symbol duration.
u	number of codewords.
v	number of data words.
v_{n_t}	coefficient of variation defined as $v_{n_t} = \sqrt{\text{VAR}\{\cdot\}}/\,\text{E}\{\cdot\}$.
$\mathbf{x}$	input vector to the transmitter inverse fast Fourier transformation (IFFT).
x_{RX}	position offset of receiver array on the x-axis relative to room centre.
$\mathbf{y}$	N_r-dimensional received signal vector.
$y(t)$	received waveform.
y_{RX}	position offset of receiver array on the y-axis relative to room centre.
z	height.
$*$	complex conjugation.
$\otimes$	convolution.
$\propto$	proportionality.
$\lvert\cdot\rvert$	absolute value.
$\lVert\cdot\rVert_{\text{F}}$	Frobenius norm.
$[\cdot]^T$	matrix/vector transpose.
$\zeta(\cdot,\cdot)$	averaged correlation coefficient.
argmax	argument of the maximum.
argmin	argument of the minimum.
$\cos(\cdot)$	cosine function.
$\text{d}_{\text{H}}(\cdot,\cdot)$	Hamming distance of two bit assignments.
$\text{E}\{\cdot\}$	expected value.
$\exp(\cdot)$	natural exponential function.
$\Im$	imaginary part.
$\widehat{\Im}$	imaginary part of equalised symbol.

$\ln(\cdot)$	logarithm to base e.
$\log_2(\cdot)$	logarithm to base 2.
$\log_{10}(\cdot)$	logarithm to base 10.
$p(\cdot)$	probability density function.
$\mathrm{Q}(\cdot)$	Q-function defined as $\mathrm{Q}(a) = \frac{1}{\sqrt{2\pi}} \int_a^{+\infty} \exp(\frac{-t^2}{2})\, \mathrm{dt}$.
$\Re$	real part.
$\widehat{\Re}$	real part of equalised symbol.
VAR $\{\cdot\}$	variance.

Chapter 1
Introduction

In recent years, the deployment of wireless communication systems has increased steadily. Current and future multimedia services such as web browsing, music and video downloads, video telephony and television on demand require higher data rates, and thus enlarged transmission capacity. Moreover, the demand for mobility, ubiquitous connectivity and pervasive communications is tremendously increasing. Figure 1.1 illustrates the global mobile data traffic growth for the years 2009 to 2012 ascertained by Cisco [1, 2]. As shown, the

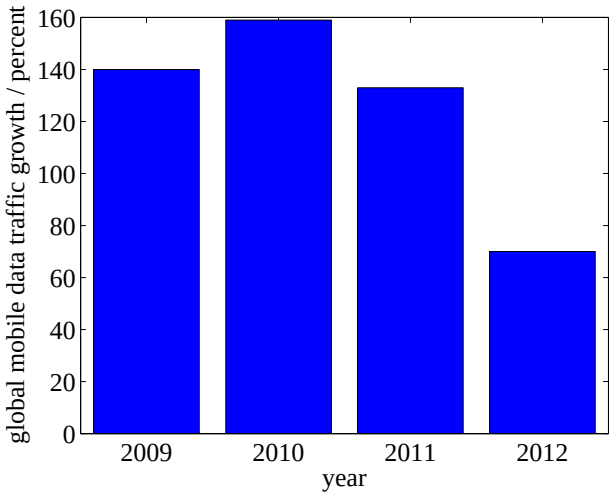

Figure 1.1: *Global mobile data traffic growth. Source: Cisco Visual Networking Index [1,2].*

global mobile data traffic has more than doubled each year from 2009 to 2011 with a slight decrease in 2012 due to the increasing offload of mobile traffic onto wireless local area networks (WLANs). According to Cisco's *Global Mobile Data Traffic Forecast* [2], this growth is predicted to persist. For instance, the projections say that

- the number of mobile-connected devices will exceed the worlds population by the end of 2013 and by 2017 there will be 1.4 mobile devices per capita.
- the average smartphone will generate 2.7 GB of traffic per month in 2017 which is an eight-fold increase over the 2012 average of 342 MB per month.

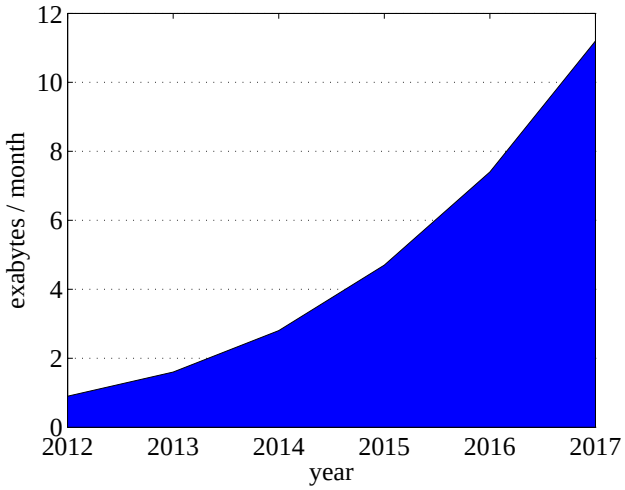

Figure 1.2: *Global mobile data traffic forecast. Source: Cisco Visual Networking Index [2].*

- the average mobile connection speed (526 kbit/s in 2012) will surpass 1 Mbit/s in 2014 and will exceed 3.9 Mbit/s in 2017.

Moreover, Cisco forecasts that the global mobile data traffic will increase 13-fold between 2012 and 2017 resulting in a compound annual growth rate of 66 %. Figure 1.2 illustrates this global mobile data traffic forecast. In 2012, the global mobile data traffic was 885 petabytes per month. This amount of traffic was nearly twelve times larger than the total global Internet traffic in 2000 which was 75 petabytes per month. It is predicted that the monthly global mobile data traffic will surpass 10 exabytes in 2017.

This increase in mobile data traffic also affects wireless data transfer in home and office environments. The major amount of wireless data traffic is generated in indoor environments due to home-based mobile Internet access and telephony. For instance, more than 50 % of all voice calls and more than 70 % of data traffic are generated indoors [3]. According to [2], there were 161 million laptops on the mobile network in 2012, and each laptop generated seven times more data traffic than an average smartphone. Within a user's home, the data traffic generated by mobile and portable devices can be offload from mobile networks to WLANs. In 2012, 33 % of the total mobile data traffic was offload, *i.e.* 429 petabytes each month. Without offload, mobile data traffic would have grown by 96 % rather than by 70 % in 2012. This mobile offload will increase to 46 % (9.6 exabytes per month) in 2017 [2]. Consequently, there is a largely increasing demand for wireless data transmission in indoor environments.

The major bottleneck in coping with this growth is the available radio frequency (RF) spectrum. Nearly all of the RF spectrum in the range of 3 kHz to 300 GHz is allocated by diverse wireless services and applications [4, 5]. As a result, RF spectrum gets a precious commodity and becomes scarce. For instance, as more and more WLANs are being installed in home and office environments, the unlicensed industrial, scientific and medical (ISM) frequency band gets congested and spectral interference increases. If several RF communication systems operate in the same frequency band (at the same time and within the same area), the overall system performance is largely degraded due to mutual interference. In fact, the available bandwidth constitutes a limiting factor for achieving higher transmission rates and for providing wireless services to more and more users. Therefore, the enhancement of spectral efficiency, *i.e.* the usage of the available bandwidth in a more efficient way, and the utilisation of unused frequency ranges above 300 GHz for wireless communications are in the spotlight of ongoing research activities.

1.1 Multiple transmitter-receiver techniques for wireless communications

Multiple transmitter-receiver techniques have gained much attention in the field of RF communications as they enable large spectral efficiencies and improve the performance of wireless systems [6–10]. Therefore, these techniques are an appropriate means to mitigate the scarcity of available bandwidth. In addition to conventional data transmission in the time and frequency domain, multiple transmitter-receiver techniques exploit the spatial domain for data transmission. The benefits of these techniques rely on multipath signal propagation and on the fading effects of wireless channels caused by reflection, diffraction and scattering. These effects induce characteristic "spatial signatures" of the multiple wireless links which are exploited by the communication system to achieve better performance.

Due to their potential, multiple transmitter-receiver techniques are already widely used in several RF communication systems. For instance, multiple transmitter-receiver techniques are employed in WLAN standards such as Institute of Electrical and Electronics Engineers (IEEE) 802.11n to provide data rates of 100 Mbit/s and higher [11] as well as in third-generation (3G) and fourth-generation (4G) wireless communication systems [12–17]. As shown in Figure 1.3, multiple transmitter-receiver techniques can be characterised by four basic configurations

depending on the number of antennas at the transmitter (TX) and at the receiver (RX):

- single-input-single-output (SISO) systems employ only one transmit and one receive antenna. This configuration represents conventional single antenna transmission systems.
- single-input-multiple-output (SIMO) systems employ one transmit antenna and several receive antennas.
- multiple-input-single-output (MISO) systems employ several transmit antennas and one receive antenna.
- multiple-input-multiple-output (MIMO) systems employ several transmit and several receive antennas.

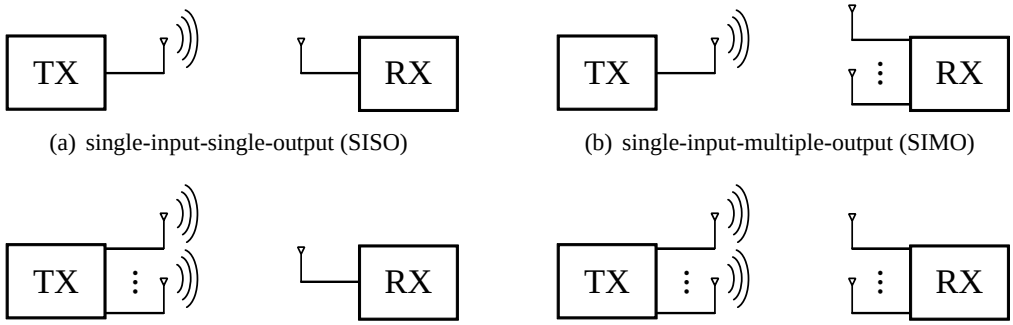

(a) single-input-single-output (SISO) (b) single-input-multiple-output (SIMO)

(c) multiple-input-single-output (MISO) (d) multiple-input-multiple-output (MIMO)

Figure 1.3: *Illustration of different multiple transmitter-receiver configurations.*

Besides these four configurations, multiple transmitter-receiver systems can be categorised in three types according to their implementation and functionality [18]. The first category comprises spatial multiplexing techniques. Spatial multiplexing techniques send independent data sequences from several transmit antennas at the same time. This parallel data transmission provides a multiplexing gain, and thus enhances transmission capacity by enabling higher data rates. This gain is achieved without any increase in transmission power or bandwidth. The total transmission power is split between the several TX antennas which simultaneously transmit in the same frequency band. Consequently, given a fixed transmission bandwidth, the spectral efficiency is enhanced resulting in more bits per second per Hertz. The Bell Laboratories layered space-time (BLAST) technique originally proposed by Foschini [7] is a well-known spatial multiplexing scheme. By using the BLAST architecture, the data sequence to be transmitted is demultiplexed into a number of parallel substreams (corresponding to the

number of transmit antennas) which are modulated independently. These substreams, also referred to as layers, are simultaneously emitted by the multiple transmit antennas. As the substreams are transmitted in parallel in time and frequency, they superimpose at the receiver leading to inter-channel interference (ICI). The performance of spatial multiplexing techniques mostly relies on the separation of the parallel data streams. In order to correctly reconstruct the transmitted data at the receiver, the multiple links must have different spatial signatures which have to be known at the receiver. The propagation characteristics induce distinctive differences between the multiple links which are evaluated by the receiver to separate the superimposed substreams. The separation is done by using specific decoding algorithms such as zero-forcing (ZF) or successive interference cancellation (SIC). For these algorithms to work properly, the number of receive antennas must be at least as large as the number of transmit antennas. Depending on the actual configuration, the BLAST technique can achieve more than 40 bit/s/Hz [19], and thus outperforms conventional SISO systems to a large extent assuming a single link.

The second category of multiple transmitter-receiver systems is based on spatial diversity. These systems rely on the transmission and/or the reception of redundant signals which contain the same information. This redundancy improves the reliability of the wireless transmission by reducing the bit error ratio (BER). The BER is the ratio between the number of erroneously received bits and the total number of transmitted bits. Typical BER values are about 10^{-3} for voice transmission and about 10^{-7} to 10^{-5} for data applications. If the receiver is equipped with several antennas, like a SIMO system for instance, the receiver is able to capture multiple replicas of the same transmitted signal. Hence, an enlarged portion of the emitted power can be collected. If the antenna spacing is large enough (typically in the range of the signal wavelength or larger), the multiple wireless links can be considered as largely independent. Consequently, the outage probability of the entire link is significantly reduced compared to a conventional SISO system. As a result, the multiple receptions provide a diversity gain [20]. According to Tse *et al.*, a transmission system has a diversity gain g if its average error probability decays for large signal-to-noise ratio (SNR) like SNR^{-g} [21, 22]. In order to exploit diversity reception, the receiver combines the multiple signal replicas. There are various combining techniques such as selection combining (SC), where only the signal with the largest SNR is processed. All other signals are neglected. Hence, SC can also be considered as an antenna selection scheme. In contrast to SC, maximum ratio combining (MRC) weights the received signals according to their individual SNR and combines all of them for further processing.

As a result, MRC maximises the SNR at the combiner output [23, Ch. 7.2.4]. A simplified version of MRC is equal gain combining (EGC) which weights all signals equally before they are combined. Besides diversity reception, there are also techniques which provide transmit diversity. These techniques perform a 2-dimensional spatio-temporal coding of the data to be transmitted, *i.e.* the data is coded in the time and the space domain [24, 25]. These schemes are called space-time codes (STCs). The Alamouti scheme [9] is the best known space-time coding scheme. It is a simple transmit diversity technique which employs two transmit antennas and one receive antenna. The scheme uses two symbol periods to transmit two symbols. In the first symbol period, two independent symbols s_1 and s_2 are simultaneously sent from both antennas. In the second symbol period, s_1^* and $-s_2^*$ are transmitted which are the complex conjugate copies of both symbols. Additionally, the assignment of the symbols to the transmit antennas is swapped for the second symbol period. Alamouti shows that this scheme provides the same diversity order as a MRC scheme which uses one transmit antenna and two receive antennas [9]. However compared to MRC, his transmit diversity scheme requires a 3 dB larger transmission power to provide the same BER performance. Additionally, his scheme requires that the channel remains constant over the two symbol periods. The Alamouti scheme can be generalised and extended to higher order STCs which use more than two transmit antennas. For instance, orthogonal space-time block codes (OSTBCs) [26] and space-time Trellis codes [10, 27] are practical extensions. Altogether, STCs enhance only the reliability of wireless links, whereas spectral efficiency is not increased. The maximum spectral efficiency of full-diversity STCs is one symbol per symbol duration as the number of used time slots is equal to the number of transmitted symbols. Consequently, STCs provide the same (or an even lower) throughput as conventional SISO systems due to the introduced redundancy.

The third category of multiple transmitter-receiver systems employs beamforming techniques. These so-called smart antenna systems improve the quality of wireless communications by shaping the antenna radiation pattern. The antenna beam is steered towards the desired target (or source) by adaptively adjusting the antenna weight vector [28–31]. Simultaneously, the radiation patterns for directions which cause interference are suppressed. As a result, the received signal power is increased and ICI as well as fading effects are mitigated. Consequently, the SNR, respectively the signal-to-interference-plus-noise ratio (SINR) is improved. This improvement is the so-called antenna gain. In [32] it is shown that smart antenna systems can largely increase the capacity of wireless communication systems. A simple example of a smart antenna system is the switched beam system. This system monitors the received signal

strength and switches to another antenna if the receiver gets better coverage by this antenna beam. If transmit beamforming is to be used, the transmitter requires knowledge about the propagation channel [6,33]. This knowledge can be provided by feedback information from the receiver. However, the transmission of this channel state information (CSI) requires a dedicated feedback channel. Using the CSI, the signals to be transmitted are appropriately pre-coded by the transmitter. For instance, the water-filling algorithm distributes the transmission power across the multiple transmit antennas depending on the channel state. Links with a high SNR are allocated more transmission power than links with a low SNR. As a result, this algorithm induces an optimal allocation of the transmission power to optimise system performance.

The multiple transmit and receive antennas have not to be integrated into the same hardware device but can also be distributed across several devices. For instance, several individual transmitter and receiver devices can jointly cooperate within a wireless network and share their antennas. This results in cooperative or virtual MIMO systems [34, 35]. Typical shortcomings of multiple transmitter-receiver techniques are their increased hardware costs because of the multiple antennas and multiple transmitter/receiver chains. Moreover, as these techniques couple several transmission symbols in time and space, they require sophisticated detection or pre-coding algorithms as presented above. These signal processing algorithms lead to high system intricacy and considerable computational complexity. A comprehensive literature survey on multiple transmitter-receiver techniques for wireless communications is given in [18] for instance. Section 2.2 introduces some selected MIMO techniques in more detail. Despite the fact that multiple transmitter-receiver techniques are already widely deployed in RF implementations, it is clear that they are not sufficient to cope with the exponential increase in mobile data traffic. Consequently, there is a demand for a new paradigm shift for wireless communication technologies.

1.2 Optical wireless communications

As mentioned above, the entire electromagnetic spectrum up to 300 GHz is almost completely allocated. Consequently, to cope with the increasing demand for wireless communications, the spectrum above 300 GHz, the optical spectrum, has to be used. The optical spectrum is much larger than the microwave spectrum as it covers the range from about 300 GHz to 790 THz. Up to now, the optical spectrum is mostly unused for wireless data transmission.

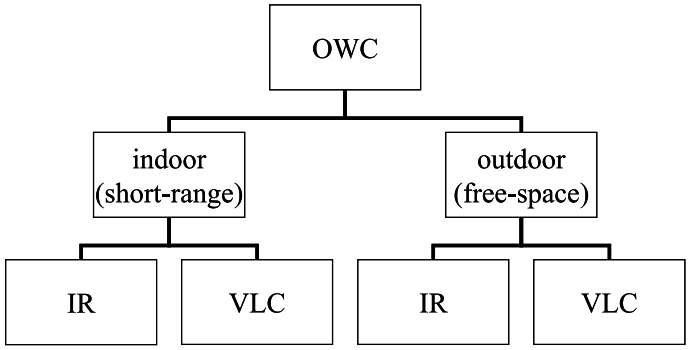

Figure 1.4: *Classification of optical wireless communications.*

In outdoor applications, optical wireless communications (OWC) can be used to establish point-to-point links between buildings for instance. The typical transmission distance of these free-space optical (FSO) links is in the order of some km. Besides, FSO can also be used for spacecraft communications in outer space [36]. In indoor environments, OWC can provide flexible and efficient data transmission as shown by Gfeller and Bapst in the 1970s [37]. The authors have considered infra-red (IR) light transmission. IR systems use wavelengths in the range of $800 - 1500$ nm [38] that are invisible to the human eye. Further optical wireless IR systems are presented for instance in [39, 40]. In 1993, the Infrared Data Association (IrDA) was founded which promotes the development and proliferation of IR enabled products, services and technology [41]. Since its foundation, IrDA has contributed to the creation of more than 30 technical specifications, mainly related to short-range wireless IR communications in personal communication systems, *e.g.* for data transmission between portable devices. For instance, the IrDA Giga-IR Special Interest Group has recently developed specifications for 1 Gbit/s IR communications [41]. Due to the advances in solid-state-lighting technology, the visible optical spectrum in the range of about $380 - 700$ nm can now be used for communication purposes as well [42–44]. Visible light communications (VLC) transmits data using visible (*e.g.* white) light. Current research activities intend to use illumination devices, such as ceiling lights or desk lamps, for data transmission [45–49]. For instance, the ceiling lights can be used to transmit data to a receiver which is placed on a desk within a room. As illumination devices are installed almost everywhere, VLC might be applied to various applications in order to establish pervasive communication networks. The Visible Light Communications Consortium (VLCC) [50] in Japan pioneered the research on VLC and supports the on-going standardisation [51, 52]. In addition, the IEEE $802.15.7$ Visible Light Communication Task Group [53] issued a standard for VLC in 2011 [54] which defines amongst

others the physical layer for short-range VLC. Practical research work on VLC has been done in the frame of the European Union (EU) project OMEGA [55] and the D-Light project at the University of Edinburgh [56] for instance. In comparison to IR transmission, VLC does not require the installation of additional emitters as it can make use of the existing illumination installations. These lighting devices are designed to provide uniform illumination within a room, thus providing good signal coverage. Moreover, visible light sources can emit much larger intensities, and consequently enable higher SNR compared to invisible IR transmitters which are subject to strict eye safety regulations. Altogether, VLC enables the installation of visible communication cells, so called data hotspots. However, in order to enable VLC, the light sources have to be switched on permanently. This prevents the application of VLC for instance in aircraft cabins where the light has to be switched off during take-off and landing. For these scenarios, IR transmission is preferred.

Since OWC is not subject to frequency regulations, it can be freely used worldwide. OWC can even be applied to sensitive environments which have stringent electromagnetic compatibility (EMC) restrictions like hospitals and manufacturing plants. This is due to the fact that optical signals do not interfere with existing electronic systems. Therefore, OWC provides better EMC than RF communications. Optical signals do not pass through walls and can be easily contained by opaque boundaries. The signals can only be detected by a receiver which is placed within the emitted light beam. Hence, the propagation and the transmission range of optical signals can be restricted to specific spots or areas. This characteristic enables a large spatial reuse of optical wireless systems. For instance, it is possible to employ multiple optical WLANs in the same building or even in the same room without mutual interference. Additionally, the constriction of optical signals provides a security feature as fraudulent interception of the data transmission can be prevented. This is in contrast to RF signals which propagate through walls and can be detected outside buildings they originate in. Moreover, compared to RF systems, OWC systems do not require high-frequency circuit designs. As a result, OWC enables the implementation of simple transceivers [57, 58]. OWC can also be used for vehicle-to-vehicle and vehicle-to-infrastructure communication by using, *e.g.*, the head and tail lamps of cars for data transmission.

Altogether, OWC can evolve into an efficient low-cost transmission technique for wireless indoor communications and can serve as a supplement to established RF technologies. This is due to the fact that OWC has the potential to provide a significant RF spectrum relief. Chapter 2

deals with OWC in more detail and introduces some common optical wireless transmission techniques.

1.3 Contributions

The aim of this thesis is the evaluation of spectrally efficient optical wireless transmission techniques in indoor environments. The first pioneering studies in optical wireless transmission for indoor environments have been focused on IR light transmission [37]. These studies have shown the potential of OWC to provide flexible and efficient data transmission. With the advent of high luminance light emitting diodes (LEDs), efficient and inexpensive illumination devices are available which will progressively replace existing light bulbs and fluorescent lamps paving the way for VLC. LEDs, being electronic devices, represent appropriate optical transmitters which can be used in home and office scenarios. However, off-the-shelf LEDs have a limited modulation capability. For instance in the case of visible light, the achievable bandwidth of common white-light phosphor-based LEDs is typically in the range of 5 - 20 MHz. Therefore, there is no abundance of bandwidth for practical OWC systems. Consequently, achieving large spectral efficiencies, and thus high data rates, is of great concern for OWC systems.

The contribution of this research work is threefold: Firstly, the potential of MIMO schemes for indoor OWC shall be analysed. Suitable MIMO techniques have been investigated starting from possible candidate techniques in RF communications. Particularly, these MIMO techniques are adapted for OWC and its specific characteristics. A framework is developed to analytically approximate the BERs of these techniques. The theoretical bounds are verified by numerical computer simulations. Moreover, the effect of induced power imbalance between the multiple transmitters is investigated. In this context, the usage of different optical wavelengths is studied as well. It is found that power imbalance and the application of different optical wavelengths can substantially improve the performance of optical MIMO techniques. Therefore, one of the main contributions of this work is the in-depth study of the specific characteristics and the various trade-offs of optical MIMO techniques. These techniques are essential to enable high-speed OWC in indoor environments.

Secondly, a novel transmitter concept for OWC is proposed. Conventional optical wireless transmitters are subject to non-linearities, restricted dynamic range and complex system designs. Therefore, intricate hardware implementations are required to build optical wireless

transmitters that are able to provide high data rates in the region of ten to hundred Mbit/s. This research provides a solution to these shortcomings by developing a low-complex and power efficient optical transmitter design. Transmission experiments prove the functionality of the implemented optical wireless transmitter.

Finally, a novel approach for wireless data transmission within an aircraft cabin is presented. The proposed application constitutes a highly parallel optical MIMO system which uses visual codes for data transmission. This transmission system can be easily applied to existing aircraft cabins without the need for additional hardware installations. For proof of concept, the system is evaluated in an aircraft cabin mock-up under realistic conditions.

1.4 Thesis structure

This chapter has provided a brief motivation and introduction for OWC in general, and spectrally efficient MIMO techniques in particular. The importance of spectrally efficient transmission techniques for OWC is highlighted. This is the area of primary concern in this thesis. The remainder of this thesis is structured as follows:

Chapter 2 overviews the concept and the fundamentals of optical wireless data transmission in indoor environments. It reviews optical digital modulation techniques. Specifically, the properties and the shortcomings of pulsed modulation schemes and of multi-carrier techniques are discussed. In addition, optical MIMO techniques are reviewed and are investigated in more detail. The final part of Chapter 2 introduces the optical wireless channel model considered in this thesis. Measurement results are presented which substantiate the considered channel model.

Chapter 3 is dedicated to an in-depth performance evaluation of MIMO techniques for OWC. To this end, a generic indoor scenario is considered. The performance is evaluated by numerical computer simulations and by analytical calculations. Moreover, the considered MIMO techniques are compared with regard to their computational complexities to account for practical system implementations. Altogether, the results show that optical MIMO techniques can provide high spectral efficiencies. This translates into high data rates, even under static line-of-sight (LOS) conditions.

Chapter 4 presents a novel optical wireless transmitter concept. This concept employs discrete

power level stepping for optical wireless signal transmission. The transmitter design enables the implementation of simple low-cost optical wireless transmitters which provide good power efficiency and linearity characteristics. Experimental results stemming from a proof-of-concept demonstrator are presented. Various experiments are conducted to evaluate the performance of the new transmitter concept. The measurements show that the developed transmitter concept enables high-speed optical wireless data transmission in indoor environments without the need for complex or costly transmitter implementations.

Chapter 5 introduces a novel wireless data transmission method for in-flight applications. The proposed approach uses visual codes to transmit data. This method constitutes a highly parallel optical MIMO system. Results of transmission experiments are presented which are taken within an aircraft cabin mock-up. The experiments demonstrate the functionality of the implemented system under realistic illumination conditions and geometric configurations. In order to provide reliable data transfer, a sequence-wise forward error correction (FEC) coding method is implemented.

Chapter 6 summarises and concludes the presented work. The main findings are highlighted. Moreover, the limitations of the presented work are discussed and potential future work is identified.

Chapter 2
Optical wireless data transmission in indoor environments

Since the last decade, there has been an exponentially increasing demand for wireless communications. More and more data is to be transmitted wireless and steadily enlarging data rates are required. However, this growing demand causes a shortage of the available radio frequency (RF) spectrum. In [59], optical wireless communications (OWC) is highlighted as a potential solution to the global wireless spectrum shortage. Especially in indoor networking systems, OWC can mature into an alternative or complementary technology to RF communications which could provide supplementary capacity. In office and home environments, OWC can offload data traffic from cellular and wireless local area network (WLAN) systems as the latter are also becoming more and more congested. Therefore, OWC is envisioned to be essential for wireless data transmission in indoor environments for short-range and low-mobility applications [60].

Typical indoor light fixtures provide illumination levels of more than 400 lux. The ceiling light installations enable a line-of-sight (LOS) link to a potential receiver placed within a room. This LOS characteristic enables bandwidths of at least 88 MHz [47]. Consequently, practical bandwidth limitations are not imposed by the channel but by the modulation capability of the light sources. Moreover, these illumination levels yield high signal-to-noise ratios (SNRs) of more than 60 dB within the room [47,61,62]. Therefore, it is desirable to use these illumination devices additionally for transmitting data. The data to be transmitted can be transferred to the light fixtures via the existing electrical wiring using power line communications (PLC) for instance.

Both infra-red (IR) and visible light communications (VLC) systems primarily use light emitting diodes (LEDs) as transmitters and photo-diodes as receivers. These components enable efficient and low-cost transceiver implementations. The data to be transmitted acts as input to an electronic circuitry that modulates the light source. Specifically, the intensity of the emitted light is modulated. As a result, the electrical signal is transferred into an optical signal.

As the modulation is done by using high-frequency pulsed light, it cannot be perceived by the human eye. Consequently, the changes in brightness are imperceptible and the generated illumination (in the case of VLC) appears constant to the human eye. The emitted optical signal impinges on the photo-detector of the receiver and generates a photo-current which is converted into digital signals. This means that the optical signal is reconverted into an electrical signal. The digital signals are decoded using signal processing techniques. Typically, the receiver comprises of an optical filter to mitigate optical noise, a concentrator (lens) to focus the light on the detector and an amplifier to amplify the received signal.

In contrast to laser diodes, LEDs are low-cost optical devices providing high reliability. Moreover, LEDs generally have widely divergent beams compared to laser diodes. The latter can be regarded as optical point sources emitting high radiant power by collimated laser beams. Therefore, laser diodes are subject to stringent eye safety regulations. Due to these reasons, LEDs are typically favoured in indoor applications [60]. LEDs are incoherent light sources which modulate the desired waveform onto the instantaneous power of the optical carrier. At the receiver side, low-cost positive intrinsic negative (PIN) photo-diodes are commonly employed. PIN photo-diodes are temperature-stable and can operate with a lower reverse bias voltage in comparison to avalanche photo-diodes. The photo-diodes directly convert the received optical power into electrical current. Consequently, intensity modulation (IM) techniques with direct detection (DD) are typically employed in indoor OWC. IM and DD offer easy implementation, and therefore promote simple optical modulation and demodulation equipment [57,58]. The up- and down-conversion of the baseband signals to/from the optical transmission frequency can be done by low-cost diodes without the need for sophisticated high-frequency circuit designs. However, this simplicity is gained at the expense of losing the optical carrier's frequency and phase information as only the intensity of the optical carrier is detected. This means that conventional RF modulation/demodulation techniques cannot be directly applied to IM/DD based OWC, and thus specific new approaches have to be developed. Moreover, given the restricted bandwidth of commercial LEDs and photo-diodes, spectrally efficient transmission techniques are vitally important for indoor OWC in order to provide the envisaged data rates of tens to hundreds of Mbit/s. This thesis investigates spectrally efficient OWC techniques in indoor environments with an emphasis on multiple-input-multiple-output (MIMO) techniques. Throughout this thesis, intensity modulated optical wireless links are considered.

This chapter provides background on optical wireless data transmission in indoor

environments. It contains an overview of common optical digital modulation techniques. Section 2.1 introduces conventional pulsed modulation techniques as well as optical wireless multi-carrier techniques. The specific characteristics and shortcomings of these techniques are discussed. A survey of optical MIMO techniques is presented in Section 2.2. Furthermore, an analytical framework is given to calculate the theoretical bit error bounds of three specific MIMO techniques which are considered for indoor OWC. In Section 2.3, the optical wireless channel model is introduced. This model is substantiated by channel measurements which are presented in Section 2.4. The chapter is summarised in Section 2.5.

2.1 Optical digital modulation techniques

This section overviews several modulation schemes which are widely used for OWC. Specifically, pulsed modulation techniques and multi-carrier techniques are considered in the following. All these techniques have to satisfy the non-negativity constraint of OWC: the transmitted signal has to be non-negative since the emitted optical power cannot be negative [57, 58]. Therefore, these techniques modulate the intensity of the optical carrier to convey information. Modulation techniques which depend on coherent signal detection cannot be applied to optical wireless systems that use IM and DD. This is due to the fact that coherent detection requires knowledge about the frequency and the phase of the signal. However, in IM/DD based OWC which is considered throughout this thesis, this information is not available at the receiver. Due to eye and skin safety regulations, the emitted optical power is commonly restricted [63–65]. In detail, the accessible emission limit (AEL) depends on the optical wavelength, on the emitter's geometry and on the emitted intensity.

In [58], Kahn and Barry provide a common baseband channel model for OWC:

$$y(t) = h(t) \otimes s(t) + n(t), \tag{2.1}$$

where $s(t)$ is the transmitted waveform, $y(t)$ is the received waveform and $h(t)$ is the channel impulse response. The symbol $\otimes$ denotes the convolution operator. The noise is represented by $n(t)$. It is assumed to be the sum of thermal noise and shot noise due to intense ambient light. These are the two main noise sources considered in DD based OWC systems. Shot noise is caused by background light sources like the sun and additional illumination devices which are not used for data transmission. This ambient light effects high intensity shot noise

which is dominant compared to the signal generated noise. Such noise can be modelled as zero mean additive white Gaussian noise (AWGN) which is independent of $s(t)$ [58, 66]. Thermal noise is induced in the receiver electronics like the pre-amplifier of the receiver front-end. It is independent of $s(t)$ and independent of the shot noise. Consequently, $n(t)$ can be modelled as real-valued AWGN with zero mean and a variance $\sigma^2 = \sigma^2_{\text{shot}} + \sigma^2_{\text{thermal}}$, where σ^2_{shot} is the shot noise variance and $\sigma^2_{\text{thermal}}$ is the thermal noise variance [58]. The noise power is given by $\sigma^2 = N_0 B$, where N_0 is the noise power spectral density and B is the bandwidth. As for IM/DD based OWC the transmitted signal represents optical power, $s(t)$ has to be non-negative, and thus $s(t) \geq 0$ holds. In contrast to RF communications where the average transmitted power depends on $|s(t)|^2$, the average transmitted power in OWC is given by

$$I = \lim_{T \to \infty} \frac{1}{2\,T} \int_{-T}^{T} s(t)\,\mathrm{dt} \tag{2.2}$$

and the average received optical power can be written as

$$I_{\mathrm{RX}} = h\,I, \tag{2.3}$$

where h denotes the channel coefficient of the optical link [58]. As further discussed in Section 2.3, intensity modulated optical links can be represented by the direct-current (DC) channel gain h due to the flat frequency response of the optical wireless channel.

2.1.1 Pulsed modulation techniques

In the following, different pulsed modulation techniques are introduced which are commonly used in intensity modulated OWC. These techniques provide different power and bandwidth efficiencies. In this thesis, rectangular pulses are considered in conjunction with these pulsed modulation techniques.

2.1.1.1 On-off-keying

On-off-keying (OOK) is the simplest optical modulation technique as it is a binary modulation scheme. Depending on the data to be transmitted, *i.e.* a binary "1" or "0", the optical signal is switched on or off for a given symbol duration. This means that OOK employs two intensity

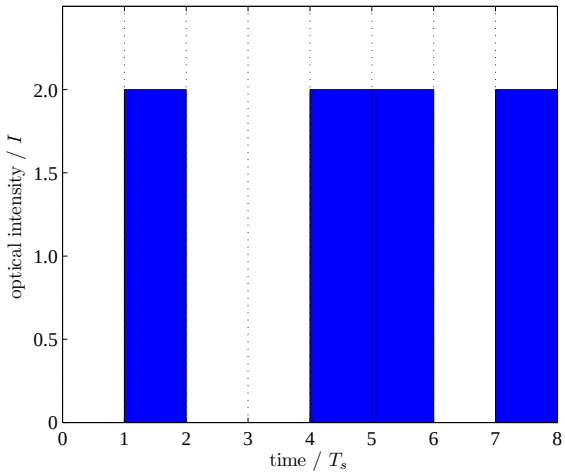

Figure 2.1: *Illustration of OOK modulation.*

levels of the optical signal:

$$I_0^{\mathrm{OOK}} = 0 \quad \text{and} \quad I_1^{\mathrm{OOK}} = 2\,I, \tag{2.4}$$

where I is the mean optical power emitted as introduced above. Figure 2.1 illustrates an OOK modulated optical signal. The bit rate of OOK is $1/T_s$ bit/s, where T_s denotes the symbol (*i.e.* the pulse) duration in seconds. Consequently, only one bit can be transmitted per symbol duration. This results in a first-null bandwidth of $1/T_s$ Hz and in a bandwidth efficiency of 1 bit/s/Hz [57, Ch. 3.3.1]. Since OOK is a binary modulation scheme, its symbol error rate corresponds to its bit error ratio (BER). According to [57, Ch. 3.3.1], the BER of OOK is given by

$$\mathrm{BER}_{\mathrm{OOK}} = \mathrm{Q}\left(\sqrt{\frac{E_{\mathrm{RX}}}{N_0}}\right), \tag{2.5}$$

where $\mathrm{Q}(a) = \frac{1}{\sqrt{2\pi}} \int_a^{+\infty} \exp(\frac{-t^2}{2})\,\mathrm{dt}$ is the Q-function. The mean received electrical energy is given by $E_{\mathrm{RX}} = (\rho\, I_{\mathrm{RX}})^2\, T_s$, where ρ is the optical-to-electrical conversion coefficient. The optical-to-electrical conversion coefficient is defined as $\rho = \frac{q_{\mathrm{e}}\sqrt{R_{\mathrm{load}}}}{h_{\mathrm{Planck}}\, f}$, where q_{e} is the electron charge, R_{load} is the load resistance over which the received current is measured, h_{Planck} is the Planck constant and f is the frequency of the optical signal. For the sake of simplicity, ρ is assumed to be 1 $\mathrm{A}\sqrt{\Omega}/\mathrm{W}$ in this thesis. In intensity modulated optical communications, the electrical energy is proportional to the square of the optical power [58]. Due to its simplicity, OOK enables low-complex and low-cost transceiver implementations. However, as OOK is a

binary modulation scheme, it provides only low spectral efficiencies.

2.1.1.2 Pulse position modulation

Corresponding to OOK, pulse position modulation (PPM) employs also two intensity levels of the optical signal. However, the symbol interval is subdivided into M subintervals resulting in M-PPM. Only during one subinterval within the symbol duration, the optical signal is switched on. During all remaining subintervals, the optical signal is switched off. This means that the data to be transmitted is represented by the position of the optical pulse within the symbol interval, *i.e.* by the index of the subinterval which contains the pulse. The intensity levels which are used for M-PPM are given by:

$$I_0^{\mathrm{PPM}} = 0 \quad \text{and} \quad I_1^{\mathrm{PPM}} = M\, I. \tag{2.6}$$

Figure 2.2 illustrates a PPM modulated optical signal with $M = 4$. According to [57, Ch. 3.3.1], the BER of M-PPM can be lower bounded by

$$\mathrm{BER}_{\mathrm{PPM}} \geq \frac{M}{2}\, \mathrm{Q}\left(\sqrt{\frac{M\, E_{\mathrm{RX}}}{2\, N_0}}\right). \tag{2.7}$$

In comparison to OOK, M-PPM provides an enhanced bit rate of $\log_2(M)/T_s$ bit/s, *i.e.* $\log_2(M)$ bits can be transmitted per symbol duration. However, PPM operates with shorter optical pulses. Specifically, the actual pulse duration is divided by factor M. Therefore, PPM

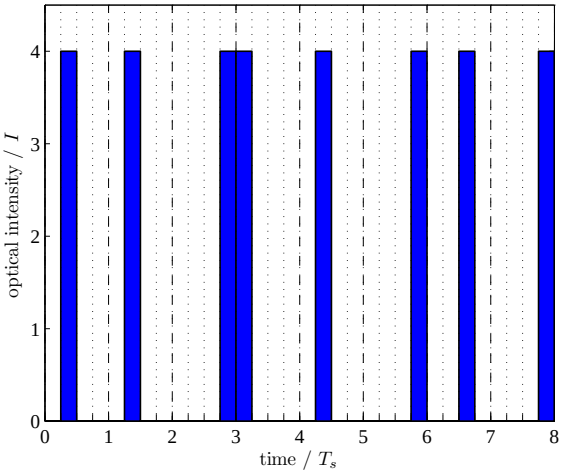

Figure 2.2: *Illustration of* 4*-PPM.*

requires a larger bandwidth compared to OOK resulting in a lower bandwidth efficiency of $\log_2(M)/M$ bit/s/Hz. Moreover, PPM has a larger peak power emission and requires both symbol interval and subinterval synchronisation.

2.1.1.3 Pulse amplitude modulation

In contrast to OOK, pulse amplitude modulation (PAM) is a higher order modulation scheme which employs multiple intensity levels to convey data. In order to provide non-negative optical signals, unipolar M-level PAM is used in OWC. Specifically, M denotes the signal constellation size, *i.e.* the number of employed optical intensity levels. The intensity levels are given by:

$$I_m^{\mathrm{PAM}} = \tfrac{2\,I}{M-1}\, m \quad \text{for} \quad m = 0, 1, \ldots (M-1). \tag{2.8}$$

Figure 2.3 illustrates a 4-PAM modulated optical signal. M-PAM provides a bit rate of $\log_2(M)/T_s$ bit/s and a bandwidth efficiency of $\log_2(M)$ bit/s/Hz. Consequently, PAM has a higher bandwidth efficiency compared to OOK and PPM. As given in [57, Ch. 3.3.2], the BER of unipolar M-PAM can be lower bounded by

$$\mathrm{BER}_{\mathrm{PAM}} \geq \frac{2\,(M-1)}{M\,\log_2(M)}\,\mathrm{Q}\left(\frac{1}{M-1}\sqrt{\frac{E_{\mathrm{RX}}}{N_0}}\right). \tag{2.9}$$

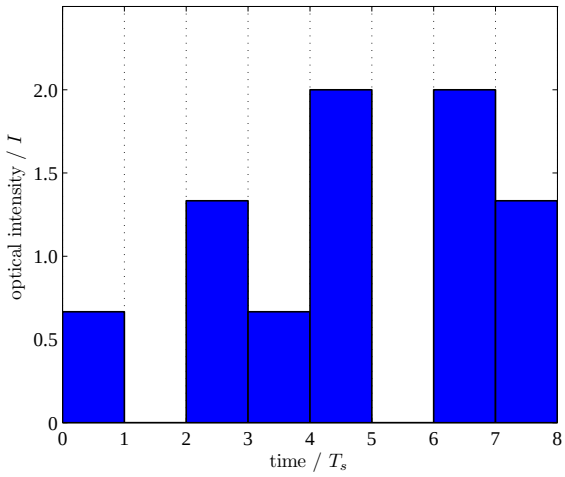

Figure 2.3: *Illustration of* 4*-PAM.*

2.1.2 Multi-carrier techniques

In [67], Ohtsuki shows that multi-carrier modulation techniques can be applied to OWC. Especially, the multi-carrier technique orthogonal frequency division multiplexing (OFDM) has attracted attention for OWC [42, 60, 68–73]. This is due to the fact that OFDM is a bandwidth efficient transmission technique. It can cope with inter-symbol interference (ISI) caused by multipath propagation and with frequency selectivity caused by the LEDs frequency response. OFDM conveys digital data on multiple orthogonal sub-carrier frequencies [23, 74, 75]. Hence, a wideband channel is subdivided into several narrowband sub-channels. These orthogonal sub-carrier channels are used to transmit independent data streams in parallel in the frequency domain. The frequency division multiplexed channels are summed up and transformed into a time domain waveform by using an inverse Fourier transformation. In IM/DD based OWC, the time domain waveform modulates the intensity of the light. To this end, the time domain waveform has to be unipolar to account for the non-negativity of the optical signal. The utilisation of narrowband sub-channels enables a low-complex channel equalisation: each sub-channel can be regarded as a non-frequency-selective channel which is individually equalised in the frequency domain using a single-tap equaliser. Consequently, OFDM enables efficient signal processing implementations.

The pulsed modulation techniques presented above suffer from ISI in the presence of multipath propagation. Multipath effects decrease the performance of OWC systems to a large extent by constraining both bandwidth and data rate. In contrast to pulsed modulation techniques, OFDM provides high data rates even in severe multipath scenarios. In order to mitigate multipath effects and to avoid ISI, OFDM uses a guard interval, the so-called cyclic prefix, which is placed between the OFDM symbols. Moreover, the actual OFDM symbol duration is typically much longer than the delay spread caused by multipath propagation. This property makes OFDM an ideal candidate for diffuse and scattered optical wireless transmission scenarios. Moreover, due to the use of fast Fourier transformation (FFT) and inverse fast Fourier transformation (IFFT), OFDM enables simple and efficient implementations. For instance, compared to M-PAM, OFDM requires approximately three times less computational complexity because PAM requires complex equalisation schemes like decision-feedback equalisation [76]. However, OFDM suffers from high peak-to-average power ratios making it sensitive to clipping effects. Additionally, the performance of OFDM is largely affected by inter-channel interference (ICI) and non-linearities. A further shortcoming of OFDM is the

fact that it requires sophisticated transceiver designs having good linearity characteristics and large dynamic ranges.

Each OFDM sub-carrier is modulated using a conventional modulation scheme. Typically, quadrature amplitude modulation (QAM) is applied. According to [77, Ch. 5.2.9] and [23, Ch. 6.1.4], rectangular M-QAM with square signal constellation size $M = K^2$ can be derived from two K-PAM systems. One K-PAM signal is transmitted on the in-phase signal component and the other one on the quadrature signal component. The transmission power is equally split between the in-phase and quadrature component. Therefore, the BER of optical QAM with square signal constellation size $M = K^2$ can be approximated by

$$\mathrm{BER}_{\mathrm{QAM}} \geq \frac{2\left(\sqrt{M}-1\right)}{\sqrt{M}\,\log_2(\sqrt{M})}\,\mathrm{Q}\left(\frac{1}{\sqrt{M}-1}\sqrt{\frac{E_{\mathrm{RX}}}{4\,N_0}}\right). \tag{2.10}$$

M-QAM provides a bit rate of $\log_2(M)/T_s$ bit/s.

As IM/DD based OWC requires real-valued non-negative time domain signals, QAM cannot be directly applied to optical OFDM. Therefore, the input vector $\mathbf{x}$ to the transmitter IFFT is constrained to have Hermitian symmetry. The input vector provides Hermitian symmetry if its elements fulfil $x_{L-l} = x_l^*$ ($l = 1, 2, \ldots \frac{L}{2} - 1$), where $*$ represents complex conjugation and L is the IFFT size. The complex-valued data symbols are denoted by x_l, with $x_0 = x_{\frac{L}{2}} = 0$. The zero sub-carrier is not modulated as it results in a DC bias. Due to the Hermitian symmetry constraint, only half of the sub-carriers contain independent data symbols. The Hermitian symmetry of the input vector creates a real-valued time domain waveform by cancelling the imaginary components of the IFFT output. This real-valued signal can be sent by incoherent light sources. However, the time domain signal is still bipolar. In order to provide unipolar signals which can modulate the intensity of the optical carrier, further processing is required. In the following, three multi-carrier techniques are introduced which generate real-valued non-negative time domain signals.

2.1.2.1 Direct-current-biased optical OFDM

As presented above, a real-valued time domain signal is generated by constraining the input vector to the transmitter IFFT to have Hermitian symmetry. In order to provide unipolar time domain signals, direct-current-biased optical orthogonal frequency division multiplexing (DCO-OFDM) adds a fixed DC bias to the IFFT input. Alternatively, an analogue DC offset

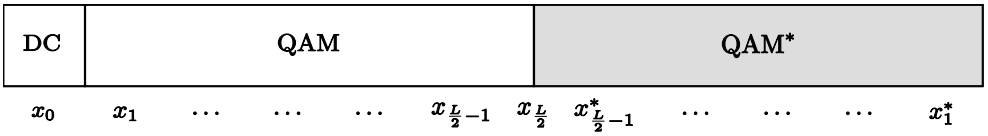

Figure 2.4: *Illustration of input vector to the transmitter IFFT used by DCO-OFDM.*

can be added to the bipolar time domain signal by adjusting the bias point of the transmitter LED. Figure 2.4 shows the input vector to the transmitter IFFT used by DCO-OFDM. The DC bias has to be chosen appropriately to provide non-negativity of the time domain signals, while keeping upper and lower clipping effects to a minimum [72]. Finally, the real-valued unipolar signal is intensity modulated onto the optical carrier. Figure 2.5 illustrates a DCO-OFDM time domain signal. As shown, the signal contains a DC bias. Since OFDM signals have a high peak-to-average power ratio, the required DC bias can be high. A high DC bias results in a low power efficiency which is the main shortcoming of DCO-OFDM.

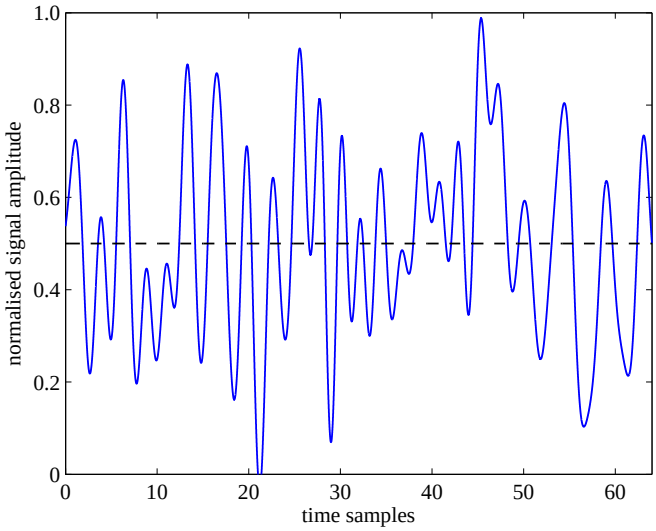

Figure 2.5: *Illustration of DCO-OFDM time domain signal. IFFT size is* 64 *and* 4*-QAM is used for signal modulation. Moreover, the added DC bias is illustrated.*

2.1.2.2 Asymmetrically clipped optical OFDM

In [69], Armstrong and Lowery propose a power efficient optical OFDM technique. The scheme is called asymmetrically clipped optical orthogonal frequency division multiplexing (ACO-OFDM). ACO-OFDM is more power efficient than DCO-OFDM because it operates without an additional DC bias. Figure 2.6 illustrates the input vector to the transmitter IFFT used by ACO-OFDM. As shown, the DC bias is set to zero. In order to provide real-valued time

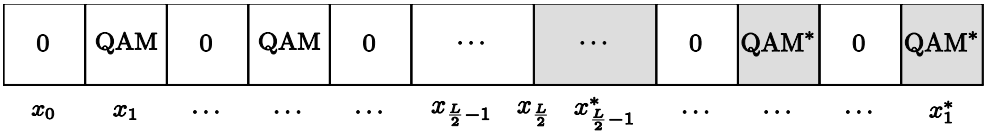

Figure 2.6: *Illustration of input vector to the transmitter IFFT used by ACO-OFDM.*

domain signals, Hermitian symmetry is applied. However, only the odd-numbered sub-carriers are modulated, whereas the even-numbered sub-carriers are set to zero. This composition of the input vector to the transmitter IFFT generates a real-valued bipolar time domain signal. As shown in Figure 2.7, the negative amplitude values are also contained in the positive signal parts and vice versa. The second half of the ACO-OFDM time domain signal is identical to its inverted first half. Armstrong and Lowery show that a hard-clipping can be applied to the entire negative signal amplitudes without affecting the data conveyed in the OFDM signal. This clipping converts the bipolar signal into a unipolar waveform as all negative amplitude values are set to zero. The clipped time domain signal is intensity modulated onto the optical carrier. The noise resulting from clipping the negative parts of the waveform falls only onto the even-numbered sub-carriers, which convey no data. As a consequence, the clipping noise does not impair the data symbols on the odd-numbered sub-carriers. The asymmetric clipping reduces the emitted average optical power. However, as only the odd-numbered sub-carriers convey data symbols, ACO-OFDM provides only half the spectral efficiency of DCO-OFDM.

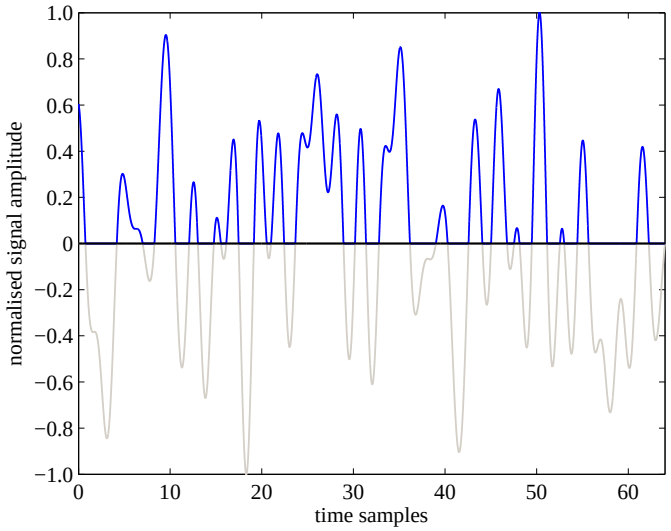

Figure 2.7: *Illustration of ACO-OFDM time domain signal. IFFT size is* 64 *and* 16*-QAM is used for signal modulation. Moreover, the hard-clipped negative amplitude values are illustrated.*

2.1.2.3 Pulse-amplitude-modulated discrete multitone modulation

In [78], Lee *et al.* propose pulse-amplitude-modulated discrete multitone modulation (PAM-DMT) for IM/DD based optical communication systems. In contrast to DCO-OFDM and ACO-OFDM which employ complex-valued QAM symbols, PAM-DMT uses real-valued PAM symbols to modulate the sub-carriers. Figure 2.8 illustrates the input vector to the transmitter IFFT used by PAM-DMT. As shown, the real parts of the input vector $\mathbf{x}$ are set to zero and only the imaginary parts are pulse amplitude modulated. As a result, $x_l = j\, I_l^{\text{PAM}}$ ($l = 1, 2, \ldots \frac{L}{2} - 1$) holds, where j is the unit imaginary number. Additionally, Hermitian symmetry is applied, and thus $x_{L-l} = x_l^* = -j\, I_l^{\text{PAM}}$. Figure 2.9 shows the resulting real-valued time domain signal. It can be seen that the positive and negative amplitudes of the PAM-DMT waveform are centrically symmetric, *i.e.* the same amplitude values are conveyed in the positive and negative parts of the time domain signal. Therefore,

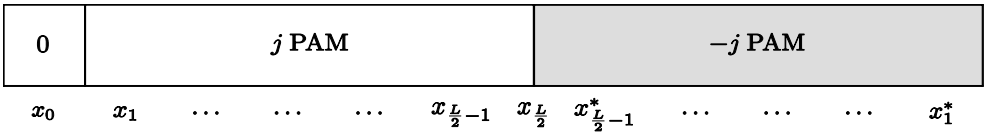

Figure 2.8: *Illustration of input vector to the transmitter IFFT used by PAM-DMT.*

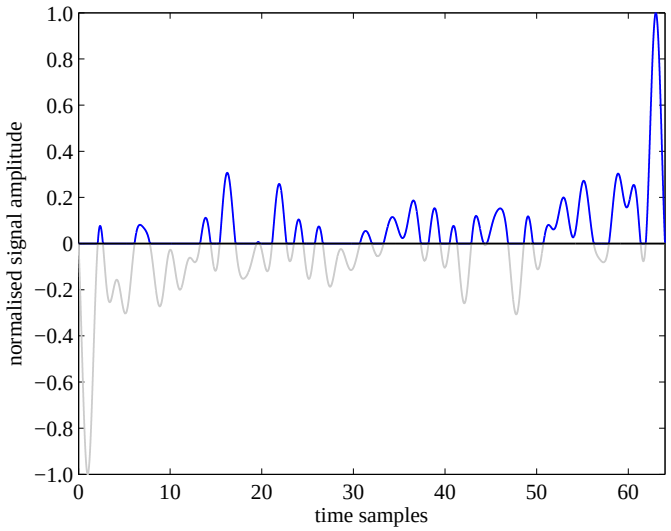

Figure 2.9: *Illustration of PAM-DMT time domain signal. IFFT size is* 64 *and* 4*-PAM is used for signal modulation. Moreover, the hard-clipped negative amplitude values are illustrated.*

similar to ACO-OFDM, the negative amplitude values can be hard-clipped without affecting the data symbols. Only the positive amplitude values are used to modulate the intensity of the optical carrier. Lee *et al.* show in [78] that the clipping noise is orthogonal to the actual PAM symbols. In contrast to ACO-OFDM, PAM-DMT uses all sub-carriers to convey data. However, only the quadrature component is used to transmit information as the real-valued PAM symbols are multiplied by j. As shown in [76, 78], PAM-DMT and ACO-OFDM provide similar performance at any spectral efficiency.

2.2 Optical MIMO techniques

MIMO techniques are well-established and widely implemented in many RF systems. The parallel usage of multiple transmitters and receivers offers high data rates by increasing the spectral efficiency [6, 8]. For outdoor free-space optical (FSO) transmission, the effects of MIMO have already been studied. The use of multiple optical emitters and receivers provides several spatially separated optical wireless channels. These multiple channels increase the system capacity and enable high data rates. It has been shown that spatial diversity can combat the fading effects caused by scattering and scintillation due to atmospheric turbulence [79–81]. However, a precise alignment of the transmitter and detector array is required for outdoor FSO transmission. For indoor OWC, it is still not clear to what extent MIMO techniques can provide gains. This is because in indoor environments there are no fading effects caused by turbulence. Potential spatial multipath interference effects are averaged by the integrating effect of the photo-detector that has a diameter which is orders of magnitude larger than the optical wavelength [38]. Moreover, a strict transmitter-receiver alignment is undesirable for indoor OWC. Imaging receivers, like the fly-eye receivers proposed by Yun and Kavehrad [82], are well suited for optical MIMO as they increase link robustness by providing angular diversity channels. The receivers consist of an imaging concentrator (a lens) which forms an image of the received light on a collection of photo-detectors. This setup enables the separation of signals which arrive from different directions without the need for a precise alignment. For diffuse OWC scenarios, Jivkova *et al.* propose a multispot diffusing configuration to improve the link margin by using multiple transmitters and receivers [83, 84]. This concept utilises a spot array generator to ensure a more uniform signal power distribution in comparison to a pure diffuse configuration. In [85], multibeam transmitters and imaging diversity receivers are considered. It is shown that these devices can reduce the required transmitter power by

up to 20 dB compared to single-input-single-output (SISO) systems. Additionally, multibeam transmitters and imaging receivers enable space-division multiple access to provide channel access for several users.

In order to increase link reliability and system performance, space-time codes (STCs) are used. In [86], the performance of space-time block codes (STBCs) for diffuse OWC systems is investigated. The authors consider a setup with two transmitters and show that STBCs can increase the coverage of the optical wireless system. Garfield *et al.* propose a system in [87] which allows parallel communications in a diffuse environment employing a 2×2 Alamouti-type space-time coding. The RF Alamouti code [9] is adapted for OWC to apply only real-valued non-negative signals resulting in on-off-keyed symbols. The coding is reported to outperform SISO and multiple-input-single-output (MISO) configurations. In [88], the authors also propose a modification of the RF Alamouti code to apply it to IM/DD based optical scenarios. This approach is generalised in [89] where a design criterion for FSO STCs is derived. The authors show that full diversity RF STCs also achieve full diversity in FSO. However, these STCs provide a lower coding gain compared to repetition coding (RC). Safari and Uysal show in [90] that for FSO links, RC can outperform single-input-multiple-output (SIMO) setups and orthogonal space-time block codes (OSTBCs) like the Alamouti scheme. RC works by the principle that the same information is simultaneously sent from multiple transmitters. It is shown that OWC systems can achieve diversity gains from RC due to the use of IM and the resulting constructive superposition of the optical signals. Therefore, RC is a more efficient technique for IM/DD based OWC compared to OSTBCs. Section 2.2.1 introduces RC in more detail.

Further research activities intend to enhance the channel capacity of indoor OWC systems by spatial multiplexing approaches. To this end, multiple LEDs are used to transmit independent data streams simultaneously [45, 91]. A multiplexing MIMO system is considered in [92]. The system uses zero-forcing (ZF) detection to eliminate the channel interference. The authors assume a directed LOS connection between the transmitters and the receivers. Furthermore, they assume limited cross-talk between the multiple emitters as they consider a transmitter spacing of up to 3 m. This work is further extended in [93] where the authors analyse the signal-to-interference-plus-noise ratio (SINR) and the BER of an optical wireless MIMO scheme employing simple OOK modulation. It is shown that optical beat interference can cause error floors. Zeng *et al.* study non-imaging and imaging spatial multiplexing MIMO approaches

in [94]. The authors show that symmetries in the geometry of the non-imaging system limit the transmission capacity. The limited capacity is caused by the fact that the channel matrix might not have full rank at some receiver positions. However, the imaging MIMO system is reported to operate properly at all receiver positions. All these spatial multiplexing schemes cause ICI which requires complex and computationally intensive interference cancellation techniques. Section 2.2.2 deals with optical spatial multiplexing (SMP) in more detail. A power and bandwidth efficient pulsed modulation technique called spatial modulation (SM) is investigated by Mesleh *et al.* in [62] for indoor OWC. This technique provides increased spectral efficiency by utilizing multiple transmitters to convey data, while completely avoiding ICI. Section 2.2.3 introduces SM in detail.

Preliminary experimental work on optical wireless MIMO transmission is undertaken for instance in [91]. The authors report experiments for a simple 2×9 LOS system. Two independent non-return-to-zero sequences are transmitted from two lasers over a short distance of 20 cm. In [95], O'Brien describes a four channel MIMO system that uses white light LEDs for data transmission at a channel data rate of 2 Mbit/s. Moreover, MIMO experiments over a short distance in a diffuse environment are reported. In [96], an experimental demonstration of a 4×9 MIMO system is reported. The system employs imaging receivers and achieves 2 Mbit/s/channel with a BER of less than 10^{-9} at certain positions of the receiver array. This work is extended in [97] where an experimental demonstration of a 4 channel MIMO-OFDM system is reported which achieves 1 Gbit/s with a BER of 10^{-3} over a distance of 1 m.

Although all this work shows that MIMO techniques might be applied to indoor OWC, there are still many unanswered research questions in this area. Indoor optical wireless links are highly correlated [91]. Provided that MIMO techniques mostly rely on spatially uncorrelated channels, it is unclear whether the optical propagation channel in indoor environments can offer practical link differentiability. Moreover, a detailed performance comparison of different MIMO schemes to analyse which one is the most suitable for OWC is still an open research issue. To the best of the author's knowledge, an extensive comparison of RC, SMP and SM for indoor OWC has not been done so far.

In the following, the optical MIMO techniques RC, SMP and SM are investigated in detail. These MIMO techniques have specific and distinct characteristics, and thus fundamentally differ from each other. Particularly, a framework is developed to analytically approximate the BERs of these schemes. An optical wireless MIMO transmission system is considered

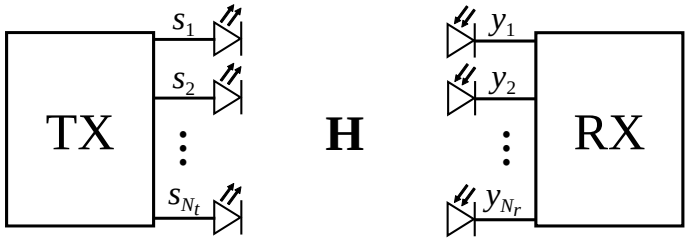

Figure 2.10: *Illustration of optical wireless MIMO transmission system.*

which employs IM and DD of the optical carrier. The system is equipped with N_t optical transmitters and N_r photo-detectors at the receiver side. Figure 2.10 illustrates the considered optical wireless MIMO transmission system. Using the baseband channel model for OWC given in (2.1) and the definition of the received optical power given in (2.3), the received signal vector can be defined as

$$\mathbf{y} = \mathbf{H}\,\mathbf{s} + \mathbf{n} \;\text{ with }\; \mathbf{y} \in \mathbb{R}^{N_r}, \tag{2.11}$$

where $\mathbf{n}$ is the N_r-dimensional real-valued AWGN vector. The noise is modelled as zero mean and independent of the transmitted signal. The transmitted signal vector is denoted by $\mathbf{s} = [s_1 \ \ldots \ s_{N_t}]^T$, where $[\cdot]^T$ is the transpose operator. The elements of $\mathbf{s}$ indicate which signal is emitted by each optical transmitter, *i.e.* s_{n_t} denotes the signal emitted by transmitter n_t. The $N_r \times N_t$ channel matrix $\mathbf{H}$ is given by

$$\mathbf{H} = \begin{pmatrix} h_{11} & \cdots & h_{1N_t} \\ \vdots & \ddots & \vdots \\ h_{N_r1} & \cdots & h_{N_rN_t} \end{pmatrix}, \tag{2.12}$$

where $h_{n_rn_t}$ represents the transfer factor of the optical wireless link between transmitter n_t and receiver n_r. As for indoor OWC the multiple optical transmitters are typically in close proximity, they can be jointly driven by exactly the same baseband hardware and electronic driver. Hence, a perfectly synchronised transmission can be considered. As the multiple receivers are commonly integrated into the same receiving device, they are also in close proximity. Consequently, there is only a very small path difference between the multiple transmitter-receiver links, especially if LOS propagation is considered. Therefore, there is negligible temporal delay between the multiple links. Consequently, the system model given in (2.11) is considered without time dispersion.

Practical optical wireless links in indoor environments provide high SNR but low bandwidth

due to the limited modulation capability of off-the-shelf LEDs. Therefore, the available bandwidth has to be used in the most efficient way. This characteristic necessitates spectrally efficient transmission techniques. The usage of multiple transmitters and receivers can perfectly fulfil this need. For this reason, MIMO techniques are considered in this thesis which enhance spectral efficiency and provide multiplexing gains.

2.2.1 Repetition coding

The simplest MIMO transmission technique is RC which simultaneously emits the same signal from all N_t transmitters. Therefore, for RC $s_1 = s_2 = \ldots = s_{N_t}$ holds. RC is known to achieve good performance in free-space OWC because of transmit diversity [80]. Safari and Uysal show in [90] that RC can outperform OSTBCs like the Alamouti scheme [9] and SIMO setups. This is due to the fact that for IM/DD based links the intensities coming from several transmitters constructively add up at the receiver. In this thesis, unipolar M-level PAM is considered as modulation scheme for RC. Consequently, RC in combination with M-PAM achieves a spectral efficiency of $\log_2(M)$ bit/s/Hz. PAM is considered because it is more bandwidth efficient compared to the other pulsed modulation techniques OOK and PPM. Moreover, PAM has shown to have similar optical power efficiency compared to DCO-OFDM [71]. In [73, 76], the authors show that PAM outperforms DCO-OFDM because the latter requires a high constant DC bias. This DC bias power affects the effective SNR of DCO-OFDM in contrast to unipolar PAM which operates without an additional DC bias.

In the following, $E_s = (\rho\, I)^2\, T_s$ denotes the mean *emitted* electrical energy of the intensity modulated optical signals. In order to ensure comparability of different setups and transmission techniques, the mean optical power emitted has to be fixed. As RC simultaneously emits the same signal from several transmitters, the optical transmission power is equally distributed across all emitters. This means that the intensities given in (2.8) have to be divided by factor N_t. As a result, the mean optical power emitted is constant, irrespective of the number of employed transmitters. The BER of M-PAM given in (2.9) can be generalised for an arbitrary $N_r \times N_t$ scenario which employs RC:

$$\mathrm{BER}_{\mathrm{RC}} \geq \frac{2\,(M-1)}{M\,\log_2(M)}\,\mathrm{Q}\left(\frac{1}{M-1}\sqrt{\frac{E_s}{N_0\,N_t^2}\sum_{n_r=1}^{N_r}\left(\sum_{n_t=1}^{N_t} h_{n_r n_t}\right)^2}\right). \tag{2.13}$$

The intensities emitted by the multiple transmitters constructively add up at the receiver leading to a mean received optical power of $I_{\mathrm{RX}_{n_r}} = \sum_{n_t=1}^{N_t} \frac{I}{N_t} h_{n_r n_t}$ at receiver n_r. Consequently, the single channel gains $h_{n_r n_t} \in [0; 1]$ induce a distinctive attenuation of the transmitted signals (path loss) depending on the specific link characteristic. The N_r received signals are combined by maximum ratio combining (MRC) [23, Ch. 7.2.4]. Thus by applying MRC, the received signals with a high SNR are weighted more than signals with a low SNR. Consequently, the electrical SNR after the combiner becomes:

$$\frac{E_{\mathrm{RX}}}{N_0} = \frac{T_s}{N_0} \sum_{n_r=1}^{N_r} \left(\rho\, I_{\mathrm{RX}_{n_r}}\right)^2 = \frac{T_s}{N_0} \sum_{n_r=1}^{N_r} \left(\sum_{n_t=1}^{N_t} \frac{\rho\, I}{N_t} h_{n_r n_t} \right)^2 = \frac{E_s}{N_0\, N_t^2} \sum_{n_r=1}^{N_r} \left(\sum_{n_t=1}^{N_t} h_{n_r n_t} \right)^2, \tag{2.14}$$

which corresponds to the SNR given in the argument of the Q-function in (2.13). Moreover, (2.14) comprises the mean *received* electrical energy of the MIMO system given by

$$\begin{aligned} E_{\mathrm{RX}} &= \sum_{n_r=1}^{N_r} \left(\rho\, I_{\mathrm{RX}_{n_r}}\right)^2 T_s \\ &= \sum_{n_r=1}^{N_r} \left(\frac{\rho\, I}{N_t} \sum_{n_t=1}^{N_t} h_{n_r n_t} \right)^2 T_s \\ &= E_s \sum_{n_r=1}^{N_r} \left(\frac{1}{N_t} \sum_{n_t=1}^{N_t} h_{n_r n_t} \right)^2. \end{aligned} \tag{2.15}$$

Consequently, the BER of RC given in (2.13) is only affected by the transfer factors of the wireless optical links, respectively by the received optical power. Therefore, RC can be represented by a simple SISO scheme which provides the same received electrical energy. For this reason, RC is considered in this thesis as a benchmark scheme for the MIMO techniques presented in the following sections.

2.2.2 Spatial multiplexing

Another well-known MIMO technique is SMP. By applying SMP, independent data streams are simultaneously emitted from all optical transmitters. Therefore, SMP provides an enhanced spectral efficiency of $N_t \log_2(M)$ bit/s/Hz. Like for RC, PAM is used as signal modulation scheme for SMP in the following. The optical power is equally distributed across all emitters to ensure that both techniques use the same mean transmission power. For SMP, the signal vector $\mathbf{s}$ has N_t elements which are independent M-PAM modulated signals according to (2.8),

whereas their respective emitted intensities are divided by N_t. Provided that the SMP receiver performs a maximum-likelihood (ML) detection, the pairwise error probability (PEP) is the probability that the receiver mistakes the transmitted signal vector $\mathbf{s}_{m^{(1)}}$ for another vector $\mathbf{s}_{m^{(2)}}$, given knowledge of the channel matrix $\mathbf{H}$ [24, Ch. 6.3.2]. Therefore, the PEP of SMP can be calculated by

$$\mathrm{PEP}_{\mathrm{SMP}}(\mathbf{s}_{m^{(1)}} \to \mathbf{s}_{m^{(2)}}|\mathbf{H}) = \mathrm{Q}\left(\sqrt{\frac{\rho^2\, T_s}{4\, N_0}\ \|\mathbf{H}\,(\mathbf{s}_{m^{(1)}} - \mathbf{s}_{m^{(2)}})\|_{\mathrm{F}}^2}\right), \tag{2.16}$$

where $\|\cdot\|_{\mathrm{F}}$ denotes the Frobenius norm. Using this PEP and considering all M^{N_t} possible combinations of the transmitted signal vector, the BER of SMP can be approximated by union bound methods. The upper bound is given in (2.17), with $\mathrm{d_H}(b_{m^{(1)}}, b_{m^{(2)}})$ denoting the Hamming distance of the two bit assignments $b_{m^{(1)}}$ and $b_{m^{(2)}}$ of the signal vectors $\mathbf{s}_{m^{(1)}}$ and $\mathbf{s}_{m^{(2)}}$:

$$\begin{aligned}\mathrm{BER}_{\mathrm{SMP}} \leq \frac{1}{M^{N_t}\ \log_2(M^{N_t})} \sum_{m^{(1)}=1}^{M^{N_t}} \sum_{m^{(2)}=1}^{M^{N_t}} \mathrm{d_H}(b_{m^{(1)}}, b_{m^{(2)}}) \cdot \\ \mathrm{Q}\left(\sqrt{\frac{\rho^2\, T_s}{4\, N_0}\ \|\mathbf{H}\,(\mathbf{s}_{m^{(1)}} - \mathbf{s}_{m^{(2)}})\|_{\mathrm{F}}^2}\right).\end{aligned} \tag{2.17}$$

For instance, if $N_t = 4$ and $M = 2$ are assumed, the bit sequence "1 0 0 1" is assigned to $\mathbf{s}_{10} = \left[\frac{I}{2}\ 0\ 0\ \frac{I}{2}\right]^T$ and "1 0 0 0" is assigned to $\mathbf{s}_9 = \left[\frac{I}{2}\ 0\ 0\ 0\right]^T$. These two bit assignments result in a Hamming distance of $\mathrm{d_H}(b_{10}, b_9) = 1$. Therefore, $\mathrm{d_H}(\cdot,\cdot)$ states the number of bit errors when erroneously detecting $\mathbf{s}_{m^{(2)}}$ at the receiver instead of the actually transmitted signal vector $\mathbf{s}_{m^{(1)}}$.

2.2.3 Spatial modulation

SM is a combined MIMO and digital modulation technique proposed in [98] and further investigated in [99–105]. As considered above, PAM is used for the digital signal modulation of SM in the following. In SM, the conventional signal constellation diagram is extended to an additional dimension, namely the spatial dimension. The spatial dimension is used to transmit additional bits. Each transmitter in the transmitting array is assigned a unique binary sequence, the spatial symbol. A transmitter is only activated when the random spatial symbol to be transmitted matches the pre-allocated spatial symbol. This means that only one transmitter

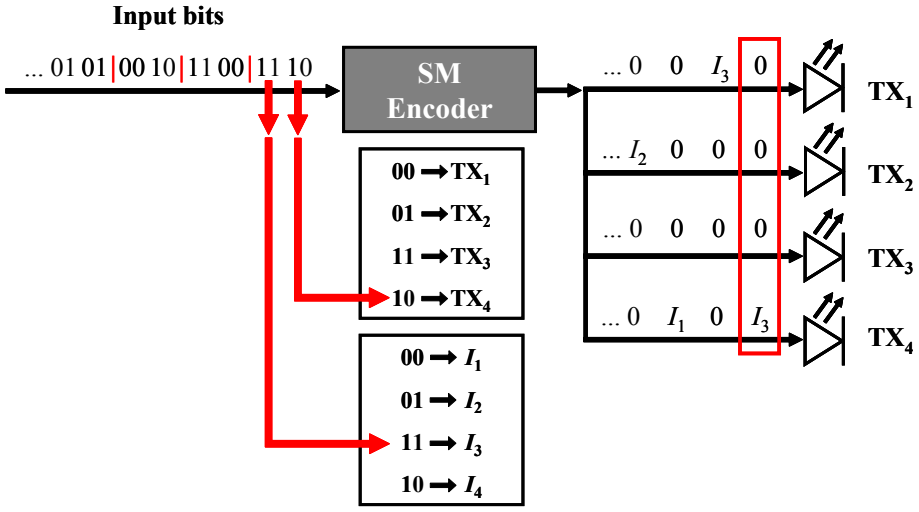

Figure 2.11: *Illustration of SM operation with $N_t = 4$ and $M = 4$ providing a spectral efficiency of 4 bit/s/Hz. The first two bits in the block of four bits determine the PAM symbol and the second two bits determine the active LED.*

is activated at any PAM symbol duration. Therefore, only one element of the signal vector $\mathbf{s}$ to be transmitted is non-zero. The element is the digitally modulated signal to be sent, *i.e.* the PAM symbol. The index of the non-zero element is the spatial symbol. SM simultaneously transmits data in the signal domain and the spatial domain. Consequently, SM provides an enhanced spectral efficiency of $\log_2(N_t) + \log_2(M) = \log_2(MN_t)$ bit/s/Hz. Moreover, as only one transmitter is activated at any symbol duration, SM completely avoids ICI. As a result, SM has a lower decoding complexity compared to other MIMO schemes [104–106]. Due to the distinct channel transfer factor between a particular transmitter and the receiver, the receiver is able to detect which transmitter is activated, and hence is able to detect the spatial symbol. Figure 2.11 illustrates the functionality of SM for a setup with $N_t = 4$ optical emitters and a signal constellation size of $M = 4$. This setup provides a spectral efficiency of 4 bit/s/Hz. The bits to be transmitted are passed to the SM encoder, which maps them to the respective signal and transmitter index. In this example, the last two bits denote the index of the transmitter which emits the signal, whereas the first two bits represent the actual signal to be sent. For instance, the bit sequence "$1\,1\,1\,0$" is represented by transmitter number 4 emitting signal I_3, *i.e.* an optical pulse with intensity I_3. In contrast to RC and SMP, signals with intensity $I_m = 0$ cannot be used for the signal modulation of SM. In this case, no transmitter would be active and the spatial information would be lost. Therefore, the intensities of conventional PAM given

in (2.8) have to be modified to be suitable for SM leading to:

$$I_m^{\mathrm{SM}} = \tfrac{2\,I}{M+1}\, m \quad \text{for} \quad m = 1, 2, \ldots M. \tag{2.18}$$

Consequently, the minimum distance between two SM signals is $\frac{2\,I}{M+1}$, whereas the minimum distance for conventional PAM is $\frac{2\,I}{M-1}$. The smaller signal distance of SM might induce a worse BER performance because the error probability depends on the Euclidean distance of the signals. However, as SM additionally encodes data bits in the spatial domain, it provides the same spectral efficiency as conventional M-PAM with a lower signal constellation size. Hence, the distance of the signal points is effectively enlarged. The SM receiver has to perform a twofold detection task: Firstly, it has to detect the transmitted PAM symbol. Secondly, the SM receiver has to detect which transmitter has sent the signal. Only if both the symbol and the transmitter index are detected correctly, the bit sequence can be reconstructed properly. Both estimation tasks are jointly done by applying ML detection for instance. Therefore, the performance of SM depends on the differentiability of the multiple channels and is affected by the channel correlation [107, 108]. The PEP of SM for IM/DD based OWC is

$$\begin{aligned} \mathrm{PEP}_{\mathrm{SM}}(\mathbf{s}_{m^{(1)}} \to \mathbf{s}_{m^{(2)}} | \mathbf{H}) &= \mathrm{Q}\left(\sqrt{\frac{\rho^2\, T_s}{4\, N_0}\, \left\| \mathbf{H}\left(\mathbf{s}_{m^{(1)}} - \mathbf{s}_{m^{(2)}}\right) \right\|_{\mathrm{F}}^2} \right) \\ &= \mathrm{Q}\left(\sqrt{\frac{\rho^2\, T_s}{4\, N_0} \sum_{n_r=1}^{N_r} \left| I_{m^{(2)}}^{\mathrm{SM}}\, h_{n_r n_t^{(2)}} - I_{m^{(1)}}^{\mathrm{SM}}\, h_{n_r n_t^{(1)}} \right|^2} \right), \end{aligned} \tag{2.19}$$

where $|\cdot|$ represents the absolute value. This PEP denotes the probability that the receiver decides for intensity $I_{m^{(2)}}^{\mathrm{SM}}$ being emitted by transmitter $n_t^{(2)}$, whereas actually transmitter $n_t^{(1)}$ has emitted intensity $I_{m^{(1)}}^{\mathrm{SM}}$. Using this PEP and considering all possible MN_t signal combinations, the BER of SM can be approximated by union bound methods. The upper bound of its BER is given in (2.20), where $b_{m^{(1)} n_t^{(1)}}$ is the bit assignment which is conveyed when intensity $I_{m^{(1)}}^{\mathrm{SM}}$ is emitted by transmitter $n_t^{(1)}$ and $b_{m^{(2)} n_t^{(2)}}$ is the bit assignment which is encoded when intensity $I_{m^{(2)}}^{\mathrm{SM}}$ is emitted by transmitter $n_t^{(2)}$:

$$\begin{aligned} \mathrm{BER}_{\mathrm{SM}} \leq \frac{1}{MN_t\, \log_2\left(MN_t\right)} & \sum_{m^{(1)}=1}^{M} \sum_{n_t^{(1)}=1}^{N_t} \sum_{m^{(2)}=1}^{M} \sum_{n_t^{(2)}=1}^{N_t} \mathrm{d_H}\left(b_{m^{(1)} n_t^{(1)}}, b_{m^{(2)} n_t^{(2)}} \right) \cdot \\ & \mathrm{Q}\left(\sqrt{\frac{\rho^2\, T_s}{4\, N_0} \sum_{n_r=1}^{N_r} \left| I_{m^{(2)}}^{\mathrm{SM}}\, h_{n_r n_t^{(2)}} - I_{m^{(1)}}^{\mathrm{SM}}\, h_{n_r n_t^{(1)}} \right|^2} \right). \end{aligned} \tag{2.20}$$

Consequently, $\mathrm{d_H}\left(b_{m^{(1)}n_t^{(1)}}, b_{m^{(2)}n_t^{(2)}}\right)$ states the number of bit errors when erroneously decoding the bit sequence $b_{m^{(2)}n_t^{(2)}}$ at the receiver instead of the actually transmitted sequence $b_{m^{(1)}n_t^{(1)}}$.

A special mode of SM is the so-called space shift keying (SSK) technique [109]. SSK conveys data bits only in the spatial domain. Digital signal modulation is not applied in SSK, and consequently $M = 1$ holds. This means that each activated LED emits the same optical intensity I. Given independent identically distributed (iid) ones and zeros as data bits, each transmitter is activated with equal probability. In order to decode the transmitted bit sequence, the SSK receiver has to estimate only the index of the activated optical transmitter, *i.e.* the actual signal is not demodulated. Therefore, SSK is a low-complex implementation of SM and its PEP reduces to:

$$\begin{aligned}\mathrm{PEP_{SSK}}(\mathbf{s}_{m^{(1)}} \rightarrow \mathbf{s}_{m^{(2)}}|\mathbf{H}) &= \mathrm{Q}\left(\sqrt{\frac{\rho^2\, T_s}{4\, N_0}\ \|\mathbf{H}\left(\mathbf{s}_{m^{(1)}} - \mathbf{s}_{m^{(2)}}\right)\|_{\mathrm{F}}^2}\right) \\ &= \mathrm{Q}\left(\sqrt{\frac{\rho^2\, T_s}{4\, N_0}\ \sum_{n_r=1}^{N_r}\left|I\, h_{n_r n_t^{(2)}} - I\, h_{n_r n_t^{(1)}}\right|^2}\right) \\ &= \mathrm{Q}\left(\sqrt{\frac{E_s}{4\, N_0}\ \sum_{n_r=1}^{N_r}\left|h_{n_r n_t^{(2)}} - h_{n_r n_t^{(1)}}\right|^2}\right).\end{aligned} \tag{2.21}$$

Using this PEP and considering all N_t transmitters which can be activated, the BER of SSK can be approximated by union bound methods. The upper bound of its BER is given by:

$$\begin{aligned}\mathrm{BER_{SSK}} \leq \frac{1}{N_t\ \log_2\left(N_t\right)}\ &\sum_{n_t^{(1)}=1}^{N_t}\ \sum_{n_t^{(2)}=1}^{N_t}\ \mathrm{d_H}\left(b_{n_t^{(1)}}, b_{n_t^{(2)}}\right) \cdot \\ &\mathrm{Q}\left(\sqrt{\frac{E_s}{4\, N_0}\ \sum_{n_r=1}^{N_r}\left|h_{n_r n_t^{(2)}} - h_{n_r n_t^{(1)}}\right|^2}\right),\end{aligned} \tag{2.22}$$

where $b_{n_t^{(1)}}$ is the bit assignment which is conveyed when transmitter $n_t^{(1)}$ is activated and $b_{n_t^{(2)}}$ is the bit assignment which is encoded when transmitter $n_t^{(2)}$ is activated. Consequently, the Hamming distance $\mathrm{d_H}\left(b_{n_t^{(1)}}, b_{n_t^{(2)}}\right)$ states the number of bit errors when erroneously decoding the bit sequence $b_{n_t^{(2)}}$ at the receiver instead of the actually transmitted sequence $b_{n_t^{(1)}}$. As SSK is a pulsed modulation technique and requires only power-signals, it is an ideal candidate for low-complex IM/DD based OWC. However, SSK provides a reduced spectral efficiency of

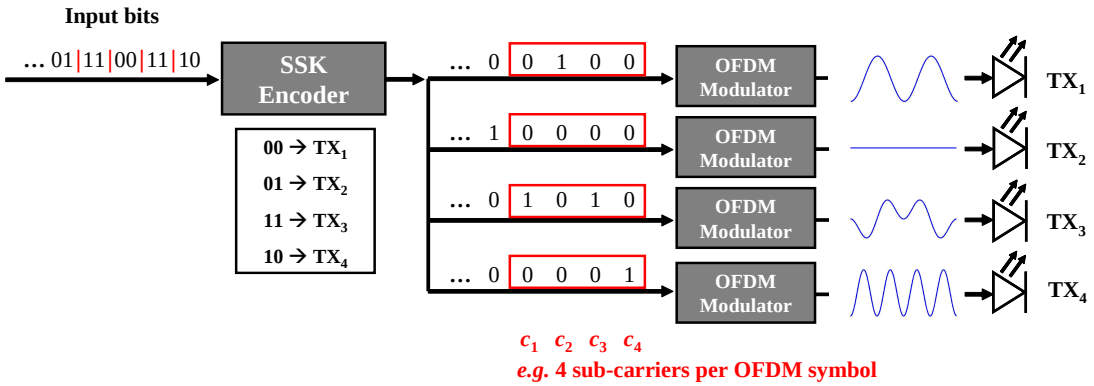

Figure 2.12: *Illustration of SSK in combination with OFDM.*

$\log_2(N_t)$ bit/s/Hz.

In [110, 111], the authors show that SM, respectively SSK can also be combined with OFDM transmission to cope with multipath propagation and frequency-selective fading for instance. Figure 2.12 illustrates this combination for a setup using $N_t = 4$ transmitters. As shown, the SSK technique is individually applied to each sub-carrier in the frequency domain. Each sub-carrier is mapped to one of the optical transmitters and all other transmitters emit zero power on this particular frequency bin. As a result, the SSK encoder generates a specific set of allocated and unassigned sub-carriers for each transmitter. These N_t sub-carrier sets are separately processed by a conventional OFDM modulator implementing an IFFT. In order to generate real-valued time domain signals at the OFDM modulator output, Hermitian symmetry of the modulator input has to be applied (see Section 2.1.2). The OFDM modulators generate N_t intensity modulated time domain waveforms which contain the SSK modulated data bits. This method accomplishes several parallel SSK transmissions in the frequency domain. As each sub-carrier is allocated to only one optical transmitter, the N_t signals superimpose without ICI. At the receiver side, the superimposed signal is processed by an OFDM demodulator. The SSK modulated data bits are separately decoded for each sub-carrier using the conventional SSK decoding algorithm.

2.3 Optical wireless channel model

In [58], Kahn and Barry derive models to analytically calculate the channel coefficients of optical wireless links. The authors state that the DC channel gain is the most distinctive parameter describing an intensity modulated optical link. This is due to the fact that the

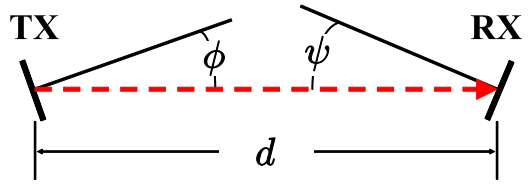

(a) LOS link.

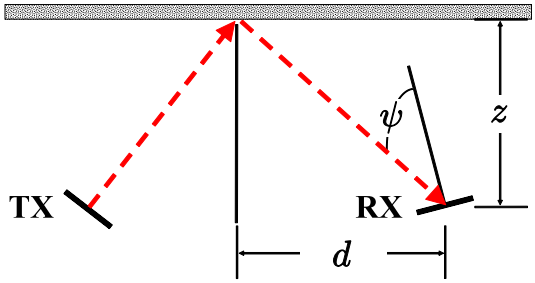

(b) Directed NLOS link.

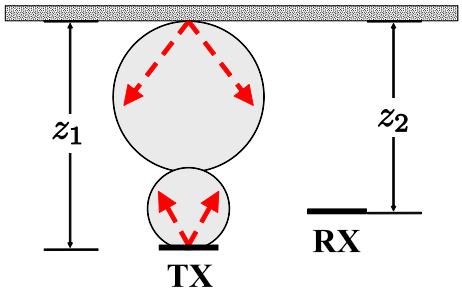

(c) Diffuse NLOS link.

Figure 2.13: *Geometric scenario used for calculation of channel coefficients.*

frequency response of the channel is flat near DC and due to the low-pass characteristic of the optical wireless channel because of DD. From this follows that the channel gain h affects the received optical power by inducing a specific path loss as given by (2.3). The optical path loss is given by $-10\log_{10} h$, whereas the electrical path loss is given by $-10\log_{10} h^2$. Kahn and Barry differentiate between three link models depending on the geometric constellation: LOS links, directed non-line-of-sight (NLOS) links and diffuse NLOS links.

Figure 2.13(a) illustrates a directed LOS link. As shown, ϕ is the angle of emergence with respect to the transmitter (TX) axis and ψ is the angle of incidence with respect to the receiver (RX) axis. Furthermore, d depicts the distance between transmitter and receiver. According

to [58], the channel coefficient of this LOS link can be calculated as follows:

$$h = \begin{cases} \frac{(k+1)\,A\,r}{2\,\pi\,d^2}\cos^k(\phi)\cos(\psi) & 0 \le \psi \le \Psi_{\frac{1}{2}} \\ 0 & \psi > \Psi_{\frac{1}{2}} \end{cases} \tag{2.23}$$

with the order $k = \frac{-\ln(2)}{\ln\left(\cos(\Phi_{\frac{1}{2}})\right)}$ and the transmitter semiangle $\Phi_{\frac{1}{2}}$ (at half power). The field-of-view (FOV) semiangle of the receiver is denoted by $\Psi_{\frac{1}{2}}$. The detector area of the receiver is represented by A and r is the detector responsivity, which is related to the optical wavelength. Clearly, the channel coefficient h depends on the specific position of the transmitter and the receiver. If a receiver and a transmitter are not in each others FOV, $h = 0$ holds.

Figure 2.13(b) illustrates a directed NLOS link. As shown, both transmitter and receiver are directed towards the ceiling. For this scenario, Kahn and Barry assume that the transmitter illuminates only a spot at the ceiling. The diameter of this spot is assumed to be smaller than the horizontal distance d between the spot and the receiver. The ceiling has a diffuse reflectivity $\Gamma \in [0;1]$ and is located at height z (relative to the position of the receiver). Using these geometries, the channel coefficient of a directed NLOS link can be calculated as follows:

$$h = \begin{cases} \frac{\Gamma\,A\,r\,z}{\pi(z^2+d^2)^{\frac{3}{2}}}\cos(\psi) & 0 \le \psi \le \Psi_{\frac{1}{2}} \\ 0 & \psi > \Psi_{\frac{1}{2}} \end{cases} \tag{2.24}$$

Finally, Kahn and Barry consider a diffuse NLOS link. Figure 2.13(c) illustrates the geometries used for calculating the channel coefficient of this link. As shown, both transmitter and receiver are oriented upwards to point straight up at the ceiling. For simplification, Kahn and Barry consider only the first order reflections on the ceiling. Moreover, they assume that the transmitter emits a Lambertian radiation pattern ($60°$ semiangle). In this scenario, the transmitter is located at position $x_1 = 0$ and $y_1 = 0$ on the x- and y-axis, whereas the receiver is located at position x_2 and y_2. The distance between the ceiling and the transmitter is z_1 and z_2 is the distance between the ceiling and the receiver. The optical power reflected from the ceiling is integrated at the receiver position resulting in:

$$h = \frac{\Gamma\,A\,r\,z_1^2\,z_2^2}{\pi^2}\int\limits_{\text{ceiling}}\int \frac{1}{\left(z_1^2+x^2+y^2\right)^2\left[z_2^2+(x-x_2)^2+(y-y_2)^2\right]^2}\,\mathrm{dx}\,\mathrm{dy}. \tag{2.25}$$

2.4 Optical wireless channel measurements

Figure 2.14 illustrates an optical wireless setup which is used for channel measurements. A basic MISO setup with $N_t = 2$ optical transmitters and one receiver ($N_r = 1$) is employed. The setup consists of two identical transmitters TX_1 and TX_2 which have a directed LOS connection towards the receiver. Both transmitters use the same optical transmission power. The spacing of the two transmitters is fixed to be 30 cm while their distance to the receiver d_1, respectively d_2, is varied. Both transmitters are oriented towards the receiver so that $\phi_1 = \phi_2 = 0^\circ$ holds. As TX_1 is directly placed on the receiver axis, $\psi_1 = 0^\circ$ holds. TX_2 has an angular misalignment ψ_2 with respect to the receiver axis. The practical parameters of the employed optical devices are as follows: at the transmitter side, off-the-shelf DL-6147-040 diodes [112] are used. These diodes have a transmitter semiangle of $\Phi_{\frac{1}{2}} \approx 8^\circ$ and a wavelength of 658 nm. The optical receiver consists of a circuitry applying a BPX 61 silicon PIN photo-diode [113]. This photo-diode has a responsivity (spectral sensitivity) of $r \approx 0.434$ at 658 nm, a detector area of $A \approx 7$ mm^2 and a FOV semiangle of $\Psi_{\frac{1}{2}} \approx 55^\circ$. The -3 dB cut-off frequency of the photo-diode is about 17 MHz.

Figure 2.15 shows the measured channel gains for two scenarios. The gains are plotted for a frequency range of $1 - 10$ MHz. For scenario 2.15(a), $d_1 = 50$ cm, $d_2 \approx 58$ cm and $\psi_2 \approx 31^\circ$. For scenario 2.15(b), $d_1 = 70$ cm, $d_2 \approx 76$ cm and $\psi_2 \approx 23^\circ$. The measurements show that the links are highly correlated and differ only by their absolute gain. This difference is caused by the larger distance and angular misalignment of TX_2. The different channel gains result in an imbalance of the received optical power between both links. In order to verify the high channel

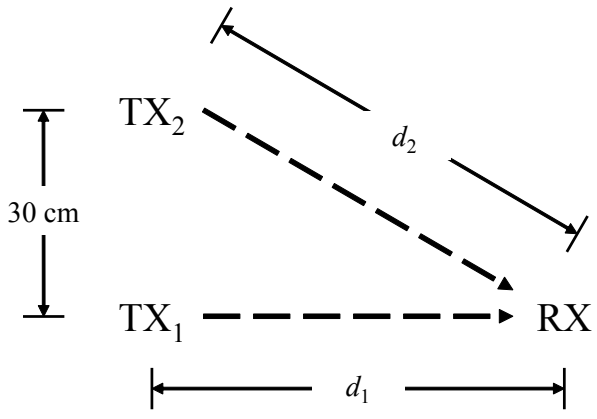

Figure 2.14: *Illustration of optical wireless channel measurement setup.*

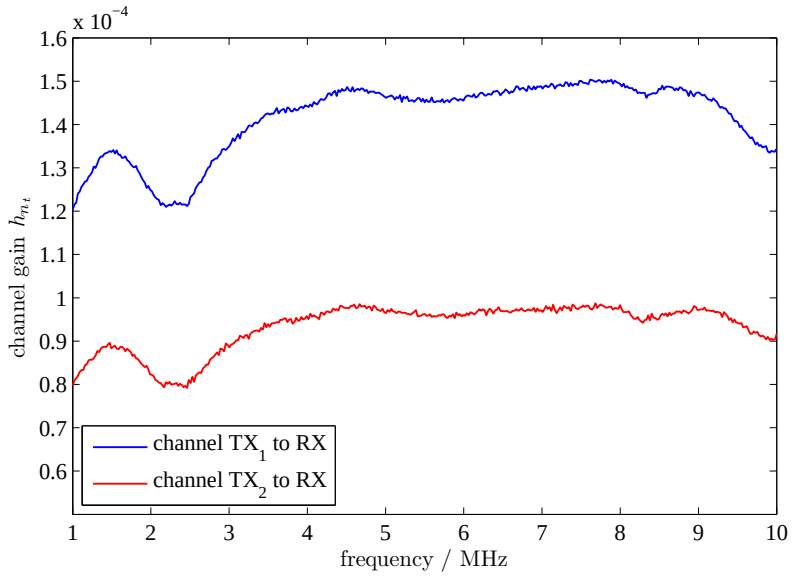

(a) Channel gains for $d_1 = 50$ cm and $d_2 \approx 58$ cm.

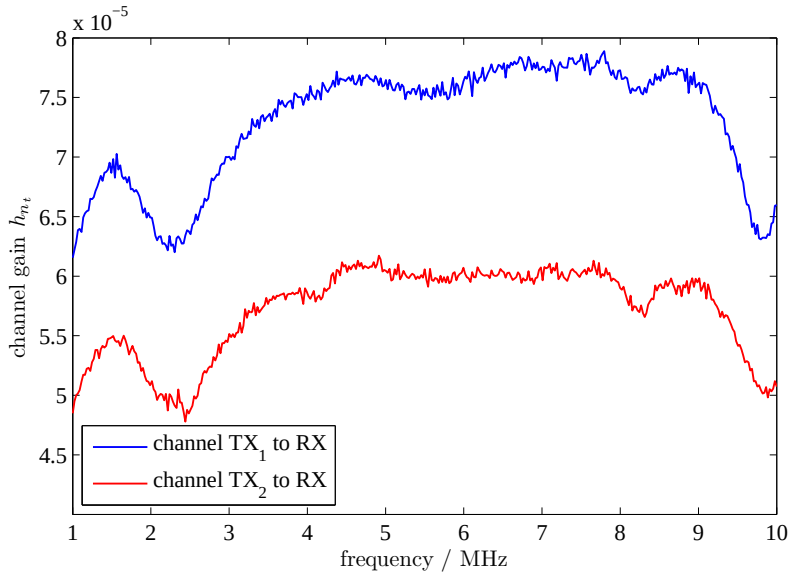

(b) Channel gains for $d_1 = 70$ cm and $d_2 \approx 76$ cm.

Figure 2.15: *Measured gains of the optical wireless channels obtained from measurement setup. The shape of the measured gains is affected by the frequency response of the diodes.*

	scenario 2.15(a)	**scenario 2.15(b)**
theoretical gain	$h_1 \approx 139.01\ 10^{-6}$ $h_2 \approx\ \ 87.65\ 10^{-6}$	$h_1 \approx 70.93\ 10^{-6}$ $h_2 \approx 55.07\ 10^{-6}$
measured gain	$\overline{h_1} \approx 141.59\ 10^{-6}$ $\overline{h_2} \approx\ \ 93.34\ 10^{-6}$	$\overline{h_1} \approx 73.05\ 10^{-6}$ $\overline{h_2} \approx 57.17\ 10^{-6}$
relative difference	$\Delta_1 \approx 1.86\,\%$ $\Delta_2 \approx 6.49\,\%$	$\Delta_1 \approx 2.99\,\%$ $\Delta_2 \approx 3.81\,\%$

Table 2.1: *Comparison of measured and theoretical channel gains.*

correlation, the time averaged correlation coefficient of the gains is calculated:

$$\zeta(h_1, h_2) = \frac{\mathrm{E}\left\{(h_1 - \mathrm{E}\left\{h_1\right\})(h_2 - \mathrm{E}\left\{h_2\right\})\right\}}{\sqrt{\mathrm{VAR}\left\{h_1\right\}\mathrm{VAR}\left\{h_2\right\}}} \approx 0.97, \tag{2.26}$$

where $\mathrm{E}\left\{\cdot\right\}$ denotes the expectation operator and $\mathrm{VAR}\left\{\cdot\right\}$ is the variance operator. Moreover, the measured optical channels show only little variations within the considered frequency range as their maximum coefficient of variation, $v_{n_t} = \sqrt{\mathrm{VAR}\left\{h_{n_t}\right\}} / \mathrm{E}\left\{h_{n_t}\right\}$, is only about 0.07. Therefore, the links can be represented by flat, non-frequency-selective AWGN channels with constant attenuation. Table 2.1 displays the mean measured channel gains $\overline{h_{n_t}}$ and the theoretical channel gains h_{n_t} for scenario 2.15(a) and 2.15(b). The theoretical gains are calculated using (2.23). Furthermore, the relative difference, $\Delta_{n_t} = \left|\overline{h_{n_t}} - h_{n_t}\right| / h_{n_t}$, between the measured gains and the theoretical gains is also given in Table 2.1. As the maximum difference is only about $6.49\,\%$, the measured channel gains and the calculated channel gains closely match. Therefore, the analytical channel model given in (2.23) is used in this thesis to derive the channel coefficients of different indoor OWC scenarios (see Chapter 3).

2.5 Summary

This chapter has given a brief review of optical wireless transmission techniques for indoor applications. The key concepts and models that will be considered within the remainder of this thesis have been introduced. Strengths and weaknesses of optical modulation techniques which employ IM and DD have been presented and discussed. To summarise, PAM provides larger spectral efficiency compared to OOK and PPM. However, these pulsed modulation techniques

are sensitive to multipath propagation due to ISI. Especially in diffuse propagation scenarios, the performance of pulsed modulation schemes is degraded. Multi-carrier techniques, such as OFDM, mitigate ISI by long symbol durations and the usage of guard intervals. However, these techniques are affected by the non-negativity constraint of the optical carrier. For instance, DCO-OFDM requires a high constant DC bias to make the bipolar OFDM waveform non-negative. This DC bias power affects the effective SNR of DCO-OFDM in contrast to unipolar PAM which operates without an additional DC bias. ACO-OFDM operates also without a DC bias, however at the expense of providing only half of the spectral efficiency of DCO-OFDM. In contrast to pulsed modulation techniques which enable low-complex and low-cost transceiver implementations, OFDM transmission requires sophisticated optical transceivers having good linearity characteristics and high dynamic ranges.

MIMO techniques provide high spectral efficiencies. Therefore, these techniques enable high data rates for indoor OWC. However, indoor optical wireless links are highly correlated as shown by the channel measurements presented in this chapter. Consequently, indoor scenarios represent challenging environments for MIMO techniques which commonly rely on uncorrelated links. Furthermore, the channel measurements substantiate the analytical channel model presented in Section 2.3. For this reason, this model is chosen in the following chapter to calculate the channel coefficients of indoor optical wireless links.

These highlighted aspects set the foundation for the work presented in the following chapters. Chapter 3 and Chapter 5 deal with optical MIMO techniques in order to provide high spectral efficiencies in indoor environments. Moreover in Chapter 3, the analytical error bounds of RC, SMP and SM derived above are substantiated by computer simulations. In Chapter 4, an optical wireless transmitter concept is presented which addresses the complexity issue of conventional optical transceiver designs entailed by OFDM transmission.

Chapter 3
Performance evaluation of MIMO techniques for optical wireless communications

In order to provide sufficient illumination, recent light fixtures are typically equipped with multiple light emitting diodes (LEDs). This property can readily be exploited to create optical multiple-input-multiple-output (MIMO) communication systems. Off-the-shelf incoherent-light-producing LEDs are characterised by achieving only a limited bandwidth of about $30 - 50$ MHz in the case of infra-red (IR) light and even less for visible light. Therefore, the available bandwidth of practical optical wireless communications (OWC) systems is restricted. Consequently, achieving high spectral efficiencies is of great concern for OWC systems. For free-space optical (FSO) transmission the effects of MIMO have already been studied. It has been shown that spatial diversity can combat the fading effects due to scattering and scintillation caused by atmospheric turbulence [79, 80]. However, for indoor OWC it is still not clear to what extent MIMO techniques can provide gains. This is because in indoor environments there are no fading effects, especially if line-of-sight (LOS) scenarios are considered. As a result, indoor optical wireless links are highly correlated. Provided that MIMO techniques mostly rely on spatially uncorrelated channels, it is unclear whether the optical propagation channel in indoor environments can offer sufficiently low channel correlation and adequate channel differentiability.

This chapter aims to evaluate the performance of MIMO techniques for OWC in an indoor environment with LOS characteristics. Three different transmission schemes are considered, namely repetition coding (RC), spatial multiplexing (SMP) and spatial modulation (SM). Throughout this chapter, pulse amplitude modulation (PAM) is considered for signal modulation due to its simple implementation and its high bandwidth efficiency.

Firstly, in Section 3.1, RC, SMP and SM are compared with regard to their computational complexity and their bit error ratio (BER) performance for different spectral efficiencies.

The error ratios are determined by numerical computer simulations as well as by analytical calculations using union bound approximations. Moreover, the effect of induced power imbalance between the multiple transmitters is studied. Link blockage is investigated as a means to enhance the performance of optical MIMO techniques. It is found that link blockage improves the channel characteristics by easing the differentiability of the links. The enhanced channel differentiability outweighs the loss in received energy, thus improving BER performance. Additionally, the performance of SM and RC is evaluated for varying numbers of optical transmitters and receivers.

Secondly, in Section 3.2, the performance of optical SM using colour LEDs is studied. To this end, the BER performance of SM is analysed i) for scenarios which use transmitters having the *same* optical wavelength and ii) for scenarios which use transmitters having *different* optical wavelengths. It is found that the utilisation of different optical wavelengths in combination with intensity modulation (IM) and direct detection (DD) enhances the differentiability of multiple optical channels.

Finally, based on the results of both preceding sections, Section 3.3 evaluates the performance of optical SM in combination with forward error correction (FEC). Specifically, an enhanced coded SM scheme is proposed. This scheme jointly encodes the bits conveyed in the spatial domain as well as in the signal domain. It is found that the jointly FEC coding achieves higher coding gains than the originally proposed Trellis coded spatial modulation (TCSM) scheme [101, 114] if applied to OWC.

3.1 Performance comparison of RC, SMP and SM

In this section, the performance of three different MIMO techniques applied to indoor OWC is compared, namely of RC, SMP and SM. The computational complexity of these schemes is determined and their BER performance is evaluated. Particularly, the analytical BER approximations of these schemes derived in Section 2.2 are verified by computer simulations. To this end, several LOS setups with different transmitter spacings and different positions of the receiver array are considered. In this context, the effect of both induced power imbalance and link blockage in investigated.

3.1.1 System model and setup scenario

In this chapter, an IM/DD based optical MIMO transmission system is considered. This MIMO system employs N_t optical transmitters (LEDs) and N_r receivers (photo-diodes). It is assumed that the multiple LEDs as well as the multiple photo-diodes are in close proximity. In addition, there is only a small path difference between the multiple transmitter-receiver links of some cm (as shown in Section 3.1.3). Consequently, the system model given in (2.11) is considered without time dispersion. Moreover, optical wireless links with LOS characteristics are assumed. Figure 3.1 illustrates the indoor setup scenario used for calculation of the channel coefficients. On the basis of this scenario, the channel coefficients of the optical wireless links are derived using (2.23). The channel measurements presented in Section 2.4 substantiate this optical wireless channel model. In this section, both the transmitter semiangle $\Phi_{\frac{1}{2}}$ (at half power) and the field-of-view (FOV) semiangle of the receiver are assumed to be $15°$. These semiangles have been chosen with regard to a practical LOS indoor OWC system which has been developed and implemented within the European Union (EU) project OMEGA [115, 116]. The detector area A of the receiver is assumed to be 1 cm^2 and the detector responsivity r is assumed to be 1. The angle of emergence with respect to the transmitter axis ϕ and the angle of incidence with respect to the receiver axis ψ as well as the distance d between transmitter and receiver are derived from the actual positions of the transmitters and receivers within the considered scenario.

In the following, a 4×4 indoor scenario ($N_r = 4$ and $N_t = 4$) is considered which is located within a $4.0\,\mathrm{m} \times 4.0\,\mathrm{m} \times 3.0\,\mathrm{m}$ room. It is assumed that the transmitters are placed

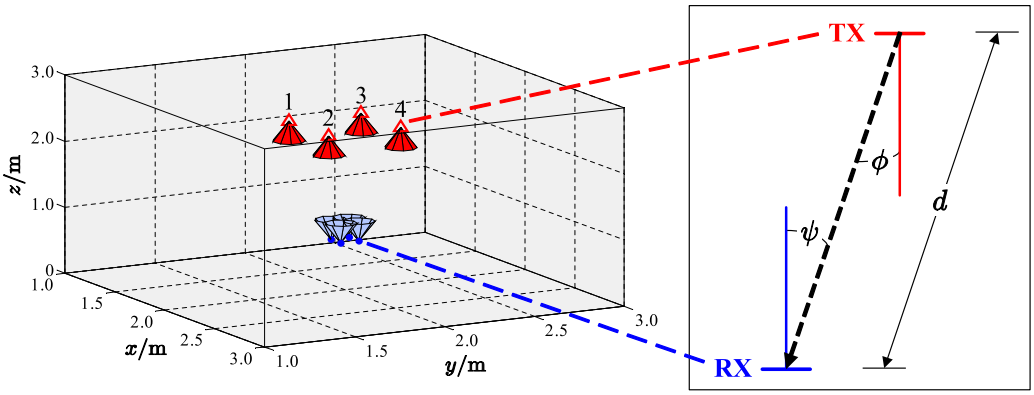

Figure 3.1: *Indoor setup scenario used for calculation of channel coefficients. Downwards pointing LEDs (transmitters) are placed at ceiling height of* 2.50 *m, and upwards pointing photo-diodes (receivers) are placed at table height of* 0.75 *m.*

at a height of $z = 2.50$ m and are oriented downwards to point straight down from the ceiling. The receivers are located at a height of $z = 0.75$ m (*e.g.* height of a table) and are oriented upwards to point straight up at the ceiling. Both transmitters and receivers are aligned in a square 2×2 array which is centred in the middle of the room. On the basis of this scenario, different static setups are investigated which have varying spacings of the single transmitters on the x- and y-axis, depicted by d_{TX}. The spacing of the receivers is assumed to be 0.1 m on the x- and y-axis for all considered setups. This receiver spacing would enable the integration of the receiver array into typical laptop computers. Figure 3.1 shows the positioning of the 4×4 setup. The receivers are displayed as dots and the transmitters as triangles. The plotted cones represent the orientation of the transmit beams and the orientation of the FOVs of the receivers, respectively. The cone angles are related to the semiangles of the transmitting LEDs and the receiving photo-diodes.

3.1.2 Computational complexity

For means of comparison, it is assumed in the following that all considered MIMO techniques use maximum-likelihood (ML) detection at the receiver side with perfect knowledge of the channel and ideal time synchronisation. Therefore, the decoder decides for the signal vector $\widehat{\mathbf{s}}$ which minimises the Euclidean distance between the actual received signal vector $\mathbf{y}$ and all potential received signals leading to

$$\widehat{\mathbf{s}} = \underset{\mathbf{s}}{\operatorname{argmax}}\, p_{\mathbf{y}}(\mathbf{y}|\mathbf{s},\mathbf{H}) = \underset{\mathbf{s}}{\operatorname{argmin}}\, \|\mathbf{y} - \mathbf{H}\,\mathbf{s}\|_{\mathrm{F}}^{2}\,, \tag{3.1}$$

where $p_{\mathbf{y}}$ is the probability density function of $\mathbf{y}$ conditioned on $\mathbf{s}$ and $\mathbf{H}$ with $p_{\mathbf{y}}(\mathbf{y}|\mathbf{s},\mathbf{H}) \propto \exp\left(-\|\mathbf{y} - \mathbf{H}\,\mathbf{s}\|_{\mathrm{F}}^{2}/\sigma^{2}\right)$. The symbol $\propto$ represents proportionality.

On the basis of this detection algorithm, the computational complexity of the considered optical MIMO techniques is analysed. The computational complexity is defined as the total number of mathematical operations, *i.e.* multiplications, additions and subtractions, that are required for ML detection. The numbers are listed in Table 3.1. It can be seen that RC and SMP need the same number of operations to provide equal spectral efficiency R, whereas the detection of SM is less computationally expensive. This is due to the fact that SM avoids inter-channel interference (ICI) as only one transmitter is active at any symbol duration in contrast to SMP. Moreover, as SM conveys additional bits in the spatial domain, it can achieve the same spectral efficiency as RC but with a reduced signal constellation size. Thus for SM, there are less signal

MIMO technique	**Spectral efficiency R in bit/s/Hz**	**Number of mathematical operations at receiver**
RC	$\log_2(M)$	$2^R\,(2\,N_t\,N_r + N_r - 1)$ $= M\,(2\,N_t\,N_r + N_r - 1)$
SMP	$N_t\ \log_2(M)$	$2^R\,(2\,N_t\,N_r + N_r - 1)$ $= M^{N_t}\,(2\,N_t\,N_r + N_r - 1)$
SM	$\log_2(M N_t)$	$2^R\,(3\,N_r - 1)$ $= M N_t\,(3\,N_r - 1)$

Table 3.1: *Comparison of spectral efficiency and computational complexity at receiver of different optical MIMO techniques.*

constellation points to be considered when performing the ML detection. For instance, if a setup with $N_t = 4$ and $N_r = 4$ is assumed which provides a spectral efficiency of $R = 4$ bit/s/Hz, RC and SMP both require 560 operations, whereas SM requires only 176 operations. Figure 3.2 displays the computational complexity of RC, SMP and SM for different setups and spectral efficiencies. Consequently, as SM requires a much lower computational complexity compared to the other MIMO techniques, it enables the implementation of efficient and simple optical MIMO receivers.

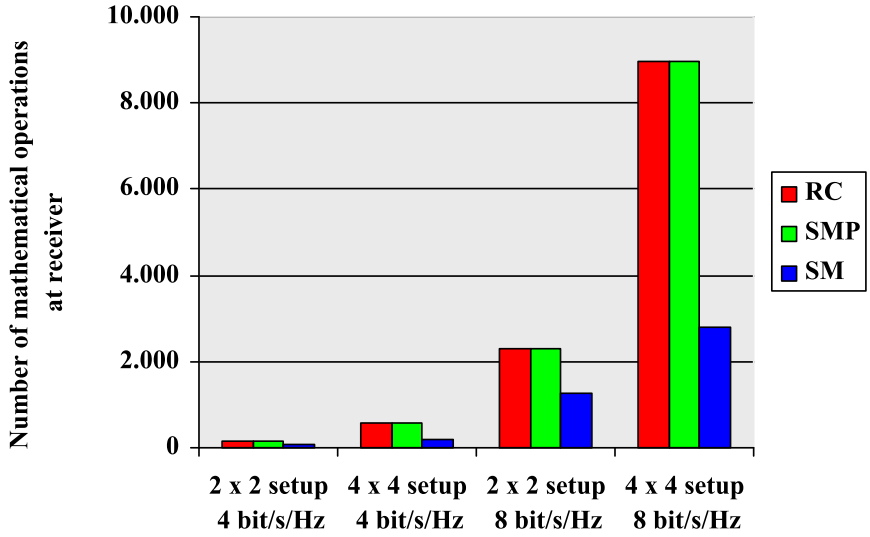

Figure 3.2: *Computational complexity at receiver of RC, SMP and SM for different setups and spectral efficiencies.*

3.1.3 Results on bit error ratio performance

In the following, the BER performance of RC, SMP and SM is analysed by considering several setup scenarios which are based on the model presented in Section 3.1.1. In order to ensure comparability, the mean emitted optical power is the same for each scenario as well as for all MIMO techniques. The error ratios at the receiver side are evaluated with regard to *transmit* energy against power spectral density of the additive white Gaussian noise (AWGN). Hence, the specific path loss of each setup caused by the particular distance and angular alignment of the single transmitters and receivers is taken into account. Consequently, the signal-to-noise ratio (SNR) is defined as $\frac{E_s}{N_0}$. This is because considering received energy to noise energy would disregard the individual path loss of the different setups, thus disallowing a fair performance comparison. The AWGN is independent of the transmitted signals and has zero mean.

The 4×4 setup with transmitter spacings on the x- and y-axis of $d_{\mathrm{TX}} = 0.2, 0.4$ and 0.6 m is considered. Applying (2.23) to these scenarios gives the following channel matrices (without noise):

$$\begin{aligned}
\mathbf{H}_{d_{\mathrm{TX}}=0.2} &\approx 10^{-4} \begin{pmatrix} 1.0708 & 0.9937 & 0.9937 & 0.9226 \\ 0.9937 & 1.0708 & 0.9226 & 0.9937 \\ 0.9937 & 0.9226 & 1.0708 & 0.9937 \\ 0.9226 & 0.9937 & 0.9937 & 1.0708 \end{pmatrix}, \\
\mathbf{H}_{d_{\mathrm{TX}}=0.4} &\approx 10^{-4} \begin{pmatrix} 0.9226 & 0.7964 & 0.7964 & 0.6888 \\ 0.7964 & 0.9226 & 0.6888 & 0.7964 \\ 0.7964 & 0.6888 & 0.9226 & 0.7964 \\ 0.6888 & 0.7964 & 0.7964 & 0.9226 \end{pmatrix}, \\
\mathbf{H}_{d_{\mathrm{TX}}=0.6} &\approx 10^{-4} \begin{pmatrix} 0.6888 & 0.5559 & 0.5559 & 0.0000 \\ 0.5559 & 0.6888 & 0.0000 & 0.5559 \\ 0.5559 & 0.0000 & 0.6888 & 0.5559 \\ 0.0000 & 0.5559 & 0.5559 & 0.6888 \end{pmatrix}.
\end{aligned} \tag{3.2}$$

The symmetrical arrangement of the transmitters and receivers leads to equal channel gains for links having the same geometrical alignment. Note that due to the high precision of the simulation software (MATLAB represents floating-point numbers in 64 bit double-precision [117]), these gains are identical. However, in an actual application scenario, there will be larger differences between the gains due to device and implementation imperfections. Therefore, the considered simulation scenario constitutes a worst case scenario

with regard to channel differentiability. As shown in (3.2), if the spacing between the transmitters is small, the gains are quite similar, whereas if d_{TX} gets larger, the differences between the links increase. If $d_{\mathrm{TX}} = 0.6$ m, some transmitters and receivers are not in each others FOV resulting in $h_{n_r n_t} = 0$. As the channel coefficients are in the region of 10^{-4}, the electrical path loss at the receiver side is about -80 dB. Because the SNR is defined as the ratio of *transmitted* signal energy to noise energy, the BER curves displayed in the following figures have an approximate SNR offset of about 80 dB with respect to the *received* energy to noise ratio. Therefore, in the following, a normalised SNR is considered given by $\frac{E_s}{N_0} - 80\,\mathrm{dB}$. Furthermore, if the diffuse transmission portion induced by first order reflections on the surfaces (walls) is considered, the reflected optical intensity impinging on the receivers is in the range of $10^{-10}\,I$ (assuming ideal conditions such as Lambertian reflectors and a reflectivity of $\Gamma = 1$). This results in an electrical path loss which is about $110 - 120$ dB larger than the path loss of the LOS transmission. As the path loss of higher order reflections is even larger, reflections can be neglected in the following and only the LOS gains given in (3.2) are considered without any diffuse transmission portions. However, additional multipath reflections would enhance the differentiability of the MIMO channels and would reduce channel correlation. Hence, as there are no reflections, the considered LOS scenario is subject to highly correlated links and constitutes a worst case scenario with regard to channel correlation.

Enlarging d_{TX} increases the path loss. Therefore, the impairment in received energy can be denoted for different transmitter spacings:

$$\Delta^{E_{\mathrm{RX}}}_{d_{\mathrm{TX}}=x} = 10\,\log_{10}\left(\frac{E_{\mathrm{RX}_{d_{\mathrm{TX}}=x}}}{E_{\mathrm{RX}_{d_{\mathrm{TX}}=0.2}}}\right), \tag{3.3}$$

where $E_{\mathrm{RX}_{d_{\mathrm{TX}}=x}}$ denotes the received electrical energy for $d_{\mathrm{TX}} = x$ m. The impairment is related to the $d_{\mathrm{TX}} = 0.2$ m setup which provides the lowest path loss yielding to

$$\begin{aligned} \Delta^{E_{\mathrm{RX}}}_{d_{\mathrm{TX}}=0.2} &= \quad 0.00\,\mathrm{dB}, \\ \Delta^{E_{\mathrm{RX}}}_{d_{\mathrm{TX}}=0.4} &\approx -1.88\,\mathrm{dB}, \\ \Delta^{E_{\mathrm{RX}}}_{d_{\mathrm{TX}}=0.6} &\approx -6.89\,\mathrm{dB}. \end{aligned} \tag{3.4}$$

The maximum difference in path length of the multiple transmitter-receiver links is about 33.30 mm. This difference results in a maximum delay variation of 111.06 ps. A delay

variation of several ps only has an effect for switching speeds in the region of several GHz. As off-the-shelf LEDs are considered which provide a bandwidth of about $30 - 50$ MHz, this delay variation can be neglected and ideal synchronisation of all links is assumed without time dispersion.

Figure 3.3(a) shows the BER performance of RC, SMP and SM for the three setup scenarios for a spectral efficiency of $R = 4$ bit/s/Hz. For $d_{\mathrm{TX}} = 0.2$ m and 0.4 m, RC gives the best performance, whereas SMP performs worst with a low slope of the BER curve within the depicted SNR range. This is due to the fact that for both scenarios the channel gains are quite similar providing low channel differentiability. Although the performance of SM also depends on the differences between the links, SM is more robust to these channel conditions. SM provides a lower error ratio and a steeper slope of the BER curve compared to SMP. If $d_{\mathrm{TX}} = 0.6$ m, SMP and SM outperform RC at a BER of 10^{-5} by about 10 dB, respectively by 9 dB. RC performs about 7 dB worse compared to the $d_{\mathrm{TX}} = 0.2\,\mathrm{m}$ case because of less received energy as $\Delta^{E_{\mathrm{RX}}}_{d_{\mathrm{TX}}=0.6} \approx -6.89$ dB. Despite this larger path loss for $d_{\mathrm{TX}} = 0.6$ m, SMP and SM even outperform RC for the two other scenarios, which provide a lower path loss. SMP outperforms SM by about 1 dB for high SNRs. Because of its multiplexing gain, SMP can operate with a reduced signal constellation size of $M = 2$ as opposed to SM which has to operate with $M = 4$ to provide the same data rate. But at low SNR regions, SM provides the best BER performance. This implies that SM profits from conveying information in the spatial domain especially at low SNRs. Whereas at high SNR regions, SM suffers from the fact that it has to use a larger signal constellation size to provide the same spectral efficiency as SMP. Accordingly, SMP requires a high SNR to separate the single signal streams at the receiver side and to benefit from its multiplexing gain. Moreover, the theoretical lower and upper error bounds (shown by markers) given in (2.13), (2.17) and (2.20) closely match the simulation results (shown by lines). As a result, the error bounds provide an accurate approximation of the BERs at high SNRs.

Figure 3.3(b) shows the BER performance of the three schemes for the same setup scenarios but with an enhanced spectral efficiency of $R = 8$ bit/s/Hz. RC requires an SNR increase of about 24 dB to achieve the same BER of 10^{-5} compared to the $R = 4$ bit/s/Hz case. For $d_{\mathrm{TX}} = 0.2$ m and $d_{\mathrm{TX}} = 0.4$ m, SMP still performs worst. However, SM outperforms RC up to an SNR of about 50 dB for $d_{\mathrm{TX}} = 0.2$ m, respectively 54 dB for $d_{\mathrm{TX}} = 0.4$ m. If $d_{\mathrm{TX}} = 0.6$ m, SMP provides the best performance as it achieves an SNR benefit of about 25 dB compared to RC

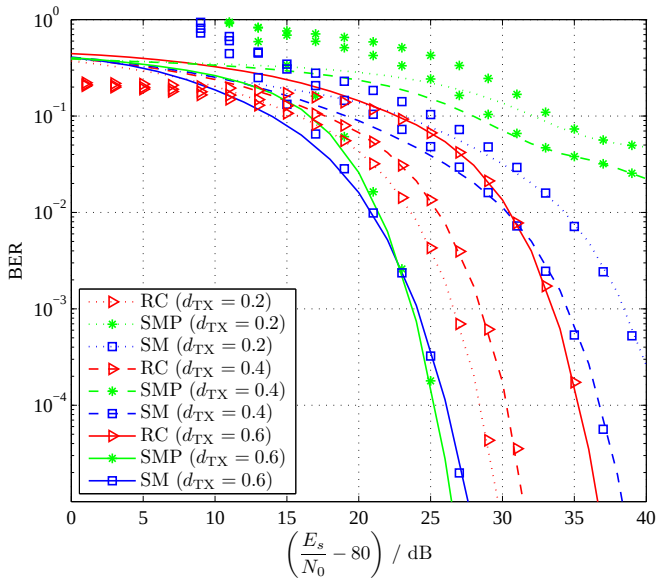

(a) $R = 4$ bit/s/Hz.

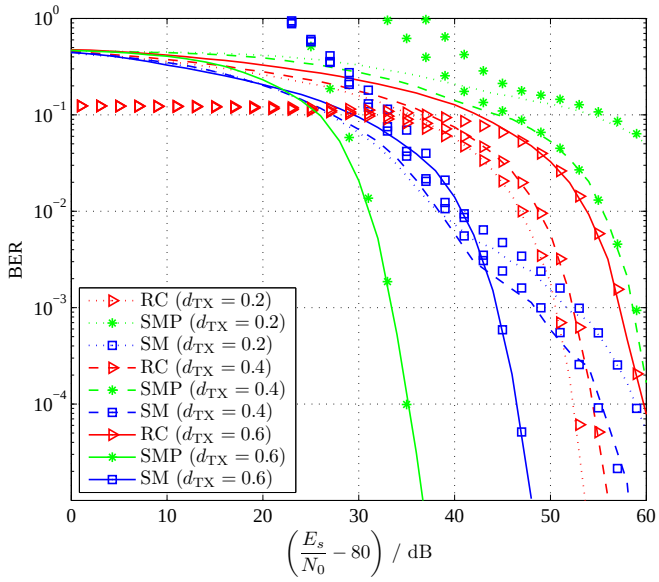

(b) $R = 8$ bit/s/Hz.

Figure 3.3: *Comparison of RC, SMP and SM for spectral efficiency of $R = 4$ and $R = 8$ bit/s/Hz in 4×4 setup scenario with varying distance d_{TX} of transmitters on the x- and y-axis (lines show simulation results and markers analytical error bounds).*

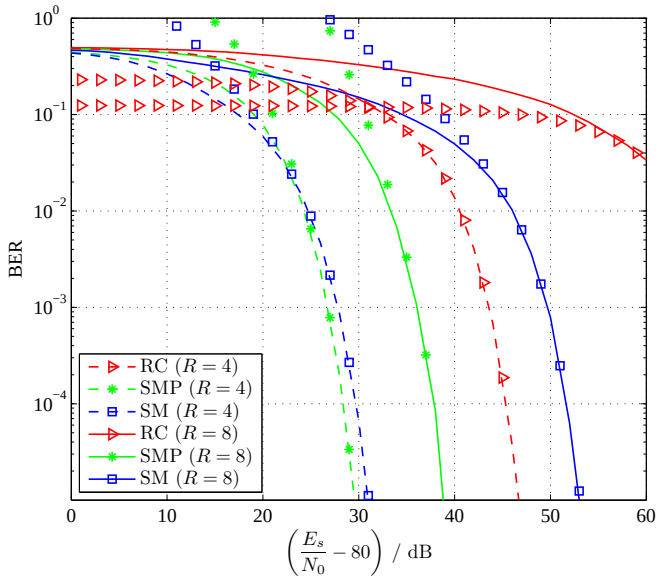

Figure 3.4: *Comparison of RC, SMP and SM for spectral efficiency of $R = 4$ and $R = 8$ bit/s/Hz in 4×4 setup scenario with $d_{\mathrm{TX}} = 0.7$ m (lines show simulation results and markers analytical error bounds).*

and of about 12 dB compared to SM. Hence, due to its multiplexing gain, SMP requires an SNR improvement of only 10 dB to provide the same BER performance when doubling the spectral efficiency from 4 to 8 bit/s/Hz, whereas SM needs additional 21 dB.

Assuming $d_{\mathrm{TX}} = 0.7\,\mathrm{m}$ results in

$$\mathbf{H}_{d_{\mathrm{TX}}=0.7} \approx 10^{-4} \begin{pmatrix} 0.5658 & 0 & 0 & 0 \\ 0 & 0.5658 & 0 & 0 \\ 0 & 0 & 0.5658 & 0 \\ 0 & 0 & 0 & 0.5658 \end{pmatrix}, \tag{3.5}$$

which corresponds to an aligned system where only one transmitter and one receiver are in each others FOV. This leads to a direct alignment with four completely independent links. Figure 3.4 displays the BER results for a spectral efficiency of $R = 4$ and $R = 8$ bit/s/Hz for this scenario. In comparison to the $d_{\mathrm{TX}} = 0.6$ m scenario, all MIMO schemes perform worse because there is less energy received. This is due to the missing cross-connects between transmitter n_t and receiver n_r for $n_t \neq n_r$ leading to $\Delta^{E_{\mathrm{RX}}}_{d_{\mathrm{TX}}=0.7} \approx -16.95$ dB. Whereas SM and SMP undergo a minor performance decrease of only about 3 dB, the performance of RC is degraded by about 10 dB. Consequently, RC suffers much more from the direct alignment, whereas SMP and

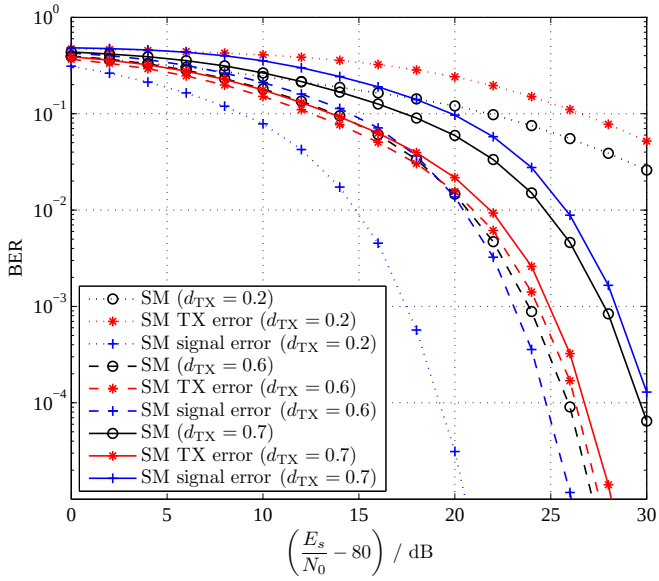

Figure 3.5: *BER of SM segmented into bit errors caused by transmitter misdetection and signal misdetection for spectral efficiency of* 4 *bit/s/Hz in* 4×4 *setup scenario with varying distance* d_{TX} *of transmitters on the* x*- and* y*-axis.*

SM can compensate for the less received energy by improved channel differentiability. For $R = 4$ bit/s/Hz, SM again outperforms SMP at low SNR regions. At higher SNRs, SMP outperforms SM due to its larger multiplexing gain. This issue is even more evident for the $R = 8$ bit/s/Hz case, where SMP achieves major performance gains as it provides this spectral efficiency with $M = 4$ compared to SM which has to operate with a signal constellation size of $M = 64$.

In the following, it is evaluated why SM achieves performance gains especially in the low SNR region. Therefore, the BER of SM is segmented into errors arising from transmitter misdetection and from signal misdetection. If $R = 4$ bit/s/Hz, SM conveys the same number of bits in the spatial domain and in the signal domain. Figure 3.5 shows that for $d_{\mathrm{TX}} = 0.2$ m, the errors caused by inaccurate detection of the transmitter mainly affect the BER, whereas the mere signal detection provides much lower error ratios. If $d_{\mathrm{TX}} = 0.6$ m, the transmitter detection provides a lower error ratio up to an SNR of about 19 dB, thus improving the overall BER of SM. At higher SNRs the signal detection can be performed more reliably and the errors caused by an erroneous detection of the transmitter get decisive again. In the aligned system ($d_{\mathrm{TX}} = 0.7$ m), the signal misdetection is the dominating source of errors due to less energy received. In contrast, the detection of the active transmitter can be performed more reliably because the direct alignment provides the best channel differentiability. Therefore,

the inherent nature of SM, which is conveying information in the spatial domain, can be exploited most distinctively by direct alignment of the optical transmitters and receivers. Thus, despite less energy received, independent links enable the most reliable detection of the active transmitter. Summing up, these results highlight the impact of the trade-off between SNR and differentiability of the multiple links. The performance of the optical MIMO techniques depends on both parameters. Consequently, both SNR and channel differentiability have to be considered to achieve good error performance.

3.1.3.1 Varying position of receiver array

In the following, the situation is considered when the position of the receiver array is varied. To this end, x_{RX} and y_{RX} are defined as the position offsets of the receiver array on the x- and y-axis relative to the centre of the room. These offsets increase both the distance and the misalignment between the transmitter array and the receivers. In order to still be able to detect the TX beams, a larger FOV semiangle of the receivers of $\Psi_{\frac{1}{2}} = 45^\circ$ is assumed. The considered position offsets are: $x_{\mathrm{RX}} = 0.5$ m, $y_{\mathrm{RX}} = 0$ m; $x_{\mathrm{RX}} = 0.25$ m, $y_{\mathrm{RX}} = 0.75$ m and $x_{\mathrm{RX}} = 0.5$ m, $y_{\mathrm{RX}} = 1.0$ m. Applying (2.23) to these scenarios results in the following channel matrices:

$$\begin{aligned}
\mathbf{H}_{x_{\mathrm{RX}}=0.5,\, y_{\mathrm{RX}}=0} &\approx 10^{-4} \begin{pmatrix} 0.2293 & 0.2013 & 0.1462 & 0.1290 \\ 0.2013 & 0.2293 & 0.1290 & 0.1462 \\ 0.7964 & 0.6888 & 0.6410 & 0.5559 \\ 0.6888 & 0.7964 & 0.5559 & 0.6410 \end{pmatrix}, \\
\mathbf{H}_{x_{\mathrm{RX}}=0.25,\, y_{\mathrm{RX}}=0.75} &\approx 10^{-4} \begin{pmatrix} 0.0461 & 0.0272 & 0.0358 & 0.0213 \\ 0.2573 & 0.1798 & 0.1917 & 0.1352 \\ 0.0735 & 0.0424 & 0.0713 & 0.0412 \\ 0.4426 & 0.3040 & 0.4275 & 0.2940 \end{pmatrix}, \\
\mathbf{H}_{x_{\mathrm{RX}}=0.5,\, y_{\mathrm{RX}}=1.0} &\approx 10^{-4} \begin{pmatrix} 0.0061 & 0.0035 & 0.0044 & 0.0025 \\ 0.0442 & 0.0283 & 0.0299 & 0.0194 \\ 0.0150 & 0.0082 & 0.0128 & 0.0071 \\ 0.1290 & 0.0792 & 0.1071 & 0.0663 \end{pmatrix}.
\end{aligned} \tag{3.6}$$

Figure 3.6 shows the BER of RC, SMP and SM for a spectral efficiency of 8 bit/s/Hz in the

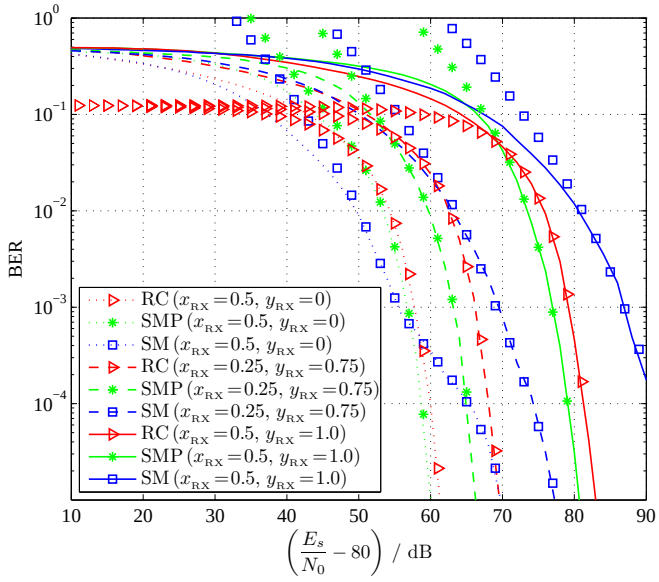

Figure 3.6: *Comparison of RC, SMP and SM for spectral efficiency of* 8 *bit/s/Hz in* 4×4 *setup scenario with* $d_{\mathrm{TX}} = 0.4$ *m and varying position offsets of receiver array on the* x*- and* y*-axis (lines show simulation results and markers analytical error bounds).*

4×4 setup scenario with $d_{\mathrm{TX}} = 0.4\,\mathrm{m}$ using these position offsets. The increased distance between the transmitters and the receivers leads to a larger path loss and an increased $\frac{E_s}{N_0}$ offset compared to the scenario with $x_{\mathrm{RX}} = y_{\mathrm{RX}} = 0\,\mathrm{m}$. However, the larger distance also increases the differences between the channels. This improves the performance of SMP. While SMP performs worst when the x-axis and y-axis offsets are zero (due to channel similarities), it performs better than RC and SM when position offsets are applied. This is because of favourable channel conditions and the fact that the spatial multiplexing gain of SMP grows linearly with the number of transmitters. In contrast, the spatial multiplexing gain grows only logarithmically in the case of SM, and there is no spatial multiplexing gain in the case of RC.

3.1.3.2 Power imbalance between transmitters

In the following, the effect of induced power imbalance between the multiple transmitters is analysed. This means that the transmission power is not uniformly distributed across all N_t transmitters but imbalanced. The optical power imbalance factor in dB is defined as δ and $\alpha = 10^{\frac{\delta}{10}}$ is the imbalance factor on a linear scale. Therefore, α denotes the optical power surplus factor assigned to one transmitter in comparison to another one. Note that the mean optical power emitted by all transmitters, I, is still the same as before. Consequently, the

total transmission power is not increased by driving individual LEDs in the array with different powers. Moreover, the power distribution is done without any channel state information (CSI) at the transmitter side.

The induced power imbalance factors for each transmitter can be calculated by

$$\begin{aligned} \gamma_1 &= \frac{N_t}{\sum_{i=0}^{N_t-1} \alpha^i}, \\ \gamma_{j+1} &= \alpha\,\gamma_j \quad \text{for} \quad j = 1, 2, \ldots (N_t - 1). \end{aligned} \tag{3.7}$$

For instance, assuming $\delta = 3$ dB and $N_t = 4$ results in $\gamma_1 \approx \frac{4}{15}$, $\gamma_2 \approx \frac{8}{15}$, $\gamma_3 \approx \frac{16}{15}$ and $\gamma_4 \approx \frac{32}{15}$. Using these factors, the optical transmission power assigned to emitter n_t applying RC or SMP is $\tilde{I}_{n_t} = \frac{I}{N_t}\,\gamma_{n_t}$ and for SM it is $\tilde{I}_{n_t} = I\,\gamma_{n_t}$. Note that the signal modulation technique is still PAM according to (2.8) and (2.18), whereas now $\tilde{I}_{n_t}$ is the mean optical power used for modulation by transmitter n_t.

Figure 3.7 depicts the BER of RC, SMP and SM for a spectral efficiency of 4 bit/s/Hz in the 4×4 setup scenario with $d_{\mathrm{TX}} = 0.2$ m and $d_{\mathrm{TX}} = 0.6$ m for varying power imbalances. As shown, adding an imbalance to the transmission powers can enhance the performance of both SMP and SM, whereas it has no influence on RC. By imbalancing the power, the differentiability of the single links is improved making them more distinguishable at the receiver side. The receiver does not need any knowledge about the induced power imbalance because it implicitly gets this information by channel estimation which it needs to perform in any case. Therefore to the receiver, the power imbalance appears to be due to the actual channel propagation. Consequently, imbalancing transmit powers does not increase the receiver's detection complexity. The performance of RC is not related to link differences but only to the absolute channel gains. Therefore, power imbalance has no effect on the performance of RC given the symmetrical arrangement of the channel gains denoted in (3.2). The results for the $d_{\mathrm{TX}} = 0.2$ m scenario shown in Figure 3.7(a) indicate that a power imbalance of about $\delta = 1$ dB results in the best BER performance for SM, whereas for SMP $\delta = 3$ dB gives the lowest BER. More pronounced power imbalances lead to worse error ratios. While the differentiability of the links may be enhanced, the transmission power for some of the links is largely decreased in this case. This leads to a low SNR on these links, and consequently to a worse BER performance. Therefore, a compromise between channel differentiability and appropriate signal detection is required. This is also the reason why SMP can operate

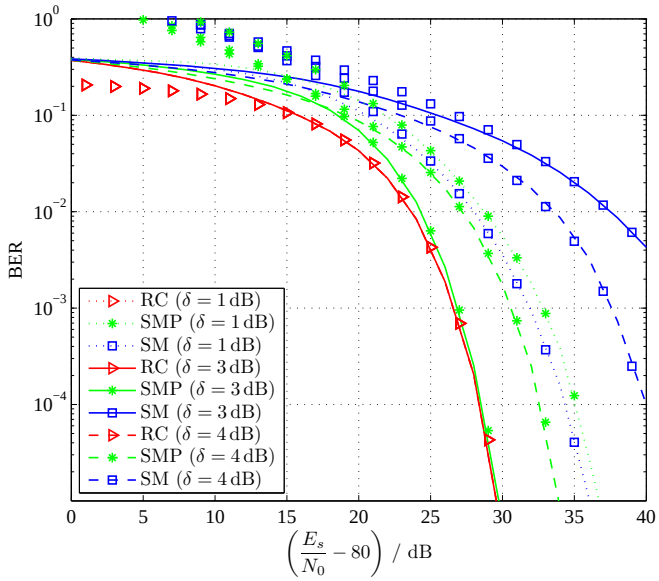

(a) $d_{\mathrm{TX}} = 0.2$ m.

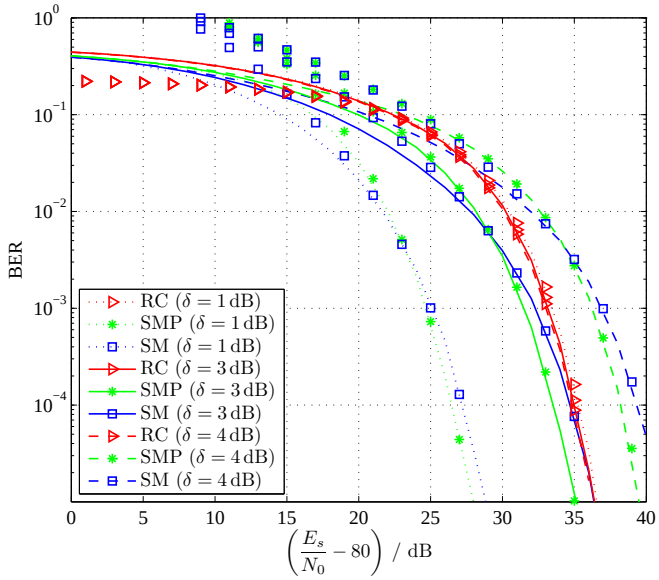

(b) $d_{\mathrm{TX}} = 0.6$ m.

Figure 3.7: *Comparison of RC, SMP and SM for spectral efficiency of* 4 *bit/s/Hz in* 4×4 *setup scenario for varying power imbalances* δ *(lines show simulation results and markers analytical error bounds).*

with higher power imbalances compared to SM. SM has to operate with a larger signal constellation size to provide the same data rate, thus making it more susceptible to low SNRs. Consequently, SMP can profit to a larger extent by power imbalancing and is able to achieve the same performance as RC. Note that the channel conditions without power imbalancing caused SMP to perform significantly worse than RC and SM in this scenario (see Figure 3.3(a)). For $d_{\mathrm{TX}} = 0.6$ m, power imbalance has a negative effect on SMP and SM as their performance decreases with rising δ as shown in Figure 3.7(b). Therefore, no further benefits can be achieved and $\delta = 0$ dB gives the best performance for both SMP and SM. The optimal power imbalance factors for each specific scenario can be calculated using the BER equations given in (2.17) and (2.20). However, this calculation requires CSI at the transmitter and consequently a dedicated feedback channel which increases system complexity.

3.1.3.3 Link blockage

In the following, the $d_{\mathrm{TX}} = 0.2$ m and 0.4 m setups with an induced link blockage between some transmitters and receivers are considered. This can be achieved by installing opaque boundaries in the receiver device or by smaller FOVs of the optical receivers. The channel coefficients are assumed as given in (3.2) and the same links of the 4×4 setup are blocked as in the $d_{\mathrm{TX}} = 0.6$ m scenario: the links between TX_1 and RX_4; TX_2 and RX_3; TX_3 and RX_2; TX_4 and RX_1. This results in the following channel matrices for the two setups with induced link blockage:

$$\widehat{\mathbf{H}}_{d_{\mathrm{TX}}=0.2} \approx 10^{-4} \begin{pmatrix} 1.0708 & 0.9937 & 0.9937 & 0.0000 \\ 0.9937 & 1.0708 & 0.0000 & 0.9937 \\ 0.9937 & 0.0000 & 1.0708 & 0.9937 \\ 0.0000 & 0.9937 & 0.9937 & 1.0708 \end{pmatrix} \tag{3.8}$$

resulting in $\widehat{\Delta}^{E_{\mathrm{RX}}}_{d_{\mathrm{TX}}=0.2} \approx -2.29\,\mathrm{dB}$ and

$$\widehat{\mathbf{H}}_{d_{\mathrm{TX}}=0.4} \approx 10^{-4} \begin{pmatrix} 0.9226 & 0.7964 & 0.7964 & 0.0000 \\ 0.7964 & 0.9226 & 0.0000 & 0.7964 \\ 0.7964 & 0.0000 & 0.9226 & 0.7964 \\ 0.0000 & 0.7964 & 0.7964 & 0.9226 \end{pmatrix} \tag{3.9}$$

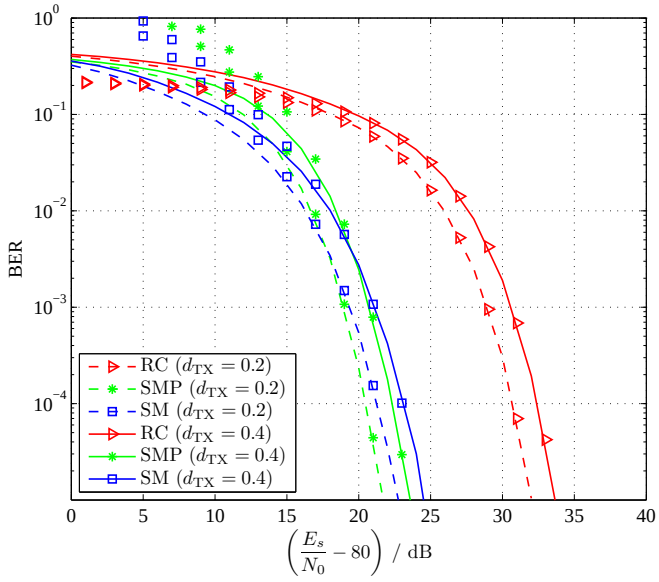

Figure 3.8: *Comparison of RC, SMP and SM for spectral efficiency of* 4 *bit/s/Hz in* 4×4 *setup scenario with* $d_{\mathrm{TX}} = 0.2$ *m and* 0.4 *m with induced link blockage (lines show simulation results and markers analytical error bounds).*

resulting in $\widehat{\Delta}^{E_{\mathrm{RX}}}_{d_{\mathrm{TX}}=0.4} \approx -3.99\,\mathrm{dB}$.

Figure 3.8 depicts the BER of RC, SMP and SM for a spectral efficiency of 4 bit/s/Hz in these two setups. Relative to the results without link blockage (see Figure 3.3(a)), RC performs about 2 dB worse. This is because the induced link blockage leads to a lower SNR at the receiver. However, the performance of SM and SMP is significantly enhanced. Although there is less energy received, both MIMO schemes profit from the enhanced channel differentiability. Especially SMP, which performs worst without link blockage, benefits from the improved channel differentiability and provides the lowest error ratio in this scenario. The $d_{\mathrm{TX}} = 0.2$ m setup with induced link blockage provides the best compromise between channel differentiability and received energy. As shown, both SM and SMP perform about 2 dB better compared to the setup with $d_{\mathrm{TX}} = 0.4$ m and induced link blockage. Relative to the $d_{\mathrm{TX}} = 0.6$ m setup (see Figure 3.3(a)), SM and SMP achieve an even larger SNR performance gain of about 5 dB.

3.1.3.4 Comparison of RC and SM for varying numbers of transmitters and receivers

In the following, the BER performance of RC and SM is evaluated for varying numbers of optical transmitters and receivers. Due to its high computational complexity for large numbers

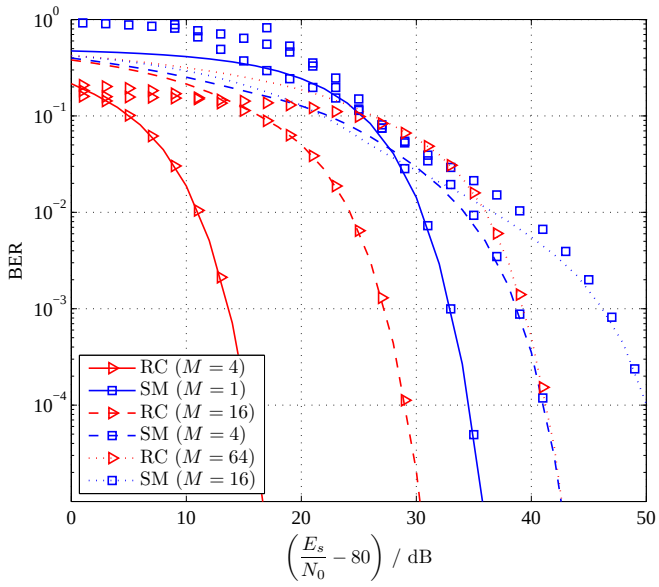

Figure 3.9: *Comparison of RC and SM for spectral efficiency of* 2*,* 4 *and* 6 *bit/s/Hz in* 4×4 *setup scenario (lines show simulation results and markers analytical error bounds).*

of transmitters and receivers, SMP is not taken into account for these evaluations. The basic wireless indoor scenario as presented in Section 3.1.1 is considered. However, the number of optical transmitters and receivers is increased resulting in different $N_r \times N_t$ setup scenarios. The spacing of the single transmitters on the x- and y-axis is set to $d_{\mathrm{TX}} = 0.2$ m. The spacing of the optical receivers is kept as considered above, *i.e.* 0.1 m. Both transmitters and receivers are aligned in rectangular arrays, which are centred within the room.

First of all, the standard 4×4 setup scenario is considered. For this scenario, Figure 3.9 depicts the BER of SM and RC assuming a spectral efficiency of 2, 4 and 6 bit/s/Hz. As shown, for a spectral efficiency of 2 and 4 bit/s/Hz, RC applying 4-PAM, respectively 16-PAM, achieves a better performance than SM. However, if an increased spectral efficiency of 6 bit/s/Hz is considered, SM outperforms RC up to an SNR of about 36 dB. This is because SM operates with a reduced signal constellation size of $M = 16$ compared to 64-PAM RC transmission. At SNRs above 36 dB, RC gets superior because of the constructive superposition of the multiple optical signals.

As SM uses only one transmitter at any symbol duration, there is no superposition of the optical signals. However, compared to RC, SM offers higher SNR gains with increasing number of receivers. This finding is shown in Figure 3.10, where the performance of SM and RC is studied

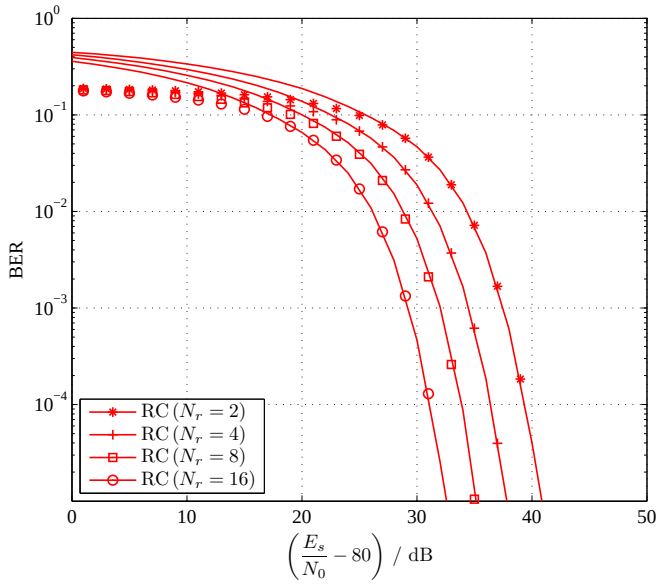

(a) 32-PAM RC.

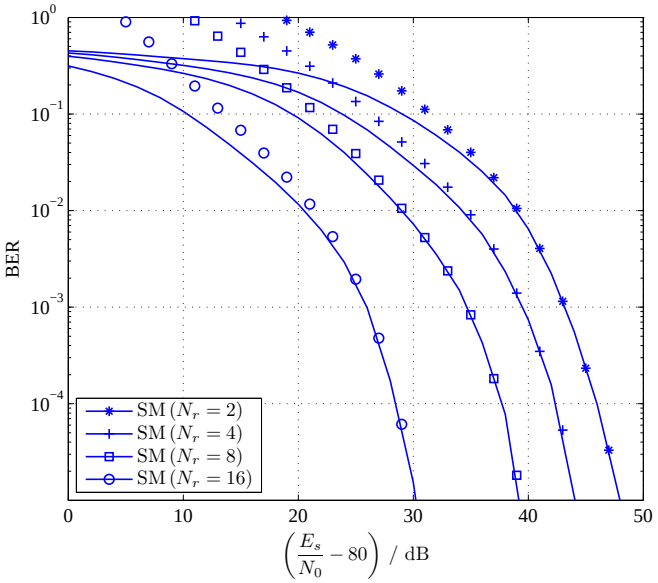

(b) SM with $M = 4$.

Figure 3.10: *Comparison of RC and SM for spectral efficiency of* 5 *bit/s/Hz with* $N_t = 8$ *and varying number of optical receivers* N_r *(lines show simulation results and markers analytical error bounds).*

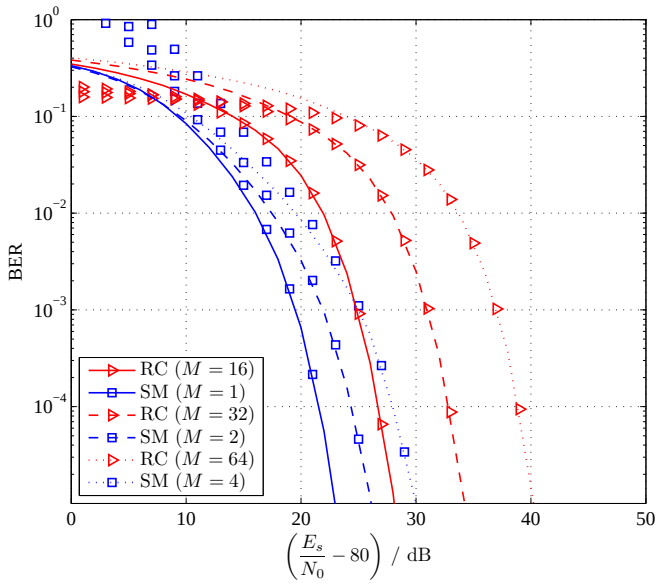

Figure 3.11: *Comparison of RC and SM for spectral efficiency of* 4, 5 *and* 6 *bit/s/Hz in* 16×16 *setup scenario (lines show simulation results and markers analytical error bounds).*

for 5 bit/s/Hz for a scenario with $N_t = 8$ and varying number of optical receivers. It can be seen that when consecutively doubling N_r from 2 up to 16, RC achieves an SNR performance gain of about 3 dB in each step. In contrast, SM achieves larger improvements as it provides an SNR performance gain of about 5 dB by moving from $N_r = 4$ to $N_r = 8$ and of about 9 dB by moving from $N_r = 8$ to $N_r = 16$. Consequently, in the 16×8 scenario SM even outperforms RC by about 2 dB.

Besides these improvements, SM has another essential advantage over RC transmission. If more bits are to be transmitted per channel use, RC needs a higher increase in SNR to be able to provide the same BER performance. This observation is taken from Figure 3.11, which shows the error ratios for a 16×16 transmission system providing different spectral efficiencies (4, 5 and 6 bit/s/Hz). It can be seen that RC needs an SNR improvement of about 6 dB to achieve the same BER when providing 5 instead of 4 bit/s/Hz, whereas SM requires an increase of only 3 dB. Consequently, SM with $M = 2$ outperforms 32-PAM RC by about 8 dB and even 16-PAM RC by about 2 dB. If the spectral efficiency is increased by 1 bit to 6 bit/s/Hz, RC requires additional 6 dB, in contrast to SM which needs only an increase of about 4 dB. In summary, for a spectral efficiency of 6 bit/s/Hz SM outperforms RC by about 10 dB and even outperforms the less efficient 32-PAM RC transmission by about 4 dB. Hence, the benefits of SM over RC largely increase with greater spectral efficiencies as well as with

increased numbers of optical transmitters and receivers. Additionally, SM even provides less computational complexity. Consequently, SM is a suitable modulation technique for OWC to provide high data rates at good BER performance.

3.2 Optical spatial modulation using colour LEDs

As shown in the previous section, SM is an ideal candidate for IM/DD based systems due to its low complexity. However, the performance of SM largely depends on the channel characteristics. As a consequence, its performance is degraded in scenarios with high link correlation and low differentiability of the multiple channels. Therefore in this section, further investigations are carried out in order to improve the performance of optical SM. To this end, optical SM in combination with colour LEDs is analysed. The BER performance of SM is analysed i) for scenarios which use transmitters having the *same* optical wavelength and ii) for scenarios which use transmitters having *different* optical wavelengths.

3.2.1 System model and setup scenario

In the following, the basic $N_r \times N_t$ indoor scenario introduced in Section 3.1.1 is maintained. However, different numbers of optical transmitters (LEDs) are considered, whereas the number of receivers (photo-diodes) is kept by setting $N_r = 4$ for each setup. This means that $4 \times N_t$ scenarios are considered. The N_t transmitters are equidistantly arranged in a circle. This circle is centred in the middle of the room and has a diameter of 0.5 m. A circular arrangement is chosen because it provides smaller distances between the transmitters, and consequently lower intrinsic channel differentiability compared to the square arrangement considered in Section 3.1.1. The 4 receivers are aligned in a square 2×2 array which is centred in the middle of the room. The spacing of the receivers is assumed to be 0.1 m on the x- and y-axis as considered above. Figure 3.12 shows the positioning of the simulation setup within the room for the case of $N_t = 16$. The receivers are displayed as dots and the transmitters as triangles. Off-the-shelf SD 445-14-21-305 silicon photo-diodes [118], which have a detector area of about $1\,\text{cm}^2$, are considered as photo-detectors. The FOV semiangle of the photo-diodes is assumed to be $60°$. Figure 3.13 shows the responsivity of the photo-diodes for different optical wavelengths. The optical transmitters are assumed to be off-the-shelf LEDs from OSRAM's Golden Dragon Plus product family [119]. These light sources have a transmitter semiangle of

$85°$ and are available in different colours. Table 3.2 shows the wavelengths of the considered LEDs and the corresponding responsivity of the photo-diodes according to Figure 3.13.

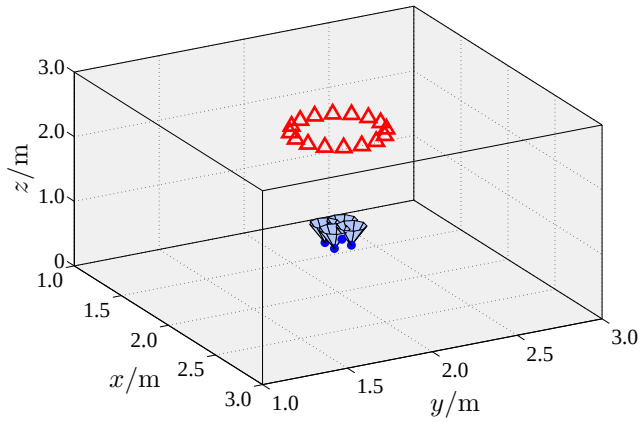

Figure 3.12: *Indoor setup scenario for the case of $N_t = 16$. Downwards pointing LEDs (transmitters) are placed at ceiling height of 2.50 m, and upwards pointing photo-diodes (receivers) are placed at table height of 0.75 m.*

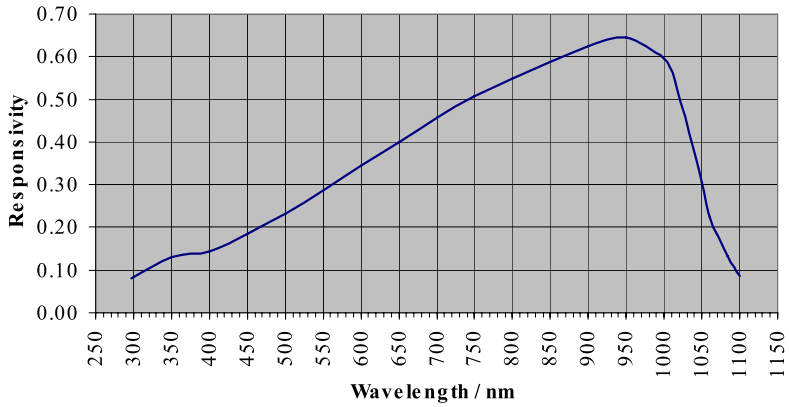

Figure 3.13: *Responsivity of photo-diode SD 445-14-21-305. The figure is taken from the data sheet [118] of the photo-diode.*

Wavelength of LED	**Responsivity of photo-diode**
462 nm (deep blue)	0.1963
467 nm (blue)	0.2019
505 nm (verde green)	0.2407
528 nm (true green)	0.2565
590 nm (yellow)	0.3343
617 nm (amber)	0.3611
625 nm (red)	0.3713
656 nm (hyper red)	0.4102

Table 3.2: *Wavelengths of LEDs and corresponding responsivity of photo-diodes.*

3.2.2 Results on bit error ratio performance

As shown in (2.23), the responsivity of the photo-detector affects the transfer factor of optical links. Since the responsivity is related to the optical wavelength, using LEDs with different wavelengths affects the differentiability of multiple optical links. As space shift keying (SSK) conveys only bits in the spatial domain, its performance is highly dependent on the differentiability of the multiple links, respectively of the multiple optical transmitters. Therefore, in the following, SM's low-complex implementation SSK is considered as transmission technique. The BER performance of SSK is analysed for two different scenarios: i) all optical transmitters have the same wavelength and ii) the optical transmitters have different wavelengths. Both scenarios are based on the $4 \times N_t$ setup presented in Section 3.2.1. For scenario ii), Table 3.3 shows the assignment of the different wavelengths to the individual transmitters. Four specific setups which have $N_t = 4, 8, 16$ and 32 optical transmitters are considered. For scenario i), all optical transmitters have a wavelength of 656 nm as this wavelength provides the highest responsivity. Therefore, this scenario provides the largest mean received electrical energy. The SNR is again defined as $\frac{E_s}{N_0}$. This is because considering received energy to noise energy would disregard the difference in path loss caused by the specific responsivities. As the channel coefficients are in the region of 10^{-6}, the electrical path loss is about -120 dB. As a consequence, the BER curves displayed in the following figures have an approximate SNR offset of about 120 dB. Therefore, in the following, a normalised SNR is considered given by $\frac{E_s}{N_0} - 120\,\mathrm{dB}$.

Wavelength of LED	**Transmitter using wavelength**			
	$N_t = 4$	$N_t = 8$	$N_t = 16$	$N_t = 32$
462 nm		1	1, 9	1, 9, 17, 25
467 nm		3	3, 11	3, 11, 19, 27
505 nm		5	5, 13	5, 13, 21, 29
528 nm		7	7, 15	7, 15, 23, 31
590 nm	2	2	2, 10	2, 10, 18, 26
617 nm	4	4	4, 12	4, 12, 20, 28
625 nm	3	6	6, 14	6, 14, 22, 30
656 nm	1	8	8, 16	8, 16, 24, 32

Table 3.3: *Wavelengths of LEDs used in setup scenarios.*

Figure 3.14 shows the BER performance of SSK for a 4×4 and 4×8 setup. It can be seen that the scenario that employs different transmitter wavelengths achieves an SNR performance gain of about 5 dB. Although using the same transmitter wavelength provides a larger received electrical energy, this results in a higher BER. This is due to the fact that using different wavelengths improves the differentiability of the multiple channels. As the performance of SSK is affected by the differentiability of the multiple channels, the use of colour LEDs enhances its performance. Figure 3.15 shows the BER performance of SSK for a 4×16 and 4×32 setup. For these two setups, using different transmitter wavelengths achieves an even larger SNR performance gain of about 10 dB. Note that the receiver does not need any knowledge about the different wavelengths because it implicitly gets this information by channel estimation which it needs to perform in any case. The wavelengths are distinguished on the basis of the specific power levels which they induce at the detector without the need for special optical filters. This is in contrast to the colour-shift-keying (CSK) transmission scheme proposed by the Institute of Electrical and Electronics Engineers (IEEE) $802.15.7$ Visible Light Communication Task Group [53] in the IEEE standard [54]. CSK uses red, green and blue (RGB) type LEDs to transmit data. The data is conveyed by the combination of the three different colours, *i.e.* each CSK constellation point is defined by a specific combination of the three colours. In order to decode the data, the combined colour has to be separated into the three individual RGB channels. To this end, the receiver employs three separate photo-diodes each with a special red, green and blue optical filter. This setup results in a complex receiver design. In contrast, the

proposed SSK scheme enables low-complex system implementations as shown above.

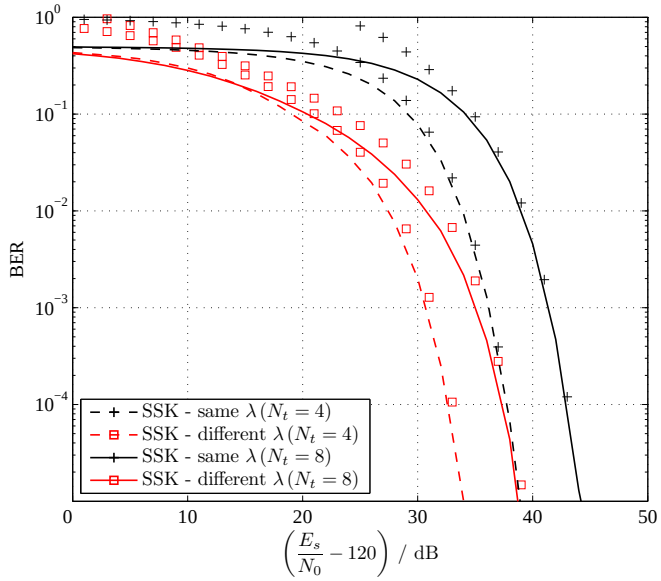

Figure 3.14: *BER of SSK for* 4×4 *and* 4×8 *setup using i) same transmitter wavelength* λ *and ii) different transmitter wavelengths* λ *(lines show simulation results and markers analytical error bounds).*

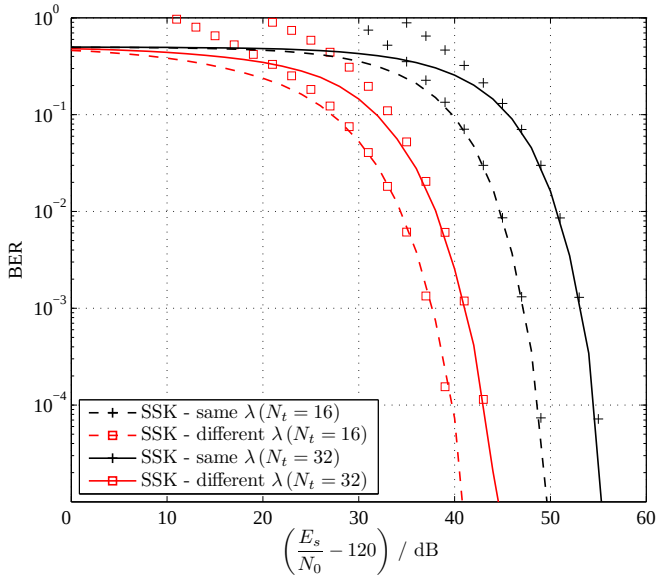

Figure 3.15: *BER of SSK for* 4×16 *and* 4×32 *setup using i) same transmitter wavelength* λ *and ii) different transmitter wavelengths* λ *(lines show simulation results and markers analytical error bounds).*

3.3 Coded optical spatial modulation

In order to improve the performance of SM over correlated channels, TCSM has been proposed [101, 114]. TCSM encodes the bits conveyed in the spatial domain to assist the detection of the active transmitter. In this section, the performance of coded optical SM is evaluated. An enhanced coded SM technique is proposed which jointly encodes the bits conveyed in the signal and spatial domains. It is found that this enhanced coded SM technique can achieve gains in SNR compared to the originally proposed TCSM scheme.

3.3.1 System model and setup scenario

TCSM applies FEC coding to the bits conveyed in the transmitter index in order to increase the free distance between sequences of spatial constellation points. Consequently, the transmitter detection is made more robust and the error ratio is reduced. As shown in Figure 3.16 (b), TCSM works by the principle that it splits the data bits into two subsets. The first subset

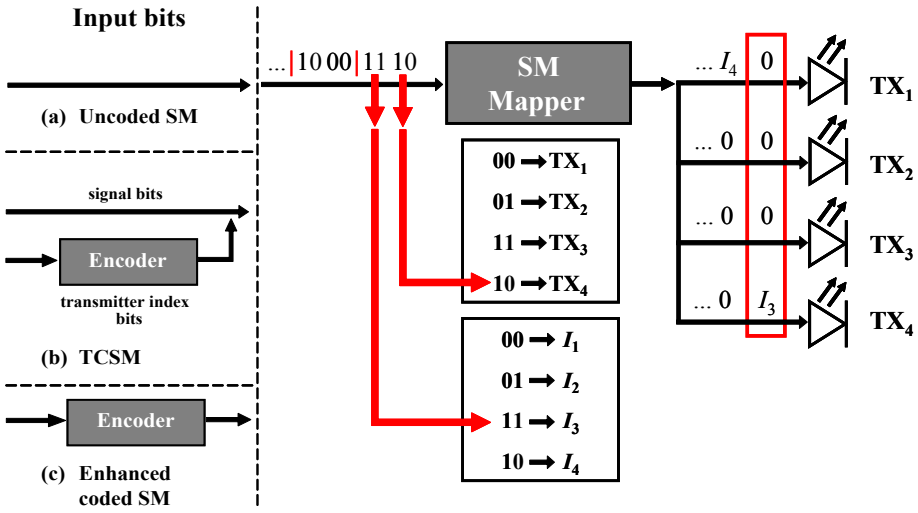

Figure 3.16: *Illustration of uncoded SM, TCSM and enhanced coded SM with* $N_t = 4$ *and* $M = 4$.

directly specifies the digitally modulated signal to be emitted, whereas the second subset is first passed to an FEC encoder and then used to determine the emitter (LED) to be activated. Despite this additional FEC encoding, the general SM principle is maintained, *i.e.* only one transmitter is active during any symbol duration. As shown, TCSM differentiates between the bits represented by digital signal modulation and the bits conveyed in the spatial domain, thus disallowing a joint decoding at the receiver side. Consequently, the basic SM principle of

simultaneously encoding bits in the spatial and signal domains is not fully exploited. Therefore, in the following, the TCSM technique is extended to an enhanced coded SM scheme which jointly encodes the bits conveyed in the spatial domain as well as in the signal domain.

For FEC encoding at the transmitter side, a convolutional encoder with an octal representation of $(161, 133)$, a coding rate of $c = \frac{1}{2}$, a constraint length of $l = 7$ and a free distance of $d_{\text{free}} = 10$ is assumed. Furthermore, the encoded bits are additionally interleaved by a random block interleaver. As proposed in [101, 114], by applying TCSM, only the bits which determine the transmitter index are passed to the convolutional encoder, while the bits denoting the digitally modulated signal to be transmitted remain uncoded and are directly passed to the SM mapper (see Figure 3.16 (b)). The encoded and interleaved bits are then used to determine the emitter (LED) which is activated according to the standard SM transmission scheme. In contrast, the proposed enhanced coded SM scheme passes *all* data bits to the convolutional encoder, *i.e.* the FEC encoding is applied to all data bits *before* they are split into the two subsets which determine the digitally modulated signal and the active transmitter. The FEC encoded bits are also interleaved and then passed to the standard SM mapper which maps them to the signal constellation points and transmitter indices as depicted in Figure 3.16 (c). Note that for the sake of comparison, both coded SM schemes use the same $(161, 133)$ convolutional encoder in the following.

At the receiver side, the FEC encoded bits of both coded SM schemes are deinterleaved. The actual detection is based on the ML principle given in (3.1). Consequently, the ML detector jointly estimates the emitter index and the transmitted signal by a common operation. If FEC coding is applied, the ML detection principle can be used to realise a soft decision ML detector for SM by employing log-likelihood ratios (LLRs). According to [111], the *a posteriori* LLR for the i^{th} bit conveyed in the transmitted signal vector $\mathbf{s}$ is

$$L(\mathbf{s}^i) = \log \frac{\sum\limits_{\mathbf{s} \in \mathbf{S}_1^i} \exp\left(-\frac{\|\mathbf{y}-\mathbf{H}\,\mathbf{s}\|_{\text{F}}^2}{\sigma^2}\right)}{\sum\limits_{\mathbf{s} \in \mathbf{S}_0^i} \exp\left(-\frac{\|\mathbf{y}-\mathbf{H}\,\mathbf{s}\|_{\text{F}}^2}{\sigma^2}\right)}, \tag{3.10}$$

where $\mathbf{S}_1^i$ and $\mathbf{S}_0^i$ represent the set of signal vectors which have "1" and "0" at the i^{th} bit position, respectively. The calculated LLRs can be processed by a soft decision Viterbi decoder in order to retrieve the transmitted data bits. It is assumed that the receiver has perfect knowledge of the channel, whereas $\mathbf{H}$ is not known at the transmitter side. Moreover, a soft decision Viterbi

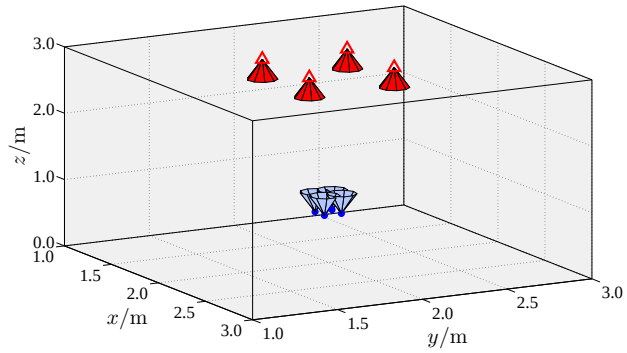

Figure 3.17: *Positioning of* 4×4 *simulation setup with* $d_{\mathrm{TX}} = 0.5$ *m. Downwards pointing LEDs (transmitters) are placed at ceiling height of* 3.00 *m, and upwards pointing photo-diodes (receivers) are placed at table height of* 0.75 *m.*

decoder is considered which has a traceback length of five times the constraint length.

In the following, the generic 4×4 indoor scenario and system model presented in Section 3.1.1 are considered. However, in this section, it is assumed that the transmitters are placed at a height of $z = 3.00$ m. The performance of the optical SM schemes is studied using the optical devices and parameters given in Section 2.4: The optical transmitters employ the DL-6147-040 diode [112] which has a transmitter semiangle of $\Phi_{\frac{1}{2}} \approx 8°$. The optical receivers employ the BPX 61 photo-diode [113] which has a responsivity of $r \approx 0.434$, a detector area of $A \approx 7\,\mathrm{mm}^2$ and a FOV semiangle of $\Psi_{\frac{1}{2}} \approx 55°$. Using these parameters, the channel coefficients are calculated according to (2.23). The values of d, ϕ and ψ are again derived from the geometric alignment within the considered setup. Figure 3.17 shows the positioning of the 4×4 simulation setup. Transmitter spacings of $d_{\mathrm{TX}} = 0.3$ m, 0.5 m and 0.7 m are assumed, which yield the following channel matrices:

$$\begin{aligned}
\mathbf{H}_{d_{\mathrm{TX}}=0.3} &\approx 10^{-5} \begin{pmatrix} 0.5934 & 0.4775 & 0.4775 & 0.3847 \\ 0.4775 & 0.5934 & 0.3847 & 0.4775 \\ 0.4775 & 0.3847 & 0.5934 & 0.4775 \\ 0.3847 & 0.4775 & 0.4775 & 0.5934 \end{pmatrix}, \\
\mathbf{H}_{d_{\mathrm{TX}}=0.5} &\approx 10^{-5} \begin{pmatrix} 0.3847 & 0.2691 & 0.2691 & 0.1889 \\ 0.2691 & 0.3847 & 0.1889 & 0.2691 \\ 0.2691 & 0.1889 & 0.3847 & 0.2691 \\ 0.1889 & 0.2691 & 0.2691 & 0.3847 \end{pmatrix},
\end{aligned} \tag{3.11}$$

$$\mathbf{H}_{d_{\mathrm{TX}}=0.7} \approx 10^{-5} \begin{pmatrix} 0.1889 & 0.1157 & 0.1157 & 0.0713 \\ 0.1157 & 0.1889 & 0.0713 & 0.1157 \\ 0.1157 & 0.0713 & 0.1889 & 0.1157 \\ 0.0713 & 0.1157 & 0.1157 & 0.1889 \end{pmatrix}.$$

3.3.2 Results on bit error ratio performance

In the following, the BER performance of the proposed enhanced coded optical SM scheme is evaluated and compared to the original TCSM scheme as well as to uncoded SM. Figure 3.18 shows the BER performance of the enhanced coded SM scheme, TCSM and uncoded SM for a spectral efficiency of 2 bit/s/Hz using the channel coefficients given in (3.11). In order

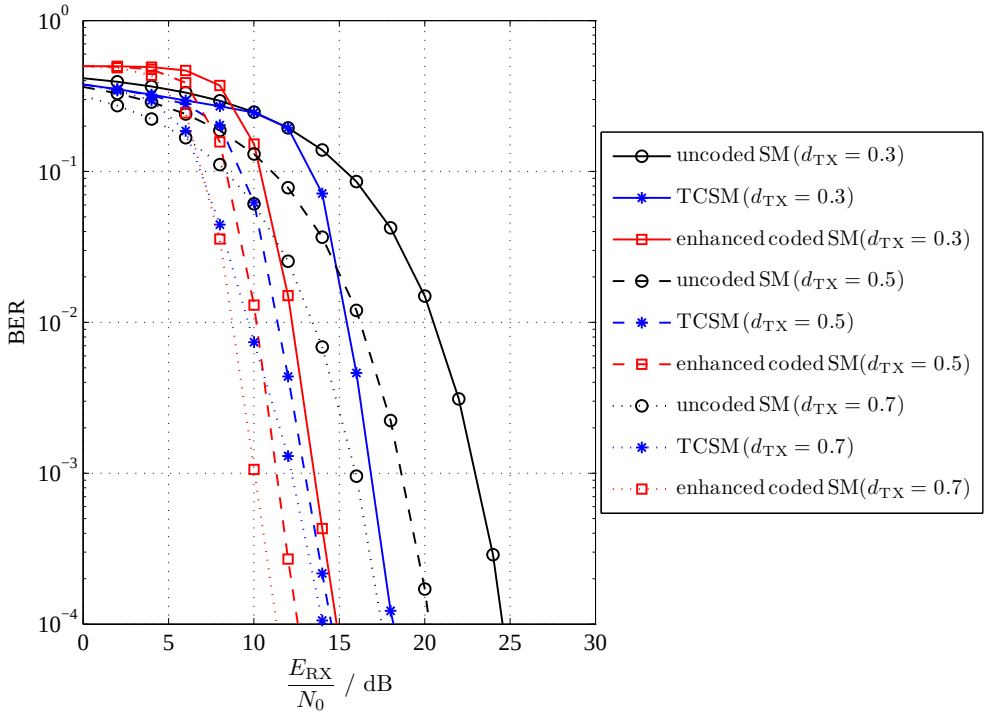

Figure 3.18: *BER of coded and uncoded SM for spectral efficiency of* 2 *bit/s/Hz in* 4×4 *setup scenario with varying distance* d_{TX} *of transmitters on the* x*- and* y*-axis.*

to provide this spectral efficiency, uncoded SM operates with a signal constellation size of $M = 1$, *i.e.* all bits to be transmitted are conveyed in the spatial domain. In contrast, TCSM has to operate with $M = 2$ to compensate for the redundancy induced by the FEC encoder. Moreover, the enhanced coded SM scheme has to operate with an even larger signal constellation size of $M = 4$ to provide the same data rate. As shown, despite this enlarged

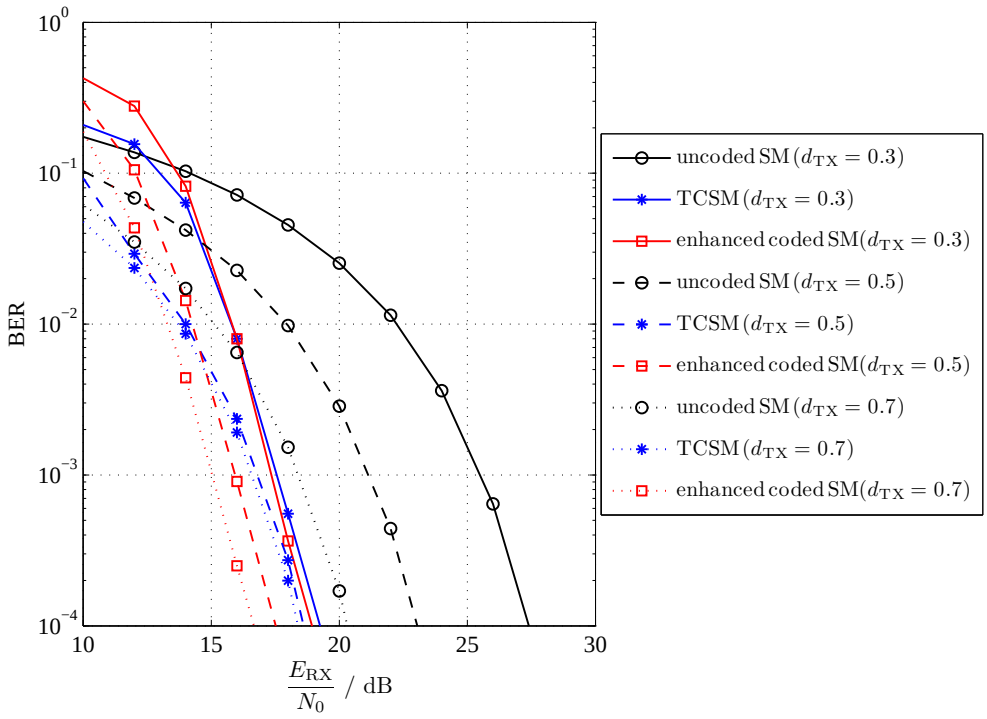

Figure 3.19: *BER of coded and uncoded SM for spectral efficiency of* 3 *bit/s/Hz in* 4×4 *setup scenario with varying distance* d_{TX} *of transmitters on the* x*- and* y*-axis.*

signal constellation size, the enhanced coded SM scheme can achieve gains in SNR of about $2 - 3$ dB compared to TCSM and outperforms uncoded SM by about $6 - 10$ dB. Moreover, it can be seen that an enlargement of the transmitter spacing increases the channel differentiability and improves the BER performance of both coded and uncoded SM. Figure 3.19 displays the BER of the considered schemes for a spectral efficiency of 3 bit/s/Hz. In this scenario, uncoded SM operates with a signal constellation size of $M = 2$ and TCSM with $M = 4$. The enhanced coded SM scheme has to operate with $M = 16$. As depicted, the new enhanced coded SM scheme can also outperform both other schemes for a spectral efficiency of 3 bit/s/Hz and achieves SNR gains of about $1 - 2$ dB compared to TCSM, respectively of about $4 - 8$ dB compared to uncoded SM. These SNR performance gains are achieved even though the proposed scheme has to use a much larger signal constellation size to compensate for the induced FEC coding and to provide the same spectral efficiency.

3.4 Summary

In this chapter, the performance of MIMO techniques applied to OWC in indoor environments has been studied. Several $N_r \times N_t$ setups with different spacings of the transmitters and different positions of the receiver array have been considered. It has been shown that for OWC, MIMO schemes can provide gains even under static LOS conditions – channel conditions which commonly disallow the use of MIMO techniques in the radio frequency (RF) domain.

In detail, the contribution of this chapter is threefold: Firstly, the performance of the MIMO techniques RC, SMP and SM has been compared. It has been shown that SMP improves the spectrum efficiency in IM/DD based transmission systems by exploiting multiplexing gains. In order to achieve these improvements, adequate channel differentiability is required. Similarly, SM achieves improved spectral efficiencies and it is more robust to low channel differentiability. SM enjoys additional implementation advantages as it only requires low complexity detection algorithms. Since SM prevents ICI, it requires a much lower computational complexity compared to SMP. Additionally, SM is also less computationally expensive than RC. This is due to the fact that SM conveys data bits in the spatial domain which enables high spectral efficiencies with lower signal constellation sizes compared to RC. RC is insensitive to different transmitter-receiver alignments because of the constructive superposition of the optical signals. However, as RC does not provide spatial multiplexing gains, it requires large signal constellation sizes to provide high data rates. This drawback degrades the BER performance of RC at high spectral efficiencies. It has been found that induced power imbalance between the transmitters is an effective technique to improve the BER performance. Under conditions which cause low channel differentiability, power imbalance can substantially improve the performance of both SMP and SM. Consequently, if the transmission power is imbalanced, SMP and SM can even be used in scenarios which typically disallow the application of MIMO schemes. As shown, the best performance for the considered 4×4 indoor scenario can be achieved by blocking some of the 16 links between the transmitters and receivers. This induced blocking reduces the SNR at the receiver side. However, the blocking improves the BER of both SMP and SM since it outweighs the loss in SNR by enhancing the channel differentiability. These two MIMO techniques capitalise on both SNR and channel differences. For instance, blocking 4 of the 16 links of the 4×4 setup improves the BER performance of SMP by more than 20 dB, while the effective SNR is reduced by about 2 dB due to the blocking. Therefore, the induced link blockage represents

the most suitable compromise between channel differentiability and received energy for the considered 4×4 scenarios. However, it requires the implementation of opaque boundaries at the receiver device, respectively small FOVs of the optical receivers. It has been further found that SM provides larger SNR improvements with increasing number of optical transmitters and receivers compared to RC. Additionally, SM can achieve better error ratios particularly at low SNRs because the superposition gain of RC prevails only at higher SNRs. SM is a low-complex transmission scheme that can be adopted to the channel characteristics of OWC by interchanging signal constellation size and number of optical transmitters. Consequently, SM is a suitable modulation technique for OWC to provide high data rates at good BER performance. Furthermore, the analytical error bounds of the three schemes derived in Section 2.2 have been substantiated by computer simulations. It has been shown that these error bounds provide accurate BER approximations.

Secondly, on the basis of the previous findings, the performance of optical SM has been further analysed. It has been found that using colour LEDs with different optical wavelengths can significantly improve the performance of SM, precisely by more than 10 dB. This finding shows that the utilisation of different optical wavelengths in combination with IM and DD enhances the differentiability of the multiple channels. This is due to the fact that the responsivity of common photo-diodes is a function of the optical wavelength. This means that different wavelengths induce specific optical power levels at the receiver. These distinctive power levels directly affect the channel characteristic as they enhance the channel differentiability. Consequently, the SM receiver can detect the activated transmitter more reliably which improves the BER performance.

Finally, the performance of coded optical SM has been studied. It has been shown that FEC coding can significantly improve the performance of SM under conditions with high link correlation and low channel differentiability. Particularly, an enhanced coded SM scheme has been proposed which jointly encodes the bits conveyed in the spatial and signal domains. It has been found that this approach can achieve gains in SNR of about 1 – 3 dB compared to the originally proposed TCSM scheme [101, 114]. This is because the jointly encoding conveys the coded bits in the spatial domain as well as in the signal domain. Consequently, the enhanced coded SM scheme can make better use of the basic SM detection principle which jointly detects the emitter index and the transmitted signal by a common operation. As a result, the enhanced coded SM scheme utilises the output of the ML detector more efficiently than

the originally proposed TCSM scheme, thus providing larger coding gains. Summing up, the MIMO techniques considered in this chapter can actually provide high data rates and enhance the performance of OWC in indoor environments even under mere LOS conditions.

Chapter 4
Optical wireless transmitter employing discrete power level stepping

Orthogonal frequency division multiplexing (OFDM) is widely used in modern radio frequency (RF) standards as well as in optical wireless communications (OWC) [42, 60, 68–73]. This is due to the fact that OFDM is a bandwidth efficient transmission technique which can cope with inter-symbol interference (ISI). In contrast to pulsed modulation techniques, OFDM provides high data rates even in severe multipath scenarios which mostly occur in diffuse and scattered propagation scenarios [37, 120]. Moreover, OFDM enables low-complex signal processing implementations by the use of fast Fourier transformation (FFT) and inverse fast Fourier transformation (IFFT). However, a major drawback of OFDM is the fact that it requires sophisticated transceiver designs which must have good linearity characteristics and large dynamic ranges. Non-linear distortions, *e.g.* caused by amplifiers, largely decrease the system performance [121–124]. Compared to RF communications, OWC does not require high-frequency circuit designs because the signals are transmitted in the baseband representation and directly modulate the intensity of the light sources, *e.g.* light emitting diodes (LEDs). However, LEDs are highly non-linear due to their optical-power-versus-current characteristic. This non-linearity largely restricts the dynamic range and the transmission power of common optical wireless transmitters [125–129]. Moreover, the non-linearity of LEDs necessitates the implementation of complex pre-distortion and/or complex equalisation techniques [130, 131]. Consequently, conventional optical wireless transmitter front-ends cannot provide the required linearity in a power- and cost-efficient way.

In this chapter, a novel optical wireless transmitter concept is presented which addresses the shortcomings of conventional optical transmitters. In particular, the concept addresses: non-linearities, restricted dynamic range and complex system designs. The proposed transmitter employs discrete power level stepping which enables simple and power-efficient front-end designs. Sophisticated pre-distortion or intricate equalisation techniques to mitigate transmitter induced non-linearities are not required. As a result, a conventional low-complex

single-tap equalisation is sufficient. The concept can be used to implement transmitters for visible and infra-red (IR) light transmission as well as for line-of-sight (LOS) and diffuse propagation scenarios.

The remainder of this chapter is organised as follows: In Section 4.1, the considered system model is introduced. Section 4.2 reviews conventional transmitter front-end designs and discusses implementation issues. In Section 4.3, the effects of quantization on the bit error ratio (BER) performance are shown. Based on this analysis, appropriate bit resolutions are determined which provide sufficient precision. In Section 4.4, the proposed transmitter concept is introduced which employs discrete power level stepping. Moreover, the focus is set on several realisation aspects and the developed optical wireless transmitter is described. In Section 4.5, the results of several transmission experiments are presented. The transmitter performance is evaluated in terms of error vector magnitude (EVM) and BER. Measurements prove the functionality of the developed transmitter. Finally, Section 4.6 concludes the chapter.

4.1 System model

Figure 4.1 illustrates an OWC system which consists of an optical transmitter (TX) and receiver (RX). The optical transmitter comprises a modulator that transforms the incoming data stream into a signal that is to be transmitted by the light source. The output of the modulator is a digital signal. For higher order modulation techniques, such as M-pulse amplitude modulation (PAM) or OFDM, the modulator output is a bit vector representing an analogue signal value. The TX front-end transforms the bit vector into an analogue optical waveform by adequately controlling the light source. As a result, the front-end performs intensity modulation (IM) by changing the intensity of the emitted light according to the

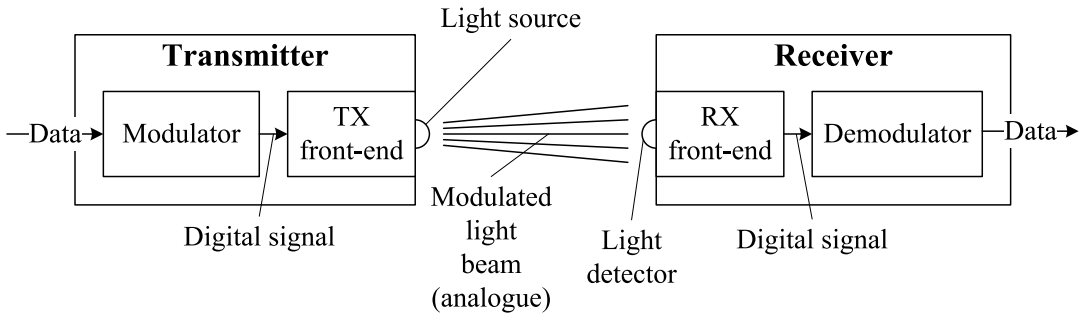

Figure 4.1: *Optical wireless transmission system.*

signal (data) to be sent. At the receiver side, a light detector retransforms the impinging optical waveform into an electrical signal. Commonly, this component is a photo-diode which transforms optical power into current by direct detection (DD). Additionally, the RX front-end contains an anti-aliasing filter, *i.e.* a low-pass filter to restrict the signal bandwidth in order to satisfy the sampling theorem, and an amplifier. After the received signal has been filtered and amplified, it is converted into a digital signal by an analogue-to-digital converter (ADC). The demodulator processes the digital signal and reconstructs the transmitted data. The remainder of this chapter focuses on the TX front-end and the generation of the optical waveform. In the following, direct-current-biased optical orthogonal frequency division multiplexing (DCO-OFDM) is considered as transmission technique. However, the transmitter concept proposed in this work is not restricted to DCO-OFDM but can also be used with any other multi-carrier transmission scheme, such as asymmetrically clipped optical orthogonal frequency division multiplexing (ACO-OFDM) or pulse-amplitude-modulated discrete multitone modulation (PAM-DMT). Moreover, single-carrier transmission schemes like on-off-keying (OOK), M-PAM or M-pulse position modulation (PPM) can be used as well.

4.2 Conventional transmitter front-end designs

A transmitter front-end for OWC transforms the electrical signal generated by the modulator into an optical signal which has sufficient power to enable its detection at the receiver. The block diagram of such a transmitter front-end is displayed in Figure 4.2. The modulator output of common transmission techniques, such as OFDM, is a bit vector of size N. This bit vector is a binary digital representation of the signal to be transmitted. Conventional optical transmitter front-ends transform this bit vector into an analogue voltage signal by using a

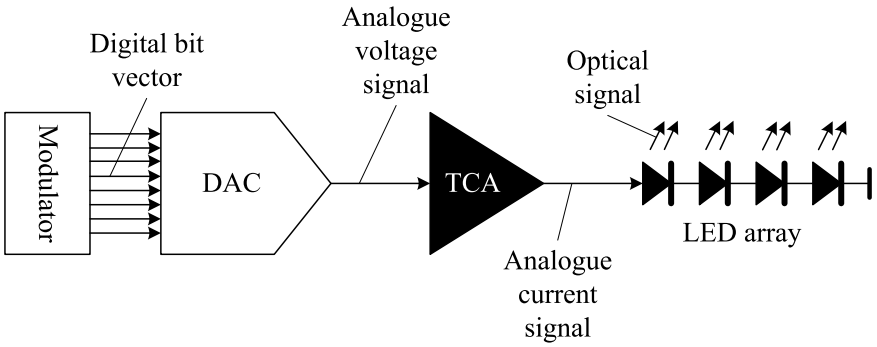

Figure 4.2: *Conventional optical wireless transmitter front-end.*

digital-to-analogue converter (DAC). The generated voltage signal is converted into a current signal using a transconductance amplifier (TCA). The TCA finally drives the light source. Commonly, the optical light source is a LED, either in the visible or IR light range. Only LEDs are fast enough to transform a modulated current signal into an optical signal of several MHz bandwidth. Therefore, sufficiently low rise and fall times of the LEDs are required. Moreover, arrays of several LEDs are commonly used to increase the emitted optical power. To this end, the LEDs are connected in series and are modulated by the same current signal. Laser diodes are an alternative light source. However, laser diodes are not considered as illumination devices because of their high costs and issues regarding eye safety.

The main drawback of LEDs is their optical-power-versus-current characteristic which is highly non-linear. Particularly in combination with OFDM transmission, non-linearities are a critical issue. Non-linearities result in a degraded signal-to-interference-plus-noise ratio (SINR), and consequently in a degraded system performance [121–124]. Therefore, OWC requires elaborate pre-distortion techniques at the transmitter or complex equalisation techniques at the receiver to compensate for the non-linear characteristic of LEDs. Without these techniques, LEDs can only be modulated in a narrow, quasi-linear operational area. Consequently, the operating point of LEDs has to be carefully chosen. However, this limited operational area largely restricts the dynamic range and the transmission power of OWC systems. Moreover, in order to enable high data rate transmission, the whole transmitter chain has to operate at several tens to hundreds of MHz. For instance in [115], a visible light transmitter system is reported which employs a DAC operating at a sampling rate of 275 mega-samples per second (Msps) to provide a data rate of about 100 Mbit/s. In order to provide the required bandwidth, broadband amplifier circuits have to be used as well. However, these circuit designs result in a high parasitic electrical power consumption, which is not transformed into optical power and is therefore wasted. Additionally, these circuit designs have to provide a good linearity characteristic. Therefore, conventional optical wireless transmitters are subject to complex and elaborate front-end designs.

4.3 Quantization

In the following, the effect of transmitter induced quantization on the BER performance is analysed. Figure 4.3 illustrates a continuous OFDM symbol which is not quantized (dashed line) and a quantized OFDM symbol with a resolution of 5 bits (solid line). Due to the considered resolution of 5 bits, the quantized symbol can take only 32 discrete amplitude

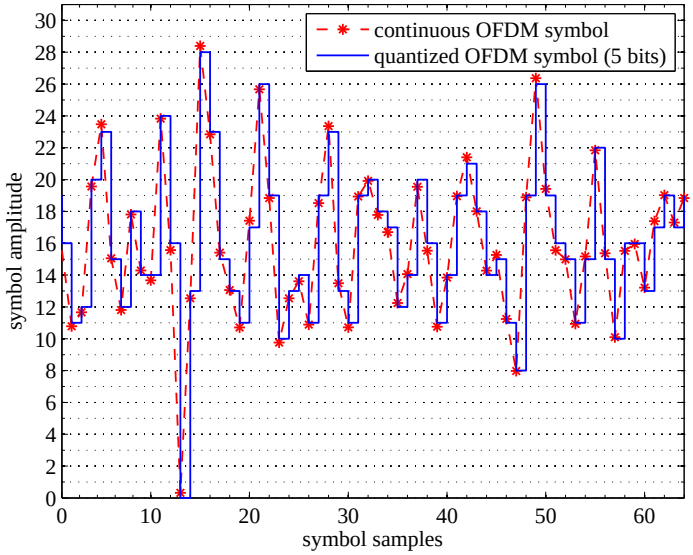

Figure 4.3: *Continuous OFDM symbol and quantized OFDM symbol.*

levels, whereas the continuous OFDM symbol has a (nearly) unlimited precision (depending on the precision of the computer system, which is commonly 32 or 64 bits). As DCO-OFDM is considered within this work, the illustrated symbols have a direct-current (DC) offset to provide non-negative amplitude values.

Figure 4.4 shows the BER performance of 16- and 64-quadrature amplitude modulation (QAM) for different bit resolutions. Note that any effects caused by channel estimation or synchronisation are not considered in these simulations to highlight the effect of bit resolution on the BER performance. Table 4.1 shows the considered OFDM system parameters. An FFT/IFFT size of $L = 256$ and a cyclic prefix length of $L_{\text{cp}} = 5$ samples is applied. Due to Hermitian symmetry, the amount of data sub-carriers is $\frac{L}{2} - 1 = 127$. The signal-to-noise ratio (SNR) is defined as $\frac{E_{\text{RX}}}{N_0}$. The BER curves in Figure 4.4 show that a low resolution of only 2 or 3 bits leads to an error floor due to insufficient precision and low SINR. For 16-QAM a resolution of 5 bits is sufficient as it provides only a minor SNR performance degradation (less than 1 dB) compared to 16-QAM without quantization. For 64-QAM a resolution of at least 7 bits is required to provide sufficient precision. Consequently, the simulation results show that M-level QAM transmission can operate with a reduced bit resolution without major performance degradation.

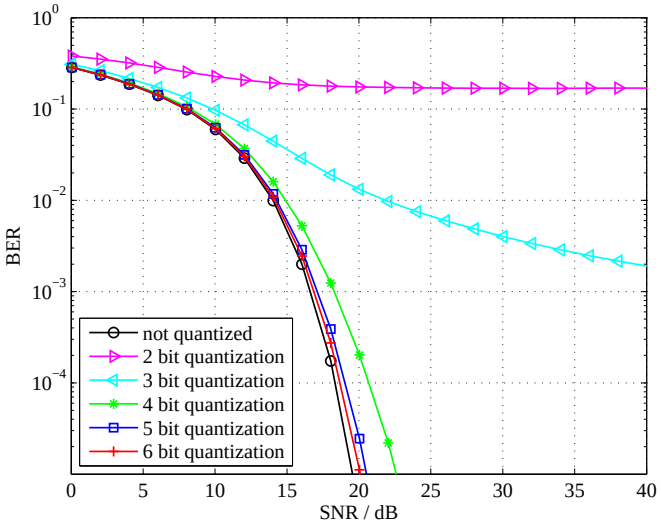

(a) 16-QAM.

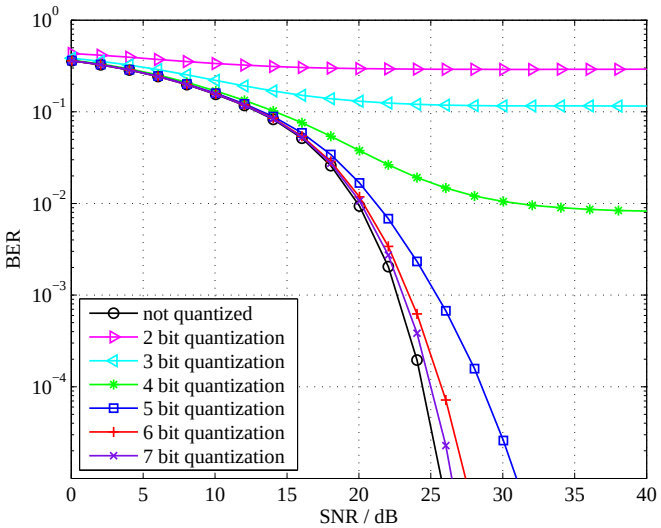

(b) 64-QAM.

Figure 4.4: *Effect of quantization on BER performance.*

OFDM system parameters	
FFT/IFFT size L	256
amount of data sub-carriers[1]	$\frac{L}{2} - 1 = 127$
cyclic prefix length L_{cp}	5 samples
sampling frequency f_{s}	25 Msps
modulation technique	2-, 4-, 16-QAM
data rate	$12, 24, 48$ Mbit/s

Table 4.1: *System parameters used for DCO-OFDM transmission.*

4.4 Proposed transmitter concept

The proposed transmitter concept addresses the shortcomings of conventional optical wireless transmitter front-ends like complex circuit designs, non-linearities and low power efficiency due to the required high-speed DACs and high-bandwidth/high-current TCAs. The architecture of the proposed optical wireless transmitter front-end is shown in Figure 4.5. The basic idea

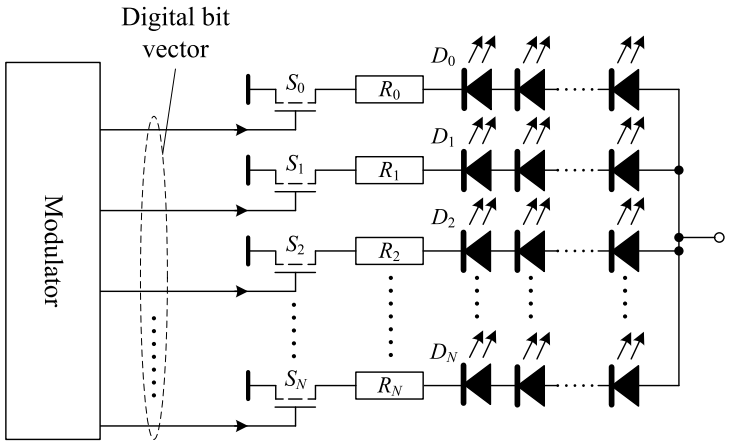

Figure 4.5: *Proposed optical wireless transmitter front-end architecture.*

of this transmitter concept is to omit both the DAC and the analogue current control circuit which powers the LEDs. Instead of this analogue signal shaping, an array of LEDs is used which applies discrete power scaling. The LEDs are arranged in several groups which can be switched on and off individually. Each LED group emits a specific optical intensity resulting in a discrete power level stepping. Equal to conventional optical transmitter front-ends, the

[1] Hermitian symmetry is considered.

waveform to be sent is represented by a digital bit vector whose elements are binary values, *i.e.* ones and zeros. These binary values determine which LED groups are switched on or off. Consequently, the baseband modulator switches a specific combination of LED groups on or off according to the signal to be sent. This means that each signal sample is represented by a specific optical power level which is generated by a particular combination of activated LED groups.

As shown in Figure 4.5, the transmitter circuit consists of $N+1$ groups of LEDs, D_0 to D_N. Each group D_i is set to emit a constant optical power level (intensity) P_i using a series resistor R_i. The value of R_i determines the electrical current I_i which powers the LED group D_i. Consequently, I_i determines the optical power level P_i which is emitted by D_i. Assuming $P_{\max}$ is the maximum power level that the LEDs can emit, the current I_0 driving the first group of LEDs D_0 is set accordingly to result in an emitted power level of $P_{\max}$. The remaining LED groups are driven with scaled currents to result in: $P_0 = P_{\max}$, $P_1 = P_{\max}/2$, $P_2 = P_{\max}/4, \ldots$ and $P_N = P_{\max}/2^N$. The LED group D_0 is modulated (switched on/off) by the most significant bit of the digital bit vector generated by the baseband modulator. Group D_1 is modulated by the second most significant bit, down to group D_N which is controlled by the least significant bit of the vector. Consequently, each bit of the signal vector to be sent is assigned to a specific emitter group radiating a defined optical intensity. As the discrete power levels emitted by the single LED groups constructively add up at the receiver, the proposed transmitter concept performs a digital-to-analogue conversion in the optical domain. Consequently, the circuit can be considered as a direct digital input to analogue optical output converter with a resolution of $N+1$ bits. The bit resolution can be chosen with regard to the required precision as analysed in Section 4.3. If a resolution of 5 bits is considered, the quantized signal waveform can take 32 discrete intensity levels. For instance, the intensity level "12" is represented by the binary sequence "$0\,1\,1\,0\,0$". If this intensity level is to be emitted, the LED groups D_1 and D_2 are activated, whereas the groups D_0, D_3 and D_4 are switched off. If DCO-OFDM is considered, the LED group D_0 represents the DC bias offset which has an optical power level of P_0. For $L \geq 64$, the OFDM time domain signal samples have approximately Gaussian distribution [71].

In order to increase the maximum transmission power and range, it is additionally proposed to combine two or more LED groups to one common group. For instance, two groups can be jointly switched on and off to commonly build group D_0. If both groups emit the maximum power level $P_{\max}$, the overall transmission power is doubled. This results in: $P_0 = 2\,P_{\max}$,

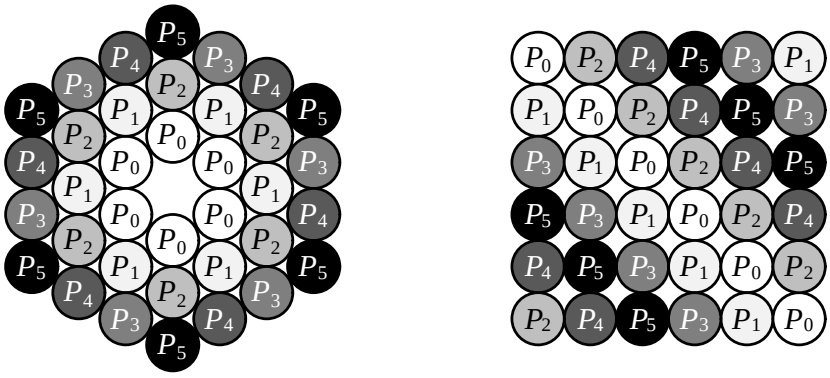

Figure 4.6: *Proposed LED arrangements for optical wireless transmitter front-end employing* 6 *LED groups with* 6 *LEDs per group.*

$P_1 = P_{\max}$, $P_2 = P_{\max}/2, \ldots$ and $P_N = P_{\max}/2^{N-1}$. This implementation constitutes a compromise between signal precision and transmission power, respectively SNR. The combination of two LED groups provides a reduced resolution of only N bits if the same number of groups is used as above. Alternatively, the amount of LEDs per emitter group D_i can also be varied in order to create different power levels P_i.

The power levels of the individual LED groups can be adjusted using an optical power meter for instance. This adjustment guarantees that the optical signal generated by the superposition of all groups has best linearity. Hence, the appropriate values of the series resistors R_i, respectively the currents I_i, can be determined using an optical power meter. Moreover, it is beneficial to align the LEDs in an arrangement which generates a light beam with most homogeneous emitted optical power. First transmission experiments using a line-by-line arrangement of the LED groups (with a simple serial arrangement of the LEDs within each group) provided an inhomogeneous light beam. Therefore, more elaborate LED arrangements are proposed. Two possible LED arrangements are illustrated in Figure 4.6. The figures show a hexagonal (left hand side) and a diagonal (right hand side) arrangement for an implementation with 6 LED groups and 6 LEDs per group. As shown, the single LEDs belonging to a specific group, and thus emitting a specific optical power level P_i, are distributed across the LED array. For the hexagonal arrangement, the groups form inner and outer circles. For the diagonal arrangement, the single LEDs are diagonally arranged within the emitter square. It is also advisable to use LEDs with wide beam angles to ensure a broad coverage and a homogeneous illumination of the emitted light beam. The switching stages S_i (see Figure 4.5) that digitally control the different LED groups are realised by fast solid state switching devices, such as transistors or gate drivers for metal-oxide-semiconductor field-effect transistors (MOSFETs). The switching

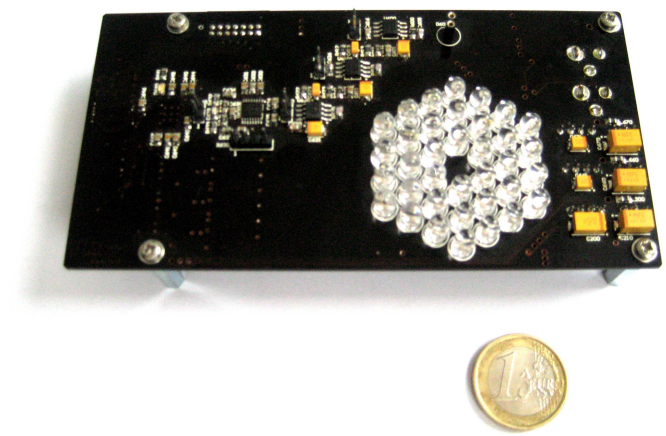

Figure 4.7: *Developed optical wireless transmitter front-end.*

speed of the stages S_i affects the achievable bandwidth of the optical transmitter. Only by fast switching speeds, a bandwidth in the range of 5 – 50 MHz or higher can be achieved. However, the bandwidth also depends on the typical rise and fall time of the LEDs. Since simple low-cost transistors are used as switching components, the proposed design enables the implementation of low-complex optical transmitters. A DAC and linear power amplifiers are not required. The OFDM signal processing can be done by an off-the-shelf field programmable gate array (FPGA) for instance, which enables flexible transceiver designs.

Figure 4.7 shows the developed optical wireless transmitter front-end. The transmitter front-end has the proposed hexagonal LED arrangement. It consists of 6 LED groups. Two of these groups are combined to be jointly switched on and off in order to increase the transmission power and the SNR at the receiver. Consequently, the implemented transmitter provides a resolution of 5 bits. The emitting diodes are off-the-shelf SFH 4502 IR LEDs [132] which have a wavelength of 950 nm. These diodes have a rise and fall time of about 10 ns and a typical radiant power of 40 mW. The semiangle of the LEDs is $18°$. The overall value of raw materials of the transmitter is less than $\$25$. As neither heat sinks nor fans are required for cooling, the implemented transmitter has a good power efficiency. The used receiver employs a SD 445-14-21-305 silicon positive intrinsic negative (PIN) photo-diode [118] with a detector area of 1 cm^2. The response time of the photo-diode is about 13 ns and the responsivity at 950 nm is about 0.65. Elaborate optical components like lenses or concentrators are not used.

4.5 Transmission experiments

In this section, the results of some transmission experiments using the implemented optical wireless transmitter front-end are presented. Table 4.1 shows the considered OFDM system parameters. The transmitter front-end has a resolution of 5 bits which is sufficient to perform a 16-QAM transmission with appropriate precision as shown in Section 4.3. The switching speed f_s of the LED groups is set to 25 Msps. The achievable bit rate of DCO-OFDM employing M-QAM can be approximated by:

$$b \approx \log_2(M)\, f_\mathrm{s}\, \frac{\frac{L}{2}-1}{L+L_\mathrm{cp}}. \tag{4.1}$$

Note that this calculation does not take additional symbols into account which are required for frame synchronisation and channel estimation. These parameters depend on the specific OFDM system implementation. Considering the system parameters given in Table 4.1, the implemented optical wireless transmitter provides a data rate of about 12, 24 or 48 Mbit/s if 2-, 4- or 16-QAM is used. The data rate can be increased by employing higher order M-QAM. For instance, 64-QAM provides a data rate of about 72 Mbit/s. However, the application of 64-QAM requires an increased resolution of at least 7 bits as shown in Figure 4.4(b). In order to further increase the data rate, higher switching speeds can also be applied if the LEDs provide sufficiently low rise and fall times. For instance, applying 64-QAM with a switching speed of $f_\mathrm{s} = 50$ Msps provides a data rate of more than 144 Mbit/s.

The maximum optical output power (all 6 LED groups with 6 LEDs per group are switched on) emitted by the transmitter is $P_\mathrm{opt} = \sum_{i=0}^{5} 6\, P_i \approx 930$ mW. The overall electrical power consumption of all LED groups is $P_\mathrm{LED} \approx 3.218$ W, which results in a total power dissipation of $P_\mathrm{LED} - P_\mathrm{opt} \approx 2.288$ W. Consequently, the LEDs have a power efficiency of $P_\mathrm{opt}/P_\mathrm{LED} \approx 28.90\,\%$. The total electrical power consumption of the transmitter front-end is $P_\mathrm{elec} \approx 4.956$ W if all LED groups are switched on. Therefore, the major portion of power is consumed by the LEDs resulting in a percentage of consumed power of $P_\mathrm{LED}/P_\mathrm{elec} \approx 64.93\,\%$. Therefore, the implemented optical transmitter has a low parasitic electrical power consumption and has an overall power efficiency of $P_\mathrm{opt}/P_\mathrm{elec} \approx 18.77\,\%$. For a continous DCO-OFDM transmission, the mean electrical power consumed is $\overline{P}_\mathrm{elec} \approx 2.760$ W and the mean emitted optical power is $\overline{P}_\mathrm{opt} \approx 441$ mW.

Table 4.2(a) shows the electrical SNR at the receiver for different distances between the

(a) LOS transmission

distance	SNR
1.0 m	35.81 dB
2.0 m	25.77 dB
3.0 m	19.21 dB
4.0 m	14.31 dB
5.0 m	10.69 dB
6.0 m	7.86 dB
7.0 m	6.35 dB

(b) NLOS transmission

distance	SNR
1.0 m	30.75 dB
1.5 m	23.98 dB
2.0 m	20.14 dB
2.5 m	17.31 dB
3.0 m	13.78 dB
3.5 m	10.58 dB
4.0 m	8.29 dB

Table 4.2: *SNR over distance for LOS and NLOS transmission.*

transmitter and the receiver. The transmitter and the receiver are aligned towards each other to provide a directed LOS link. The SNR is ascertained by measuring the mean electrical signal energy of the received OFDM symbols and by measuring the mean noise energy. The noise energy is measured in the interframe gaps between the OFDM frames since in these gaps no optical signal is emitted. Table 4.2(b) shows the electrical SNR for a non-line-of-sight (NLOS) transmission. Figure 4.8 illustrates the measurement setup for the NLOS transmission. As shown, the transmitter and the receiver are straightly directed towards a wall. The wall is a typical office wall with white paint and non-glossy surface. This setup provides a merely diffuse transmission scenario as an opaque obstacle between the transmitter and the receiver blocks the LOS link. The distance of the transmitter, respectively of the receiver towards the wall is $\frac{d}{2}$. This means that the entire optical path length is about d. Since uncoded wireless data transmission requires an SNR of at least 10 dB to provide reasonable BER (less than 10^{-5}) in additive white

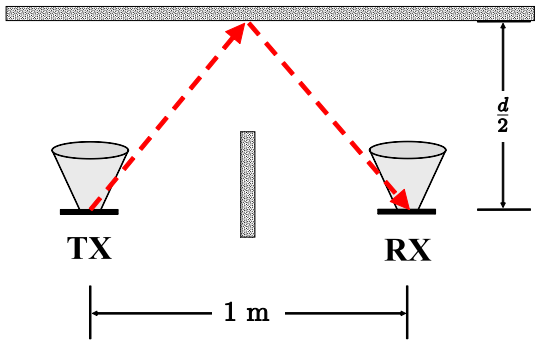

Figure 4.8: *NLOS transmission setup.*

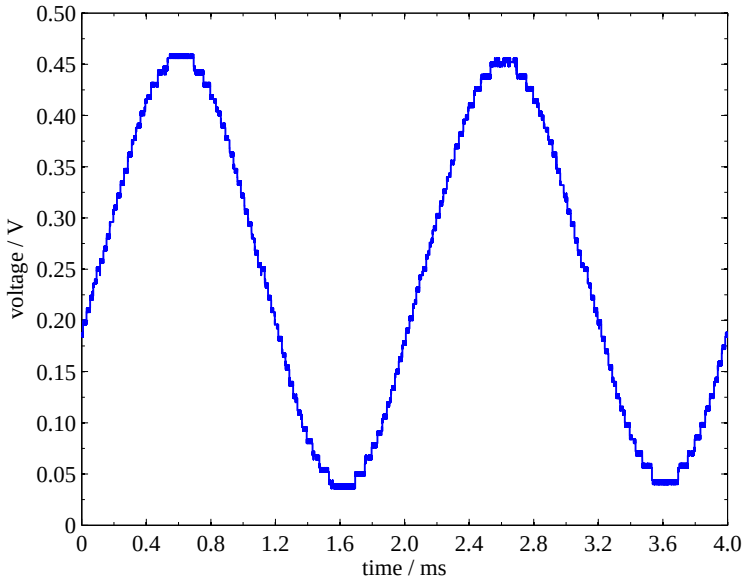

Figure 4.9: *Received sine wave transmitted by optical wireless transmitter front-end employing discrete power level stepping.*

Gaussian noise (AWGN) channels [23], the implemented transmitter enables a transmission of up to 5.0 m in LOS scenarios and up to 3.5 m in NLOS scenarios. The achievable transmission distance can be increased if more powerful LEDs are used. Additionally, the amount of LEDs per emitter group can be enlarged to further increase the optical transmission power. The comparison of Table 4.2(a) and 4.2(b) shows that for the same transmission distance, the SNRs of the LOS and NLOS link differ by about 5.5 dB. This difference is induced by the higher transmission loss of the NLOS link due to the wall reflections.

Figure 4.9 displays a received sine wave (with transmission induced noise) transmitted by the optical wireless front-end. The transmission distance is 1 m and a LOS link is considered. As shown, the discrete power level stepping generates a quantized sine wave with discrete amplitude values. Moreover, the sine wave has a DC offset of about 0.2 V due to the non-negativity constraint of the emitted optical signal. The displayed wave closely matches an ideal sine wave. Figure 4.10(a) shows the spectrum of a quantized sine wave which is transmitted by the optical wireless front-end. For means of comparison, Figure 4.10(b) shows the spectrum of a sine wave which is generated by a conventional signal generator. This sine wave is electrically generated without quantization effects and is transmitted via cable. Since a conventional signal generator is applied which provides ideal linearity characteristics, this electrical setup corresponds to an ideal conventional optical transceiver as shown in Figure 4.1

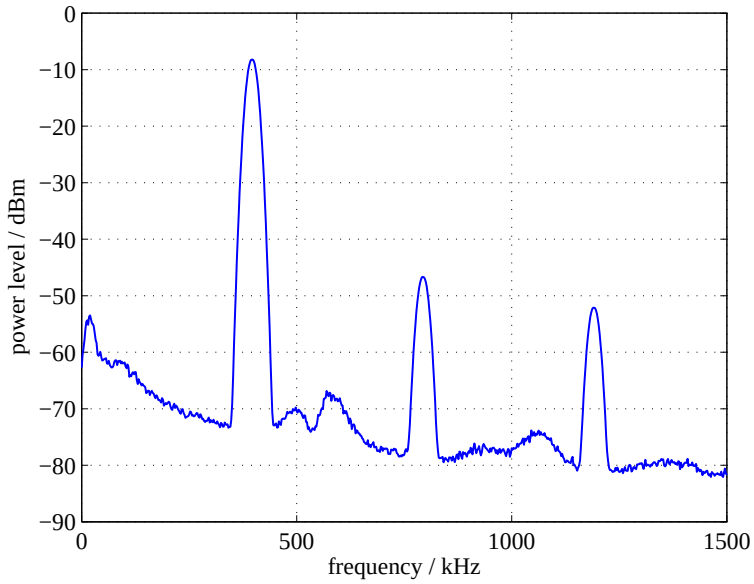

(a) Optical wireless transmission using implemented transmitter front-end.

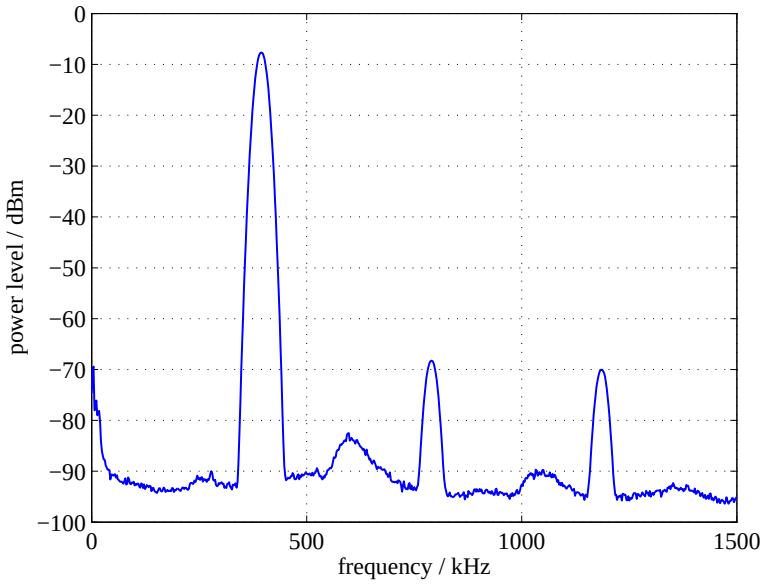

(b) Electrical transmission via cable using signal generator.

Figure 4.10: *Spectrum of sine wave.*

and Figure 4.2. Therefore, the implemented optical transmitter is compared in the following to an electrical transmission using a conventional signal generator. The electrical signal generator represents the reference performance for the implemented optical wireless transmitter. As shown in Figure 4.10, the spectra of the optically and electrically generated sine waves closely match. Besides the actual frequency of the emitted sine wave, the harmonic frequencies can also be seen. Note that both transmission methods use a similar power level to enable a fair comparison. Moreover, it can be seen that the noise level of the electrical transmission is lower. This is due to the fact that the electrical transmission uses a cable connection in comparison to the optical wireless transmission which undergoes ambient light shot noise. Since both spectra closely match, the implemented optical wireless transmitter shows good linearity characteristics. Additionally, Figure 4.11 shows the spectrum of a DCO-OFDM signal. An IFFT size of $L = 256$ is used and 16-QAM is applied. The spectrum of the optical wireless transmission (1 m LOS) and the spectrum electrically generated by the signal generator (transmitted via cable) closely match. Again, the optical wireless transmission undergoes a higher noise level. Figure 4.12 displays the measured frequency gain of the optical wireless transceiver (transmitter *and* receiver). A directed 1 m LOS link between the transmitter and the receiver is established. The optical wireless transceiver has a -3 dB cut-off frequency of about 18 MHz and a -6 dB cut-off frequency of about 25 MHz.

In the following, a M-QAM DCO-OFDM transmission is considered. Each transmitted OFDM frame contains a symbol used for frame detection and synchronisation. Furthermore, each frame comprises several data symbols and a dedicated symbol used for channel estimation. The estimation of the channel coefficient h_l of each OFDM sub-carrier is done by using this pilot symbol. The estimated channel coefficients $\widehat{h}_l$ are used for maximum-likelihood (ML) detection at the receiver. Therefore, for the l^{th} OFDM sub-carrier, the decoder decides for the symbol $\widehat{s}_l$ which minimises the Euclidean distance between the actual received symbol y_l and all potential symbols leading to

$$\widehat{s}_l = \underset{s_l}{\operatorname{argmin}} \left| y_l - \widehat{h}_l \, s_l \right|^2 . \tag{4.2}$$

The QAM symbol transmitted on the l^{th} OFDM sub-carrier is given by s_l. Figure 4.13(a) shows the signal constellation diagram for a simulated 16-QAM DCO-OFDM transmission with 5 bit resolution. This simulation result is obtained for an ideal transmission in a mere AWGN channel without any fading and hardware effects, *i.e.* the received symbol on the l^{th}

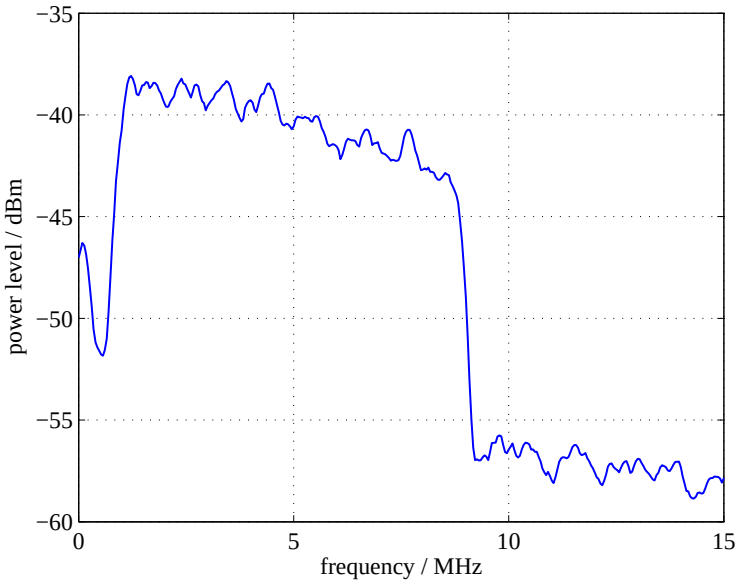

(a) Optical wireless transmission using implemented transmitter front-end.

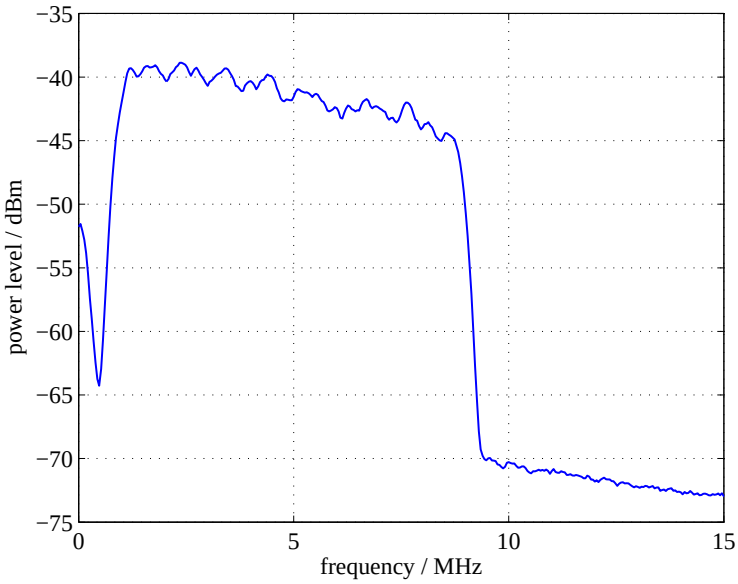

(b) Electrical transmission via cable using signal generator.

Figure 4.11: *Spectrum of DCO-OFDM signal. IFFT size is* 256 *and* 16*-QAM is applied.*

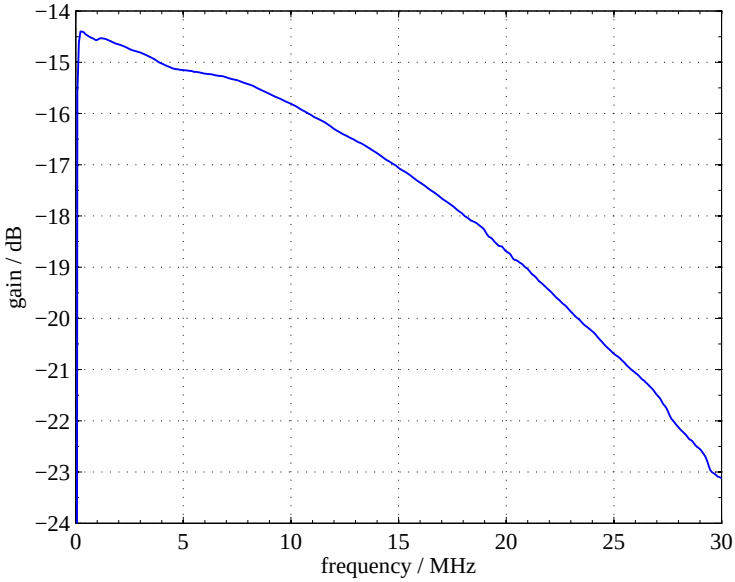

Figure 4.12: *Frequency gain of optical wireless transceiver.*

OFDM sub-carrier is given by $y_l = h_l\, s_l + n_l$ with $h_l = 1$. The AWGN is denoted by n_l. The crosses plotted in Figure 4.13 illustrate the transmitted signal constellation points s_l. The dots represent the equalised received symbols. As a single-tap zero-forcing (ZF) channel equaliser is considered, the equalised received symbols are given by $y_l/\widehat{h}_l$. The simulated SNR is 38 dB which leads to an EVM of about $7.63\,\%$. The EVM is definded as follows:

$$\begin{aligned} \text{EVM} &= \sqrt{\frac{\sum_{k=1}^{K} \left| s_k - \frac{y_k}{\widehat{h}_k} \right|^2}{\sum_{k=1}^{K} |s_k|^2}} \\ &= \sqrt{\frac{\sum_{k=1}^{K} \left(\Im_k - \widehat{\Im}_k \right)^2 + \left(\Re_k - \widehat{\Re}_k \right)^2}{\sum_{k=1}^{K} \left(\Im_k^2 + \Re_k^2 \right)}}, \end{aligned} \tag{4.3}$$

where $\Im_k$ and $\Re_k$ are the imaginary and the real part of the k^{th} transmitted symbol. The imaginary and the real part of the k^{th} equalised QAM symbol $y_k/\widehat{h}_k$ are represented by $\widehat{\Im}_k$ and $\widehat{\Re}_k$. The number of transmitted symbols is given by K. Figure 4.13(b) shows the signal constellation diagram for an actual 16-QAM DCO-OFDM transmission using the implemented optical wireless transmitter. The measured SNR is about 38 dB for a LOS transmission over

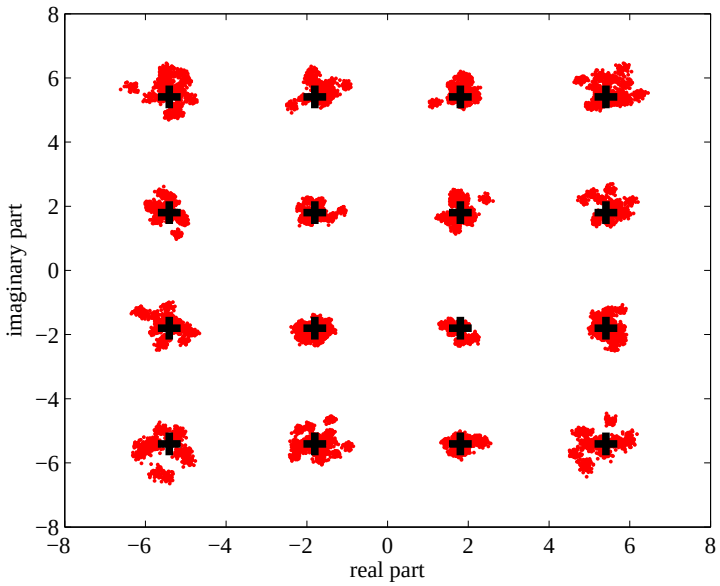

(a) Results for AWGN channel (simulated).

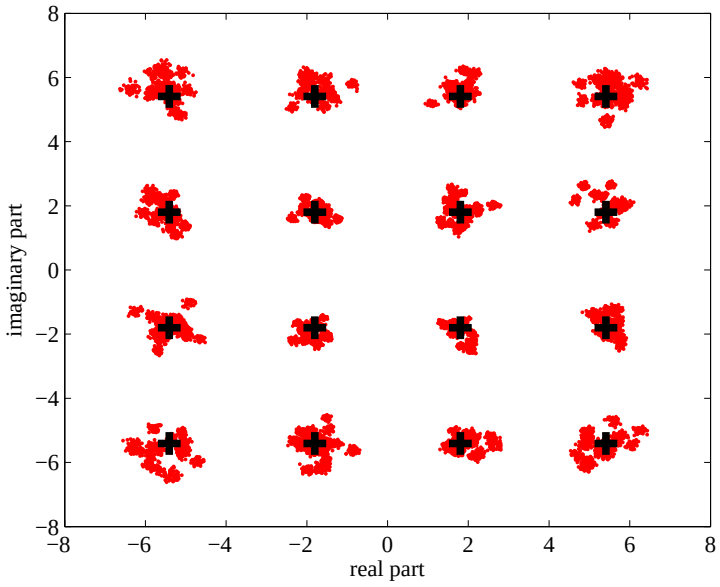

(b) Results using optical wireless transmitter front-end (measured).

Figure 4.13: 16-*QAM signal constellation diagram for DCO-OFDM transmission with* 5 *bit quantization and an SNR of* 38 *dB.*

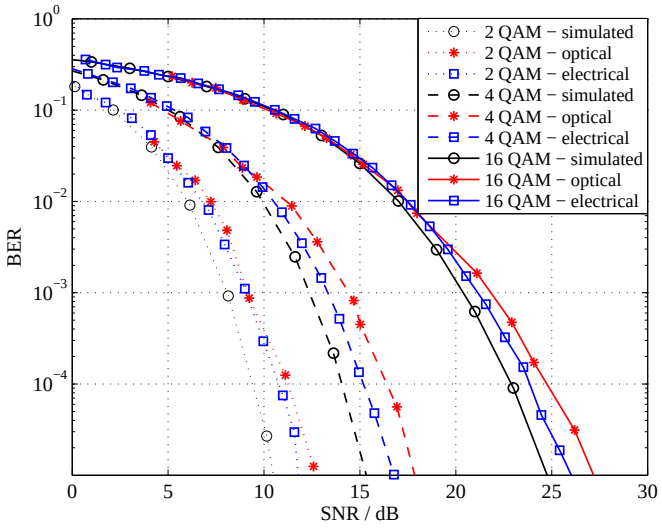

Figure 4.14: *Comparison of simulated BER performance and measured BER performance of DCO-OFDM transmission experiments.*

a distance of 0.75 m. The measured EVM is about $8.42\,\%$. Consequently, the transmission experiments fairly comply with the simulation results.

Figure 4.14 shows the BER performance of a simulated DCO-OFDM transmission using 2-, 4- and 16-QAM. For these simulations, an ideal AWGN channel is assumed as considered above. Moreover, the measured BERs of an actual optical wireless transmission using the implemented transmitter front-end are displayed. A relation between SNR and transmission distance for the optical wireless transmission is given in Table 4.2. Additionally, the results of an electrical DCO-OFDM transmission are shown as well. The electrical transmission is done using the same (de)modulating hardware (waveform generator and oscilloscope) and signal processing as for the optical wireless transmission. However, the optical transmitter and receiver front-ends are replaced by a DAC generating analogue electrical signals. Moreover, the optical wireless link is replaced by a cable which directly connects the transmitter and the receiver. Since the electrical signal generator has ideal linearity characteristics, it can be regarded as an ideal conventional optical transceiver. As shown, the BER performance of the three scenarios is identical for low SNR values. This is due to the fact that at low SNRs, the noise is the most predominant impairment affecting the link performance. However for higher SNR values, the electrical transmission has a performance loss of about 1 dB compared to the simulation results. This is due to practical realisation issues and hardware effects like frequency offsets between the transmitter and the receiver. These effects are not

considered in the AWGN simulations. Because of these hardware limitations, the performance of the electrical transmission represents the practical performance bound of the transmission experiments. This bound cannot be exceeded with the used setup and devices. Consequently, the performance of the wired electrical transmission system can be considered as the target performance for the optical wireless transmission. As illustrated, the performance of the implemented optical wireless transmitter closely matches the performance of the wired electrical transmission. The minor performance loss is due to the actual transmitter *and* receiver implementations. The receiver implementation is not within the scope of this work but it might be optimised separately. Moreover, the optical transmission is wireless compared to the electrical transmission which is wired. This results in an additional performance degradation due to the nature of wireless transmission. Therefore, the proposed optical wireless transmitter concept shows good performance as its BER closely matches the theoretical and practical error bounds.

4.6 Summary

An optical wireless transmitter which employs discrete power level stepping has been developed. The transmitter consists of several LED groups which can be switched on and off individually. The LED groups emit specific stepped optical intensities which constructively add up at the receiver. Therefore, the optical wireless transmitter can be used for intensity modulated signal transmission using techniques like PAM or OFDM. The proposed transmitter concept has good linearity characteristics and is not subject to the non-linear optical-power-versus-current characteristic of LEDs compared to conventional optical wireless transmitter front-ends. Complex pre-distortion techniques are not required. The transmitter is controlled by simple digital signal modulation, *i.e.* on-off-switching of the LED groups. Therefore, the implemented transmitter provides a larger dynamic range and higher optical output power compared to conventional optical transmitter front-ends which have to carefully adjust the bias point and operating area of the LEDs. Moreover, the proposed solution enables a very simple and cost-effective transmitter design without the need for DACs or complex amplifier circuits. The digital-to-analogue conversion is done in the optical domain by the superposition of the emitted discrete intensities. Additionally, the proposed transmitter concept has a better power efficiency as it does not require high-bandwidth/high-current TCAs which waste power. Transmission experiments prove the functionality of the implemented optical

wireless transmitter as its performance closely matches the theoretical and practical error bounds. The performance of the implemented optical wireless transmitter is nearly similar to an electrical transmission. The latter provides ideal linearity characteristics, and therefore corresponds to an ideal conventional optical transceiver.

Chapter 5
Wireless data transmission for in-flight applications using visual codes

As shown in Chapter 3, multiple-input-multiple-output (MIMO) techniques improve the spectral efficiency of intensity modulation (IM) and direct detection (DD) based optical wireless transmission systems. The parallel transmission of data on multiple links provides spatial multiplexing gains which enable increased data rates. Consequently, these gains can compensate for the limited modulation capability of off-the-shelf optical devices. In this chapter, a novel approach for wireless data transmission within an aircraft cabin is presented which makes practical use of spatial multiplexing gains. The proposed transmission system constitutes a highly parallel optical MIMO system which applies spatial multiplexing (SMP) to compensate for the low bandwidth of the employed optical transmitter (display) and receiver (camera). The line-of-sight (LOS) characteristic of the considered setup and the employed optical devices provide a large number of separate optical wireless channels. In contrast to the work presented in Chapter 3.2, different optical wavelengths (colours) are not used to improve the differentiability of the multiple channels, but to increase the data rate. Forward error correction (FEC) schemes are used to improve the reliability of the data transmission. In accordance with Chapter 4, where the importance and benefits of a simple and cost-effective transceiver design are discussed, the approach presented in the following represents a low-complex and low-cost optical wireless transmission system.

The increasing demand for pervasive connectivity also affects the aviation sector. More and more users want to use wireless services also during flights. In order to increase passenger comfort during flights, airlines intend to provide, *e.g.*, information about on-board shopping, in-flight magazines, news or information about the destination such as airport maps, hotels, rental cars and public transportation. Besides this general information, passenger specific data and services, like direction information for connecting gates, departure time of connecting flights and travel plan updates, are to be provided as well. This information is often not fully known before the passenger boards the aircraft, especially if the current flight is delayed. It

is desirable that the passengers can download the information on their own mobile devices for easy and ubiquitous access. In order to provide a reasonable amount of information, several kB of data have to be transferred. Typical file sizes are about $300 - 400$ kB. As passenger specific data is to be transmitted, aspects like security and privacy have to be considered. Interception and fraudulent access of the passengers' data have to be prevented. Even more important, the transmission system has to comply with high safety requirements as potential access to the sensitive on-board systems has to be prevented. Additionally, the data transmission must not interfere with the on-board systems. Within the aircraft cabin, the data transmission service has to be provided to all passengers. This results in several hundreds of users which might simultaneously use the service to download passenger specific data. Consequently, the bandwidth has to be shared between all passengers if common wireless transmission techniques are applied. Conventional radio frequency (RF) communications cannot be easily employed in sensitive environments like aircraft cabins. Firstly, RF signals can interfere with the electronic on-board systems. Secondly, as aeroplanes are operated globally, wireless in-flight RF communications is subject to stringent frequency regulation of local authorities.

A few airlines already provide wireless services to their passengers on some selective flights [133, 134]. However, the airlines have to make large investments to provide the necessary infrastructure within the aircraft cabin and to upgrade existing aeroplanes. This is due to the fact that wireless communications requires the installation of complex and costly hardware equipment such as access points and transceivers. Moreover, these installations cause maintenance effort and increase the weight, and consequently the fuel consumption of the aircraft. A large number of existing aeroplanes is still not equipped with wireless in-flight services.

Instead of using dedicated RF based data transmission, optical wireless communications (OWC) can be applied within the aircraft cabin. Optical signals are neither subject to frequency regulation nor do they interfere with electronic devices. The application of OWC for aircraft intra-cabin communication has already been studied in [135–138] for instance. However, all these systems require additional complex hardware equipment, *i.e.* special optical transmitters and receivers which have to be installed into the aircraft cabin. This hardware equipment is not commercially available up to now. Moreover, the studies presented in [135–138] imply the division of the aircraft cabin into several individual communication cells. The available bandwidth has to be shared between all users (passengers) and elaborate medium access

control schemes have to be implemented. Due to these reasons, a simple wireless transmission system is favoured which is cost-efficient, safe and easy to maintain. Moreover, a software based solution which reuses available hardware is largely preferred as it can be readily integrated into existing aeroplanes.

In the following, a simple optical wireless data transmission method for in-flight applications is proposed. The developed solution addresses the shortcomings of conventional wireless systems such as complex system implementations and required hardware installations. In detail, the proposed application uses visual codes to transmit data. The data to be transmitted, *e.g.* text documents or images, is encoded into a sequence of several visual codes. This "visual code video" is displayed on the screen of the in-flight entertainment (IFE) system. The visual code sequence is captured and decoded by a user device which acts as receiver. Conventional visual codes are only black-and-white. In this work, the black-and-white visual codes are extended to coloured visual codes in order to increase data rate. The contributions of this chapter are as follows: Firstly, a novel approach for wireless in-flight data transmission is presented. The functionality of the proposed approach is demonstrated under realistic conditions within an aircraft cabin mock-up. Secondly, a sequence-wise FEC encoding scheme is implemented. This FEC encoding scheme is evaluated and compared to the existing FEC schemes of conventional visual codes. Typically, visual codes employ a frame-wise FEC encoding. Finally, a synchronisation approach is developed which enables the reconstruction of the transmitted data and the detection of frame transition artefacts.

The remainder of this chapter is organised as follows: In Section 5.1, the concept of using visual codes for data transmission is shown and related work is reviewed. Section 5.2 introduces the in-flight application scenario and overviews the proposed transmission system. It is shown how passenger specific data can be transferred to a user device via the IFE system of an aircraft. Section 5.3 presents the visual encoding and decoding approach developed within this work. In Section 5.4, the FEC techniques of conventional visual codes, specifically of quick response (QR)-codes, are introduced. The limitations of these techniques are analysed and a sequence-wise FEC encoding approach is developed which overcomes these limitations. Section 5.5 shows the results of transmission experiments which have been conducted within an aircraft cabin mock-up under realistic application conditions. Finally, Section 5.6 concludes this chapter.

5.1 Visual codes for data transmission

Visual codes are optical machine-readable representations of data which can be decoded by appropriate code readers. These so-called scanners are equipped with photo-sensors to capture the visual code. Visual codes have become popular due to their fast readability and data storage capacity. The encoded information can be made up of any kind of data, *e.g.* binary or alphanumeric data. There exist several different codes like 1-dimensional barcodes [139] or more sophisticated 2-dimensional codes such as Data-Matrix-codes [140], Maxi-codes [141], Aztec-codes [142] and QR-codes [143]. For instance, QR-codes consist of black modules arranged in a square pattern on a white background as shown in Figure 5.1. The upper

Figure 5.1: *Structure of a QR-code.*

left, upper right and lower left corners of these visual codes contain three identical position detection patterns. These patterns comprise three superimposed concentric squares. The capturing receiver identifies the location and the orientation of the visual code by detecting these patterns. The inner part of the QR-code contains various sections. Besides some meta information about size and encoding format, the code contains additional alignment patterns to assist the reading process in determining the module grid and maintaining its accuracy. A horizontal and a vertical line pattern enable the detection of the module density. These patterns consist of a row, respectively of a column of alternating black-and-white modules. The complete visual code is surrounded by a white “quite zone”. The data section contains the actual payload and additional error correction codewords. These error correction codewords enable the QR-code reader to compensate for module errors without loss of data. This induced

redundancy allows the recovery of the encoded data even if some parts of the QR-code cannot be fully recovered, *e.g.* due to damage or erroneous capturing of the visual code. According to [143], 4 different redundancy levels and 40 different sizes of QR-codes, referred to as version $1 \ldots 40$, are defined. Due to their specific shape, these 2-dimensional visual codes are robust to visual distortion and enable fast readability. Typically, visual codes comprise only black-and-white elements as they are mainly designed for print media and have to be robust to abrasion. However, there also exist special coloured codes like Microsoft's Tag [144]. Commonly, visual codes encode only simple information like uniform resource locators (URLs) or the name of a product. As visual codes provide only low data density [145, 146], extensions are required that mitigate the limitations in data capacity if these codes are to be applied to wireless communications.

In order to enable practical wireless data transmission by visual codes for the envisaged scenario, the following requirements have to be fulfilled:

- A data rate of at least several kbit/s has to be provided.
- The application has to be independent of the viewpoint, *i.e.* there is no fixed alignment.
- The application has to be able to recover frame loss.
- Low-cost user devices and existing displays have to be employed.
- The camera and the display are not synchronised and work independently.
- The system has to be simple and has to be easily operated by the user.
- The system has to operate under realistic conditions with regard to ambient illumination and transmission distance.

There has been some work on using visual codes for wireless data transmission. For instance, in [147], unsynchronised 4-dimensional visual codes are used for wireless data transfer. The authors combine three different 2-dimensional Data-Matrix-codes in the complementary colour channels red, green and blue to one common frame. Several of these frames are displayed in a temporal sequence resulting in a coloured visual code video. The authors count time and colour as third and fourth dimensions. The goal of their work is to provide high robustness of the transmission system by adding redundancy instead of providing high data rates. To this end, the authors propose a redundancy concept which uses frame-duplication to restore lost frames

and to address synchronisation issues. Due to the high redundancy caused by frame-duplication, the reported system achieves a low throughput of only 23 characters per second with a success rate of $82\,\%$. The total size of the transmitted text is 700 characters. This amount of data can be encoded into a single visual code by the application presented in this work. As shown in Section 5.5, the developed application provides a data capacity of up to 1158 bytes per frame. In [148], another transmission system using coloured visual codes is presented. The setup uses a current high-end smartphone (Samsung Galaxy SII [149]) for capturing the visual codes. The system is reported to achieve a theoretical throughput of only 430 byte/s. Consequently, the transfer of 1 MB takes more than 20 minutes which disallows a practical application. In [57, Ch. 8] and [150] a LOS image transfer system is described, which uses a pixelated display (a liquid crystal display (LCD)) as transmitter and a digital camera as receiver. In order to transfer data, a sequence of 2-dimensional intensity images is displayed on the LCD. The intensity images are generated by applying a 2-dimensional orthogonal frequency division multiplexing (OFDM) transmission scheme. The authors investigate the capacity of this 2-dimensional OFDM approach and report a low speed point-to-point transmission experiment. The authors consider a static setup and employ a high-end camera in their experiments. Frame loss is not taken into account by the authors. In [151], a similar system called *PixNet* is proposed. The encoding of the images is also based on an OFDM scheme, whereas the corner detection uses the Data-Matrix detection algorithm [140]. The authors report to achieve a data rate of up to 12 Mbit/s at a distance of 10 m. However, this performance is achieved by using static setups. Additionally, sophisticated high-definition cameras and a large 30 inch display are employed within the setup. A low-complex implementation which can be applied to simple mobile devices is not within the scope of the authors. Moreover, effects caused by frame loss are not taken into account by the authors.

A detailed comparison of different visual codes and visual encoding techniques is beyond the scope of this thesis. A simple encoding technique is envisaged which can be efficiently implemented on common mobile devices. Therefore, the widely used QR-codes are employed in the following, whereas other visual codes might be used as well. Specifically, the corner detection, rectification and binarization techniques of these codes are used as shown in Section 5.3. Since QR-codes are well-established, they can be reliably received and decoded by nearly all current mobile devices. To the best of the author's knowledge, all work done so far does not specifically handle the aspect of encoding redundancy into the visual code sequence to compensate for frame loss while providing practical data rate.

5.2 System overview: in-flight transmission of passenger specific data

In order to address the requirements of wireless in-flight applications presented above and to overcome the shortcomings of conventional wireless techniques, a new approach for wireless data transmission within the aircraft cabin is proposed. This approach enables the download of passenger specific data, *e.g.* files, from the on-board IFE system onto a user device. The data is transferred by a sequence of visual codes. Figure 5.2 illustrates the proposed transmission system. The central IFE server transfers the visual code sequence to the IFE display at the passenger's seat. The detailed procedure of the data transmission via visual codes is displayed in Figure 5.3. Firstly, the file, *e.g.* text documents or images, is compressed to reduce the amount of data which is to be transmitted. In addition, the file can be encrypted to provide security and privacy of the passenger specific information. Secondly, the encrypted and compressed file is FEC encoded to compensate for potential transmission errors. In a third step, the FEC encoded data is segmented into several packets. Each of these packets is visually encoded by a visual code resulting in a sequence of several visual codes. Fourthly, this visual code sequence is displayed in a continuous loop on the IFE screen like a common video film. The intended receiver, *i.e.* the user device, can start the capturing at any time without the need for an initial synchronisation. This asynchronous transmission enables a simple handling as the passenger has only to record a video of the IFE display using the built-in camera of the user device. In a fifth step, the captured visual codes are visually decoded. The visually decoded data packets are reassembled in the correct order by means of additionally encoded meta information which provides the packet number. The reassembling reconstructs the originally FEC encoded

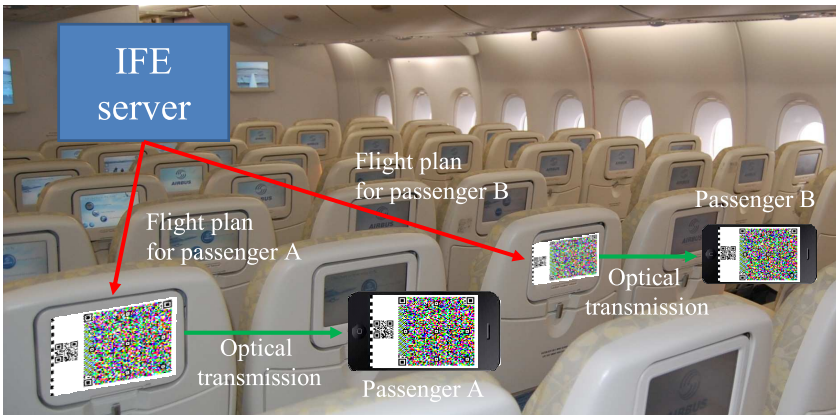

Figure 5.2: *Setup for transmission of passenger specific data.*

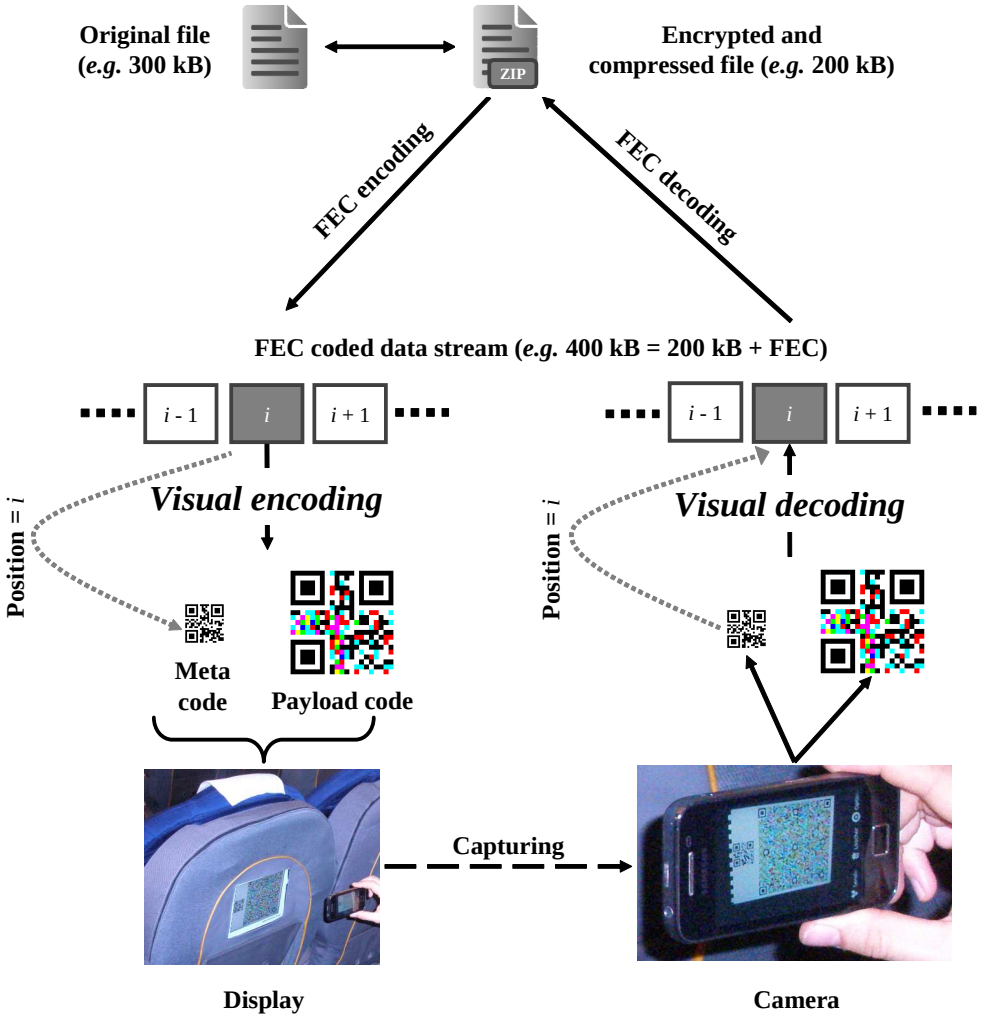

Figure 5.3: *Data transmission using visual codes.*

data stream. In a sixth step, the FEC encoded data is decoded. Due to the induced FEC, errors which arise during the transmission and capturing process can be corrected. Finally, the FEC decoded data is decrypted and uncompressed, and the reconstructed file is stored on the user device. As a result, the users can access the data on their own devices at any time, can edit the data (*e.g.* fill out documents) or zoom into maps for instance. The passengers interact with the transmission system via the touch-screen of the IFE system [152–154]. For instance, they can choose the desired data and apply settings for the data transfer via the touch-screen.

As the IFE system can display the desired content on-demand [155], the wireless data transfer can be individually and simultaneously used by each passenger via the respective IFE display. The bandwidth has not to be shared between several passengers. Moreover, the proposed

application enables only the transmission of data to the passenger's mobile device. This uni-directional communication provides a fundamental safety feature as there is no uplink connection from the user device to the sensitive on-board systems, *i.e.* the user device cannot send data to the aircraft system. The major benefit of the proposed transmission system is that it reuses the existing IFE equipment without the need for any additional hardware installations. The system requires only a software update of the existing IFE system and an application to be installed on the user device. This software comprises the visual coding algorithms and a simple communication protocol to provide some meta information for the data transfer. Therefore, the proposed transmission system is a low-complex and low-cost solution which is especially suitable for so-called retro-fits as it can be easily applied to existing aeroplanes.

5.3 Visual encoding and decoding

As the application is to be used within the aircraft cabin, specific conditions like illumination constraints or motion of the hand-held camera have to be considered. Moreover, the visual transmission is largely affected by the employed hardware equipment. The intended transmitter and receiver devices have specific characteristics. On the one hand, displays usually build up images line-wise. This means that the display is not completely refreshed at once. On the other hand, cameras typically have a so-called rolling-shutter. The rolling-shutter causes a vertical or horizontal scanning of the camera across an image. Additionally, low-cost built-in cameras have a small aperture. Therefore, these cameras require long exposure times, especially in lowly illuminated environments.

Since there is no synchronisation between the IFE display and the built-in camera of the user device, these hardware characteristics cause distortions if the displayed image changes during the capturing process. As a consequence, transition artefacts between two consecutive frames arise. A potential transition effect which may occur is frame splitting. The effect of frame splitting is illustrated in Figure 5.4(a). As shown, two consecutive frames partially overlap. Both frames form the top and the bottom part of the captured image. This transition artefact is caused by the line-wise rendering of the display and by the rolling-shutter of the camera. Another potential transition effect is frame shadowing. Frame shadowing is caused by the superposition of two consecutive frames. Cameras capture images by integrating the impinging light over a period of time (exposure time). If the displayed frame changes during this period of time, two consecutive frames are superimposed by the camera. As illustrated in

(a) Effect of frame splitting: complete frame (left) and split frame (right).

(b) Effect of frame shadowing.

(c) Effect of motion blur.

Figure 5.4: *Illustration of distortions and transition artefacts caused by visual transmission (images captured with Apple iPhone* 4 *smartphone).*

Figure 5.4(b), this interference causes a grey-scale image which impedes the correct detection of the black-and-white modules of the visual code. Finally, if the hand-held camera is moved during the capturing process, motion blur occurs. The effect of motion blur is shown in Figure 5.4(c). Due to the movement of the camera, the captured image represents an integration of the impinging light along the direction of movement causing a blurred image.

If coloured visual codes are considered, additional distortions occur and further effects have to be taken into account. In Figure 5.5, a captured coloured visual code is decomposed into the three colour channels red, green and blue (RGB). Compared to black-and-white visual codes, coloured visual codes have a reduced optical contrast. The reduced contrast corresponds

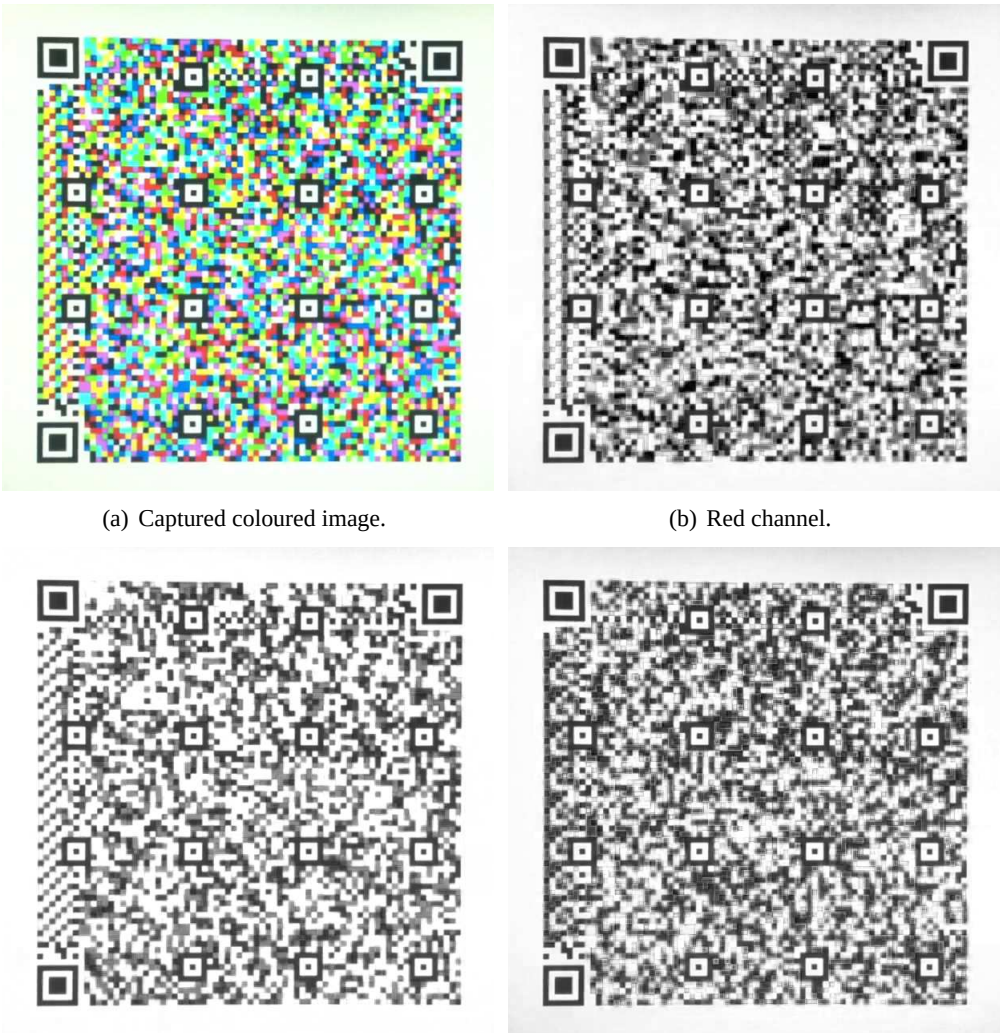

(a) Captured coloured image. (b) Red channel.

(c) Green channel. (d) Blue channel.

Figure 5.5: *Captured coloured image and decomposed colour channels red, green and blue.*

to a reduced distance of the signal constellation points which are encoded in the RGB colour space. For instance, the colour red has a value of $(255, 0, 0)$ in the RGB colour space and the colour blue has a value of $(0, 0, 255)$. The colour white has a value of $(255, 255, 255)$ and the colour black has a value of $(0, 0, 0)$. As a result, the Euclidean distance between the colours red and blue is smaller than the distance between the colours white and black. Moreover, colour channels suffer from cross-talk causing "colour mixing", especially if low-cost image sensors are used. Cross-talk occurs when photons impinging on one pixel are additionally sensed by other pixels of the image sensor. For instance, green coloured light pointing to a green pixel can additionally hit an adjacent blue pixel. As a consequence, the blue pixel shows a response and registers more blue coloured light than is actually present in the captured image. This

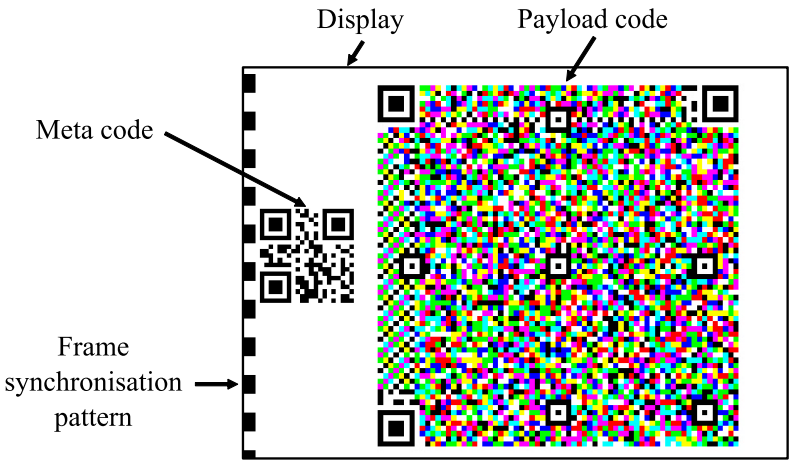

Figure 5.6: *Frame setup of visual codes. The proposed visual codes consist of three parts: payload code, meta code and frame synchronisation pattern.*

optical cross-talk between the pixels reduces the colour resolution and creates noisy images. As shown in Figure 5.5, the red and blue channel undergo higher noise, and thus higher distortions compared to the green channel. Nonetheless, the green channel suffers also from higher noise compared to pure black-and-white visual codes which provide the highest optical contrast (see Figure 5.4(a) left hand side). All these effects and the resulting distortions have to be taken into account to enable a reliable data transfer via visual codes.

In the following, the employed visual encoding and decoding techniques are described which address these effects. Figure 5.6 illustrates the proposed frame setup of the visual codes. As shown, the frames are composed of two individual visual codes: a meta code and a payload code. The payload code comprises the actual data to be transmitted. This code is displayed on the right hand side of the IFE screen. The payload code contains the conventional QR-code detection patterns (concentric squares) used by the receiver for detection and rectification of the visual code. The implemented visual encoding application uses code of the *libqrencode library* [156] which generates conventional black-and-white QR-codes for a given input data. In order to generate the payload code, this open source code has been modified by removing the conventional frame-wise FEC coding scheme. Instead of the conventional FEC coding, the payload data is encoded using the proposed sequence-wise FEC scheme to compensate for detection errors and frame loss caused by motion blur for instance. Details about the FEC scheme are given in Section 5.4. The FEC encoded data bits are visually encoded by

black-and-white modules using the modified *libqrencode library* code, respectively by coloured modules using an additionally implemented merging scheme (see Figure 5.8). Since the data to be transmitted is encoded into a sequence of multiple visual codes, the receiver has to reassemble the captured frames in the correct order. To this end, the receiver has to know the frame number, *i.e.* the index of each visual code within the sequence. This meta information is crucial for the reconstruction of the transmitted data as the receiver and the transmitter are not synchronised and since frame loss may occur. Therefore, this information is separated from the actual payload. For a first implementation approach, the frame number is encoded into an additional meta code. A conventional QR-code is used as meta code which is displayed on the left hand side of the IFE screen (see Figure 5.6). As there is only a small amount of meta information to be transmitted, a small QR-code having a low version number (*e.g.* version $1 - 2$) is sufficient. Moreover, the meta code has the highest QR-code redundancy level to guarantee its correct detection. As the IFE screen has a rectangular shape, there is enough space to enlarge the square payload code to maximum size while still having space for simultaneously displaying the meta code on the left hand side. In order to detect frame transitions and transition artefacts, an additional frame synchronisation pattern is included into the visual code. As shown in Figure 5.6, a black-and-white pattern is added on the left hand side of each visual code. Specifically, two black-and-white patterns (called even- and odd-pattern) are used which alternate frame by frame. The patterns differ only in colour: The even-pattern is a sequence of black-and-white modules and the odd-pattern is the inverted sequence of white-and-black modules.

For visual decoding, the receiver localises the payload code and rectifies it. To this end, the QR-code detection patterns are used. In detail, the localisation and rectification procedure uses the pattern detector algorithm of the open source image processing implementation *ZXing* [157] which is designed for conventional black-and-white visual codes. Figure 5.7 illustrates the visual decoding procedure. In this figure, the grey marked text boxes indicate operations that are done by the image processing implementation *ZXing* [157], *i.e.* corner detection, rectification and binarization, whereas the white marked text boxes indicate additionally implemented operations, *i.e.* colour separation, reassembling of the data packets and FEC decoding. Firstly, the receiver identifies the location and the orientation of the visual code by detecting the concentric squares. Once the corners of the visual code are found, a projective transformation, a so-called homography, is applied. Perspective distortions are rectified by aligning the patterns of the captured image with the known square structure of the visual code. After rectification,

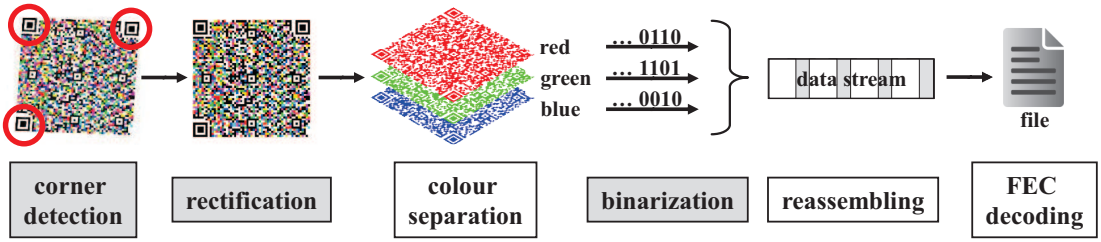

Figure 5.7: *Visual decoding procedure. Grey boxes indicate operations done by image processing implementation ZXing [157] and white boxes indicate additionally implemented operations.*

the rectified visual code is binarized. To this end, a histogram of the intensity values of the captured image is generated. The two maximum peaks of this histogram are considered as the white reference point and the black reference point. The intensity value that optimally separates this two points in the histogram is considered as threshold for the binarization. Using this threshold, the decoder decides if a pixel is black or white, respectively if it is a binary one or zero.

In order to enhance the data rate, coloured payload codes are used. As illustrated in Figure 5.8, three independent single-coloured payload codes, which correspond to three consecutive data packets, are combined to one common coloured payload code. The first payload code is coloured red, the second code is coloured green and the third code is coloured blue. Each colour corresponds to the red, green and blue photo-receptors on the camera chip. Therefore, these colours represent three complementary colour channels. The three colour channels, and thus the three payload codes, are simultaneously displayed on the screen of the IFE

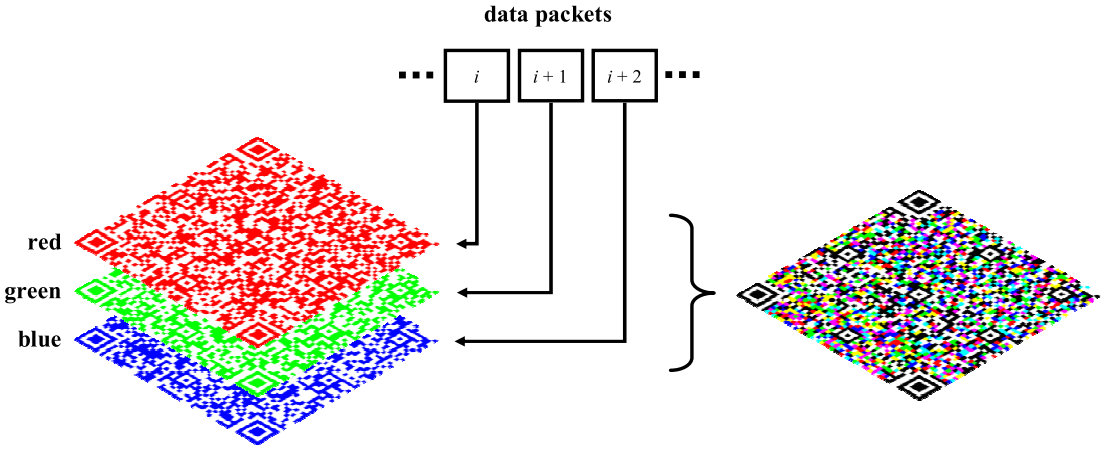

Figure 5.8: *Merging of three single-coloured payload codes into a coloured payload code.*

system. Consequently, the throughput is increased by a factor of three compared to simple black-and-white payload codes. Depending on the data to be transmitted, the combination of the three visual codes results in one coloured visual code which can have 8 different colours: white, black, red, green, blue, yellow, cyan and magenta. As the three visual codes have the same basic shape, their detection patterns are identical. Therefore, the detection patterns of the three payload codes superimpose to the conventional black-and-white patterns as shown in Figure 5.8. As a result, the receiver can employ the conventional localisation and rectification algorithm as presented above. However, each colour channel is binarized individually. The captured coloured payload code is decomposed into three separate black-and-white visual codes as shown in Figure 5.7. These three visual codes are separately binarized using three individual binarization thresholds. As a result, colour distortions caused by ambient light as well as by display and camera effects can be compensated. The binarized data packets are reassembled to reconstruct the entire data stream. Finally, the FEC encoded data stream is decoded to compensate for transmission errors and to reconstruct the original data.

As discussed above, the display and the camera are not synchronised. In order to ensure that the camera captures all displayed frames, the displaying rate of the visual codes is set to half the capturing rate of the camera. The capturing rate of the camera is about 30 frames per second (fps). Therefore, the displaying rate of the visual codes is set to $10 – 15$ fps. The screen has an image build-up time of about 17 ms, *i.e.* a response rate of about 60 Hz. The relation between displaying and capturing is shown in Figure 5.9. As illustrated, the receiver performs an oversampling and captures a displayed frame several times. This oversampling ensures that each displayed frame is at least once captured correctly without transition effects. The other captured frame copies might undergo transition effects. For optimal processing, the transition artefacts (illustrated by "X" in Figure 5.9) have to be filtered out by the receiver because they are highly distorted. This means that the receiver has to select the best captured images for the decoding process. The functionality of the developed selection process is as follows: For each captured frame, the frame synchronisation pattern (see Figure 5.6) is correlated with the original even- and odd-pattern. The captured frame is classified according to the pattern version which provides the highest correlation score, and thus is classified as even- or odd-frame. As long as the detected pattern version does not change compared to the previous one, the frame is added to a buffer. As soon as a new pattern version is detected, the frame with the highest correlation score is taken from the buffer and passed to the decoder. Consequently, the frame with the highest correlation score, and thus the frame with least transition effects is chosen for

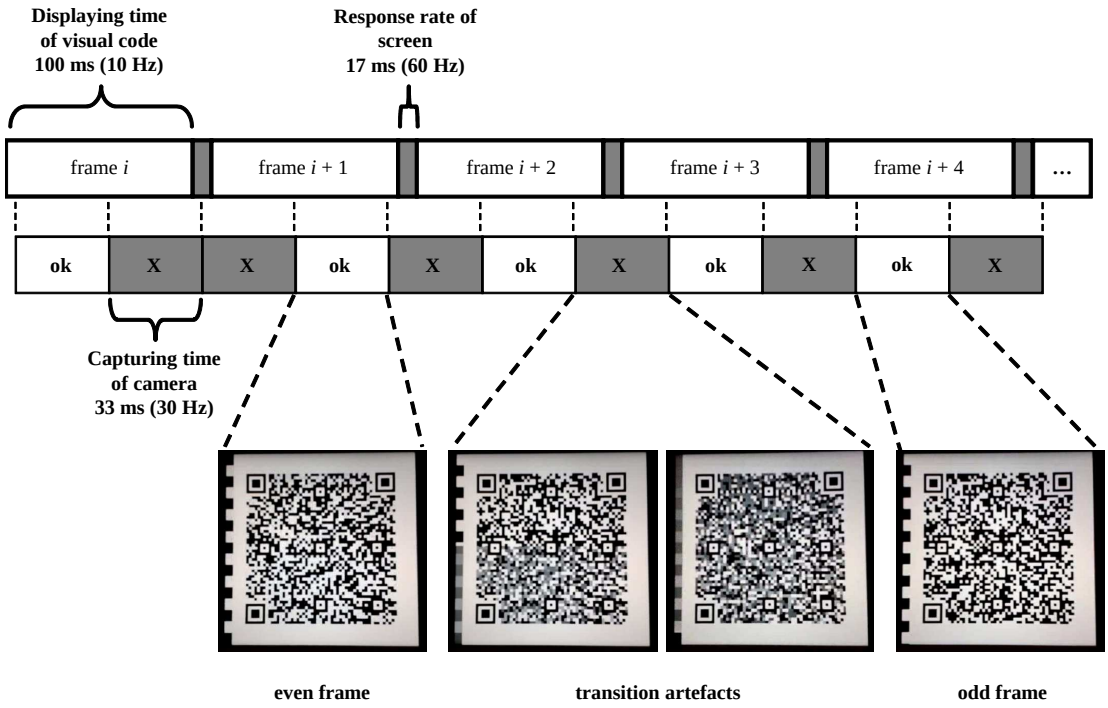

Figure 5.9: *Timing of displaying and capturing process. The upper time line shows how the screen displays the visual code sequence. The displaying is affected by the response rate of the screen and the time each visual code is shown. The lower time line shows the capturing times of the camera.*

further processing to reconstruct the transmitted data.

5.4 FEC coding techniques

Visual codes are primarily designed for print media. The codes have to be robust to abrasion and have to enable reliable decoding. Therefore, visual codes have inherent FEC capabilities to withstand damage without loss of data. In the following, the FEC coding techniques of conventional visual codes are introduced using the example of QR-codes. Commonly, QR-codes employ a frame-wise FEC encoding, *i.e.* error correction codewords are added to the actual data words contained in the visual code. According to [143], four different error correction levels can be employed. Table 5.1 shows these error correction levels and their particular recovery capacity. The recovery capacity depicts the percentage of damaged codewords that can be recovered. The error correction codewords are able to correct two types of erroneous codewords: i) erasures, *i.e.* erroneous codewords at known locations within the

Error Correction Level	**Recovery Capacity**
L	$\approx 7\,\%$
M	$\approx 15\,\%$
Q	$\approx 25\,\%$
H	$\approx 30\,\%$

Table 5.1: *QR-code error correction levels.*

QR-code Version	**Total Number of Words**	**Error Correction Level**	**Number of Error Correction Codewords**	**Error Correction Code**
6	172	L	36	$(86, 68, 9)$
6	172	H	112	$(43, 15, 14)$

Table 5.2: *FEC coding of QR-codes.*

QR-code, and ii) errors, *i.e.* erroneous codewords at unknown locations. An erasure is caused by an unscanned or undecodable symbol character within the visual code. An error is caused by a misdecoded symbol character. For instance, erroneously converting a module from black to white or vice versa results in a misdecoding of the affected symbol character. In this case, the decoder decides for an apparently valid but different codeword than was actually transmitted. QR-codes use Reed-Solomon FEC coding under a Galois field of GF(2^8) as they operate on byte characters. The number of erasures and errors which can be corrected by Reed-Solomon block-codes is given by [143]:

$$e + 2t \leq q - p, \tag{5.1}$$

where e is the number of erasures and t is the number of errors. The number of error correction codewords is denoted by q. Consequently, at least two error correction codewords are required to correct an error. The number of codewords for error detection is denoted by p. These codewords can detect (but not correct) additional errors. If the number of errors exceeds the error correction capacity, the data cannot be reconstructed correctly. Table 5.2 shows two error correction schemes as specified in [143]. The notation of the shown error correction code is

(u, v, m), where u is the total number of words used by the FEC code, v is the number of data words and m denotes the error correction capacity. For instance, a version 6 QR-code contains a total number of 172 words (see Table 5.2). If the error correction level H is used, only $172\,\frac{v}{u} = 172\,\frac{15}{43} = 60$ of the words are actual data words, and thus 112 of the words are error correction codewords. The 112 error correction codewords are able to correct $172\,\frac{m}{u} = 172\,\frac{14}{43} = 56$ misdecoded words. This is $\frac{56}{172} \approx 32.6\,\%$ of the total symbol capacity of the version 6 QR-code. The actual data capacity of this QR-code is $\frac{60}{172} \approx 34.9\,\%$ which corresponds to $\frac{v}{u} = \frac{15}{43}$.

As shown above, the FEC coding of conventional visual codes is done on a per frame basis, *i.e.* the data and the error correction codewords are contained in the same visual code. If a large amount of data, *e.g.* a text-file, is distributed across several visual codes, multiple visual codes have to be decoded individually in order to reconstruct the transmitted data. However, if just one or even several of the visual codes are corrupted and cannot be reconstructed correctly, the complete information is lost. As shown in Section 5.5, frame loss can occur during the capturing process, even though the highest FEC level is employed. Therefore, a sequence-wise FEC encoding of the complete visual code sequence is developed. In the following, this sequence-wise FEC encoding technique is presented.

The developed application is based on the conventional QR-code generation algorithm according to [143]. However, only the corner detection, the rectification and the binarization schemes of these codes (see Section 5.3) are employed. The inherent frame-wise FEC encoding scheme is completely removed. Instead of the frame-wise FEC encoding, the complete data to be transmitted is encoded resulting in a sequence-wise FEC encoding. This encoding approach is illustrated in Figure 5.10. As shown, the data, *e.g.* a text-file, to be transmitted is passed to the encoder. The FEC encoder uses a $(127, 67, 30)$ Reed-Solomon block-code. A Reed-Solomon block-code is chosen to be consistent to the conventional QR-code FEC encoding/decoding. More powerful FEC coding techniques like Turbo codes or soft-decision Viterbi decoding schemes can also be employed. However, these sophisticated coding techniques cannot be efficiently implemented on current mobile devices and may cause large processing delay, high power consumption and low battery life time. The chosen Reed-Solomon code has a data capacity of $\frac{v}{u} = \frac{67}{127} \approx 52.8\,\%$ and a recovery capacity of $\frac{m}{u} = \frac{30}{127} \approx 23.6\,\%$ which is similar to the QR-code error correction level Q. Higher, respectively lower error correction levels can also be employed if higher robustness or higher throughput is required. During a flight, higher robustness may be beneficial due to the swaying

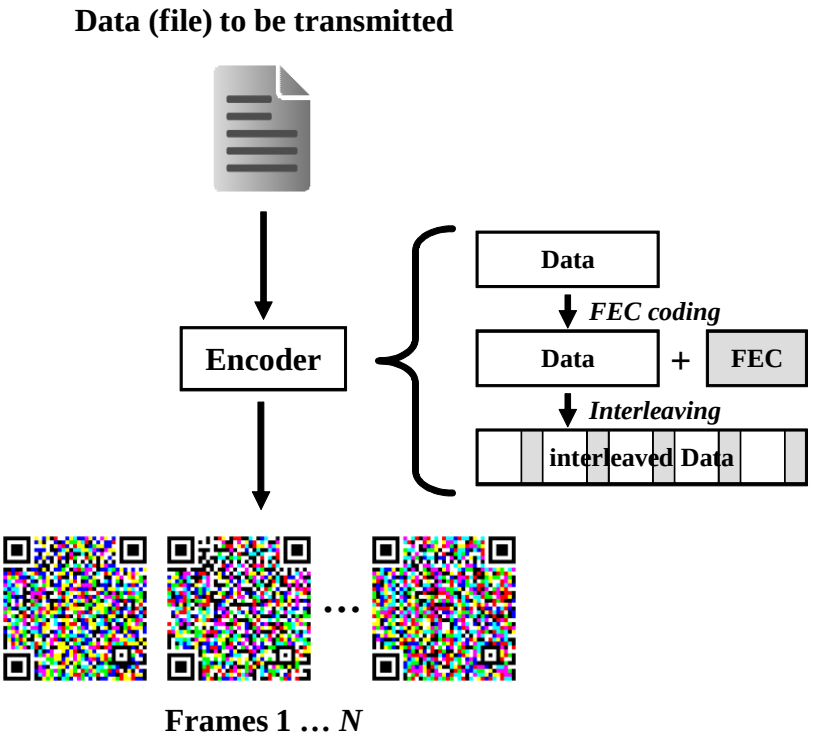

Figure 5.10: *Illustration of sequence-wise FEC encoding.*

motion of the aircraft. For instance, turbulences might cause increased motion blur. During taxiing at the ground, a higher throughput may be required due to time constraints when reaching a connecting flight. The information about the currently employed error correction level can be incorporated into the meta code which contains information to reconstruct the transmitted data, *e.g.* the frame number (see Section 5.3). In order to increase the robustness, the FEC encoded data is interleaved. This means that the FEC encoded data is "randomly" distributed across all frames within the visual code sequence. As a result, burst errors which arise from the loss of complete frames can be compensated by the receiver. Due to the chosen Reed-Solomon code, the data can be correctly reconstructed if up to about a quarter of the visual code sequence is completely missing. Consequently, the developed sequence-wise FEC encoding is able to compensate for frame losses. The encoded and interleaved data stream is segmented into several packets of fixed size. Each packet is processed by the visual encoding method presented in Section 5.3.

5.5 Transmission experiments

In the following, the results of some transmission experiments are presented. The aim of these experiments is threefold: Firstly, the performance of the frame-wise FEC encoding of conventional visual codes is evaluated. To this end, conventional black-and-white QR-codes are used. For this experiment, a low-cost user device is employed as receiver in order to perform a practical evaluation. Secondly, the performance of the developed sequence-wise FEC encoding approach is evaluated. For means of comparison, black-and-white visual codes as well as the same low-cost user device are employed. Finally, the achievable data rate is maximised. To this end, a high-end user device and coloured visual codes are employed to derive an upper performance bound. In order to evaluate the implemented transmission system under realistic conditions, the experiments have been conducted within an Airbus A330 aircraft cabin mock-up. This means that the measurements have been taken within the aspired application scenario under realistic ambient light conditions and transmitter-receiver spacings. The aircraft cabin environment is shown in Figure 5.11. The cabin mock-up is equipped with an IFE system. The screens of the IFE system are installed in the rear side of the passengers' seats. Therefore, each passenger can individually employ the respective IFE display in front of him/her. As the display is a touch-screen, the passenger can interact with the IFE system and can individually choose the content to be displayed on the screen. The IFE screen has a size of about $17\,\text{cm} \times 13\,\text{cm}$ (8.4 inch display) with a resolution of 1024×768 pixels. Figure 5.12 shows the setup of the transmission experiments within the considered application scenario. The passenger records the visual code sequence, which is displayed on the IFE screen, with the built-in camera of the user device, *e.g.* a smartphone. The distance between the transmitter (IFE screen) and the receiver (user device) is about $20 - 30$ cm. As the passenger manually aligns the user device towards the IFE screen, there is no fixed alignment between the transmitter and the receiver. Moreover, as the passengers move their hands during the capturing process, *e.g.* due to turbulences during the flight, the alignment might change for each frame of the visual code sequence. Therefore, the receiver has to individually detect the transmitted visual code within each captured image.

5.5.1 Performance of conventional visual codes with frame-wise FEC coding

In the following, the transmission performance of conventional black-and-white QR-codes with frame-wise FEC coding is evaluated. The data to be transmitted is split into several segments.

Figure 5.11: *Aircraft cabin environment used for transmission experiments. Figures show different ambient illumination conditions which can be applied.*

Figure 5.12: *Setup of transmission experiments.*

Each segment is encoded into one QR-code. These QR-codes are sequentially displayed on the IFE screen and are captured by the user device. The user device is a low-cost Samsung Galaxy Ace smartphone [158]. The built-in camera of this smartphone has a resolution of 640×480 pixels in video mode. Further details about the built-in camera, *e.g.* information about the employed lens and sensor, are not available from the technical specification. In order to compensate for transition artefacts caused by frame shadowing and splitting, the frame rate of the IFE display has to be downsampled to at least 10 fps. The transmission experiments have shown that this is the largest frame rate which ensures that each frame is captured by the employed smartphone at least once without transition effects. Several transmission experiments using different QR-code versions and error correction levels have been conducted. For the

QR-code Version	Error Correction Level	Total Rate (bytes/ frame)	Data Rate (bytes/ frame)	Mean Symbol Error Rate	Data received correctly
9	L	292	230	0	yes
9	H	292	98	0	yes
10	L	346	271	≈ 0.0392	no
10	H	346	119	0	yes
11	L	404	321	≈ 0.0465	no
11	H	404	137	0	yes
12	L	466	367	≈ 0.1060	no
12	H	466	155	0	yes
13	L	532	425	≈ 0.1643	no
13	H	532	177	≈ 0.1561	no

Table 5.3: *Performance of conventional black-and-white QR-codes with frame-wise FEC coding using Samsung Galaxy Ace smartphone.*

experiments, the smartphone is manually aligned in front of the IFE screen resulting in realistic motion effects. After a complete visual code sequence has been displayed on the IFE screen, the captured frames are decoded. For performance evaluation, it is checked if the transmitted data is received correctly and the symbol error rate is calculated.

Table 5.3 shows the data rate (throughput) which can be achieved per frame as a function of the QR-code version and the error correction level. The total rate is the sum of the data words and the error correction codewords per frame. As shown, level H codes have a lower data capacity compared to the level L codes due to the higher redundancy and enhanced error correction capability. Moreover, the measured mean symbol error rate for a transmitted QR-code sequence is shown. It can be seen that due to the lower error correction capability, the level L codes provide a higher symbol error rate compared to the level H codes. The level L codes enable a reliable data transmission, *i.e.* the transmitted data is received correctly, up to version 9. A larger QR-code version disallows the correct reconstruction of the transmitted data, and thus the whole data is lost. Compared to this, level H codes enable a reliable data transmission up to version 12. Using larger QR-codes causes increasing misdetections and erroneously received data. Summing up, version 9 L codes achieve the highest data rate provided that

QR-code Version	Total Rate (bytes/ frame)	Data Rate (bytes/ frame)	Mean Symbol Error Rate	Data received correctly
11	404	213	0	yes
12	466	245	0	yes
13	532	280	0	yes
14	581	306	≈ 0.3107	no

Table 5.4: *Performance of black-and-white visual codes with sequence-wise FEC coding using Samsung Galaxy Ace smartphone.*

the data is received without any errors. The achievable symbol rate of this scenario is about 230 data words/frame $\cdot$ 10 fps $=$ 2300 data words/second. This symbol rate results in a bit rate of 18.4 kbit/s as one data word comprises 8 bits. Note however, that this data rate is achieved without distinct motion effects which might occur during an actual flight given intermittent turbulences. This data rate represents a best case result as additional motion effects induce increased frame loss which cannot be compensated by the frame-wise FEC coding of conventional visual codes. Consequently, this frame-wise FEC coding scheme is not suitable for the proposed application which relies on the transmission of a sequence of several visual codes.

5.5.2 Performance of visual codes with sequence-wise FEC coding

In the following, the transmission performance of the developed sequence-wise FEC coding is analysed. Table 5.4 shows the performance of black-and-white visual codes using the developed FEC coding approach presented in Section 5.4. For means of comparison, the same setup scenario and user device are used as presented above. The results show that the sequence-wise FEC coding approach provides a more reliable data transmission in comparison to the frame-wise FEC coding technique. This is due to the fact that the sequence-wise FEC coding can compensate for the loss of complete frames. As a result, frames which are lost or misdetected can be reconstructed by the receiver if the error/loss rate is smaller than $23.6\,\%$ (depending on the chosen coding rate as shown in Section 5.4). Consequently, the sequence-wise FEC coding technique provides a reliable data transmission, *i.e.* the transmitted data is correctly received, up to visual code version 13. Given the chosen coding rate, this visual code version enables a symbol rate of 280 data words/frame $\cdot$ 10 fps $=$ 2800 data

QR-code Version	Total Rate (bytes/ frame)	Data Rate (bytes/ frame)	Mean Symbol Error Rate	Data received correctly
18	901	475	0	yes
19	991	522	0	yes
20	1085	572	≈ 0.4703	no

Table 5.5: *Performance of black-and-white visual codes with sequence-wise FEC coding using Apple iPhone* 4 *smartphone.*

words/second. This symbol rate results in a bit rate of 22.4 kbit/s. Consequently, the achievable data rate is increased by about $21.7\,\%$ compared to the conventional frame-wise FEC coding scheme.

5.5.3 Enhancement of data rate using coloured visual codes

In the following, the transmission performance of the developed application is analysed for the case of using a high-end user device instead of a low-cost device. Therefore, an Apple iPhone 4 smartphone [159] is used as receiver device. The built-in camera of this smartphone has a higher resolution of 1280×720 pixels in video mode. Moreover, for this user device, the frame rate of the IFE display can be increased to 13 fps. This transmission rate ensures that each frame is captured by this smartphone at least once without transition effects. Furthermore, the built-in camera has a lens focal length of 3.85 mm, a f/2.8 lens aperture and a $1/3.2$ inch back-illuminated CMOS sensor. Table 5.5 shows the transmission performance using black-and-white visual codes with sequence-wise FEC coding for this user device. It can be seen that due to the superior built-in camera and the higher resolution, this smartphone provides an enhanced performance as it enables a reliable data transmission up to visual code version 19. As a result, a symbol rate of 522 data words/frame $\cdot\, 13$ fps $= 6786$ data words/second can be achieved. This symbol rate results in a bit rate of 54.29 kbit/s. This data rate exceeds the achievable data rate of the low-cost smartphone by a factor of about 2.42.

The data rate can be additionally increased by using coloured visual codes. Figure 5.13 shows a captured coloured visual code. As shown, the captured image contains the coloured payload code and the black-and-white meta code which comprises the frame number. For decoding, the coloured payload code is decomposed into the complementary colour channels red, green and blue. This splitting generates three independent visual codes which are separately processed

QR-code Version	Total Rate (bytes/ frame)	Data Rate (bytes/ frame)	Mean Symbol Error Rate	Data received correctly
13	1596	840	0	yes
14	1743	918	0	yes
15	1965	1035	0	yes
16	2199	1158	0	yes
17	2445	1287	≈ 0.4713	no

Table 5.6: *Performance of coloured visual codes with sequence-wise FEC coding using Apple iPhone 4 smartphone.*

Figure 5.13: *Captured coloured visual code (image captured with Apple iPhone 4 smartphone).*

and decoded (see Figure 5.5). By using these three independent colour channels, the data rate can be increased by a factor of three. However, as shown in Section 5.3, coloured visual codes suffer from optical cross-talk and colour mixing. Therefore, coloured visual codes are subject to increased error rates. Table 5.6 shows the transmission performance of coloured visual codes with sequence-wise FEC coding using an Apple iPhone 4 smartphone as receiving device. It can be seen that the visual code version has to be reduced if coloured visual codes are applied. As shown, the transmitted data can be correctly received up to visual code version 16. Nonetheless, a higher symbol rate of 1158 data words/frame $\cdot$ 13 fps $=$ 15054 data words/second can be achieved by using coloured visual codes. This symbol rate results in a bit rate of 120.43 kbit/s which is an increase by a factor of about 2.22 compared to the

User Device	FEC Coding Technique	Colour of Visual Code	Frame Rate (fps)	Bit Rate (kbit/s)
Samsung Galaxy Ace	conventional frame-wise encoding	black-and-white	10	18.40
Samsung Galaxy Ace	developed sequence-wise encoding	black-and-white	10	22.40
Apple iPhone 4	developed sequence-wise encoding	black-and-white	13	54.29
Apple iPhone 4	developed sequence-wise encoding	coloured	13	120.43

Table 5.7: *Performance bounds derived from transmission experiments.*

black-and-white visual codes.

Table 5.7 summarises all performance bounds derived from the conducted transmission experiments.

5.6 Summary

A novel approach for wireless data transmission within an aircraft cabin has been identified. An in-flight optical wireless transmission system has been proposed and developed to transfer passenger specific data to a user device. By displaying visual code sequences on the IFE screen within an aircraft cabin, data can be securely and safely transmitted to a user device. As the application uses existing hardware equipment, no additional hardware installations are required. The proposed approach enables a low-cost transmission system which requires only a software application to be installed on the user device and a software update of the IFE system. Therefore, the application is especially suitable for aircraft retro-fits.

The transmitted frames consist of a meta code, which contains supplementary information like the frame number, and the payload code, which contains the actual information to be transmitted. In a future implementation, these two codes might be combined to one common visual code. The meta information might be included into the payload code by inserting a

meta data field for instance. Furthermore, a selection algorithm has been implemented which uses a synchronisation pattern to detect frame transitions. By applying this algorithm, the receiver is able to choose the captured frames with least transition effects for the decoding process. Transmission experiments within an aircraft cabin mock-up have demonstrated the functionality of the proposed application under realistic conditions. The performance of the uni-directional transmission system has been evaluated. The application provides a throughput of up to 120 kbit/s with current smartphones. This data rate corresponds to the data rate of general packet radio service (GPRS) or integrated services digital network (ISDN) with channel bundling for instance. Tests have shown that 30 seconds are a tolerable time which is accepted by a user (passenger) to capture the IFE screen with a mobile device. This duration is merely derived from subjective perception. Longer capturing runs can also be employed. Considering a capturing time of 30 seconds, a data volume of up to 450 kB can be transmitted by a single visual code sequence which is sufficient to transfer the required amount of data for the proposed application. As the bandwidth has not to be shared between several users, this data rate is available for each individual passenger. For instance in an Airbus A330, 300 – 350 passengers can simultaneously download their passenger specific flight information without any interference.

Transmission experiments have shown that complete frames can be misdetected or lost due to occlusion and movement of the receiver. In order to compensate for misdetections and frame loss, a sequence-wise FEC coding method has been developed. It has been shown that this sequence-wise encoding outperforms the frame-wise FEC coding of conventional visual codes as it provides higher reliability and larger throughput. The transmission performance of the developed application has been evaluated for current low-cost and high-end smartphones. In order to increase data rate, the black-and-white visual codes have been enhanced to coloured visual codes by using the three complementary colour channels red, green and blue for simultaneously transmitting three individual visual codes. These coloured visual codes provide a data rate which is more than two times larger than the data rate of black-and-white visual codes, even though the coloured visual codes suffer from increased noise and cross-talk.

Chapter 6
Conclusions

This chapter summarises and concludes the research work presented in this thesis. The main findings are highlighted and conclusions are drawn. Finally, limitations of this work are outlined and scope for future work is presented.

6.1 Summary and main findings

The ever increasing amount of wireless data traffic provokes alternative transmission techniques to supplement existing radio frequency (RF) communications. Optical wireless communications (OWC) can provide a remedy for the scarcity of available RF spectrum and can evolve into a complementary technology for wireless indoor communications. Chapter 1 has highlighted the motivation and the need for spectrally efficient transmission techniques for OWC. The limited modulation capability of off-the-shelf light emitting diodes (LEDs) restricts the bandwidth of practical intensity modulation (IM) and direct detection (DD) based OWC systems. Therefore, the available bandwidth has to be used in the most efficient way, and consequently spectral efficiency is of great concern for OWC. Chapter 2 has introduced several optical wireless transmission techniques which are typically used in indoor environments. Conventional pulsed modulation techniques as well as multi-carrier transmission techniques and optical multiple-input-multiple-output (MIMO) schemes have been presented. The latter enable large spectral efficiency by spatial multiplexing gains.

Based on this background, the contribution of this research work is threefold: Firstly, in Chapter 3, the applicability and the potential of different MIMO techniques for indoor OWC have been analysed. Specifically, the transmission techniques repetition coding (RC), spatial multiplexing (SMP) and spatial modulation (SM) have been transferred to the optical domain and their performance has been evaluated. The bit error ratios (BERs) of these three MIMO techniques have been derived analytically. To this end, a general framework has been developed which provides analytical error bounds. The derived bounds have been verified by numerical computer simulations. The results show that the considered optical MIMO techniques provide

enhanced spectral efficiency even under static line-of-sight (LOS) conditions which cause high channel correlation. One of the main contributions of this work is the investigation of the various trade-offs of MIMO techniques for indoor OWC systems. The author has shown that the performance of optical MIMO techniques depends on both the signal-to-noise ratio (SNR) and the differentiability of the multiple links. Consequently, both parameters have to be considered to achieve good error performance. It has been found that inducing power imbalance between the multiple optical transmitters is an advisable approach to enhance channel differentiability. Imbalanced transmission power enables the utilisation of optical MIMO techniques under channel conditions which provide only little differences between the multiple links. Without induced power imbalance, these channel conditions typically disallow the application of MIMO schemes. Besides, the power imbalance approach does not affect the decoding process of the receiver. The receiver implicitly detects the induced power imbalance by conventional channel estimation. Moreover, it has been found that blocking some of the links between the transmitter array and the receiver array can also improve the error performance of optical MIMO techniques. Although the blocking reduces the received optical power, and thus affects the SNR, it improves the channel characteristics by easing the differentiability of the multiple links. Consequently, the loss in SNR is outweighed by improved channel differentiability. However, link blockage requires the implementation of opaque boundaries at the receiver device, respectively small field-of-views (FOVs) of the optical receivers. Furthermore, the utilisation of optical transmitters having different wavelengths also improves the differentiability of multiple links. Different optical wavelengths (colours) induce specific power levels at the photo-diode as the responsivity of photo-diodes is a function of the optical wavelength. Consequently, the received power level is directly related to the optical wavelength. The utilisation of different optical wavelengths may be considered as “indirect” frequency multiplexing. This is due to the fact that in DD based OWC the information about the frequency of the optical carrier is commonly lost as only the intensity of the optical signal is detected. Therefore, multiple optical signals superimpose constructively although they have different wavelengths. As a result, the signals cannot be separated in the frequency domain unless specific optical filters are employed. However, it has been shown by the author that the signals can be distinguished according to the specific power levels which they induce at the detector without the need for optical filters. This characteristic is especially suitable for SM which relies on the detection of the activated optical transmitter within the emitter array. The comparison of RC, SMP and SM has revealed that RC is insensitive

to different transmitter-receiver alignments. However, RC requires large signal constellation sizes to achieve high data rates as it does not provide multiplexing gains. In contrast, SMP provides multiplexing gains, but requires high channel differentiability to achieve good error performance. SM is more robust to low channel differentiability and achieves improved spectral efficiency especially at low SNRs. Moreover, it has been demonstrated that SM achieves significant gains if several receivers are employed. Compared to RC, SM offers higher SNR gains with increasing number of receivers. Additionally, SM has the lowest computational complexity. Its simplicity is gained by the fact that SM completely avoids inter-channel interference (ICI) in time and space, in contrast to SMP, while providing an additional multiplexing gain, in contrast to RC. In order to further improve the performance of SM, an enhanced forward error correction (FEC) coded SM scheme has been proposed and evaluated. This scheme jointly encodes the bits conveyed in the spatial domain and the signal domain. It has been found that, compared to the originally proposed Trellis coded spatial modulation (TCSM) scheme [101, 114], this jointly encoding makes better use of the basic SM detection principle: the combined detection of the emitter index and the actually transmitted signal. As a result, the enhanced coded SM scheme provides larger coding gains. To sum up, this work has demonstrated that transmission of data across parallel optical channels is possible and that practical OWC systems could greatly benefit from adaptive MIMO techniques.

Secondly, in Chapter 4, a novel optical wireless transmitter concept has been developed. The basic principle of this concept is that the digital-to-analogue conversion of the signals is done in the optical domain. To this end, the transmitter consists of several on-off-switchable LED groups which emit scaled optical intensities. The emitted optical intensities constructively superimpose at the receiver. As a result, several intensity levels can be generated which enables the transmission of intensity modulated signals, such as orthogonal frequency division multiplexing (OFDM) waveforms. Transmission experiments have demonstrated that the proposed transmitter concept enables data rates of tens of Mbit/s depending on the switching speed of the LED groups. The benefits of the transmitter concept are its simple implementation and its cost-effectiveness. The evaluation of the developed transmitter has revealed its good linearity characteristics and its power efficiency – the key weaknesses of conventional optical wireless OFDM transmitter front-ends. Since OFDM is an effective technique to compensate for inter-symbol interference (ISI) caused by multipath propagation, the proposed transmitter concept is especially suitable to enable high-speed data transfer in diffuse transmission scenarios.

Finally, in Chapter 5, a novel approach for wireless data transmission within an aircraft cabin has been demonstrated. Black-and-white and coloured 2-dimensional visual codes are used for data transmission. The screen of the in-flight entertainment (IFE) system acts as transmitter by displaying a sequence of visual codes. This sequence is captured by the built-in camera of a user device which acts as receiver. The proposed transmission system has several benefits: Firstly, it reuses the hardware equipment which is already available within the aircraft cabin without the need for additional hardware installations. Secondly, the transmission system does not interfere with the sensitive aircraft systems since it is based on OWC. In addition, the transmission is intrinsically safe as the user device has no physical uplink connection to the on-board system. Thirdly, the application can be simultaneously used by all passengers without mutual interference and without sharing the transmission capacity. Since several pixels of the transmitting display are simultaneously captured by the image sensor of the camera, this setup represents a highly parallel optical MIMO system. In order to compensate for frame loss and misdetections caused by occlusion or motion blur, a sequence-wise FEC coding scheme has been developed. Due to the induced redundancy, this scheme is able to correct misdetected pixels and can even reconstruct entire frames. Experiments have shown that the developed sequence-wise FEC coding provides higher reliability and larger throughput compared to the frame-wise FEC coding of conventional visual codes. In addition, a selection algorithm for the frame capturing has been implemented. This algorithm can detect frame transitions which cause frame splitting and frame shadowing. To this end, a synchronisation pattern is included into the visual code sequence. This pattern is evaluated by the receiver by means of simple correlation. As a result, the receiver is able to select the captured visual codes which undergo least frame transition effects. Transmission experiments within an aircraft cabin mock-up have evaluated the transmission system under realistic illumination conditions and geometric alignments. It has been found that coloured visual codes achieve a more than two times larger data rate compared to black-and-white visual codes, even though coloured visual codes undergo increased noise and cross-talk. The tests have shown that the system achieves a throughput of more than 120 kbit/s per individual passenger seat with current smartphones.

6.2 Limitations and scope for future work

It should be noted that all analyses in this thesis are primarily based on indoor propagation environments assuming IM and DD based OWC. In addition, the computer simulations were

performed using a series of system models. Therefore, the results are subject to certain limitations with regard to the considered models and the assumptions made.

The simulations presented in Chapter 3 use realistic system parameters like transmitter-receiver separation distances as well as practical transmitter and receiver FOVs. As a result, the simulations provide a good insight into the performance of optical MIMO techniques. However, this work is based on static system and channel simulations which disregard effects such as dispersion and multipath propagation. Moreover, several specific indoor scenarios are considered. The author recognises that these assumptions constitute a simplification of the channel characteristics. Although the considered geometric channel model fairly complies with practical channel measurements, it may oversimplify actual optical wireless propagation channels. Future work may evaluate the performance of optical MIMO techniques using statistical channel models derived by ray-tracing simulations for instance. The effects of dispersion and induced ISI may be further analysed. Besides, optical MIMO techniques in diffuse non-line-of-sight (NLOS) scenarios may be subject of further investigation. These effects and propagation conditions might provide lower channel correlation, and thus larger intrinsic link differentiability. As a result, they could enable even higher gains compared to the static and highly correlated LOS channels considered in this thesis. As shown, the considered LOS scenario constitutes a worst case scenario with regard to channel correlation. In the context of link differentiability, the application of imaging receivers for optical MIMO transmission deserves further investigation as well. For instance, the "fly-eye receivers" proposed by Yun and Kavehrad [82] enable the separation of signals which arrive from different directions. It is anticipated that such imaging receivers are perfectly suitable for SM which is based on the capability of the receiver to detect the single active transmitter from an emitter array. It has been shown in this thesis that inducing power imbalance between the optical transmitters improves link differentiability. In this work, the imbalancing is done without any channel state information (CSI) at the transmitter side to enable simple practical system implementations. However, the utilisation of CSI for power imbalance might provide an optimal power allocation, and thus improved performance. A shortcoming of this extension is that the provision of CSI requires a dedicated feedback channel which increases system complexity. In the case of diffuse transmission, the combination of optical MIMO techniques with OFDM may be an interesting scope for further study since in this work only pulse amplitude modulation (PAM) has been considered. Moreover, the aspect of mobility has not been investigated in this work. Further research may consider a mobile receiver which is moving within the room. Altogether,

the simulations performed have investigated only the downlink from the ceiling lights to the receiver array. The uplink connection has not been investigated. In a practical transmission system, the uplink connection might use an optical link as well. Alternatively, an RF based uplink might be used resulting in hybrid optical and RF transmission systems.

With regard to practical realisation aspects, the effects of inaccurate channel estimates and non-perfect time synchronisation on the decoder performance may be investigated in future work. For means of simplification, perfect knowledge of the channel and ideal time synchronisation at the receiver have been assumed in this thesis. These assumptions may not be valid for practical OWC systems. Moreover, the computational complexity of the optical MIMO techniques has been analysed with regard to number of required mathematical operations. Practical implementation aspects have not been taken into account. For instance, the considered maximum-likelihood (ML) detection might not be suitable for real time implementations. Therefore, it might be necessary to implement less complex, but suboptimal schemes, like sphere decoding [160, 161]. Nonetheless, it has been shown that SM is significantly less computationally expensive than SMP and RC making it an ideal candidate for optical wireless indoor communications.

The optical wireless transmitter presented in Chapter 4 might be optimised in future work to provide higher data rates. For instance, the bit resolution can be increased to enable higher order quadrature amplitude modulation (QAM) transmission. Additionally, faster switching speeds can be applied if LEDs with lower rise and fall times are employed. In order to increase the transmission distance, the emitted optical power can be enhanced. To this end, the number of LEDs per group and/or the number of groups can be enlarged. Alternatively, more powerful LEDs can be used. This provides scope for further research to investigate which of these options provides the best performance and efficiency. In this work, a uniform quantization of the OFDM samples is applied. Future work might optimise the quantization intervals by considering statistics of the signal amplitudes. For instance, a non-uniform quantization of the OFDM samples might provide reduced quantization effects, and thus improved performance. A shortcoming of the proposed transmitter concept is the fact that a broken LED within the transmitter array directly affects the emitted optical waveform. This is in contrast to conventional transmitter front-ends where broken LEDs result only in less transmission power and lower SNR. The effect of broken LEDs on the signal waveform and on the error performance might be further investigated. However, given the high life time of LEDs

of about $35000 - 50000$ hours, this defect is unlikely to happen.

The visual code transmission system presented in Chapter 5 might be further optimised as well. Currently, the application uses code of the open source implementation *ZXing* [157] for decoding the visual codes. This code was designed to ease practical implementation and utilisation, however it is not optimised. Consequently, if the visual decoding implementation is further optimised, it might be possible to reliably decode larger visual code versions and to increase data rate. In addition, the intensity of the pixels might also be varied to encode more data into the visual codes. It is anticipated that using more than eight colours (different intensity levels) increases the data rate, even though it also increases cross-talk and noise effects. Moreover, it might be possible to use higher order PAM on the green channel and on-off-keying (OOK) on the red and blue channel as the transmission experiments have shown that the green channel is less distorted by noise. A limitation of this work is the underlying consideration of a simple receiver device with low-cost optics. More sophisticated hardware equipment, especially better optics, enables the utilisation of higher frame rates and larger visual code versions. Additionally, more powerful FEC schemes, such as Turbo codes for instance, and visual calibration techniques might be evaluated to further enhance the performance of the developed application. Currently, the transmitted frames consist of a meta code, which contains supplementary information like the frame number, and the payload code, which contains the actual information to be transmitted. In a future implementation, these two codes might be combined to one common visual code. The meta information might be included into the actual payload code by inserting a dedicated meta data field for instance. Furthermore, it might be possible to implement an adaptive turbulence aware synchronisation scheme to provide improved turbulence compensation. However, such a scheme cannot make use of the actual data of the flight control system of the aircraft as a connection of both systems is not permitted due to safety reasons.

Appendix A
Publications and patents

This chapter contains a list of journal and conference papers as well as patents related to this thesis.

A.1 Journal papers

- **T. Fath** and H. Haas, "Performance Comparison of MIMO Techniques for Optical Wireless Communications in Indoor Environments," *IEEE Transactions on Communications*, vol. 61, no. 2, pp. 733–742, Feb. 2013.
- **T. Fath**, C. Heller, and H. Haas, "Optical Wireless Transmitter Employing Discrete Power Level Stepping," *IEEE/OSA Journal of Lightwave Technology*, vol. 31, no. 11, pp. 1734–1743, Jun. 2013.
- **T. Fath**, F. Schubert, and H. Haas, "Wireless Data Transmission using Visual Codes," in *IEEE/OSA Journal of Lightwave Technology* (submitted).

A.2 Conference papers

- **T. Fath**, M. Di Renzo, and H. Haas, "On the Performance of Space Shift Keying for Optical Wireless Communications," in *Proc. of the IEEE Global Communications Conference - Workshop on Optical Wireless Communications*, Miami, Florida, USA, Dec. 10, 2010, pp. 990–994.
- **T. Fath**, H. Haas, M. Di Renzo, and R. Mesleh, "Spatial Modulation applied to Optical Wireless Communications in Indoor LOS Environments," in *Proc. of the IEEE Global Communications Conference*, Houston, Texas, USA, Dec. 5–9, 2011, pp. 1–5.

- **T. Fath**, J. Klaue, and H. Haas "Coded Spatial Modulation applied to Optical Wireless Communications in Indoor Environments," in *Proc. of the IEEE Wireless Communications and Networking Conference*, Paris, France, Apr. 1–4, 2012, pp. 1000–1004.

- **T. Fath** and H. Haas, "Optical Spatial Modulation using Colour LEDs," in *Proc. of the IEEE International Conference on Communications*, Budapest, Hungary, Jun. 9–13, 2013, pp. 3938–3942.

- F. Schubert, **T. Fath**, and H. Haas, "Coloured Video Code for In-Flight Data Transmission," in *Proc. of the International Conference on Computer Vision Systems*, St. Petersburg, Russia, Jul. 16–18, 2013, pp. 42–51.

A.3 Patents

- **T. Fath**, C. Blümm, J. Schalk, N. Schmitt, and C. Heller, "System for the optical communication of data in free spaces based on discrete power levels," *European patent application number: EP20130152787*, Jan. 2012.

- **T. Fath**, C. Blümm, J. Schalk, N. Schmitt, and C. Heller, "System for optical open space data communication based on discrete output levels," *United States patent application number: US 13/749,111*, Jan. 2012.

Appendix B
Selected publications

This chapter contains selected work already published in proceedings of academic conferences or journals.

On the Performance of Space Shift Keying for Optical Wireless Communications

Thilo Fath*‡, Marco Di Renzo† and Harald Haas‡

*EADS Innovation Works Germany
EADS Deutschland GmbH
81663 Munich, Germany
thilo.fath@eads.net

†Laboratory of Signals and Systems
French National Center for Scientific Research (CNRS)
91192 Gif-sur-Yvette (Paris), France
marco.direnzo@lss.supelec.fr

‡Institute for Digital Communications
School of Engineering and Electronics
The University of Edinburgh
EH9 3JL, Edinburgh, UK
h.haas@ed.ac.uk

***Abstract*—In this paper, we study the performance of Space Shift Keying (SSK) modulation applied to optical wireless channels. The optical Multiple-Input-Single-Output (MISO) channel used here is obtained through measurements. The experimental setup consists of two lasers and an optical receiver. Using the channel measurements, the performance of SSK is compared to the Single-Input-Single-Output (SISO) transmission case. We build upon a recent finding, obtained for a two-transmitter case, that power imbalance at the transmitters can enhance the performance of SSK, especially in highly correlated channels [1]. It is found in this paper that SSK applied to real optical wireless channels outperforms SISO and Single-Input-Multiple-Output (SIMO) transmission if more than four optical transmitters are used. Furthermore, we show that Space Shift Keying can also exceed Multiple-Input-Multiple-Output (MIMO) setups which apply repetition coding as SSK exploits receive-diversity in a better way.**

I. Introduction

The ever increasing demand for higher data rates in wireless systems makes radio frequency (RF) spectrum a precious commodity. In fact, the available bandwidth constitutes a limiting factor for achieving higher transmission rates. In sharp contrast, the spectrum in the range of visible or infra-red light offers almost limitless bandwidth and with the advent of high power light emitting diodes (LEDs) powerful and, at the same time, cheap transmitters exist. Therefore, optical wireless communications (OWC) can mature into a promising complement to RF based systems since it could potentially offload a significant amount of traffic in indoor environments from the RF domain to the optical wireless domain resulting in a noticeable RF spectrum relief.

The parallel usage of multiple transmitters and receivers in wireless RF communications can enhance the overall system performance [2], [3]. These so called Multiple-Input-Multiple-Output (MIMO) methods increase the spectral efficiency and can reduce the bit error ratio (BER) of a communication system. For instance, the Bell Laboratories layered space-time (BLAST) architecture [4] and the Alamouti scheme [5] are two well-known MIMO techniques. But as these techniques couple multiple transmission symbols in time and space by simultaneously sending them from all transmit antennas, they cause inter-channel interference (ICI). Therefore, these MIMO implementations require sophisticated detection or pre-coding algorithms which lead to high receiver or transmitter intricacy and considerable system complexity.

Recently, Spatial Modulation (SM) [6] and particularly its low complexity implementation Space Shift Keying (SSK) [7] have been proposed as promising solutions to reduce the high intricacy of MIMO systems. This is due to the fact that SM and SSK completely avoid ICI in time and space. Furthermore, these two techniques can operate with any number of receive antennas in comparison to e.g. BLAST, which requires at least as many receive antennas as transmit antennas. The basic principle of SSK is that it considers the transmitter array as a spatial constellation diagram leading to spatially encoded bits. Thus, information to be transmitted resides in the physical location of the transmitter (the transmitter index). As only one transmit antenna is active at any time instant and all others emit zero power at that time, ICI is completely avoided. The SSK receiver employs a specific detection process which identifies the transmitter that has emitted power. Results presented in [6]-[8] have demonstrated the potential and the reduced computational complexity of SM and of SSK. It has been shown that SSK can work properly even in correlated channels with power imbalance and that it exploits receive-diversity in a better way compared to common Single-Input-Multiple-Output (SIMO) setups. Besides, [9] and [10] show that SM and SSK can also be combined with Orthogonal Frequency Division Multiplexing (OFDM) transmission to enhance spectral efficiency and to cope with severe channel conditions like frequency-selective fading.

Because of its simplicity and its characteristics, Space Shift Keying seems to be a proper modulation technique for low-complex optical wireless communications. This is due to the fact that SSK is based on mere signal pulses i.e. the phase of the transmission signal is not used for conveying information. Therefore, it is especially appropriate for OWC which employs incoherent light sources and uses intensity modulation at the transmitter and direct detection at the receiver side [11]. Intensity modulation and direct detection offer easy implementation and therefore promote low-cost optical modulation and demodulation equipment [12]. But this simplicity is gained at

the expense of losing the optical carrier's frequency and phase information. Thus, common RF modulation techniques cannot be directly applied to optical communications and specific new approaches have to be developed.

Due to its appropriateness and its promising potential for OWC [13], we will study in this paper the performance of SSK modulation in an actual optical wireless propagation environment. In order to evaluate its performance, we will compare SSK to Single-Input-Single-Output (SISO) and SIMO transmission which employ the same power and spectral efficiency. Additionally, SSK is compared to MIMO scenarios which apply repetition coding as these achieve very good performance in optical wireless communications [14]. Furthermore, we will study the effect of transmit power imbalance, which is analysed in [1], where it is found that power imbalance can enhance the performance of SSK in highly correlated channels.

The remainder of this paper is organised as follows: In Section II, we introduce the basic Space Shift Keying system model. Section III describes the optical wireless test setup which is used for real time measurements to derive the optical wireless channel used in this paper. In Section IV, the performance of SSK is studied. Finally, Section V concludes the paper.

II. Space Shift Keying System Model

Notation: The following notations are used throughout the entire paper: bold symbols denote vectors. We use $(\cdot)^T$ for the transpose operator and $|\cdot|$ for the absolute value of a scalar. $\mathrm{E}\{\cdot\}$ stands for the expectation operator and $\mathrm{VAR}\{\cdot\}$ for the standard deviation.

Generally, a $N_t \times N_r$ MIMO system consists of N_t transmit and N_r receive devices. In the following, we consider a basic Multiple-Input-Single-Output (MISO) setup with $N_t = 2$ transmit devices and one receiver ($N_r = 1$). Channel coding is not taken into account within this paper.

By using Space Shift Keying modulation, a random bit sequence is passed to the SSK encoder. The encoder maps the input bits to a constellation vector $\mathbf{x} = [x_1\ x_2]^T$, where the index specifies the respective transmitter. At any given time instance, only one of the two transmitters radiates optical power. Which one is exactly active depends on the random bit sequence at the encoder input. The received signal is given by

$$y = \mathbf{h}\mathbf{x} + n_i, \tag{1}$$

where $\mathbf{h} = [h_1\ h_2]$ represents the transfer factors of the wireless 2×1 channel. Besides, n_i is the noise, which we assume as additive white Gaussian noise (AWGN) with zero mean and of power N_0, affecting the average signal to noise ratio (SNR) at the receiver. The index i is related to the transmitter being active. At the receiver, perfect knowledge of the channel and ideal time synchronisation is assumed. The detection is based on the Maximum-Likelihood (ML) principle meaning that the detector decides for the constellation vector $\widehat{\mathbf{x}}$ which minimises the Euclidean distance between the actual received signal y and all potential received signals leading to

$$\widehat{\mathbf{x}} = \arg\max_{\mathbf{x}} p_y(y|\mathbf{x},\mathbf{h}) = \arg\min_{\mathbf{x}} |y - \mathbf{h}\mathbf{x}|^2, \tag{2}$$

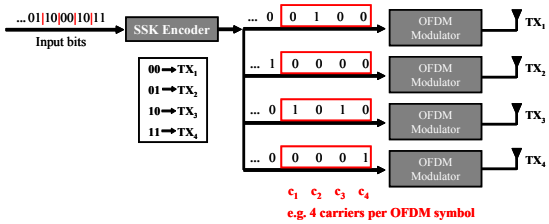

Fig. 1. Illustration of SSK in combination with OFDM.

where p_y is the probability density function of y conditioned on $\mathbf{x}$ and $\mathbf{h}$. Therefore, by applying SSK demodulation, the receiver has to estimate the index of the respective transmit device (e.g. laser or LED) which is active in order to decode the bit sequence generated at the transmitter side.

As shown in [9], Space Shift Keying can also be combined with OFDM. Fig. 1 illustrates this combination for an exemplary setup using $N_t = 4$ transmitters. Hence, SSK is individually applied to each single subcarrier in the frequency domain. Therefore, each subcarrier is mapped to one of the optical transmitters and the respective other transmitters emit zero power on this frequency. By doing so, the output of the SSK encoder delivers a specific set of subcarriers for each transmit device to which a OFDM modulator (Inverse Fast Fourier Transformation) is separately applied. In order to generate real valued signals after the OFDM modulator, Hermitian symmetry of the modulator input is enforced. This generates specific intensity modulated signals which are emitted by each optical transmitter and which contain the distinctive SSK modulated data bits. Through this we achieve several parallel SSK transmissions in the frequency domain. Because of the narrow bandwidth of the single OFDM subcarriers, each one of them can be regarded as a self-contained fading channel with its own characteristics $\mathbf{h}$. At the receiver side, the sum signal y is processed by an OFDM demodulator and the SSK modulated data bits are separately decoded for each subcarrier by using the Maximum-Likelihood principle in (2).

III. Optical Wireless Test Setup

In the following, we describe the test setup which is employed to measure the optical wireless channel and to obtain the transfer factors $\mathbf{h}$, which are used in the simulations presented in Section IV-A. The setup comprises two optical transmit devices (TX_1 and TX_2), which are two identical laser installations using a red laser diode with a wavelength of 658 nm. The optical receiver (RX) consists of a circuitry applying a BPX65 Silicon PIN (Positive Intrinsic Negative) photo diode. As Fig. 2 illustrates, both transmitters have a direct line of sight link to the optical receiver at which the distance of TX_2 to RX (displayed as d_2) is 60 cm and TX_1 is about 70 cm away from the receiver. The distance d_1 between TX_1 and TX_2 is 30 cm. As illustrated, the angle of incidence of the laser beam from TX_1 on the optical receiver is 45°,

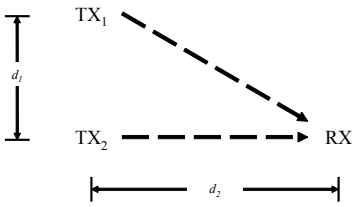

Fig. 2. Illustration of the optical wireless test setup.

whereas the beam of TX_2 directly reaches the photo detector without an angular misalignment.

Fig. 3 displays the average measured gains of the optical wireless links between both transmitters and the receiver. Within this setup, we use Space Shift Keying modulation in combination with OFDM. Thus, the gains are plotted over a frequency range of 8 MHz consisting of 80 measured subcarriers with a spacing of 100 kHz. The displayed gains are averaged over 50 independent series of measurements. It can be seen that the transmission link between TX_1 and RX undergoes a channel attenuation which is about 2.7 dB higher in comparison to the transmission between TX_2 and the optical receiver. As both lasers use the same transmission power, this deficit is caused by the misaligned angle of incidence of TX_1 leading to less received power at the photo diode and a power imbalance between both links. Furthermore, it can be seen that both transmission links are highly correlated leading to a time averaged correlation coefficient of about

$$\rho(h_1, h_2) = \frac{\mathrm{E}\left\{(h_1 - \mathrm{E}\left\{h_1\right\})(h_2 - \mathrm{E}\left\{h_2\right\})\right\}}{\sqrt{\mathrm{VAR}\left\{h_1\right\}\mathrm{VAR}\left\{h_2\right\}}} = 0.93.$$

IV. Results

In this section, we analyse the performance of Space Shift Keying modulation for the measured optical channel samples and for an enhanced $N_t \times N_r$ setup. SSK is compared to SISO, SIMO and MIMO transmissions which use simple on-off-keying (OOK) or pulse amplitude modulation (PAM). M-PAM is an extension of OOK by using a set of M scaling factors for intensity modulation of the optical carrier instead of using only two factors (on and off). In order to ensure comparability, all considered schemes (SSK, SISO, SIMO and MIMO) use the same overall transmission power E_s and provide equal spectral efficiency by transmitting the same number of bits per channel use. Furthermore, Ω_i is the power imbalance in dB between the transmit devices, where the index i displays which transmitter utilises the power surplus (note that in this scenario the overall transmission power is still E_s).

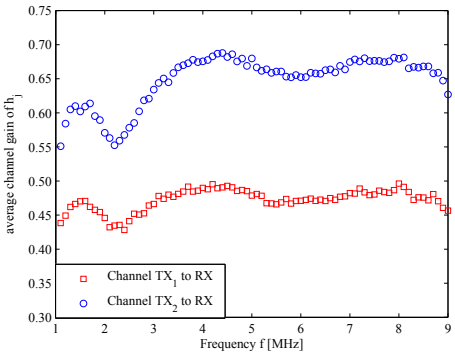

Fig. 3. Measured gains of the optical wireless channels.

A. SSK in measured optical wireless channels

First of all, we examine the performance of SSK for the measured optical wireless channels with power balance of both optical transmitters i.e. $\Omega_1 = \Omega_2 = 0$. As displayed in Fig. 4, there is a close matching between our ascertained bit error ratio performance of SSK and the analytical average bit error probability (ABEP) for two transmitters reported in [1] which is ABEP = $\mathrm{E}\left\{\mathrm{P_E}(\mathbf{h}_1, \mathbf{h}_2)\right\}$, where

$$\mathrm{E}\left\{\mathrm{P_E}(\mathbf{h}_1, \mathbf{h}_2)\right\} = \mathrm{E}\left\{ Q\left(\sqrt{\overline{\gamma} \sum_{n=1}^{N_r} |h_{2,n} - h_{1,n}|^2} \right) \right\}. \quad (3)$$

$\mathrm{P_E}(\cdot,\cdot)$ is the probability of detecting the wrong transmitter index at the receiver, when conditioning upon the channel transfer factors $\mathbf{h}_1 = [h_{1,1}\ h_{1,2}\ \ldots\ h_{1,N_r}]$ and $\mathbf{h}_2 = [h_{2,1}\ h_{2,2}\ \ldots\ h_{2,N_r}]$ of the links between the two transmitters and the N_r receivers. In our experimental setup $N_r = 1$. $Q(x) = \frac{1}{\sqrt{2\pi}} \int_x^{+\infty} \exp(\frac{-t^2}{2})\ dt$ is the Q-function and $\overline{\gamma} = \frac{E_s}{4N_0}$. In comparison to the OOK transmission for TX_1 and TX_2, SSK exhibits a larger BER in this scenario because of the high correlation of both channels.

Fig. 5 presents the effect of power imbalance on the optical wireless test setup. It can be seen that if $\Omega_1 = 3$, the performance of SSK decreases. This is due to the fact that the attenuation of both channels differs of about 3 dB. Thus, by granting TX_1 a power surplus of 3 dB, the difference between

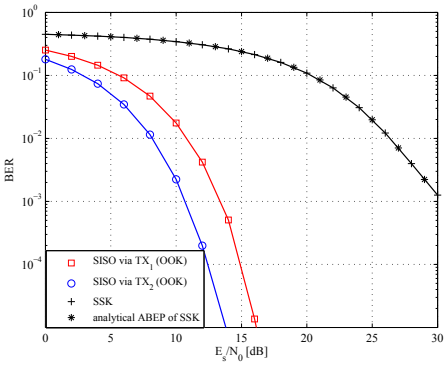

Fig. 4. BER against E_s/N_0 for the measured optical wireless channels with power balance ($\Omega_1 = \Omega_2 = 0$) for 1 bit transmission.

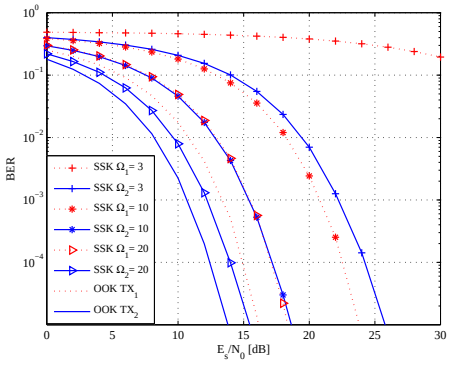

Fig. 5. BER against E_s/N_0 for the measured optical wireless channels with different power imbalance (1 bit transmission).

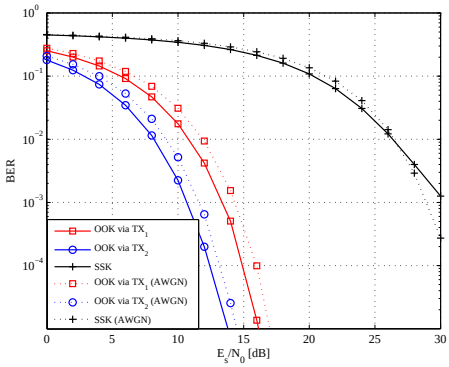

Fig. 6. Comparison of BER against E_s/N_0 for the measured optical wireless channels and for the AWGN case with constant channel attenuations $h_1 = 0.48$ and $h_2 = 0.65$ (1 bit transmission).

both channels gets even less and their unique characteristic is balanced. If applying other scenarios for Ω_1 and Ω_2, the performance of SSK steadily enhances with rising Ω_i as the difference between both channels increases making them more distinguishable, while the overall transmitted power E_s remains constant. The upper bound of the performance of SSK is the OOK scenario, where the power imbalance is maximum.

B. SSK in AWGN scenario

The measurement results of the optical channel obtained by the experimental test setup show only little variations across the single subcarriers and across time. Therefore, the channel can be assumed as a flat AWGN channel with constant attenuation. In order to evaluate this assumption, we consider in the following an AWGN channel with constant attenuation for our 2×1 optical wireless test setup. By doing so, the attenuations of the two links are set to the mean of the measured channel gains displayed in Fig. 3. Thus, the transmission link between TX_1 and RX undergoes a channel attenuation of $h_1 \approx 0.48$, whereas the transmission link between TX_2 and the optical receiver has a channel attenuation of $h_2 \approx 0.65$. This leads to a power imbalance between both links. Fig. 6 displays the comparison of the measured optical wireless channels and of the mere AWGN case with the constant channel attenuations h_1 and h_2. As both results show a good match, the AWGN scenario with constant channel gain is a good approximation for the analysed 2×1 setup with direct line of sight between the two transmitters and the optical receiver.

C. SSK in an enhanced $N_t \times N_r$ setup

As shown, SSK cannot achieve gains in a simple 2×1 setup. Thus, in the following we analyse its performance in an enhanced $N_t \times N_r$ setup with several optical transmitters and receivers. By doing so, we compare SSK to SIMO and MIMO transmissions, which use the same number of optical transmitters/ receivers and equal mean transmission power E_s. Due to comparability regarding the amount of bits sent, we compare SSK to M-PAM transmission. Since Space Shift Keying conveys $m = \log_2(N_t)$ bits per channel use and for M-PAM $m = \log_2(M)$, both techniques have the same spectral efficiency if $M = N_t$. For the following M-PAM MIMO scenarios, repetition coding is used where the same PAM-signal is simultaneously emitted from the N_t optical transmitters. In [14] it is shown that for OWC, repetition coding outperforms SIMO setups because of transmit-diversity. This is due to the fact that the optical intensities coming from sufficiently separated transmitters are orthogonally detected by the receivers. Therefore, the repetition coding scheme combines the faded signals before any noise accumulation unlike a SIMO scheme which combines the noisy faded signals. Thus, we compare SSK to these MIMO setups which apply repetition coding whereas ideal time synchronisation between the single MIMO paths is assumed.

Based on the results of Section IV-B, we use in the following AWGN channels with different gains for the wireless links between the transmitters and receivers. The channel gains are assumed to be independent values drawn from a uniform distribution on the unit interval. By doing so, the single channel links experience power imbalances between each other due to different attenuations like in the optical test setup. Fig. 7 presents the simulation results of a system setup with $N_t = 4$ transmitters and several receivers. All schemes transmit 2 bits in this scenario. Although SIMO and MIMO still perform better, it can be seen that SSK benefits from the enhanced number of transmit and receive devices. Especially with rising number of optical receivers, SSK can exploit the receive-diversity in a better way than SIMO and MIMO as the performance gap decreases. Fig. 8 and Fig. 9 show that SSK outperforms SIMO transmission in a setup employing $N_t = 8$ and $N_t = 16$ transmitters even if $N_r < N_t$. In comparison to repetition coding, SSK can outperform the MIMO scheme within a SNR range of about 10 - 27 dB if $N_t = 8$. At higher SNRs, the gain of repetition coding comes into play and makes it superior. In a $N_t = 16$ setup, SSK performs best and it can be seen that repetition coding has no benefits even compared

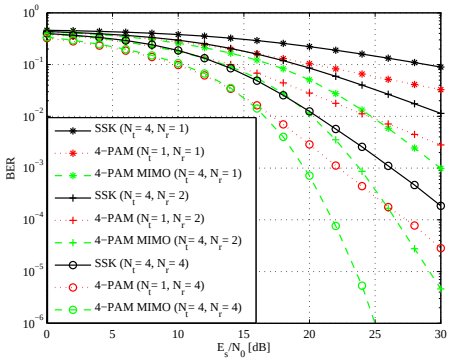

Fig. 7. BER against E_s/N_0 for AWGN scenario (2 bits transmission).

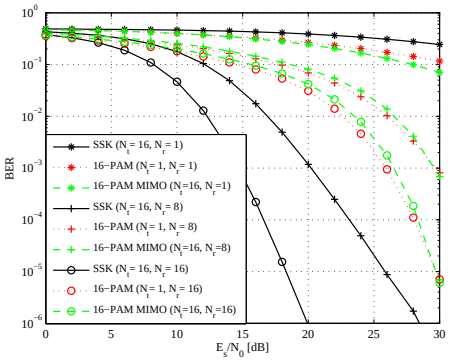

Fig. 9. BER against E_s/N_0 for AWGN scenario (4 bits transmission).

to SIMO transmission. The results show that more than four transmit devices have to be used in order to profit from SSKs potential and to achieve gains compared to SIMO and MIMO transmission. These gains increase with rising number of employed transmitters and receivers.

V. Summary and Conclusion

In this paper, we have studied the performance of Space Shift Keying modulation under optical wireless channel conditions, which have been obtained by actual channel measurements. SSK has been compared to SISO, SIMO and MIMO transmission scenarios. The results show that the performance of SSK modulation is strongly affected by the channel conditions and that simple 2×1 SSK cannot make use of transmit-diversity gains. Nevertheless, power imbalance on the different transmitters can enhance its performance, especially for highly correlated optical wireless channels with direct line of sight. Furthermore, we have shown that SSK can deploy its transmit-diversity potential and achieves benefits over SIMO and MIMO setups if more than four transmit devices are used. We have also illustrated that SSK can exploit receive-diversity in a better way. Future work will deal with further performance measurements of Space Shift Keying in an extended test setup using more than two optical transmitters and several receivers under real channel conditions.

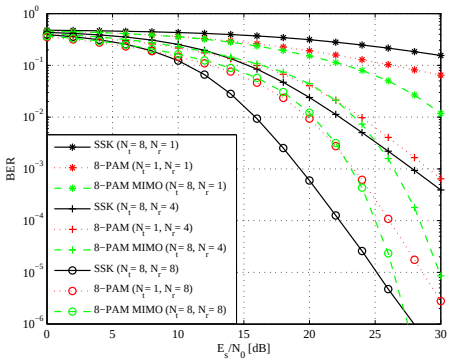

Fig. 8. BER against E_s/N_0 for AWGN scenario (3 bits transmission).

References

[1] M. Di Renzo and H. Haas, "On the Performance of Space Shift Keying MIMO Systems Over Correlated Rician Fading Channels," in *ITG International Workshop on Smart Antennas (WSA 2010)*, Bremen, Germany, Feb. 23–24, 2010.

[2] E. Telatar, "Capacity of Multi-Antenna Gaussian Channels," *European Transaction on Telecommunication*, vol. 10, no. 6, pp. 585–595, Nov. / Dec. 1999.

[3] G. J. Foschini and M. J. Gans, "On Limits of Wireless Communications in a Fading Environment when Using Multiple Antennas," *Wireless Personal Communications*, vol. 6, no. 6, pp. 311–335, 1998.

[4] G. J. Foschini, "Layered Space-Time Architecture for Wireless Communication in a Fading Environment when Using Multi-Element Antennas," *Bell Labs Technical Journal*, vol. 1, no. 2, pp. 41–59, Sep. 1996.

[5] S. M. Alamouti, "A Simple Transmit Diversity Technique for Wireless Communications," *IEEE Journal on Selected Areas in Communications*, vol. 16, no. 8, pp. 1451–1458, Oct. 1998.

[6] R. Mesleh, H. Haas, C. W. Ahn, and S. Yun, "Spatial Modulation – A New Low Complexity Spectral Efficiency Enhancing Technique," in *IEEE International Conference on Communication and Networking in China (CHINACOM)*, Beijing, China, Oct. 25–27, 2006, pp. 1–5.

[7] J. Jeganathan, A. Ghrayeb, L. Szczecinski, and A. Ceron, "Space Shift Keying Modulation for MIMO Channels," *IEEE Transaction on Wireless Communications*, vol. 8, no. 7, pp. 3692–3703, Jul. 2009.

[8] J. Jeganathan, A. Ghrayeb, and L. Szczecinski, "Spatial Modulation: Optimal Detection and Performance Analysis," *IEEE Communication Letters*, vol. 12, no. 8, pp. 545–547, 2008.

[9] R. Mesleh, H. Haas, C. W. Ahn, and S. Yun, "Spatial Modulation – OFDM," in *Proc. of the International OFDM Workshop*, Hamburg, Germany, Aug. 30–31, 2006.

[10] S. U. Hwang, S. Jeon, S. Lee, and J. Seo, "Soft-Output ML Detector for Spatial Modulation OFDM Systems," *IEICE Electronics Express*, vol. 6, no. 19, pp. 1426–1431, Oct. 2009.

[11] S. Hranilovic, *Wireless Optical Communication Systems*, 1st ed. Springer, Sep. 1996.

[12] J. M. Kahn and J. R. Barry, "Wireless Infrared Communications," *Proceedings of the IEEE*, vol. 85, no. 2, pp. 265–298, Feb. 1997.

[13] R. Mesleh, R. Mehmood, H. Elgala, and H. Haas, "Indoor MIMO Optical Wireless Communication Using Spatial Modulation," in *IEEE International Conference on Communications (ICC'10)*, Cape Town, South Africa, 22–27 May 2010, to appear.

[14] M. Safari and M. Uysal, "Do we really need OSTBCs for free-space optical communication with direct detection?" *IEEE Transactions on Wireless Communications*, vol. 7, no. 11 Part 2, pp. 4445–4448, 2008.

Spatial Modulation applied to Optical Wireless Communications in Indoor LOS Environments

Thilo Fath*†, Harald Haas†§, Marco Di Renzo‡ and Raed Mesleh§

*EADS Innovation Works Germany
EADS Deutschland GmbH
81663 Munich, Germany
thilo.fath@eads.net

†School of Engineering and Electronics
The University of Edinburgh
EH9 3JL, Edinburgh, UK
h.haas@ed.ac.uk

‡Laboratory of Signals and Systems
French National Center for Scientific Research (CNRS)
91192 Gif-sur-Yvette, France
marco.direnzo@lss.supelec.fr

§School of Engineering and Science
Jacobs University Bremen
28759 Bremen, Germany
r.mesleh@jacobs-university.de

***Abstract*—In this paper, we study the performance of Spatial Modulation (SM) applied to optical wireless communications (OWC) in indoor environments with line-of-sight (LOS) characteristics. To this end, we consider setup scenarios with different numbers of optical transmitters and receivers which are arranged within a room. SM is compared to Repetition Coding (RC). Because RC is known to achieve very good performance in OWC systems due to the use of intensity modulation and the resulting constructive superposition of the power signals. The results show that SM can outperform RC when high spectral efficiencies are desirable, e.g. 4 bit/s/Hz and greater, since it can operate with reduced signal modulation orders by conveying additional data bits in the spatial domain. We also demonstrate that SM benefits from receive-diversity to a larger extent while at the same time requiring less computational complexity. Furthermore, we give a general framework to numerically approximate the average bit error probability of both SM and RC.**

***Index Terms*—diversity, MIMO, optical wireless communications, repetition coding, spatial modulation.**

I. Introduction

The first pioneering studies in optical free-space transmissions for indoor environments [1] have shown the potential of optical wireless communications (OWC) to provide flexible and efficient indoor data transmission. With the advent of cheap and powerful light emitting diodes (LEDs), appropriate optical transmitters are available which can be used for instance in home and office scenarios. As OWC transmission does not interfere with delicate electronic systems, it can even be applied to sensitive environments like hospitals and aircraft cabins. However, like all wireless communication systems, OWC also has to cope with the ever increasing demand for higher data rates. Therefore, it is important to provide high spectral efficiencies at low error ratios.

Commonly, OWC transmission schemes employ intensity modulation of the optical carrier and direct detection at the receiver side [2], [3]. To this end, up- and down-conversion of the signals can be done by low-cost diodes without the need for sophisticated high-frequency circuit designs. Most optical wireless links use simple modulation techniques like on-off-keying (OOK) or pulse amplitude modulation (PAM) because they offer easy implementation. PAM provides an enhanced spectral efficiency by using several intensity levels of the optical signal in contrast to OOK which encodes information by simply switching the device on and off. However, the provision of enhanced spectral efficiencies by using larger constellation sizes leads to worse bit error ratio (BER) performance. Thus, the main drawback of simple single-input-single-output (SISO) systems is that the achievable data rate at reasonable BER performance is low since a high order modulation scheme is needed. A known solution to improve the error performance of wireless communication systems is by exploitation of diversity. The reliability can be enhanced by using several receiving devices, which enables receive-diversity. These so called single-input-multiple-output (SIMO) methods receive several replicas of the same transmitted signal. Hence, an enlarged portion of the emitted power can be collected and the multiple signal receptions can be combined to improve the quality of the wireless link. Besides, it is possible to use several transmit devices as well. In order to provide transmit-diversity, Repetition Coding (RC) can be used which works by the principle that the same information is sent from multiple transmitters simultaneously. RC is known to achieve very good performance in free-space optical communications with line-of-sight (LOS) as the intensities coming from the multiple transmitters constructively add up at the receiver side [4], [5]. Because of this, RC can outperform orthogonal space-time block codes (OSTBCs) and even SIMO transmission [4].

In [6], [7] a new and promising modulation technique called Spatial Modulation (SM) has been proposed. It has been shown that SM can achieve high data rates while providing good BER performance and low system complexity. Like RC, SM employs several emitters for transmitting data. But, as opposed to common modulation techniques where information is conveyed by modulating the signal, SM additionally conveys data bits in the spatial domain. In order to accomplish this, SM considers the transmitter array as an additional (spatial) constellation diagram. Unlike RC, SM works by the principle that only one transmitter is active at any time instance. In addition to modulating the signal, e.g. modulation of the signal amplitude, information is also encoded in the index of the

transmitter which emits the signal. Therefore, high spectral efficiencies can be achieved which depend not only on the signal constellation size, but also on the number of transmitters. This leads to a degree of freedom as both parameters can be traded off against each other. Furthermore, SM can deal with high channel correlation and power imbalances of wireless links [8]. As these are characteristics of optical wireless links [9], [10], SM seems to be especially suitable for OWC.

Hence, in this paper, we apply SM to OWC in indoor LOS environments. We compare SM and RC transmission with regard to their BER performance for different spectral efficiencies. Setup scenarios with different numbers of optical transmitters and receivers are considered. Furthermore, we give a numerical framework to calculate the respective average bit error probability (ABEP) of both schemes.

The remainder of the paper is organized as follows: In Section II we introduce the system model and the notations. Section III presents the optical wireless setup from which we derive the channel coefficients for the considered indoor scenarios. The BER performance of SM and RC is studied in Section IV, where numerical and simulation results are shown. Finally, Section V concludes the paper.

II. System Model

The following notations are used throughout the paper: lower case bold symbols denote vectors and upper case bold symbols denote matrices. We use $[\cdot]^T$ for the transpose operator, $|\cdot|$ for the absolute value and $\|\cdot\|_{\mathrm{F}}$ for the Frobenius norm. The signal constellation size is given by M and $\mathrm{d_H}(\cdot,\cdot)$ denotes the Hamming distance of two bit assignments. $\mathrm{Q}(a) = \frac{1}{\sqrt{2\pi}} \int_a^{+\infty} \exp(\frac{-t^2}{2})\ dt$ is the Q-function. N_t is the number of transmitters and N_r is the number of receivers, where n_t is the transmitter index and n_r is the receiver index. We assume perfect knowledge of the channel and ideal time synchronisation at the receiver side. Channel coding is not taken into account.

The received signal vector is given by:

$$\mathbf{y} = \mathbf{H}\,\mathbf{s} + \mathbf{n}, \tag{1}$$

where $\mathbf{s} = [s_1 \ \ldots \ s_{N_t}]^T$ is the signal vector to be transmitted. Consequently, the elements of $\mathbf{s}$ indicate which signal is emitted by each single optical transmitter. $\mathbf{H}$ is the $N_r \times N_t$ channel matrix. Its single elements $h_{n_r n_t}$ represent the respective channel coefficient of the wireless link between transmitter n_t and receiver n_r. Furthermore, $\mathbf{n}$ is the noise, which we assume as real valued additive white Gaussian noise (AWGN) with zero mean and a double-sided power spectral density of E_n. The detection at the receiver is based on the maximum-likelihood (ML) principle. The ML detector decides for the signal vector $\widehat{\mathbf{s}}$ which minimises the Euclidean distance between the actual received signal $\mathbf{y}$ and all potential received signals leading to

$$\widehat{\mathbf{s}} = \arg\max_{\mathbf{s}} p_{\mathbf{y}}(\mathbf{y}|\mathbf{s},\mathbf{H}) = \arg\min_{\mathbf{s}} \|\mathbf{y} - \mathbf{H}\,\mathbf{s}\|_{\mathrm{F}}^2, \tag{2}$$

where $p_{\mathbf{y}}$ is the probability density function of $\mathbf{y}$ conditioned on $\mathbf{s}$ and $\mathbf{H}$.

The intensities I_m^{PAM} which can be used for signal modulation applying $M-$PAM are given by

$$I_m^{\mathrm{PAM}} = \tfrac{2\,I}{M-1}\,m \quad \text{for } m = 0, 1, \ldots, (M-1), \tag{3}$$

with I being the mean optical intensity emitted. Hence, $M-$PAM provides a spectral efficiency of $\log_2(M)$ bit/s/Hz. As RC works by the principle that all transmitters emit the same signal, $s_1 = s_2 = \ldots = s_{N_t}$ holds. In order to ensure comparability, the mean optical power transmitted has to be fixed, irrespective of the number of transmitters. Thus, for RC transmission, the optical power is equally distributed across all N_t emitters and the intensities given in (3) have to be divided by factor N_t. In (4) we denote the ABEP of RC employing $M-$PAM for an arbitrary $N_t \times N_r$ scenario. It is a generalisation of the common $M-$PAM ABEP, which is e.g. given in [2]. At this end, $E_s = (r\ I)^2$ is the mean electrical energy of the intensity modulated optical signal, with r being the optical-to-electrical conversion coefficient (which we assume being 1 A/W). Because in intensity modulated optical communications the electrical energy is proportional to the square of the optical power [3].

By using SM, the bit sequence to be transmitted is passed to the SM encoder. As illustrated in Fig. 1, the encoder maps the bits to the signal vector $\mathbf{s}$. At any given time instance, only one transmitter radiates optical power. This means that only one element of $\mathbf{s}$ is non-zero. The index of this respective element states the index of the transmitter (e.g. LED) which is activated. Therefore, the emitter index depends on the bit sequence at the encoder input. In this way, one part of the data is transmitted. The other part of the data is conveyed in a conventional way via PAM. This means that the non-zero element of $\mathbf{s}$ is a specific signal constellation point with intensity I_m representing additional information bits. $b_{m\,n_t}$ is the bit assignment of the signal when intensity I_m is emitted from transmitter n_t. However, classical PAM must be modified because a signal with $I_m = 0$ cannot be used for conveying information as in this case all elements of $\mathbf{s}$ would be zero and the spatial information would be lost. As a consequence, the intensities I_m^{SM} which can be used for SM are

$$I_m^{\mathrm{SM}} = \tfrac{2\,I}{M+1}\,m \quad \text{for } m = 1, 2, \ldots, M. \tag{5}$$

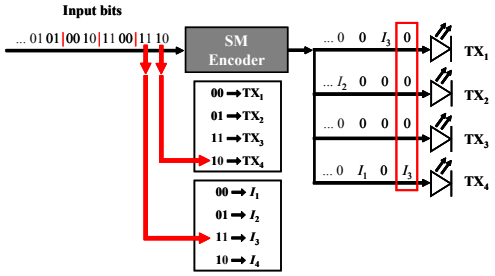

Fig. 1. Illustration of SM operation providing 4 bit/s/Hz with $N_t = 4$.

$$\mathrm{ABEP}_{\mathrm{RC}} \approx \frac{2\,(M-1)}{M\,\log_2(M)}\,\mathrm{Q}\left(\frac{1}{M-1}\sqrt{\frac{E_s}{E_n\,N_t^2}\sum_{n_r=1}^{N_r}\left(\sum_{n_t=1}^{N_t} h_{n_r n_t}\right)^2}\right) \tag{4}$$

$$\mathrm{ABEP}_{\mathrm{SM}} \leq \frac{1}{MN_t\,\log_2\left(MN_t\right)}\sum_{m^{(1)}=1}^{M}\sum_{n_t^{(1)}=1}^{N_t}\sum_{m^{(2)}=1}^{M}\sum_{n_t^{(2)}=1}^{N_t}\mathrm{d_H}\left(b_{m^{(1)}n_t^{(1)}}, b_{m^{(2)}n_t^{(2)}}\right)\cdot \mathrm{Q}\left(\sqrt{\frac{r^2}{4\,E_n}\sum_{n_r=1}^{N_r}\left|I^{\mathrm{SM}}_{m^{(2)}}\,h_{n_r n_t^{(2)}} - I^{\mathrm{SM}}_{m^{(1)}}\,h_{n_r n_t^{(1)}}\right|^2}\right) \tag{6}$$

In the example displayed in Fig. 1, the data bits are arranged in blocks of 4 bits leading to a spectral efficiency of 4 bit/s/Hz. The last two bits define the transmitter index and the first two ones the signal intensity assuming $M = 4$. As shown, for instance the bit sequence "1 1 1 0" corresponds to LED number 4 emitting an optical pulse with intensity I_3. At the receiver side, the detector has to perform two detection tasks. First, it has to estimate the index of the respective LED which is active and second it has to decode the information encoded in the signal from the received intensity level. Only if both the index and the signal constellation point are detected correctly, the bit sequence can be decoded error free. As ML detection is assumed, both estimation tasks are jointly done by the decoding algorithm given in (2).

According to (5), the minimum distance between two possible SM intensities is $\frac{2\,I}{M+1}$, whereas the minimum distance for PAM is $\frac{2\,I}{M-1}$. The lower signal distance of SM might lead to a worse BER performance as the error probability depends on the Euclidean distance of the transmitted signals. But, as SM conveys additional information bits in the spatial domain, it provides a higher spectral efficiency which is $\log_2(M) + \log_2(N_t) = \log_2(MN_t)$ bit/s/Hz. In other words: SM can achieve the same efficiency as $M-$PAM, but with a reduced signal constellation size of $\widetilde{M} = \frac{M}{N_t}$, hence effectively enlarging the distance of the signal points. In [8] and [11] it is shown that the error performance of SM depends on the differences between radio frequency channels. Moreover, it is demonstrated that the ABEP of SM can be approximated by union bound methods. Using these basics, we can derive the ABEP of SM employing intensity modulation for OWC. Due to space constraints, we omit the detailed calculation and report only the final result which is given in (6). Here, $b_{m^{(1)}n_t^{(1)}}$ is the bit assignment which is conveyed when intensity $I^{\mathrm{SM}}_{m^{(1)}}$ is emitted by transmitter $n_t^{(1)}$ and $b_{m^{(2)}n_t^{(2)}}$ is the bit assignment which is conveyed when intensity $I^{\mathrm{SM}}_{m^{(2)}}$ is emitted by transmitter $n_t^{(2)}$. Consequently, $\mathrm{d_H}\left(b_{m^{(1)}n_t^{(1)}}, b_{m^{(2)}n_t^{(2)}}\right)$ states the number of bit errors when erroneously decoding the assignment $b_{m^{(2)}n_t^{(2)}}$ at the receiver instead of the actually transmitted assignment $b_{m^{(1)}n_t^{(1)}}$.

If we consider the computational complexity at the receiver side, it can be seen that the detection of SM transmission requires fewer mathematical operations compared to RC. For RC, a total of $M\,(2\,N_t\,N_r + N_r - 1)$ multiplications, additions and subtractions are needed. In contrast, SM merely requires $\widetilde{M}\,N_t\,(3\,N_r - 1) = M\,(3\,N_r - 1)$ operations and, therefore, is less computationally expensive. For instance, if $M = 16$, $N_t = 4$ and $N_r = 4$, RC requires 560 operations, whereas SM requires only 176 operations.

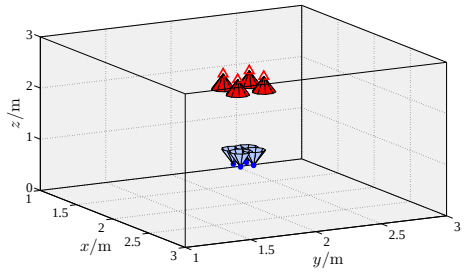

Fig. 2. Positioning of a 4×4 setup within room.

III. Optical Wireless Setup Scenario

In the following, we consider an indoor LOS environment with different $N_t \times N_r$ setup scenarios. We assume that the transmitters are placed at a height of $z = 2.5$ m and are oriented downwards to point straight down from the ceiling. The receivers are located at a height of $z = 0.75$ m (e.g. height of a table) and are oriented upwards to point straight up at the ceiling. Both transmitters and receivers are aligned in rectangular arrays, which are centred within the room. The element spacing of the single transmitters on the x- and y-axis is 0.2 m and 0.1 m for the receivers. These spacings are chosen with regard to a practical implementation of the transmitters within an illumination installation and of the receivers within a potential user device. Fig. 2 exemplarily shows the positioning of a 4×4 setup, at which the transmitters are displayed as triangulars and the receivers as dots. The plotted cones illustrate the orientation of the transmit beams and the orientation of the receiver field-of-view (FOV). The cone angles are related to the TX and RX semiangles.

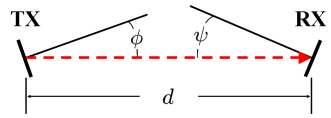

Fig. 3. Geometric scenario used for calculation of channel coefficients.

On the basis of this setup scenario, we derive the channel coefficients of the optical wireless links. Fig. 3 illustrates the geometries used to calculate the single coefficients $h_{n_r n_t}$. As shown, ϕ is the angle of emergence with respect to the transmitter axis and ψ is the angle of incidence with respect to the receiver axis. Furthermore, d depicts the distance between transmitter and receiver. According to [3], the DC channel gain is the most distinctive parameter describing an optical wireless link. Therefore, the channel coefficient of a directed LOS link can be calculated as follows:

$$h = \begin{cases} \frac{(k+1)\,A}{2\,\pi\,d^2}\cos^k\phi\cos\psi & 0 \le \psi \le \Psi_{\frac{1}{2}} \\ 0 & \psi > \Psi_{\frac{1}{2}} \end{cases} \tag{7}$$

with the order $k = \frac{-\ln(2)}{\ln(\cos\Phi_{\frac{1}{2}})}$ and the transmitter semiangle $\Phi_{\frac{1}{2}}$, which we assume being $15°$. Furthermore, $\Psi_{\frac{1}{2}}$ denotes the FOV semiangle of the receiver, assumed being $15°$, and A is the detector area of the receiver, assumed being 1 cm^2. Hence, the channel coefficients depend on the specific position of each transmitter and receiver within the setup scenario.

IV. Results on Bit Error Ratio Performance

In this section, we analyse the BER performance of SM and RC using the scenario introduced in Section III. We consider setups with different numbers of optical transmitters and receivers as well as varying spectral efficiencies. In order to ensure comparability, the mean emitted power is the same in each scenario and for both transmission techniques. Therefore, we evaluate the error ratios at the receiver side with regard to transmit power against noise power, while taking into account the specific path loss of the setups caused by the alignment of the transmitters and receivers within the room. Thus, we define the signal to noise ratio (SNR) being $\frac{E_s}{E_n}$. As the channel coefficients of the considered setups are in the range of 10^{-4}, the electrical path loss is about -80 dB.

First of all, we consider the 4×4 setup scenario illustrated in Fig. 2. For this scenario, Fig. 4 depicts the BER of SM and RC assuming a spectral efficiency of 2, 4 and 6 bit/s/Hz. It can be seen that the numerical ABEPs (markers) given in (4) and (6) very closely match the simulation results (lines). Consequently, the given ABEPs provide a good means to evaluate the BER performance of SM and RC. As shown in Fig. 4, for a spectral efficiency of 2 and 4 bit/s/Hz, RC applying 4-PAM, respectively 16-PAM, achieves a better performance than SM. But, if we consider improved spectral efficiency of 6 bit/s/Hz,

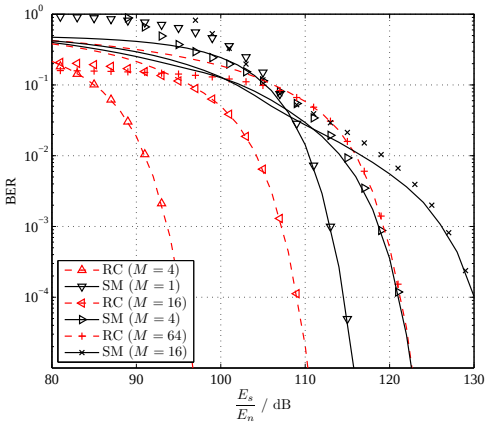

Fig. 4. Comparison of SM and RC for spectral efficiency of 2, 4 and 6 bit/s/Hz in 4×4 setup scenario (lines show simulation results and markers numerical ABEP results).

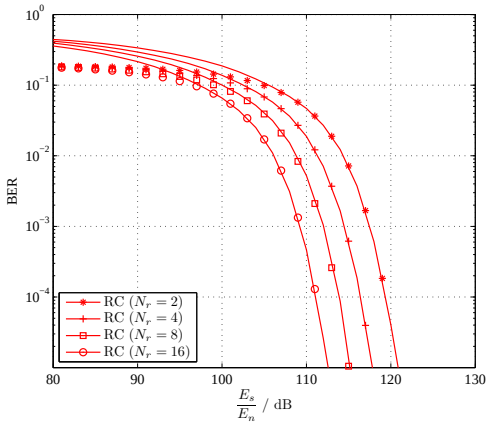

(a) 32-PAM RC

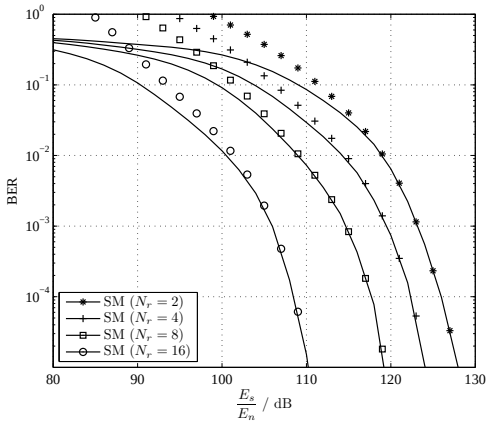

(b) SM with $M = 4$

Fig. 5. Comparison of SM and RC for 5 bit/s/Hz with $N_t = 8$ and varying number of optical receivers N_r (lines show simulation results and markers numerical ABEP results).

SM outperforms RC up to a SNR of about 116 dB. This is because SM operates with a reduced signal constellation size of $M = 16$ compared to 64-PAM RC transmission. At SNRs above 116 dB RC gets superior because of its transmit-diversity gain.

As SM only uses one transmitter at any time instance, it cannot provide transmit-diversity. However, it can utilize receive-diversity to a larger extent than RC by offering higher SNR gains with increasing N_r. This finding is shown in Fig. 5, where we study the performance of SM and RC for 5 bit/s/Hz for a scenario with $N_t = 8$ and a varying number of optical receivers. It can be seen that when consecutively doubling N_r from 2 up to 16, RC achieves a performance gain of about 3 dB in each step. In contrast, SM achieves larger improvements as it provides a performance gain of about 5 dB by moving from $N_r = 4$ to $N_r = 8$ and of about 9 dB by moving from $N_r = 8$ to $N_r = 16$. Consequently, in the 8×16 scenario SM even outperforms RC by about 2 dB.

Besides these improvements, SM has another essential advantage over RC transmission. If more bits are to be transmitted per channel use, RC needs a higher increase in SNR to be able to provide the same BER performance. This observation is taken from Fig. 6, which shows the error ratios for a 16×16 transmission system providing different spectral efficiencies (4, 5 and 6 bit/s/Hz). It can be seen that RC needs an SNR improvement of about 6 dB to achieve the same BER when providing 5 instead of 4 bit/s/Hz, whereas SM requires an increase of only 3 dB. Consequently, SM with $M = 2$ outperforms 32-PAM RC by about 8 dB and even 16-PAM by about 2 dB. If the spectral efficiency is increased by 1 bit to 6 bit/s/Hz, RC requires additional 6 dB, in contrast to SM which needs only an increase of about 4 dB. In summary, for a spectral efficiency of 6 bit/s/Hz SM outperforms RC by about 10 dB and even outperforms the less efficient 32-PAM RC transmission by about 4 dB. Hence, the benefits of SM over RC largely increase with greater spectral efficiencies.

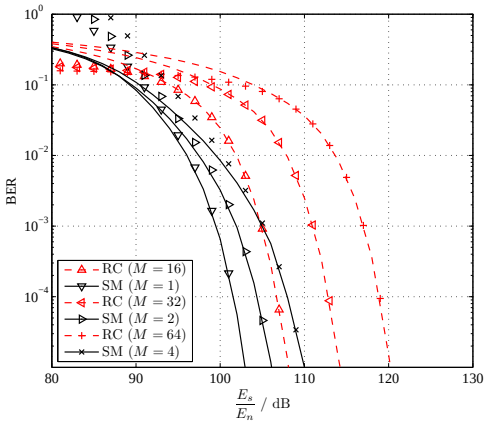

Fig. 6. Comparison of SM and RC for spectral efficiency of 4, 5 and 6 bit/s/Hz in 16×16 setup scenario (lines show simulation results and markers numerical ABEP results).

V. Summary & Conclusion

We have studied the performance of Spatial Modulation applied to OWC in indoor environments and compared it to Repetition Coding. The simulation results were substantiated by numerical ABEP calculations. We have demonstrated that SM achieves significant gains if several receivers are employed because it provides large SNR improvements with increasing number of receivers. Especially for higher spectral efficiencies, SM provides a better error performance as it can operate with a reduced signal constellation size by conveying data bits in the spatial domain. Furthermore, SM can achieve better error ratios particularly at low SNR regions because the transmit-diversity gain of RC prevails only at higher SNRs. Moreover, SM even provides less computational complexity. Thus, SM is a suitable modulation technique for OWC to provide high data rates at good BER performance. Future work will deal with the adaptation of SM in order to achieve benefits by transmit-diversity as this will enhance its performance, especially for low spectral efficiencies and at high SNR regions.

Acknowledgement

Professor Haas acknowledges the Scottish Funding Council support of his position within the Edinburgh Research Partnership in Engineering and Mathematics between the University of Edinburgh and Heriot Watt University.

References

[1] F. R. Gfeller and U. Bapst, "Wireless In-House Data Communication Via Diffuse Infrared Radiation," *Proceedings of the IEEE*, vol. 67, no. 11, pp. 1474–1486, Nov. 1979.

[2] S. Hranilovic, *Wireless Optical Communication Systems*, 1st ed. Springer, Sep. 1996.

[3] J. M. Kahn and J. R. Barry, "Wireless Infrared Communications," *Proceedings of the IEEE*, vol. 85, no. 2, pp. 265–298, Feb. 1997.

[4] M. Safari and M. Uysal, "Do we really need OSTBCs for free-space optical communication with direct detection?" *IEEE Transactions on Wireless Communications*, vol. 7, no. 11 Part 2, pp. 4445–4448, 2008.

[5] S. M. Navidpour, M. Uysal, and M. Kavehrad, "BER Performance of Free-Space Optical Transmission with Spatial Diversity," *IEEE Transactions on Wireless Communications*, vol. 6, no. 8, pp. 2813–2819, Aug. 2007.

[6] Y. A. Chau and S.-H. Yu, "Space Modulation on Wireless Fading Channels," in *VTC 2001 Fall Vehicular Technology Conference IEEE VTS 54th*, vol. 3, 7–11 Oct. 2001, pp. 1668–1671.

[7] R. Mesleh, H. Haas, C. W. Ahn, and S. Yun, "Spatial Modulation – A New Low Complexity Spectral Efficiency Enhancing Technique," in *IEEE International Conference on Communication and Networking in China (CHINACOM)*, Beijing, China, Oct. 25–27, 2006, pp. 1–5.

[8] M. Di Renzo and H. Haas, "On the Performance of Space Shift Keying MIMO Systems Over Correlated Rician Fading Channels," in *ITG International Workshop on Smart Antennas (WSA 2010)*, Bremen, Germany, Feb. 23–24 2010.

[9] T. Fath, M. Di Renzo, and H. Haas, "On the Performance of Space Shift Keying for Optical Wireless Communications," in *Proc. of the IEEE Global Communications Conference (GLOBECOM) - Workshop on Optical Wireless Communications*, Miami, Florida, USA, Dec. 10, 2010, pp. 990–994.

[10] R. Mesleh, H. Elgala, and H. Haas, "Optical Spatial Modulation," *Journal of Optical Communications and Networking*, vol. 3, no. 3, pp. 234–244, Mar. 2011.

[11] M. Di Renzo and H. Haas, "Performance analysis of spatial modulation," in *5th International ICST Conference on Communications and Networking in China*, August 2010.

Coded Spatial Modulation applied to Optical Wireless Communications in Indoor Environments

Thilo Fath*†, Jirka Klaue* and Harald Haas†

*EADS Innovation Works Germany
EADS Deutschland GmbH
81663 Munich, Germany
{thilo.fath, jirka.klaue}@eads.net

†Institute for Digital Communications
School of Engineering and Electronics
The University of Edinburgh
EH9 3JL, Edinburgh, UK
h.haas@ed.ac.uk

***Abstract*—Spatial Modulation (SM) is a combined multiple-input-multiple-output (MIMO) and digital modulation technique which besides common signal modulation conveys additional information bits in the spatial domain. To this end, only one transmitter is active at any time instance. The actual index of each emitter represents a unique spatial constellation point and thus conveys additional information. As a consequence, SM completely avoids inter-channel interference (ICI) and provides low detection complexity. Like for any MIMO scheme, the performance of SM is degraded in the presence of high channel correlation. Therefore, Trellis Coded Spatial Modulation (TCSM) applies coding techniques to the bits conveyed in the spatial domain to assist the detection of the active transmitter. As optical wireless communications (OWC) in indoor environments is subject to high spatial correlation and low channel distinctness, we evaluate the performance of coded SM applied to indoor OWC. For this purpose, we propose an enhanced coded SM technique which jointly encodes the bits conveyed in the signal and spatial domains. It is found in this paper that our enhanced coded SM technique can achieve gains in signal to noise ratio (SNR) of about $1-3$ dB compared to the originally proposed TCSM scheme.**

***Index Terms*—coding, MIMO, optical wireless communications, spatial modulation.**

I. Introduction

Due to recent advances in solid-state lighting and the associated availability of frequency spectrum of hundreds of THz, optical wireless communications (OWC) has attracted attention for indoor data transmission as a promising complement to existing radio frequency (RF) systems [1]. Commonly for OWC, incoherent light sources are used as they enable the use of simple low cost optical devices. As a consequence, optical systems are mostly based on intensity modulation (IM) and direct detection (DD) by employing light emitting diodes (LEDs) as emitters and photo diodes as receivers, thus not providing phase information in the received signals [2]. Since there is an increasing adoption of LED lighting in homes and offices, this has fueled research that aims at using these devices not only for illumination but also for wireless communications [3]. Moreover, as there typically are several LEDs in an entire LED cluster, these multiple emitters can be used for data transmission. This inherently provides the essential prerequisite for the use of multiple-input-multiple-output (MIMO) techniques in conjunction with OWC [4]. MIMO techniques are already widely used in RF communications to enhance the system performance as they increase the link reliability and provide high data rates [5].

Recently, Spatial Modulation (SM) has been proposed as a combined MIMO and digital modulation technique [6]. In addition to applying basic signal modulation, SM transmits additional bits in the spatial domain by considering the transmitter array as an extended constellation diagram. As only one transmitter is emitting a digitally modulated signal at any time instance, the index of this transmitter represents additional data bits. It has been shown that SM can outperform other MIMO schemes like Repetition Coding (RC) [7] and spatial multiplexing [6], while even providing lower computational complexity.

Like for any MIMO technique, the performance of SM is related to the channel characteristics. As a consequence, its performance is degraded in scenarios with high link correlation and low channel distinctness. Therefore, Trellis Coded Spatial Modulation (TCSM) has been proposed to improve the performance of SM over correlated channels [8], [9]. TCSM applies coding to the bits conveyed in the transmitter index in order to increase the free distance between sequences of spatial constellation points. Consequently, the transmitter detection is made more robust and the error ratio is reduced. In order to achieve these gains, TCSM splits the data bits into two subsets. The first subset directly specifies the digitally modulated signal to be emitted, whereas the second subset is first passed to an encoder and then used to determine the emitter to be activated. Consequently, TCSM differentiates between the bits represented by digital signal modulation and the bits conveyed in the spatial domain. However, this approach disallows a joint decoding at the receiver side, thus not allowing the full exploitation of the SM principle.

Therefore, in this paper we extend the TCSM technique to an enhanced coded SM scheme which jointly encodes the bits conveyed in the spatial as well as in the signal domain. To this end, a convolutional encoder is applied to all data bits *before* they are split into the two subsets which determine the digitally modulated signal and the active transmitter. It is found that our jointly encoding achieves higher coding gains than the originally proposed TCSM scheme if applied to OWC.

The remainder of this paper is organised as follows: in Section II the basic system model is given. Section III introduces the setup which is used to model the optical wireless indoor scenario. Actual channel measurements substantiate the chosen model. In Section IV the bit error ratio (BER) performance of our proposed enhanced coded SM scheme is evaluated and compared to the original TCSM scheme [8], [9] as well as to uncoded SM. Finally, Section V concludes the paper.

II. System Model

The considered system model comprises N_t optical transmitters and N_r receivers. The N_r-dimensional received signal vector is expressed as follows:

$$\mathbf{y} = \mathbf{H}\,\mathbf{s} + \mathbf{n} \;\text{ with }\; \mathbf{y} \in \mathbb{R}^{N_r}, \tag{1}$$

where the transmitted signal vector is denoted by $\mathbf{s} = [s_1 \;\ldots\; s_{N_t}]^T$ with $[\cdot]^T$ being the transpose operator and s_{n_t} depicting the signal emitted by transmitter n_t. The $N_r \times N_t$ channel matrix

$$\mathbf{H} = \begin{pmatrix} h_{11} & \cdots & h_{1N_t} \\ \vdots & \ddots & \vdots \\ h_{N_r1} & \cdots & h_{N_rN_t} \end{pmatrix} \tag{2}$$

denotes the respective channel gain of the link between transmitter n_t and receiver n_r. Moreover, $\mathbf{n}$ is the noise vector with N_r elements, assumed to be real valued additive white Gaussian noise (AWGN) with zero mean, double-sided power spectral density E_n and variance σ^2.

The basic principle of SM is that besides transmitting data by common signal modulation, *e.g.* amplitude modulation, it uses the transmitter index to convey additional bits. To this end, only one transmitter is emitting a signal at any time instance. Consequently, only one element of the signal vector $\mathbf{s}$ is non-zero and the index of this element represents the emitter to be activated. Fig. 1 illustrates the functionality of SM for a setup with $N_t = 4$ optical emitters and a signal constellation size of $M = 4$. As the spectral efficiency of SM is $\log_2(M\,N_t)$ bit/s/Hz, 4 bits can be transmitted per channel use in this example. The bits are passed to the SM mapper, which maps them to a signal constellation point and a transmitter index. As shown, the last two bits denote the index of the transmitter, whereas the first two bits represent the actual signal to be sent. For instance, the bit sequence "1 1 1 0" is represented by LED number 4 emitting signal I_3.

In the following, pulse amplitude modulation (PAM) is considered for signal modulation as it is widely used in OWC because of its simple implementation. The intensities which are used for the signal modulation of SM are given by

$$I_m = \frac{2\,I}{M+1}\,m \;\text{ for }\; m = 1 \ldots M, \tag{3}$$

with I denoting the mean optical intensity being emitted. Note that these intensities differ from common PAM as SM cannot operate with a signal intensity of $I_m = 0$. This is due to the fact that for $I_m = 0$, no emitter would be activated and the information conveyed in the spatial domain would be lost.

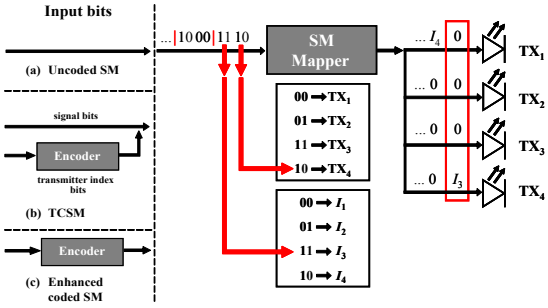

Fig. 1. Illustration of SM operation with $N_t = 4$ and $M = 4$.

The detection at the receiver side is based on the maximum-likelihood (ML) principle. Therefore, the detector decides for the constellation vector $\widehat{\mathbf{s}}$ which minimises the Euclidean distance between the actual received signal vector $\mathbf{y}$ and all potential received signals leading to

$$\widehat{\mathbf{s}} = \arg\max_{\mathbf{s}} p_{\mathbf{y}}(\mathbf{y}|\mathbf{s},\mathbf{H}) = \arg\min_{\mathbf{s}} \|\mathbf{y} - \mathbf{H}\,\mathbf{s}\|_{\mathrm{F}}^2, \tag{4}$$

where $\|\cdot\|_{\mathrm{F}}$ denotes the Frobenius norm and $p_{\mathbf{y}}$ is the probability density function of $\mathbf{y}$ conditioned on $\mathbf{s}$ and $\mathbf{H}$ with $p_{\mathbf{y}}(\mathbf{y}|\mathbf{s},\mathbf{H}) \propto \exp\left(-\|\mathbf{y} - \mathbf{H}\,\mathbf{s}\|_{\mathrm{F}}^2/\sigma^2\right)$. Consequently, the ML detector jointly estimates the emitter index and the transmitted signal by a common operation. In the following it is assumed that the receiver has perfect knowledge of the channel, whereas $\mathbf{H}$ is not known at the transmitter side. If forward error correction (FEC) coding is applied, the ML detection principle given in (4) can be used to realise a soft decision ML detector for SM by employing log-likelihood ratios (LLRs). According to [10], the a posteriori LLR for the i^{th} bit conveyed in the transmitted signal vector $\mathbf{s}$ is

$$L(\mathbf{s}^i) = \log \frac{\sum\limits_{\mathbf{s}\,\in\,\mathbf{S}_1^i} \exp\left(-\frac{\|\mathbf{y}-\mathbf{H}\,\mathbf{s}\|_{\mathrm{F}}^2}{\sigma^2}\right)}{\sum\limits_{\mathbf{s}\,\in\,\mathbf{S}_0^i} \exp\left(-\frac{\|\mathbf{y}-\mathbf{H}\,\mathbf{s}\|_{\mathrm{F}}^2}{\sigma^2}\right)}, \tag{5}$$

where $\mathbf{S}_1^i$ and $\mathbf{S}_0^i$ represent the set of signal vectors which have "1" and "0" at the i^{th} bit position, respectively. The calculated LLRs can be processed by a soft decision Viterbi decoder in order to retrieve the transmitted data bits.

III. Optical Wireless Setup

In this paper, intensity modulated optical wireless links with line-of-sight (LOS) characteristics are considered. According to [2], the channel gain of a directed LOS link can be determined using its geometric alignment yielding to

$$h = \begin{cases} \frac{(k+1)\,A\,r}{2\,\pi\,d^2}\cos^k(\phi)\cos(\psi) & 0 \le \psi \le \Psi_{\frac{1}{2}} \\ 0 & \psi > \Psi_{\frac{1}{2}} \end{cases} \tag{6}$$

where $\Psi_{\frac{1}{2}}$ is the field-of-view (FOV) semiangle of the receiver, $k = \frac{-\ln(2)}{\ln\left(\cos(\Phi_{\frac{1}{2}})\right)}$ and $\Phi_{\frac{1}{2}}$ is the transmitter semiangle (at half

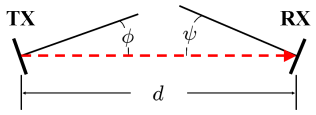

Fig. 2. Geometric scenario used for calculation of channel coefficients.

power). Moreover, r denotes the optical-to-electrical conversion coefficient and A is the detector area of the receiver. The distance between transmitter and receiver is depicted by d. As illustrated in Fig. 2, ϕ is the angle of emergence with respect to the transmitter (TX) axis and ψ is the angle of incidence with respect to the receiver (RX) axis. Consequently, the channel gain $h_{n_r n_t}$ depends on the position of both transmitter n_t and receiver n_r, *i.e.* their distance and angular alignment. Due to the use of SM, only one transmitter is emitting at any time instance and given independent identically distributed (i.i.d.) ones and zeros as data bits, each transmitter is activated with equal probability. Therefore, the average electrical power collected at each receiver is donated by $E_{\mathrm{RX}} = \left(\frac{1}{N_r} \frac{1}{N_t} \sum_{n_r=1}^{N_r} \sum_{n_t=1}^{N_t} h_{n_r n_t} I \right)^2$.

Without loss of generality, the performance of the evaluated SM schemes is studied using practical system parameters as follows: we analyse the channel gains of a setup which employs an off-the-shelf DL-6147-040 diode [11] at the transmitter side with $\Phi_{\frac{1}{2}} \approx 8°$ and a wavelength of 658 nm. The optical receiver consists of a circuitry applying a BPX 61 Silicon PIN (positive intrinsic negative) photo diode [12] with an optical-to-electrical conversion coefficient of $r \approx 0.434$ A/W at 658 nm, a detector area of $A \approx 7$ mm^2 and $\Psi_{\frac{1}{2}} \approx 55°$. The 3 dB cut-off frequency of the photo diode is about 17 MHz.

Fig. 3 displays an arbitrary optical wireless test setup which is used for channel measurements employing the diodes given above. As illustrated, the setup consists of two identical transmitters TX_1 and TX_2 which have a directed LOS connection towards the receiver. The spacing of the two transmitters is fixed to be 30 cm while their distance to the receiver d_1, respectively d_2, is varied. Both transmitters are oriented towards the receiver so that $\phi_1 = \phi_2 = 0$. As TX_1 is directly placed on the receiver axis, $\psi_1 = 0$ holds. However, TX_2 has an angular misalignment ψ_2 with respect to the receiver axis. Fig. 4 shows the measured channel gains for two scenarios,

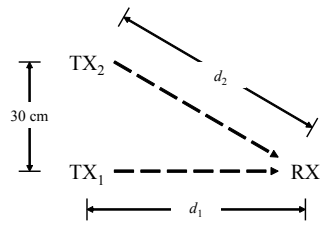

Fig. 3. Illustration of the optical wireless test setup.

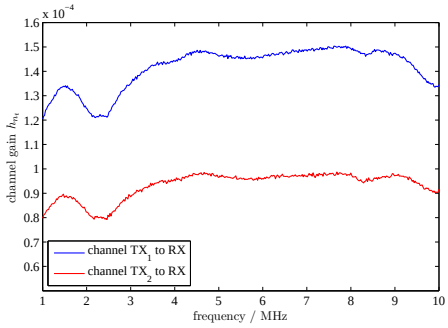

(a) channel gains for $d_1 = 50$ cm and $d_2 \approx 58$ cm.

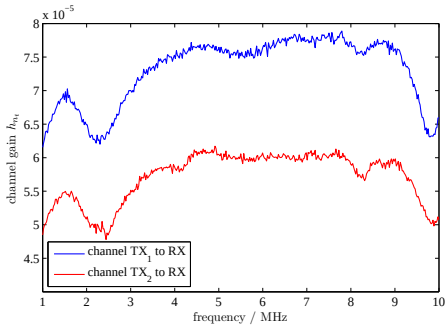

(b) channel gains for $d_1 = 70$ cm and $d_2 \approx 76$ cm.

Fig. 4. Measured gains of the optical wireless channels within the test setup.

similar to the setup presented in [13]. The gains are plotted for a frequency range of $1 - 10$ MHz. For scenario 4(a), $d_1 = 50$ cm, $d_2 \approx 58$ cm and $\psi_2 \approx 31°$. For scenario 4(b), $d_1 = 70$ cm, $d_2 \approx 76$ cm and $\psi_2 \approx 23°$. The measurements show that the links are highly correlated and differ only by their absolute gain, due to the larger distance and angular misalignment of TX_2. Consequently, the gains have a time averaged correlation coefficient of

$$\rho(h_1, h_2) = \frac{\mathrm{E}\left\{(h_1 - \mathrm{E}\{h_1\})(h_2 - \mathrm{E}\{h_2\})\right\}}{\sqrt{\mathrm{VAR}\{h_1\}\,\mathrm{VAR}\{h_2\}}} \approx 0.97,$$

with $\mathrm{E}\{\cdot\}$ denoting the expectation operator and $\mathrm{VAR}\{\cdot\}$ being the variance operator. Moreover, the measured optical channels show only little variations within the considered frequency range as their maximum coefficient of variation, $v_n = \sqrt{\mathrm{VAR}\{h_n\}}/\,\mathrm{E}\{h_n\}$, is only about 0.07. Therefore, the links can be represented by flat AWGN channels with constant attenuation. Table I displays the mean measured channel gains $\overline{h_n}$ and the theoretical channel gains h_n for scenario 4(a) and 4(b). Moreover, the relative difference, $\Delta_n = 100\,\left|\overline{h_n} - h_n\right| / h_n$, between the measured gains and the theoretical values is given. As the maximum difference is only about 6.49 %, the measured channel gains and the gains calculated using the geometrical model closely match.

TABLE I
COMPARISON OF MEASURED AND THEORETICAL CHANNEL GAINS.

	scenario 4(a)	**scenario 4(b)**
theoretical gain	$h_1 \approx 139.01\ 10^{-6}$ $h_2 \approx\ 87.65\ 10^{-6}$	$h_1 \approx 70.93\ 10^{-6}$ $h_2 \approx 55.07\ 10^{-6}$
measured gain	$\overline{h_1} \approx 141.59\ 10^{-6}$ $\overline{h_2} \approx\ 93.34\ 10^{-6}$	$\overline{h_1} \approx 73.05\ 10^{-6}$ $\overline{h_2} \approx 57.17\ 10^{-6}$
relative difference	$\Delta_1 \approx 1.86$ % $\Delta_2 \approx 6.49$ %	$\Delta_1 \approx 2.99$ % $\Delta_2 \approx 3.81$ %

Therefore, we use this model in the following to derive the channel gains of different indoor setup scenarios. To this end, we consider a generic 4×4 indoor scenario ($N_r = 4$ and $N_t = 4$), which is located within a $4.0\,\mathrm{m} \times 4.0\,\mathrm{m} \times 3.0\,\mathrm{m}$ room. We assume that the transmitters are placed at a height of $z = 3.00$ m and are oriented downwards to point straight down from the ceiling. The receivers are located at a height of $z = 0.75$ m (*e.g.* height of a table) and are oriented upwards to point straight up at the ceiling. Both transmitters and receivers are aligned in a quadratically 2×2 array which is centered in the middle of the room. On the basis of this scenario, we investigate different static setups with varying element spacings of the single transmitters on the x- and y-axis, depicted by d_{TX}, while the element spacing of the receivers is assumed to be 0.1 m on the x- and y-axis for all considered setups. This receiver spacing is chosen with regard to a practical implementation within a potential (hand-held) user device. Fig. 5 exemplarily shows the positioning of the 4×4 setup, at which the receivers are displayed as dots and the transmitters as triangulars. The plotted cones illustrate the orientation of the transmit beams and the orientation of the receiver FOV. Applying (6) to this setup with $d_{\mathrm{TX}} = 0.3$ m, 0.5 m and 0.7 m, results in the following channel matrices:

$$\mathbf{H}_{d_{\mathrm{TX}}=0.3} \approx 10^{-5} \begin{pmatrix} 0.5934 & 0.4775 & 0.4775 & 0.3847 \\ 0.4775 & 0.5934 & 0.3847 & 0.4775 \\ 0.4775 & 0.3847 & 0.5934 & 0.4775 \\ 0.3847 & 0.4775 & 0.4775 & 0.5934 \end{pmatrix},$$

$$\mathbf{H}_{d_{\mathrm{TX}}=0.5} \approx 10^{-5} \begin{pmatrix} 0.3847 & 0.2691 & 0.2691 & 0.1889 \\ 0.2691 & 0.3847 & 0.1889 & 0.2691 \\ 0.2691 & 0.1889 & 0.3847 & 0.2691 \\ 0.1889 & 0.2691 & 0.2691 & 0.3847 \end{pmatrix}, \quad (7)$$

$$\mathbf{H}_{d_{\mathrm{TX}}=0.7} \approx 10^{-5} \begin{pmatrix} 0.1889 & 0.1157 & 0.1157 & 0.0713 \\ 0.1157 & 0.1889 & 0.0713 & 0.1157 \\ 0.1157 & 0.0713 & 0.1889 & 0.1157 \\ 0.0713 & 0.1157 & 0.1157 & 0.1889 \end{pmatrix}.$$

It can be seen that the symmetrical arrangement of the transmitters and receivers leads to equal channel gains for the wireless links with the same alignment, *e.g.* $h_{n_r n_t} = h_{n_t n_r}$. Moreover, if the spacing d_{TX} between the transmitters is small, the gains are quite similar, whereas if d_{TX} gets larger, the differences between the links increase due to the geometry of the setup scenario, *i.e.* the enlarged angular misalignment.

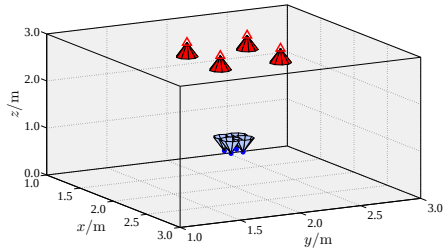

Fig. 5. Positioning of 4×4 setup with $d_{\mathrm{TX}} = 0.5$ m within room.

IV. BIT ERROR RATIO PERFORMANCE OF CODED SPATIAL MODULATION

In the following, we evaluate the BER performance of coded SM applied to the optical wireless setup presented above. For encoding at the transmitter side, we assume a convolutional encoder with an octal presentation of $(161, 133)$, a coding rate of $c = \frac{1}{2}$, a constraint length of $l = 7$ and a free distance of $d_{\mathrm{free}} = 10$. Furthermore, the encoded bits are additionally interleaved by a random block interleaver. As proposed in [8], [9], by applying TCSM, only the bits which determine the transmitter index are passed to the convolutional encoder, while the bits denoting the digitally modulated signal to be transmitted remain uncoded and are directly passed to the SM mapper (see Fig. 1 (b)). The encoded and interleaved bits are then used to determine the emitter which is activated according to the standard SM transmission scheme. In contrast, our proposed enhanced coded SM scheme passes *all* information bits to the convolutional encoder. The encoded bits are also interleaved and then passed to the standard SM mapper which maps them to the signal constellation points and transmitter indices as depicted in Fig. 1 (c). Note that for the sake of comparison, both coded SM schemes use the same $(161, 133)$ convolutional encoder. At the receiver side, the encoded bits of both coded SM schemes are deinterleaved and processed by a soft decision Viterbi decoder which has a traceback length of five times the constraint length.

Fig. 6 shows the BER performance of our enhanced coded SM scheme, TCSM and uncoded SM for a spectral efficiency of $R = 2$ bit/s/Hz in the considered 4×4 setup with different transmitter spacings of $d_{\mathrm{TX}} = 0.3$ m, 0.5 m and 0.7 m. In order to provide this spectral efficiency, uncoded SM operates with a signal constellation size of $M = 1$, *i.e.* all bits to be transmitted are conveyed in the spatial domain because $R = \log_2(N_t)$. In contrast, TCSM has to operate with $M = 2$ to compensate for the redundancy induced by the encoder. Moreover, the enhanced coded SM scheme has to operate with an even larger constellation size of $M = 4$ to provide the same data rate. As shown, despite this enlarged signal constellation size, our enhanced coded SM scheme can achieve gains in signal to noise ratio (SNR) of about $2 - 3$ dB compared to TCSM and outperforms uncoded SM by about $6 - 10$ dB. Moreover, it can be seen that an enlargement of the transmitter spacing,

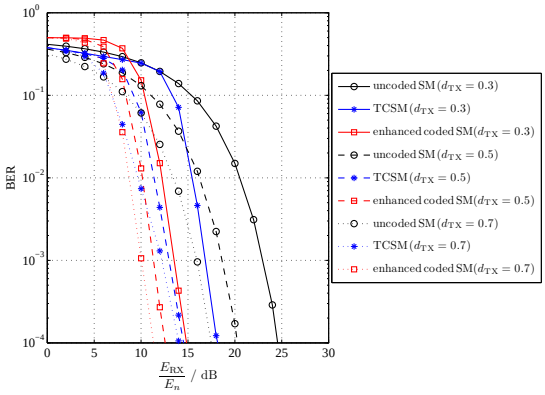

Fig. 6. BER of coded and uncoded SM for spectral efficiency of $R = 2$ bit/s/Hz in 4×4 setup scenario with varying distance d_{TX} of transmitters on the $x-$ and $y-$axis.

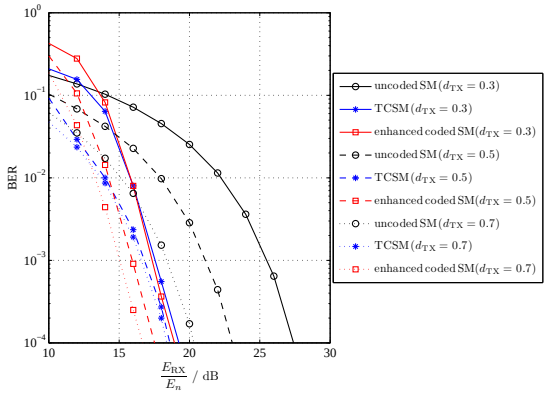

Fig. 7. BER of coded and uncoded SM for spectral efficiency of $R = 3$ bit/s/Hz in 4×4 setup scenario with varying distance d_{TX} of transmitters on the $x-$ and $y-$axis.

d_{TX}, increases the channel distinctness and improves the BER performance of both coded and uncoded SM. Fig. 7 displays the BER of the considered schemes for $R = 3$ bit/s/Hz. In this scenario, uncoded SM operates with a signal constellation size of $M = 2$ and TCSM with $M = 4$. The enhanced coded SM scheme has to operate with $M = 16$. As depicted, the new enhanced coded SM scheme can also outperform both other schemes for $R = 3$ bit/s/Hz and achieves SNR gains of about $1 - 2$ dB compared to TCSM, respectively of about $4 - 8$ dB compared to uncoded SM, despite the fact that it has to use a much larger signal constellation size to compensate for the induced FEC coding.

V. Summary and Conclusion

In this paper, we have studied the performance of coded SM applied to OWC in indoor environments. It has been shown that FEC coding can significantly improve the performance of SM under conditions with high link correlation and low channel distinctness. Moreover, we have proposed an enhanced coded SM scheme which jointly encodes the bits conveyed in the spatial and signal domains. It has been found in this paper that our approach can outperform the originally proposed TCSM scheme by several dB. This is because the jointly encoding conveys the coded bits in the spatial as well as in the signal domain. As a consequence, our enhanced coded SM scheme can make better use of the basic SM detection principle which jointly detects the emitter index and the transmitted signal by a common operation. Consequently, our enhanced coded SM scheme utilises the output of the ML detector more efficiently than the originally proposed TCSM scheme, thus providing larger coding gains. Future work might deal with the performance of coded SM for higher spectral efficiencies and different coding rates as well as its evaluation for outdoor free space optical (FSO) communications employing laser diodes.

References

[1] R. J. Green, H. Joshi, M. D. Higgins, and M. S. Leeson, "Recent Developments in Indoor Optical Wireless," *IET Communications*, vol. 2, no. 1, pp. 3–10, Jan. 2008.

[2] J. M. Kahn and J. R. Barry, "Wireless Infrared Communications," *Proceedings of the IEEE*, vol. 85, no. 2, pp. 265–298, Feb. 1997.

[3] Y. Tanaka, T. Komine, S. Haruyama, and M. Nakagawa, "Indoor Visible Communication Utilizing Plural White LEDs as Lighting," in *Proceedings of the 12^{th} IEEE International Symposium on Personal, Indoor and Mobile Radio Communications*, vol. 2, San Diego, CA, USA, Sep. 30–Oct. 3, 2001, pp. 81–85.

[4] D. C. O'Brien, Q. Shabnam, Z. Sasha, and G. E. Faulkner, "Multiple Input Multiple Output Systems for Optical Wireless; Challenges and Possibilities," in *Proceedings of SPIE*, San Diego, California, USA, Aug. 15–17 2006.

[5] E. Telatar, "Capacity of Multi-Antenna Gaussian Channels," *European Transaction on Telecommunication*, vol. 10, no. 6, pp. 585–595, Nov. / Dec. 1999.

[6] R. Mesleh, H. Haas, C. W. Ahn, and S. Yun, "Spatial Modulation – A New Low Complexity Spectral Efficiency Enhancing Technique," in *IEEE International Conference on Communication and Networking in China (CHINACOM)*, Beijing, China, Oct. 25–27, 2006, pp. 1–5.

[7] T. Fath, H. Haas, M. Di Renzo, and R. Mesleh, "Spatial Modulation applied to Optical Wireless Communications in Indoor LOS Environments," in *Proc. of the IEEE Global Communications Conference*, Houston, Texas, USA, Dec. 5–9, 2011, pp. 3001–3005.

[8] R. Mesleh, I. Stefan, H. Haas, and P. Grant, "On the Performance of Trellis Coded Spatial Modulation," in *ITG International Workshop on Smart Antennas (WSA'09)*, Berlin, Germany, Feb. 16–19 2009.

[9] R. Mesleh, M. Di Renzo, H. Haas, and P. M. Grant, "Trellis Coded Spatial Modulation," *IEEE Trans. on Wireless Commun.*, vol. 9, no. 7, pp. 2349–2361, July 2010.

[10] S. U. Hwang, S. Jeon, S. Lee, and J. Seo, "Soft-Output ML Detector for Spatial Modulation OFDM Systems," *IEICE Electronics Express*, vol. 6, no. 19, pp. 1426–1431, Oct. 2009.

[11] Tottori SANYO Electric Co., Ltd., "Datasheet: RED LASER DIODE DL-6147-040," Retrieved Sep. 08, 2011 from http://combinlasers.com/1sanyo/dl-6147-040.pdf, May 2005.

[12] OSRAM Opto Semiconductors GmbH, "Datasheet: BPX 61 Silicon PIN Photodiode, Lead (Pb) Free Product - RoHS Compliant," Retrieved Sep. 08, 2011 from http://catalog.osram-os.com, Mar. 2007.

[13] T. Fath, M. Di Renzo, and H. Haas, "On the Performance of Space Shift Keying for Optical Wireless Communications," in *Proc. of the IEEE Global Communications Conference - Workshop on Optical Wireless Communications*, Miami, Florida, USA, Dec. 10, 2010, pp. 990–994.

Performance Comparison of MIMO Techniques for Optical Wireless Communications in Indoor Environments

Thilo Fath and Harald Haas, *Member, IEEE*

***Abstract*—In this paper, we compare the performance of multiple-input-multiple-output (MIMO) techniques applied to indoor optical wireless communications (OWC) assuming line-of-sight (LOS) channel conditions. Specifically, several 4×4 setups with different transmitter spacings and different positions of the receiver array are considered. The following MIMO algorithms are considered: Repetition Coding (RC), Spatial Multiplexing (SMP) and Spatial Modulation (SM). Particularly, we develop a framework to analytically approximate the bit error ratios (BERs) of these schemes and verify the theoretical bounds by simulations. The results show that due to diversity gains, RC is robust to various transmitter-receiver alignments. However, as RC does not provide spatial multiplexing gains, it requires large signal constellation sizes to enable high spectral efficiencies. In contrast, SMP enables high data rates by exploiting multiplexing gains. In order to provide these gains, SMP needs sufficiently low channel correlation. SM is a combined MIMO and digital modulation technique. We show that SM is more robust to high channel correlation compared to SMP, while enabling larger spectral efficiency compared to RC. Moreover, we investigate the effect of induced power imbalance between the multiple transmitters. It is found that power imbalance can substantially improve the performance of both SMP and SM as it reduces channel correlation. In this context, we also show that blocking some of the links is an acceptable method to reduce channel correlation. Even though the blocking diminishes the received energy, it outweighs this degradation by providing improved channel conditions for SMP and SM. For example, blocking 4 of the 16 links of the 4×4 setup improves the BER performance of SMP by more than 20 dB, while the effective signal to noise ratio (SNR) is reduced by about 2 dB due to the blocking. Therefore, MIMO techniques can provide gains even under LOS conditions which provide only little channel differences.**

***Index Terms*—MIMO, optical wireless communications, repetition coding, spatial modulation, spatial multiplexing.**

I. Introduction

RECENTLY, there has been increasing interest in optical wireless communications (OWC) because of the tremendous advancements in solid-state-lighting technology. It is now possible to harnesses vast, free and largely unused wireless transmission resources in the infra-red (IR) and visible light spectrum for communication purposes. Especially for indoor scenarios, like office and home environments, OWC can provide significant spectrum relief for the crowed radio frequency (RF) spectrum used by traditional wireless communications systems such as wireless local area networks (WLANs). As more and more wireless home networks are being installed, the public ISM (Industrial, Scientific and Medical) band gets increasingly crowded leading to a shortage of available bandwidth, increased interference and compromised system throughput. In addition, RF communications can interfere with electrical equipment preventing its application in sensitive environments like hospitals or aircraft cabins.

With the advent of high luminance light-emitting diodes (LEDs), efficient and inexpensive illumination devices are available which will progressively replace existing light bulbs and fluorescent lamps. In contrast to the latter, LEDs, being electronic devices, can be switched must faster. Therefore, an additional benefit can be generated if LEDs are not only used for illumination, but also for high data rate wireless communications to establish flexible and ubiquitous communication networks [1]-[3]. For instance, the ceiling lights in an office can be used to transmit data to a receiver placed on a desk within a room. Apart from the visible light spectrum, the near-IR band between about 780 nm and 950 nm is also a potential transmission medium for indoor communications [4], [5]. Commonly, OWC transfers data by modulating the intensity of the optical signal [6]. Typical light fixtures achieve more than 400 lux to provide sufficient indoor illumination. Those illumination levels are enough to transmit data at high signal to noise ratios (SNRs). At the receiver side, a photo-detector converts the optical signals into electrical signals which are used to decode the information. This direct detection enables the implementation of simple low-cost transceiver devices without the need for complex high-frequency circuit designs. As the information can only be received by a photo-detector which is within the emitted light beam and the signals do not penetrate opaque boundaries, the propagation can be restricted to specific spots or areas (rooms). This prevents interception and creates less interference compared to RF devices whose signals propagate through walls. Moreover, the line-of-sight (LOS) characteristic between transmitter and receiver can provide high SNRs of more than 60 dB at the receiver [7], [8].

In order to provide sufficient illumination, light installations are typically equipped with multiple LEDs. This property can

Manuscript received August 29, 2011; revised May 15, 2012 and August 13, 2012.

This work was presented in part at the *IEEE Global Communications Conference GLOBECOM 2011*, Houston, Texas, USA.

Thilo Fath is with EADS Deutschland GmbH, Innovation Works, 81663 Munich, Germany and with the University of Edinburgh, Institute for Digital Communications, the Kings Buildings, Edinburgh EH9 3JL, UK (e-mail: thilo.fath@ed.ac.uk).

Harald Haas is with the University of Edinburgh, Institute for Digital Communications, the Kings Buildings, Edinburgh EH9 3JL, UK (e-mail: h.haas@ed.ac.uk).

readily be exploited to create optical multiple-input-multiple-output (MIMO) communication systems. MIMO techniques are well-established and widely implemented in many RF systems as they offer high data rates by increasing the spectral efficiency [9], [10]. Off-the-shelf LEDs provide only a limited bandwidth of about $30-50$ MHz for incoherent IR light and even less for visible light. Consequently, these incoherent light sources restrict the available bandwidth of practical OWC systems. Therefore, it is equally important to achieve high spectral efficiencies in OWC. For free-space optical transmission the effects of MIMO have already been studied. It has been shown that spatial diversity can combat the fading effects due to scattering and scintillation caused by atmospheric turbulences [11], [12]. Ongoing research activities intend to increase the capacity of OWC indoor systems by MIMO techniques [13], [14]. However, for indoor OWC it is still not clear to what extent MIMO techniques can provide gains. This is because in indoor environments there are no fading effects caused by turbulence etc., especially if LOS scenarios are considered. Therefore, indoor optical wireless links are envisaged to be highly correlated enabling only minor diversity gains. Provided that MIMO techniques mostly rely on spatially uncorrelated channels, it is unclear whether the optical propagation channel in indoor environments can offer sufficiently low channel correlation.

In this paper, we study the performance of MIMO techniques for OWC in an indoor environment with LOS characteristic. A simple 4×4 setup with different transmitter spacings is assumed. We consider three different transmission schemes, namely Repetition Coding (RC), Spatial Multiplexing (SMP) and Spatial Modulation (SM). These techniques are compared with regard to their bit error ratio (BER) performance for different spectral efficiencies. The error ratios are determined by computer simulations as well as by analytical approximations. For the latter, we give a framework to determine the theoretical BERs of the considered techniques using union bound methods. Moreover, we study the effect of induced power imbalance between the multiple transmitters. It has been shown in [15] that for a two-transmitter OWC scenario with highly correlated channels, power imbalance can improve the performance of MIMO. In addition, we investigate link blockage as a means to reduce channel correlation.

The remainder of this paper is organised as follows: In Section II we define the basic system model and the considered indoor system setup. The different MIMO techniques are introduced in Section III and their theoretical bit error bounds are determined. In Section IV we analyse the BER performance of the MIMO techniques for different scenarios. In this context, we investigate the effect of both induced power imbalance and link blockage. Finally, Section V concludes the paper.

II. System Model

We consider an optical wireless MIMO transmission system employing intensity modulation (IM) and direct detection (DD) of the optical carrier using incoherent light sources, *e.g.* LEDs. The system is equipped with N_t transmitters and

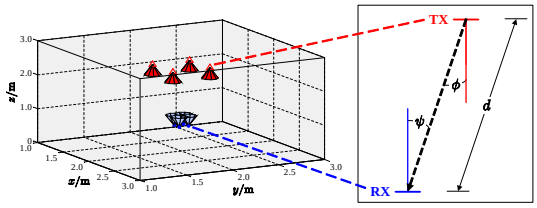

Fig. 1. Geometric scenario used for calculation of channel coefficients.

N_r photo-detectors at the receiver side. The received signal vector is

$$\mathbf{y} = \mathbf{H}\,\mathbf{s} + \mathbf{n}, \tag{1}$$

where $\mathbf{n}$ is the sum of ambient shot light noise and thermal noise. It is independent of the transmitted signals and the main noise impairment as commonly assumed in OWC [5]. Consequently, $\mathbf{n}$ is real valued additive white Gaussian noise (AWGN) with zero mean and a variance $\sigma^2 = \sigma^2_{\text{shot}} + \sigma^2_{\text{thermal}}$, where σ^2_{shot} is the shot noise variance and $\sigma^2_{\text{thermal}}$ is the thermal noise variance [5]. Thus, the noise power is given by $\sigma^2 = N_0\,B$, where N_0 is the noise power spectral density and B is the bandwidth. The transmitted signal vector is denoted by $\mathbf{s} = [s_1\ \ldots\ s_{N_t}]^T$, with $[\cdot]^T$ being the transpose operator. The elements of $\mathbf{s}$ indicate which signal is emitted by each optical transmitter, *i.e.* s_{n_t} denotes the signal emitted by transmitter n_t. The $N_r \times N_t$ channel matrix $\mathbf{H}$ is given by

$$\mathbf{H} = \begin{pmatrix} h_{11} & \cdots & h_{1N_t} \\ \vdots & \ddots & \vdots \\ h_{N_r1} & \cdots & h_{N_rN_t} \end{pmatrix}, \tag{2}$$

where $h_{n_rn_t}$ represents the transfer factor of the wireless link between transmitter n_t and receiver n_r. As the LEDs are in close proximity, they can be jointly driven by exactly the same baseband hardware and electronic driver. We, therefore, assume that the transmission is perfectly synchronised. In addition, there is only a very small path difference between the multiple transmitter-receiver links of some cm (as shown in Section IV). Therefore, there is negligible temporal delay between the multiple links and consequently, we consider the system model given in (1) without time dispersion.

In this paper, we assume optical wireless links with LOS characteristics. Fig. 1 (right hand side) illustrates a directed LOS link. As shown, ϕ is the angle of emergence with respect to the transmitter (TX) axis and ψ is the angle of incidence with respect to the receiver (RX) axis. Furthermore, d depicts the distance between transmitter and receiver. Using this geometric scenario, the channel gain of an optical propagation link can be calculated according to [5] as follows:

$$h = \begin{cases} \frac{(k+1)\,A}{2\,\pi\,d^2}\cos^k(\phi)\cos(\psi) & 0 \le \psi \le \Psi_{\frac{1}{2}} \\ 0 & \psi > \Psi_{\frac{1}{2}} \end{cases} \tag{3}$$

with the order $k = \frac{-\ln(2)}{\ln\left(\cos(\Phi_{\frac{1}{2}})\right)}$ and the transmitter semiangle $\Phi_{\frac{1}{2}}$ (at half power), which is assumed to be $15°$. Furthermore, $\Psi_{\frac{1}{2}}$ denotes the field-of-view (FOV) semiangle of the receiver,

$$\mathrm{BER}_{\mathrm{RC}} \geq \frac{2\,(M-1)}{M\,\log_2(M)}\,\mathrm{Q}\left(\frac{1}{M-1}\,\sqrt{\frac{E_s}{N_0\,N_t^2}\,\sum_{n_r=1}^{N_r}\left(\sum_{n_t=1}^{N_t} h_{n_r n_t}\right)^2}\right) \tag{7}$$

which is assumed to be $15°$. These semiangles have been chosen with regard to a practical LOS indoor OWC system which has been developed and implemented within the European Union (EU) project OMEGA [16], [17]. A is the detector area of the receiver. In this paper, we assume A to be 1 cm^2. Clearly, the channel coefficient $h_{n_r n_t}$ depends on the specific position of transmitter n_t and receiver n_r. If a receiver and a transmitter are not in each others FOV, $h_{n_r n_t} = 0$.

In the following, we consider a 4×4 indoor scenario ($N_r = 4$ and $N_t = 4$) which is located within a $4.0\,\mathrm{m} \times 4.0\,\mathrm{m} \times 3.0\,\mathrm{m}$ room. We assume that the transmitters are placed at a height of $z = 2.50$ m and are oriented downwards to point straight down from the ceiling. The receivers are located at a height of $z = 0.75$ m (*e.g.* height of a table) and are oriented upwards to point straight up at the ceiling. Both transmitters and receivers are aligned in a quadratically 2×2 array which is centered in the middle of the room. On the basis of this scenario, we investigate different static setups with varying spacings of the single transmitters on the x- and y-axis, depicted by d_{TX}. The spacing of the receivers is assumed to be 0.1 m on the x- and y-axis for all considered setups. This receiver spacing would enable the implementation of the receiver array into typical laptop computers. Fig. 1 (left hand side) shows the positioning of the 4×4 setup. The receivers are displayed as dots and the transmitters as triangles. The plotted cones represent the orientation of the transmit beams and the orientation of the FOVs of the receivers, respectively. The cone angles are related to the semiangles of the transmitter and receiver devices.

III. MIMO Techniques

In the following, we introduce the different MIMO techniques which we study for indoor OWC. We assume that all considered MIMO techniques use maximum-likelihood (ML) detection at the receiver side with perfect knowledge of the channel and ideal time synchronisation. Therefore, the decoder decides for the constellation vector $\widehat{\mathbf{s}}$ which minimises the Euclidean distance between the actual received signal vector $\mathbf{y}$ and all potential received signals leading to

$$\widehat{\mathbf{s}} = \arg\max_{\mathbf{s}} p_{\mathbf{y}}(\mathbf{y}|\mathbf{s},\mathbf{H}) = \arg\min_{\mathbf{s}} \|\mathbf{y} - \mathbf{H}\,\mathbf{s}\|_{\mathrm{F}}^2\,, \tag{4}$$

where $p_{\mathbf{y}}$ is the probability density function of $\mathbf{y}$ conditioned on $\mathbf{s}$ and $\mathbf{H}$. $\|\cdot\|_{\mathrm{F}}$ denotes the Frobenius norm.

The simplest MIMO transmission technique is RC which simultaneously emits the same signal from all transmitters. Therefore, for RC $s_1 = s_2 = \ldots = s_{N_t}$ holds. RC is known to achieve good performance in free-space OWC because of transmit-diversity [12]. In [18] it is shown that RC can outperform orthogonal space-time block codes (OSTBCs) like the Alamouti scheme [19] and single-input-multiple-output (SIMO) setups. This is due to the fact that the intensities coming from the several transmitters constructively add up at the receiver side. In this paper, unipolar M-level pulse amplitude modulation (M-PAM) is considered together with RC, where M denotes the signal constellation size. Consequently, M-PAM achieves a spectral efficiency of $\log_2(M)$ bit/s/Hz. We consider PAM because it is more bandwidth efficient compared to other pulse modulation techniques such as on-off-keying (OOK), pulse width modulation (PWM) and pulse position modulation (PPM). Moreover, PAM has shown to have similar optical power efficiency compared to direct-current-biased optical orthogonal frequency division multiplexing (DCO-OFDM) [20]. For instance, in [21] and [22] the authors show that PAM outperforms DCO-OFDM because the latter requires a high constant DC bias to make the bipolar OFDM waveform non-negative. This DC bias power affects the effective SNR of DCO-OFDM in contrast to unipolar PAM which operates without an additional DC bias. Without loss of generality, we employ rectangular pulses in conjunction with M-PAM. The intensity levels are given by:

$$I_m^{\mathrm{PAM}} = \tfrac{2\,I}{M-1}\,m \quad \text{for } m = 0, 1, \ldots, (M-1), \tag{5}$$

where I is the mean optical power emitted. According to, for instance, [6], the BER of unipolar M-PAM can be lower bounded by

$$\mathrm{BER}_{\mathrm{PAM}} \geq \frac{2\,(M-1)}{M\,\log_2(M)}\,\mathrm{Q}\left(\frac{1}{M-1}\,\sqrt{\frac{E_{\mathrm{RX}}}{N_0}}\right), \tag{6}$$

where $\mathrm{Q}(a) = \frac{1}{\sqrt{2\pi}}\int_a^{+\infty}\exp(\frac{-t^2}{2})\,\mathrm{d}t$ is the Q-function and E_{RX} is the *received* electrical energy. In the following, $E_s = (r\;I)^2\,T_s$ denotes the mean *emitted* electrical energy of the intensity modulated optical signals. r represents the optical-to-electrical conversion coefficient. Without loss of generality, we assume r to be $1\ \mathrm{A}\sqrt{\Omega}/\mathrm{W}$. T_s denotes the symbol duration in seconds. As RC simultaneously emits the same signal from several transmitters, the optical transmission power is equally distributed across all emitters. Thus, the intensities given in (5) have to be divided by factor N_t. By doing so, the mean optical power emitted is constant, irrespective of the number of employed transmitters. This ensures the comparability of different setups and transmission techniques. The BER of M-PAM given in (6) can be generalised for an arbitrary $N_r \times N_t$ scenario which employs RC. The BER of RC is shown in (7) on top of this page. The intensities emitted by the multiple transmitters constructively add up at the receiver leading to an optical power of $I_{\mathrm{RX}_{n_r}} = \sum_{n_t=1}^{N_t} \frac{I}{N_t}\,h_{n_r n_t}$ at receiver n_r. Consequently, the single channel gains $h_{n_r n_t} \in [0;1]$ induce a distinctive attenuation of the transmitted signals (path loss) depending on the specific link characteristic. The N_r received signals are combined by maximum ratio combining (MRC) [23, Ch. 7.2.4]. Thus by applying MRC, the received signals

4

$$\mathrm{BER}_{\mathrm{SMP}} \leq \frac{1}{M^{N_t}\,\log_2(M^{N_t})} \sum_{m^{(1)}=1}^{M^{N_t}} \sum_{m^{(2)}=1}^{M^{N_t}} \mathrm{d_H}(b_{m^{(1)}}, b_{m^{(2)}})\, \mathrm{Q}\left(\sqrt{\frac{r^2\,T_s}{4\,N_0}\,\|\mathbf{H}\,(\mathbf{s}_{m^{(1)}} - \mathbf{s}_{m^{(2)}})\|_{\mathrm{F}}^2}\right) \tag{10}$$

with a high SNR are weighted more than signals with a low SNR. Consequently, the electrical SNR after the combiner becomes:

$$\begin{aligned}\frac{E_{\mathrm{RX}}}{N_0} &= \frac{T_s}{N_0} \sum_{n_r=1}^{N_r} \left(r\, I_{\mathrm{RX}_{n_r}}\right)^2 \\ &= \frac{T_s}{N_0} \sum_{n_r=1}^{N_r} \left(\sum_{n_t=1}^{N_t} \frac{r\,I}{N_t}\, h_{n_r n_t}\right)^2 \\ &= \frac{E_s}{N_0\,N_t^2} \sum_{n_r=1}^{N_r} \left(\sum_{n_t=1}^{N_t} h_{n_r n_t}\right)^2,\end{aligned} \tag{8}$$

which corresponds to the SNR given in the argument of the Q-function in (7). Moreover, (8) comprises the received electrical energy given by $E_{\mathrm{RX}} = \sum_{n_r=1}^{N_r} \left(r\, I_{\mathrm{RX}_{n_r}}\right)^2 T_s$. Consequently, the given BER of RC is only affected by the transfer factors of the wireless optical links, respectively by the received optical power. Thus, RC can be represented by a simple single-input-single-output (SISO) scheme which provides the same received electrical energy.

Another well-known MIMO technique is SMP. By applying SMP, independent data streams are simultaneously emitted from all transmitters. Therefore, SMP provides an enhanced spectral efficiency of $N_t\,\log_2(M)$ bit/s/Hz. Like for RC, we use PAM for SMP and equally distribute the optical power across all emitters to ensure that both schemes use the same mean transmission power. For SMP, the signal vector $\mathbf{s}$ has N_t elements which are independent M-PAM modulated signals according to (5), whereas their respective emitted intensities are divided by N_t. Provided that the SMP receiver performs a ML detection, the pairwise error probability (PEP) is the probability that the receiver mistakes the transmitted signal vector $\mathbf{s}_{m^{(1)}}$ for another vector $\mathbf{s}_{m^{(2)}}$, given knowledge of the channel matrix $\mathbf{H}$. Thus, the PEP of SMP can be calculated by

$$\begin{aligned}\mathrm{PEP}_{\mathrm{SMP}} &= \mathrm{PEP}(\mathbf{s}_{m^{(1)}} \rightarrow \mathbf{s}_{m^{(2)}}|\mathbf{H}) \\ &= \mathrm{Q}\left(\sqrt{\frac{r^2\,T_s}{4\,N_0}\,\|\mathbf{H}\,(\mathbf{s}_{m^{(1)}} - \mathbf{s}_{m^{(2)}})\|_{\mathrm{F}}^2}\right).\end{aligned} \tag{9}$$

Using this PEP and considering all M^{N_t} possible combinations of the transmitted signal vector, the BER of SMP can be approximated by union bound methods. The upper bound is given in (10) on top of this page, with $\mathrm{d_H}(b_{m^{(1)}}, b_{m^{(2)}})$ denoting the Hamming distance of the two bit assignments $b_{m^{(1)}}$ and $b_{m^{(2)}}$ of the signal vectors $\mathbf{s}_{m^{(1)}}$ and $\mathbf{s}_{m^{(2)}}$. For instance, if we assume $N_t = 4$ and $M = 2$, the bit sequence "1001" is assigned to $\mathbf{s}_{10} = \left[\frac{I}{2}\ 0\ 0\ \frac{I}{2}\right]^T$ and "1000" is assigned to $\mathbf{s}_9 = \left[\frac{I}{2}\ 0\ 0\ 0\right]^T$, resulting in $\mathrm{d_H}(b_{10}, b_9) = 1$. Therefore, $\mathrm{d_H}(\cdot,\cdot)$ states the number of bit errors when erroneously detecting $\mathbf{s}_{m^{(2)}}$ at the receiver instead of the actually transmitted signal vector $\mathbf{s}_{m^{(1)}}$.

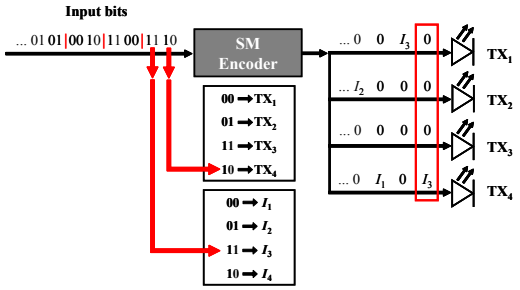

Fig. 2. Illustration of SM operation with $N_t = 4$ and $M = 4$. The first two bits in the block of four bits determine the PAM symbol and the second two bits determine the active LED.

Finally, we also consider SM, which is a combined MIMO and digital modulation technique, proposed in [24] and further investigated in [25]-[27]. In SM, the conventional signal constellation diagram is extended to an additional dimension, namely the spatial dimension. The spatial dimension is used to transmit additional bits. Each transmitter in the transmitting array is assigned a unique binary sequence – the spatial symbol. A transmitter is only activated when the random spatial symbol to be transmitted matches the pre-allocated spatial symbol. Thus, only one transmitter is activated at any PAM symbol duration. Therefore, only one element of the signal vector $\mathbf{s}$ to be transmitted is non-zero. The element is the digitally modulated signal to be sent. The index of the non-zero element is the spatial symbol. SM simultaneously transmits data in the signal domain and the spatial domain. Consequently, SM provides an enhanced spectral efficiency of $\log_2(N_t) + \log_2(M)$ bit/s/Hz. Moreover, as only one transmitter is activated at any symbol duration, SM completely avoids inter-channel interference (ICI). Thus, SM has a lower decoding complexity compared to other MIMO schemes [28]-[30]. Due to the distinct channel transfer factors between a particular transmitter and the receiver, the receiver is able to detect which transmitter is activated and hence is able to detect the spatial symbol. Fig. 2 illustrates the functionality of SM for a setup with $N_t = 4$ optical emitters and a signal constellation size of $M = 4$. The bits to be transmitted are passed to the SM encoder, which maps them to the respective signal and transmitter index. In this example, the last two bits denote the index of the transmitter which emits the signal, whereas the first two bits represent the actual signal to be sent. For instance, the bit sequence "1110" is represented by transmitter number 4 emitting signal I_3. In contrast to RC and SMP, signals with intensity $I_m = 0$ cannot be used for the signal modulation of SM. Because in this case, no transmitter would be active and the spatial information would be lost.

$$\mathrm{BER}_{\mathrm{SM}} \leq \frac{1}{MN_t \, \log_2(MN_t)} \sum_{m^{(1)}=1}^{M} \sum_{n_t^{(1)}=1}^{N_t} \sum_{m^{(2)}=1}^{M} \sum_{n_t^{(2)}=1}^{N_t} \mathrm{d_H}\left(b_{m^{(1)}n_t^{(1)}}, b_{m^{(2)}n_t^{(2)}}\right) \cdot \mathrm{Q}\left(\sqrt{\frac{r^2\,T_s}{4\,N_0} \sum_{n_r=1}^{N_r} \left| I_{m^{(2)}}^{\mathrm{SM}} \, h_{n_r n_t^{(2)}} - I_{m^{(1)}}^{\mathrm{SM}} \, h_{n_r n_t^{(1)}} \right|^2}\right) \tag{13}$$

Therefore, the intensities of common PAM given in (5) have to be modified to be suitable for SM leading to:

$$I_m^{\mathrm{SM}} = \tfrac{2\,I}{M+1}\, m \quad \text{for } m = 1 \ldots M. \tag{11}$$

Consequently, the minimum distance between two SM signals is $\frac{2\,I}{M+1}$, whereas the minimum distance for common PAM is $\frac{2\,I}{M-1}$. The smaller signal distance of SM might induce a worse BER performance because the error probability depends on the Euclidean distance of the transmitted signals. However, as SM additionally encodes data bits in the spatial domain, it can provide the same spectral efficiency as common M-PAM with a lower signal constellation size, hence effectively enlarging the distance of the signal points. As the SM receiver has to detect which transmitter has sent the signal, its performance depends on the differentiability of the multiple channels. Thus, the performance of SM is affected by the channel correlation. The PEP of SM is

$$\begin{aligned} \mathrm{PEP}_{\mathrm{SM}} &= \mathrm{PEP}(\mathbf{s}_{m^{(1)}} \to \mathbf{s}_{m^{(2)}} | \mathbf{H}) \\ &= \mathrm{Q}\left(\sqrt{\frac{r^2\,T_s}{4\,N_0} \, \|\mathbf{H}\,(\mathbf{s}_{m^{(1)}} - \mathbf{s}_{m^{(2)}})\|_{\mathrm{F}}^2}\right) \\ &= \mathrm{Q}\left(\sqrt{\frac{r^2\,T_s}{4\,N_0} \sum_{n_r=1}^{N_r} \left| I_{m^{(2)}}^{\mathrm{SM}} \, h_{n_r n_t^{(2)}} - I_{m^{(1)}}^{\mathrm{SM}} \, h_{n_r n_t^{(1)}} \right|^2}\right). \end{aligned} \tag{12}$$

This denotes the probability that the receiver decides for intensity $I_{m^{(2)}}^{\mathrm{SM}}$ being emitted by transmitter $n_t^{(2)}$, whereas actually transmitter $n_t^{(1)}$ has emitted intensity $I_{m^{(1)}}^{\mathrm{SM}}$. Using this PEP and considering all possible MN_t signal combinations, the BER of SM can be approximated by union bound methods. The upper bound of its BER is given in (13) on top of this page, where $b_{m^{(1)}n_t^{(1)}}$ is the bit assignment which is conveyed when intensity $I_{m^{(1)}}^{\mathrm{SM}}$ is emitted by transmitter $n_t^{(1)}$ and $b_{m^{(2)}n_t^{(2)}}$ is the bit assignment which is encoded when intensity $I_{m^{(2)}}^{\mathrm{SM}}$ is emitted by transmitter $n_t^{(2)}$. Consequently, $\mathrm{d_H}\left(b_{m^{(1)}n_t^{(1)}}, b_{m^{(2)}n_t^{(2)}}\right)$ states the number of bit errors when erroneously decoding the bit sequence $b_{m^{(2)}n_t^{(2)}}$ at the receiver instead of the actually transmitted sequence $b_{m^{(1)}n_t^{(1)}}$.

IV. Results on Bit Error Ratio Performance

In this section, we analyse the BER performance of the MIMO techniques introduced in Section III by considering several setup scenarios which are based on the model presented in Section II. In order to ensure comparability, the mean emitted optical power is the same for each scenario as well as for all MIMO techniques. We evaluate the error ratios at the receiver side with regard to *transmit* energy against power spectral density of the AWGN. Hence, we take into account the specific path loss of each setup caused by the particular distance and angular alignment of the single transmitters and receivers. Consequently, we define the SNR as $\frac{E_s}{N_0}$. This is because considering received energy to noise energy would disregard the individual path loss of the different setups, thus disallowing a fair performance comparison.

We consider the 4×4 setup with transmitter spacings on the x- and y-axis of $d_{\mathrm{TX}} = 0.2, 0.4$ and 0.6 m. Applying (3) to these scenarios gives the following channel matrices (without noise):

$$\begin{aligned} \mathbf{H}_{d_{\mathrm{TX}}=0.2} &\approx 10^{-4} \begin{pmatrix} 1.0708 & 0.9937 & 0.9937 & 0.9226 \\ 0.9937 & 1.0708 & 0.9226 & 0.9937 \\ 0.9937 & 0.9226 & 1.0708 & 0.9937 \\ 0.9226 & 0.9937 & 0.9937 & 1.0708 \end{pmatrix}, \\ \mathbf{H}_{d_{\mathrm{TX}}=0.4} &\approx 10^{-4} \begin{pmatrix} 0.9226 & 0.7964 & 0.7964 & 0.6888 \\ 0.7964 & 0.9226 & 0.6888 & 0.7964 \\ 0.7964 & 0.6888 & 0.9226 & 0.7964 \\ 0.6888 & 0.7964 & 0.7964 & 0.9226 \end{pmatrix}, \\ \mathbf{H}_{d_{\mathrm{TX}}=0.6} &\approx 10^{-4} \begin{pmatrix} 0.6888 & 0.5559 & 0.5559 & 0.0000 \\ 0.5559 & 0.6888 & 0.0000 & 0.5559 \\ 0.5559 & 0.0000 & 0.6888 & 0.5559 \\ 0.0000 & 0.5559 & 0.5559 & 0.6888 \end{pmatrix}. \end{aligned} \tag{14}$$

The symmetrical arrangement of the transmitters and receivers leads to equal channel gains for the links with the same geometrical alignment. Moreover, if the spacing between the transmitters is small, the gains are quite similar, whereas if d_{TX} gets larger, the differences between the links increase. If $d_{\mathrm{TX}} = 0.6$ m, some transmitters and receivers are not in each others FOV resulting in $h_{n_r n_t} = 0$. As the channel coefficients are in the region of 10^{-4}, the electrical path loss at the receiver side is about -80 dB. Because we defined the SNR as the ratio of *transmitted* signal energy to noise, the BER curves displayed in the following figures have an SNR offset of about 80 dB with respect to the *received* energy to noise ratio. Furthermore, if we consider the diffuse transmission portion induced by first order reflections on the surfaces (walls), the reflected optical intensity impinging on the receivers is in the range of $10^{-10}\,I$ (assuming ideal conditions such as Lambertian reflectors and a reflectivity of $\rho = 1$). This results in an electrical path loss which is about $110 - 120$ dB larger than the path loss of the LOS transmission. As the path loss of higher order reflections is even larger, we can neglect reflections in the following and consider only the LOS gains given in (14) without any diffuse transmission portions.

However, additional multipath reflections would enhance the differentiability of the MIMO channels and would reduce the channel correlation. Hence, as there are no reflections, the considered LOS scenario is subject to highly correlated links and constitutes a worst case scenario with regard to channel correlation.

Enlarging d_{TX} increases the path loss. Therefore, the impairment in received energy can be denoted for different transmitter spacings:

$$\Delta^{E_{\mathrm{RX}}}_{d_{\mathrm{TX}}=x} = 10\,\log_{10}\left(\frac{E_{\mathrm{RX}_{d_{\mathrm{TX}}=x}}}{E_{\mathrm{RX}_{d_{\mathrm{TX}}=0.2}}}\right). \tag{15}$$

$E_{\mathrm{RX}_{d_{\mathrm{TX}}=x}}$ denotes the received electrical energy for $d_{\mathrm{TX}} = x$ m. The impairment is related to the $d_{\mathrm{TX}} = 0.2$ m setup which provides the lowest path loss yielding to

$$\begin{aligned}\Delta^{E_{\mathrm{RX}}}_{d_{\mathrm{TX}}=0.2} &= \quad 0.00\,\mathrm{dB},\\ \Delta^{E_{\mathrm{RX}}}_{d_{\mathrm{TX}}=0.4} &\approx -1.88\,\mathrm{dB},\\ \Delta^{E_{\mathrm{RX}}}_{d_{\mathrm{TX}}=0.6} &\approx -6.89\,\mathrm{dB}.\end{aligned} \tag{16}$$

Besides, the maximum difference in path length of the multiple transmitter-receiver links is about 33.30 mm. This difference results in a maximum delay variation of 111.06 ps. A delay variation of several ps only has an effect for switching speeds in the region of several GHz. As we consider off-the-shelf LEDs which provide a bandwidth of about $30 - 50$ MHz, we can neglect this delay variation and assume ideal synchronisation of all links without time dispersion.

Fig. 3(a) shows the BER performance of RC, SMP and SM for the three setup scenarios for a spectral efficiency of $R = 4$ bit/s/Hz. For $d_{\mathrm{TX}} = 0.2$ m and 0.4 m, RC gives the best performance, whereas SMP performs worst with a low slope of the BER curve within the depicted SNR range. This is due to the fact, that for both scenarios the channel gains are quite similar providing high channel correlation. Although the performance of SM also depends on the differences between the links, SM is more robust to these channel conditions. SM provides a lower error ratio and a steeper slope of the BER curve compared to SMP. If $d_{\mathrm{TX}} = 0.6$ m, SMP and SM outperform RC at a BER of 10^{-5} by about 10 dB, respectively by 9 dB. RC performs about 7 dB worse compared to the $d_{\mathrm{TX}} = 0.2\,\mathrm{m}$ case because of less received energy as $\Delta^{E_{\mathrm{RX}}}_{d_{\mathrm{TX}}=0.6} \approx -6.89$ dB. Despite this larger path loss for $d_{\mathrm{TX}} = 0.6$ m, SMP and SM even outperform RC for the two other scenarios, which provide a lower path loss. SMP outperforms SM by about 1 dB for high SNRs. Because of its multiplexing gain, SMP can operate with a reduced signal constellation size of $M = 2$ as opposed to SM which has to operate with $M = 4$ to provide the same data rate. But at low SNR regions of up to about 103 dB, SM provides the best BER performance. This implies that SM profits from conveying information in the spatial domain especially at low SNRs. Whereas at high SNR regions SM suffers from the fact that it has to use a larger signal constellation size to provide the same spectral efficiency as SMP. Accordingly, SMP requires a high SNR to separate the single signal streams at the receiver side and to benefit from its multiplexing gain. Moreover, the

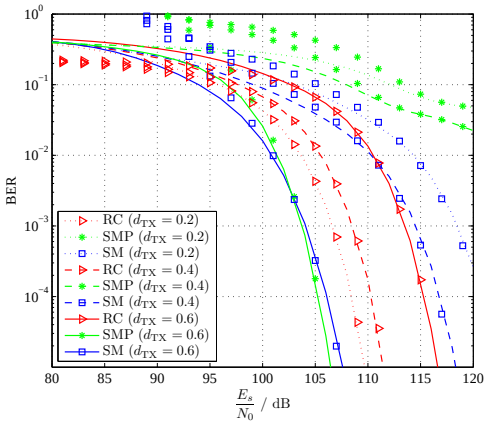

(a) $R = 4$ bit/s/Hz

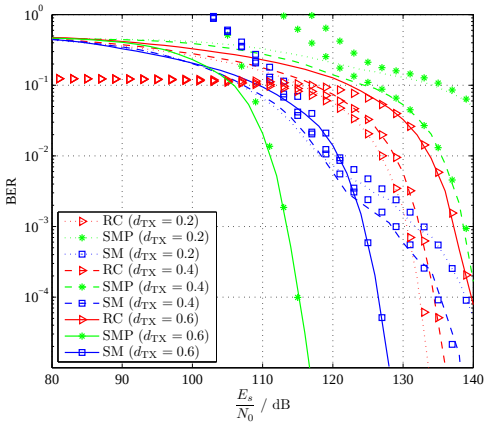

(b) $R = 8$ bit/s/Hz

Fig. 3. Comparison of RC, SMP and SM for spectral efficiency of $R = 4$ and $R = 8$ bit/s/Hz in 4×4 setup scenario with varying distance d_{TX} of transmitters on the x- and y-axis (lines show simulation results and markers analytical error bounds).

theoretical lower and upper error bounds (shown by markers) given in (7), (10) and (13) closely match the simulation results (shown by lines). Thus, the error bounds provide an accurate approximation of the BERs at high SNRs.

Fig. 3(b) shows the BER performance of the three schemes for the same setup scenarios but with an enhanced spectral efficiency of $R = 8$ bit/s/Hz. RC requires an SNR increase of about 24 dB to achieve the same BER of 10^{-5} compared to the $R = 4$ bit/s/Hz case. For $d_{\mathrm{TX}} = 0.2$ m and $d_{\mathrm{TX}} = 0.4$ m, SMP still performs worst. However, SM outperforms RC up to an SNR of about 130 dB for $d_{\mathrm{TX}} = 0.2$ m, respectively 134 dB for $d_{\mathrm{TX}} = 0.4$ m. If $d_{\mathrm{TX}} = 0.6$ m, SMP provides the best performance as it achieves an SNR benefit of about 25 dB compared to RC and of about 12 dB compared to SM. Hence, due to its multiplexing gain, SMP requires an

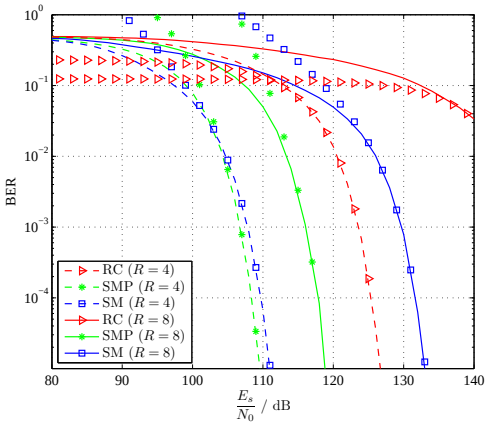

Fig. 4. Comparison of RC, SMP and SM for spectral efficiency of $R = 4$ and $R = 8$ bit/s/Hz in 4×4 setup scenario with $d_{\mathrm{TX}} = 0.7$ m (lines show simulation results and markers analytical error bounds).

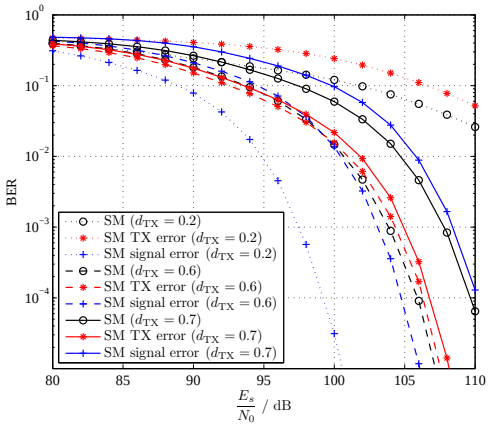

Fig. 5. BER of SM segmented into bit errors caused by transmitter misdetection and signal misdetection for spectral efficiency of $R = 4$ bit/s/Hz in 4×4 setup scenario with varying distance d_{TX} of transmitters on the x- and y-axis.

SNR improvement of only 10 dB to provide the same BER performance when doubling the spectral efficiency from 4 to 8 bit/s/Hz, whereas SM needs additional 21 dB.

If we assume $d_{\mathrm{TX}} = 0.7\,\mathrm{m}$, we get

$$\mathbf{H}_{d_{\mathrm{TX}}=0.7} \approx 10^{-4} \begin{pmatrix} 0.5658 & 0 & 0 & 0 \\ 0 & 0.5658 & 0 & 0 \\ 0 & 0 & 0.5658 & 0 \\ 0 & 0 & 0 & 0.5658 \end{pmatrix}, \tag{17}$$

which results in an aligned system where only one transmitter and receiver are in each others FOV. This leads to a direct alignment with four completely independent links. Fig. 4 displays the BER results for a spectral efficiency of $R = 4$ and $R = 8$ bit/s/Hz for this scenario. In comparison to the $d_{\mathrm{TX}} = 0.6$ m scenario, all MIMO schemes perform worse because there is less energy received. This is due to the missing cross-connects between emitter n_t and receiver n_r for $n_t \neq n_r$ leading to $\Delta^{E_{\mathrm{RX}}}_{d_{\mathrm{TX}}=0.7} \approx -16.95$ dB. Whereas SM and SMP undergo a minor performance decrease of only about 3 dB, the performance of RC is degraded by about 10 dB. Consequently, RC suffers much more from the direct alignment, whereas SMP and SM can compensate the less received energy by the reduced channel correlation. For $R = 4$ bit/s/Hz, SM again outperforms SMP at low SNR regions up to about 103 dB. At higher SNRs, SMP outperforms SM due to its larger multiplexing gain. This issue is even more evident for the $R = 8$ bit/s/Hz case, where SMP achieves major performance gains as it provides this spectral efficiency with $M = 4$ compared to SM which has to operate with $M = 64$.

In the following, we study why SM achieves performance gains especially in the low SNR region. Therefore, the BER of SM is segmented into errors arising from transmitter misdetection and from signal misdetection. If $R = 4$ bit/s/Hz, SM conveys the same number of bits in the spatial and in the signal domain. Fig. 5 shows that for $d_{\mathrm{TX}} = 0.2$ m, the errors caused by inaccurate detection of the transmitter mainly affect the BER, whereas the mere signal detection provides much lower error ratios. If $d_{\mathrm{TX}} = 0.6$ m, the transmitter detection provides a lower error ratio up to an SNR of about 99 dB, thus improving the overall BER of SM. At higher SNRs the signal detection can be performed more reliably and the errors caused by an erroneous detection of the transmitter get decisive again. In the aligned system ($d_{\mathrm{TX}} = 0.7$ m), the signal misdetection is the dominating source of errors due to less energy received. In contrast, the detection of the active emitter can be performed more reliably because the direct alignment provides the lowest channel correlation. Therefore, the inherent nature of SM, which is conveying information in the spatial domain, can be exploited most distinctively by direct alignment of the optical transmitters and receivers. Thus despite less energy received, independent links enable the most reliable detection of the active transmitter.

A. Varying position of receiver array

In this section, we consider the situation when the position of the receiver array is varied. We define x_{RX} and y_{RX} as the position offsets of the receiver array on the x- and y-axis relative to the center of the room. These offsets increase both the distance and the misalignment between the transmitter array and the receivers. In order to still be able to detect the TX beams, we assume a larger FOV semiangle of the receivers of $\Psi_{\frac{1}{2}} = 45°$. The considered position offsets are: i) $x_{\mathrm{RX}} = 0.5$ m, $y_{\mathrm{RX}} = 0$ m; ii) $x_{\mathrm{RX}} = 0.25$ m, $y_{\mathrm{RX}} = 0.75$ m and iii) $x_{\mathrm{RX}} = 0.5$ m, $y_{\mathrm{RX}} = 1.0$ m. Applying (3) to these scenarios results in the following channel matrices:

$$\mathbf{H}_{\mathrm{i}} \approx 10^{-4} \begin{pmatrix} 0.2293 & 0.2013 & 0.1462 & 0.1290 \\ 0.2013 & 0.2293 & 0.1290 & 0.1462 \\ 0.7964 & 0.6888 & 0.6410 & 0.5559 \\ 0.6888 & 0.7964 & 0.5559 & 0.6410 \end{pmatrix},$$

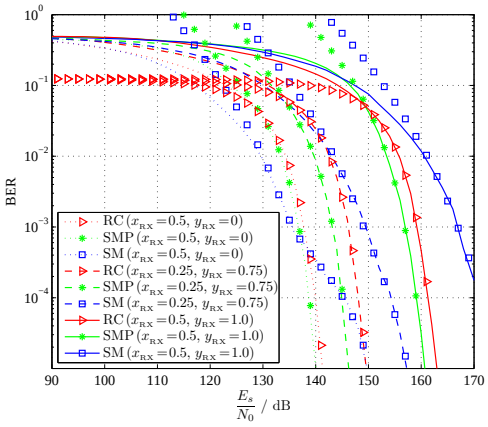

Fig. 6. Comparison of RC, SMP and SM for spectral efficiency of $R = 8$ bit/s/Hz in 4×4 setup scenario with $d_{\mathrm{TX}} = 0.4$ m and varying position offsets of receiver array on the x- and y-axis (lines show simulation results and markers analytical error bounds).

$$\mathbf{H}_{\mathrm{ii}} \approx 10^{-4} \begin{pmatrix} 0.0461 & 0.0272 & 0.0358 & 0.0213 \\ 0.2573 & 0.1798 & 0.1917 & 0.1352 \\ 0.0735 & 0.0424 & 0.0713 & 0.0412 \\ 0.4426 & 0.3040 & 0.4275 & 0.2940 \end{pmatrix},$$
$$\mathbf{H}_{\mathrm{iii}} \approx 10^{-4} \begin{pmatrix} 0.0061 & 0.0035 & 0.0044 & 0.0025 \\ 0.0442 & 0.0283 & 0.0299 & 0.0194 \\ 0.0150 & 0.0082 & 0.0128 & 0.0071 \\ 0.1290 & 0.0792 & 0.1071 & 0.0663 \end{pmatrix}. \quad (18)$$

Fig. 6 shows the BER of RC, SMP and SM for a spectral efficiency of 8 bit/s/Hz in the 4×4 setup scenario with $d_{\mathrm{TX}} = 0.4$ m using these position offsets. The increased distance between the transmitters and the receivers leads to a larger path loss and an increased $\frac{E_s}{N_0}$ offset compared to the scenario with $x_{\mathrm{RX}} = y_{\mathrm{RX}} = 0$ m. However, the larger distance also increases the differences between the channels. This improves the performance of SMP. While SMP performs worst when the x-offset and y-offset are zero (due to channel similarities), it performs better than RC and SM when assuming position offsets and larger distances. This is because of favorable channel conditions and the fact that the spatial multiplexing gain of SMP grows linearly with the minimum number of transmitters and receivers. In contrast, the spatial multiplexing gain grows only logarithmically in the case of SM, and there is no spatial multiplexing gain in the case of RC.

B. Power imbalance between transmitters

In the following, we analyse the effect of induced power imbalance between the single transmitters. Thus, the transmission power is not uniformly distributed across all N_t transmitters but imbalanced. We define δ as the optical power imbalance factor in dB and $\alpha = 10^{\frac{\delta}{10}}$ as the imbalance factor on a linear scale. Therefore, α denotes the optical power surplus factor assigned to one transmitter in comparison to another one. Note that the mean optical power emitted by all transmitters, I, is still the same as before. This means that the total transmission power is not increased by driving individual LEDs in the array with different powers. Moreover, the power distribution is done without any channel state information at the transmitter side.

The induced power imbalance factors for each transmitter can be calculated by

$$\gamma_1 = \frac{N_t}{\sum_{i=0}^{N_t-1} \alpha^i}, \qquad \gamma_{j+1} = \alpha\, \gamma_j \quad \text{for } j = 1 \ldots N_t - 1. \quad (19)$$

For instance, if we assume $\delta = 3$ dB and $N_t = 4$, we get $\gamma_1 \approx \frac{4}{15}$, $\gamma_2 \approx \frac{8}{15}$, $\gamma_3 \approx \frac{16}{15}$ and $\gamma_4 \approx \frac{32}{15}$. Using these factors, the optical transmission power assigned to emitter n_t applying RC or SMP is $\tilde{I}_{n_t} = \frac{I}{N_t}\, \gamma_{n_t}$ and for SM it is $\tilde{I}_{n_t} = I\, \gamma_{n_t}$. Note that the signal modulation technique is still PAM according to (5) and (11), whereas now $\tilde{I}_{n_t}$ is the mean optical power used for modulation by transmitter n_t.

Fig. 7 depicts the BER of RC, SMP and SM for a spectral efficiency of 4 bit/s/Hz in the 4×4 setup scenario with $d_{\mathrm{TX}} = 0.2$ m and $d_{\mathrm{TX}} = 0.6$ m for varying power imbalances. As shown, adding an imbalance to the transmission powers can enhance the performance of both SMP and SM, whereas it has no influence on RC. By imbalancing the power, the correlation of the single links is reduced making them more distinguishable at the receiver side. The receiver does not need any knowledge about the induced power imbalance because it implicitly gets this information by channel estimation which it performs anyway. Therefore to the receiver, the power imbalance appears to be due to the actual channel propagation. Consequently, imbalancing transmit powers does not increase the receiver's detection complexity. The performance of RC is not related to link differences but only to the absolute channel gains. Therefore, power imbalance has no effect on the performance of RC given the symmetrical arrangement of the channel gains denoted in (14). The results for the $d_{\mathrm{TX}} = 0.2$ m scenario shown in Fig. 7(a) indicate that a power imbalance of about $\delta = 1$ dB results in the best BER performance for SM, whereas for SMP $\delta = 3$ dB gives the lowest BER. More pronounced power imbalances lead to worse error ratios. While the correlation of the links may be reduced, the transmission power for some of the links is largely decreased in this case. This leads to a low SNR on these links and consequently, to a worse BER performance. Therefore, a compromise between channel correlation and appropriate signal detection is required. This is also the reason why SMP can operate with higher power imbalances compared to SM. SM has to operate with a larger signal constellation size to provide the same data rate, thus making it more susceptible to low SNRs. Consequently, SMP can profit to a larger extent by power imbalancing and achieves the same performance as RC. Note that the channel conditions without power imbalancing caused SMP to perform significantly worse than RC and SM in this scenario (see Fig. 3(a)). For $d_{\mathrm{TX}} = 0.6$ m, power imbalance has a negative effect on SMP and SM as their

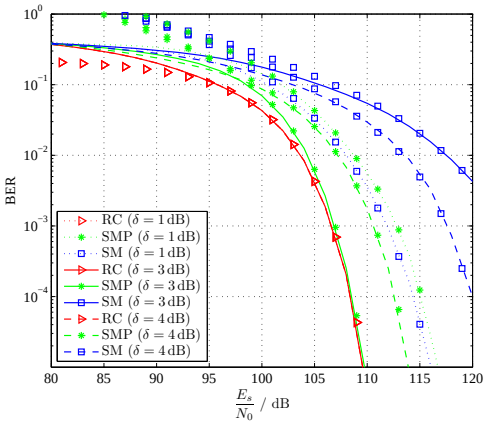

(a) $d_{\mathrm{TX}} = 0.2$ m

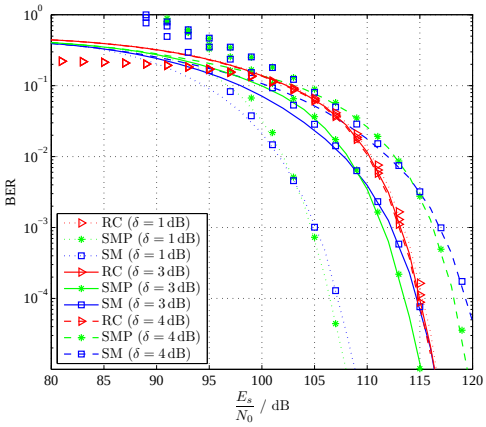

(b) $d_{\mathrm{TX}} = 0.6$ m

Fig. 7. Comparison of RC, SMP and SM for spectral efficiency of $R = 4$ bit/s/Hz in 4×4 setup scenario for varying power imbalances δ (lines show simulation results and markers analytical error bounds).

performance decreases with rising δ as shown in Fig. 7(b). Thus, no further benefits can be achieved and $\delta = 0$ dB gives the best performance for both SMP and SM.

C. Link blockage

In this section, we consider the $d_{\mathrm{TX}} = 0.2$ m and 0.4 m setups with an induced link blockage between some transmitters and receivers. This can be achieved by installing opaque boundaries in the receiver device or by smaller FOVs of the optical receivers. We assume the channel coefficients as given in (14) and block the same links of the 4×4 setup as in the $d_{\mathrm{TX}} = 0.6$ m scenario: the links between TX_1 and RX_4; TX_2 and RX_3; TX_3 and RX_2; TX_4 and RX_1. This results in the following channel matrices for the two setups with induced

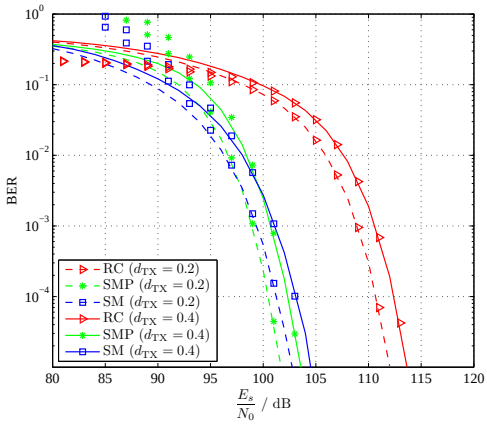

Fig. 8. Comparison of RC, SMP and SM for spectral efficiency of $R = 4$ bit/s/Hz in 4×4 setup scenario with $d_{\mathrm{TX}} = 0.2$ m and 0.4 m with induced link blockage (lines show simulation results and markers analytical error bounds).

link blockage:

$$\widehat{\mathbf{H}}_{d_{\mathrm{TX}}=0.2} \approx 10^{-4} \begin{pmatrix} 1.0708 & 0.9937 & 0.9937 & 0.0000 \\ 0.9937 & 1.0708 & 0.0000 & 0.9937 \\ 0.9937 & 0.0000 & 1.0708 & 0.9937 \\ 0.0000 & 0.9937 & 0.9937 & 1.0708 \end{pmatrix} \tag{20}$$

resulting in $\widehat{\Delta}^{E_{\mathrm{RX}}}_{d_{\mathrm{TX}}=0.2} \approx -2.29$ dB and

$$\widehat{\mathbf{H}}_{d_{\mathrm{TX}}=0.4} \approx 10^{-4} \begin{pmatrix} 0.9226 & 0.7964 & 0.7964 & 0.0000 \\ 0.7964 & 0.9226 & 0.0000 & 0.7964 \\ 0.7964 & 0.0000 & 0.9226 & 0.7964 \\ 0.0000 & 0.7964 & 0.7964 & 0.9226 \end{pmatrix} \tag{21}$$

resulting in $\widehat{\Delta}^{E_{\mathrm{RX}}}_{d_{\mathrm{TX}}=0.4} \approx -3.99$ dB.

Fig. 8 depicts the BER of RC, SMP and SM for $R = 4$ bit/s/Hz in these two setups. Relative to the results without link blockage, RC performs about 2 dB worse. This is because the induced link blockage leads to a lower SNR at the receiver. However, the performance of SM and SMP is significantly enhanced. Although there is less energy received, both MIMO schemes profit from the reduced channel correlation. Especially SMP, which performs worst without link blockage, benefits from the reduced channel correlation and provides the lowest error ratio in this scenario. The $d_{\mathrm{TX}} = 0.2$ m setup with induced link blockage provides the best compromise between channel correlation and received energy. As shown, both SM and SMP perform about 2 dB better compared to the setup with $d_{\mathrm{TX}} = 0.4$ m and induced link blockage. Relative to the $d_{\mathrm{TX}} = 0.6$ m setup (see Fig. 3(a)), SM and SMP achieve an even larger performance gain of about 5 dB.

V. Summary and Conclusion

In this paper, we have studied the performance of MIMO techniques applied to OWC in indoor environments. Several

4×4 setups with different spacings of the transmitters and different positions of the receiver array have been considered. We have shown that for OWC, MIMO schemes can provide gains even under static LOS conditions – channel conditions which commonly disallow the use of MIMO techniques in the RF domain. It has been shown that SMP improves the spectrum efficiency in IM/DD transmission systems. In order to achieve these improvements, sufficiently low channel correlations are required. Similarly, SM achieves improved spectral efficiencies especially at low SNRs and it is more robust to high channel correlation. SM enjoys additional implementation advantages as it only requires low complexity detection algorithms. This is because SM prevents ICI. RC is insensitive to different transmitter-receiver alignments, but suffers from the fact that it requires large signal constellation sizes to provide high data rates. It has been found that induced power imbalance between the transmitters is an effective technique to improve the BER performance. Under conditions which cause high channel correlation, power imbalance can enhance the performance of both SMP and SM remarkably. Consequently, if the transmission power is imbalanced, SMP and SM can even be used in scenarios which typically disallow the application of MIMO schemes. As shown, the best performance for the considered 4×4 indoor scenario can be achieved by blocking some of the 16 links between the transmitters and receivers. This induced blocking reduces the SNR at the receiver side. However, blocking 4 links, for example, improves the BER of both SMP and SM, since it outweighs the loss in SNR by reducing the channel correlation. These two MIMO techniques capitalise on both SNR and channel differences. Therefore, the induced link blockage represents the most suitable compromise between channel correlation and received energy for the considered scenarios. This work has also demonstrated that practical OWC systems could greatly benefit from adaptive MIMO techniques.

REFERENCES

[1] Y. Tanaka, T. Komine, S. Haruyama, and M. Nakagawa, "Indoor Visible Communication Utilizing Plural White LEDs as Lighting," in *Proc. of the IEEE International Symposium on Personal, Indoor and Mobile Radio Communications*, vol. 2, San Diego, California, USA, Sep. 30–Oct. 3, 2001, pp. 81–85.

[2] T. Komine and M. Nakagawa, "Fundamental Analysis for Visible–Light Communication System using LED Lights," *IEEE Transactions on Consumer Electronics*, vol. 50, no. 1, pp. 100–107, Feb. 2004.

[3] K.-D. Langer, J. Grubor, O. Bouchet, M. El Tabach, J. Walewski, S. Randel, M. Franke, S. Nerreter, D. O'Brien, G. Faulkner, I. Neokosmidis, G. Ntogari, and M. Wolf, "Optical Wireless Communications for Broadband Access in Home Area Networks," in *Proc. of the* 10^{th} *Anniversary International Conference on Transparent Optical Networks (ICTON 08)*, vol. 4, Athens, Greece, Jun. 22–26, 2008, pp. 149–154.

[4] F. R. Gfeller and U. Bapst, "Wireless In-House Data Communication Via Diffuse Infrared Radiation," *Proceedings of the IEEE*, vol. 67, no. 11, pp. 1474–1486, Nov. 1979.

[5] J. M. Kahn and J. R. Barry, "Wireless Infrared Communications," *Proceedings of the IEEE*, vol. 85, no. 2, pp. 265–298, Feb. 1997.

[6] S. Hranilovic, *Wireless Optical Communication Systems*, 1st ed. Springer, Sep. 1996.

[7] D. O'Brien, H. L. Minh, L. Zeng, G. Faulkner, K. Lee, D. Jung, Y. Oh, and E. T. Won, "Indoor visible light communications: challenges and prospects," *Proc. SPIE, Free-Space Laser Communications VIII*, vol. 7091, no. 1, p. 709106, 2008.

[8] R. Mesleh, H. Elgala, and H. Haas, "Optical Spatial Modulation," *Journal of Optical Communications and Networking*, vol. 3, no. 3, pp. 234–244, Mar. 2011.

[9] E. Telatar, "Capacity of Multi-Antenna Gaussian Channels," *European Transaction on Telecommunication*, vol. 10, no. 6, pp. 585–595, Nov. 1999.

[10] G. J. Foschini and M. J. Gans, "On Limits of Wireless Communications in a Fading Environment when Using Multiple Antennas," *Wireless Personal Communications*, vol. 6, no. 3, pp. 311–335, Mar. 1998.

[11] S. G. Wilson, M. Brandt-Pearce, Q. Cao, and M. Baedke, "Optical Repetition MIMO Transmission with Multipulse PPM," *IEEE Journal on Selected Areas in Communications*, vol. 23, no. 9, pp. 1901–1910, Sep. 2005.

[12] S. Navidpour, M. Uysal, and M. Kavehrad, "BER Performance of Free-Space Optical Transmission with Spatial Diversity," *IEEE Transactions on Wireless Communications*, vol. 6, no. 8, pp. 2813–2819, Aug. 2007.

[13] D. O'Brien, "Multi-Input Multi-Output (MIMO) indoor optical wireless communications," in *Conference Record of the Asilomar Conference on Signals, Systems and Computers*, Pacific Grove, California, USA, Nov. 1–4, 2009, pp. 1636–1639.

[14] L. Zeng, D. O'Brien, H. Minh, G. Faulkner, K. Lee, D. Jung, Y. Oh, and E. T. Won, "High Data Rate Multiple Input Multiple Output (MIMO) Optical Wireless Communications using White LED Lighting," *IEEE Journal on Selected Areas in Communications*, vol. 27, no. 9, pp. 1654–1662, Dec. 2009.

[15] T. Fath, M. Di Renzo, and H. Haas, "On the Performance of Space Shift Keying for Optical Wireless Communications," in *Proc. of the IEEE Global Communications Conference (GLOBECOM) - Workshop on Optical Wireless Communications*, Miami, Florida, USA, Dec. 10, 2010, pp. 990–994.

[16] O. Bouchet, G. Faulkner, L. Grobe, E. Gueutier, K.-D. Langer, S. Nerreter, D. O'Brien, R. Turnbull, J. Vucic, J. Walewski, and M. Wolf, "Deliverable D4.2b Physical Layer Design and Specification," *Seventh Framework Programme Information & Communication Technologies*, Feb. 2011, Retrieved Jul. 18, 2012 from http://www.ict-omega.eu.

[17] D. O'Brien, G. Faulkner, H. Le Minh, O. Bouchet, M. El Tabach, M. Wolf, J. Walewski, S. Randel, S. Nerreter, M. Franke, K.-D. Langer, J. Grubor, and T. Kamalakis, "Home access networks using optical wireless transmission," in *Proc. of the IEEE International Symposium on Personal, Indoor and Mobile Radio Communications*, Cannes, France, Sep. 15–18, 2008, pp. 1–5.

[18] M. Safari and M. Uysal, "Do we really need OSTBCs for free-space optical communication with direct detection?" *IEEE Transactions on Wireless Communications*, vol. 7, no. 11 Part 2, pp. 4445–4448, 2008.

[19] S. M. Alamouti, "A Simple Transmit Diversity Technique for Wireless Communications," *IEEE Journal on Selected Areas in Communications*, vol. 16, no. 8, pp. 1451–1458, Oct. 1998.

[20] J. Armstrong, "OFDM for Optical Communications," *IEEE/OSA Journal of Lightwave Technology*, vol. 27, no. 3, pp. 189–204, Feb. 2009.

[21] S. Dimitrov, S. Sinanovic, and H. Haas, "Signal Shaping and Modulation for Optical Wireless Communication," *IEEE/OSA Journal of Lightwave Technology*, vol. 30, no. 9, pp. 1319–1328, May 2012.

[22] D. Barros, S. Wilson, and J. Kahn, "Comparison of Orthogonal Frequency-Division Multiplexing and Pulse-Amplitude Modulation in Indoor Optical Wireless Links," *IEEE Transactions on Communications*, vol. 60, no. 1, pp. 153–163, Jan. 2012.

[23] A. Goldsmith, *Wireless Communications*, Cambridge University Press, 2005.

[24] Y. A. Chau and S.-H. Yu, "Space Modulation on Wireless Fading Channels," in *IEEE Vehicular Technology Conference (VTC 2001-Fall)*, vol. 3, 7–11 Oct. 2001, pp. 1668–1671.

[25] R. Mesleh, H. Haas, S. Sinanović, C. W. Ahn, and S. Yun, "Spatial Modulation," *IEEE Transactions Vehicular Technology*, vol. 57, no. 4, pp. 2228 – 2241, July 2008.

[26] R. Mesleh, M. Di Renzo, H. Haas, and P. M. Grant, "Trellis Coded Spatial Modulation," *IEEE Transactions on Wireless Communications*, vol. 9, no. 7, pp. 2349–2361, July 2010.

[27] E. Basar, U. Aygolu, E. Panayirci, and V. H. Poor, "Space-Time Block Coded Spatial Modulation," *IEEE Transactions on Communications*, vol. 59, no. 3, pp. 823 –832, Mar. 2011.

[28] R. Mesleh, H. Haas, C. W. Ahn, and S. Yun, "Spatial Modulation – A New Low Complexity Spectral Efficiency Enhancing Technique," in *IEEE International Conference on Communication and Networking in China (CHINACOM)*, Beijing, China, Oct. 25–27, 2006, pp. 1–5.

[29] R. Mesleh, "Spatial Modulation: A Spatial Multiplexing Technique for Efficient Wireless Data Transmission," Ph.D. dissertation, Jacobs University, Bremen, Germany, Jun. 2007.

[30] A. Younis, M. Di Renzo, R. Mesleh, and H. Haas, "Sphere Decoding for Spatial Modulation," in *Proc. of IEEE International Conference on Communications (ICC 2011)*, Kyoto, Japan, 5–9 Jun. 2011, pp. 1 –6.

Optical Wireless Transmitter Employing Discrete Power Level Stepping

Thilo Fath, Christoph Heller, and Harald Haas, *Member, IEEE*

***Abstract*—A major shortcoming of light-emitting diodes (LEDs) is their highly non-linear optical-power-versus-current characteristic. This non-linearity largely restricts the dynamic range and the transmission power of common optical wireless transmitters. This restriction degrades the performance of optical wireless communication (OWC) systems. In this paper, a novel transmitter concept for OWC is proposed which employs discrete power level stepping. The transmitter consists of several on-off-switchable emitter groups. These groups are individually controlled and emit fixed specific optical intensities in parallel. As optical intensities constructively add up, the total emitted intensity is generated by the sum of the emitted intensities of all activated emitter groups. Therefore, the proposed transmitter solution can generate several discrete optical intensity levels which can be used for optical wireless signal transmission. The transmitter design allows the utilisation of the full dynamic range of LEDs or laser diodes by avoiding non-linearity issues. Moreover, costs and complexity of the optical front-end are significantly reduced as neither a digital-to-analogue converter (DAC) nor high-speed current controllers are required. This simple design also provides improved power efficiency. Transmission experiments prove the functionality of the implemented optical transmitter. It is shown that the practical performance of the transmitter closely matches the expected performance determined by computer simulations. Moreover, the implemented optical transmitter is compared to an electrical transmission which provides ideal linearity characteristics, and therefore corresponds to an ideal conventional optical transceiver.**

***Index Terms*—intensity modulation, non-linearity, optical wireless communications, power efficiency, transmitter design.**

I. Introduction

CURRENT and future wireless data applications, such as high-speed internet access or high-quality audio/ video streaming, require wireless data links that offer large throughputs. Commonly, wireless links are based on signal transmission in the radio frequency (RF) bands. The ever increasing demand for higher data rates and the enlarging number of devices make the RF spectrum a precious commodity [1]. Besides, RF devices cannot be used in environments which have stringent electromagnetic compatibility (EMC) restrictions like hospitals, fabrication plants or aeroplanes. As RF communications transmits data by modulating electromagnetic fields in the range of several MHz and GHz, it requires complex and elaborated high-frequency circuit designs. Moreover, these designs are not power-efficient as only a small amount of the consumed power is actually radiated.

Given this situation, ongoing research activities are focusing on alternative means and media for wireless data transmission [2]. Optical wireless communications (OWC) has the potential to become a viable complement to RF signal transmission and a remedy for the shortage of the RF spectrum [1, 3]. Compared to RF transmission, OWC has better EMC and is not subject to frequency regulations. OWC is based on modulating the optical power (intensity) emitted by light sources. For instance, the light bulbs (in fact high power light-emitting diodes (LEDs)) installed at the ceiling of a room can simultaneously provide illumination and data transmission.

Commonly, OWC employs pulsed digital modulation techniques to convey information [4]. For instance, the widely used on-off-keying (OOK) technique relies on purely switching the light source on and off. However, since OOK is a binary modulation scheme, it provides low spectral efficiency. As off-the-shelf LEDs achieve only a limited modulation bandwidth of about $30 - 50$ MHz in the case of infra-red (IR) light and even less for visible light, OOK can only provide limited data rates. Consequently, more advanced modulation schemes are required to enable higher data rates. Higher order modulation schemes such as M-level pulse amplitude modulation (PAM) or M-level pulse position modulation (PPM) provide larger throughputs. However, all these pulsed modulation techniques suffer from multipath effects which mostly occur in diffuse and scattered transmission scenarios [5, 6]. Multipath effects cause inter-symbol interference (ISI), and therefore decrease the system performance to a large extent by constraining both bandwidth and data rate.

Orthogonal frequency division multiplexing (OFDM) is widely used in modern RF standards as well as in OWC [7]. This is due to the fact that OFDM is a bandwidth efficient transmission technique which can cope with frequency-selective fading [8–10]. In contrast to pulsed modulation techniques, OFDM provides high data rates even in severe multipath scenarios. In order to mitigate multipath effects and to avoid ISI, OFDM uses a guard interval, the so-called cyclic prefix, which is placed between the transmitted OFDM symbols. Moreover, the actual OFDM symbol duration is typically much longer than the delay spread caused by multipath propagation. OFDM conveys digital data on multiple orthogonal sub-carrier frequencies. Hence, a wideband

Manuscript received January 6, 2013; revised March 21, 2013; accepted March 25, 2013.

Thilo Fath is with EADS Deutschland GmbH, Innovation Works, 81663 Munich, Germany and with the University of Edinburgh, Institute for Digital Communications, the Kings Buildings, Edinburgh EH9 3JL, UK (e-mail: thilo.fath@ed.ac.uk).

Christoph Heller is with EADS Deutschland GmbH, Innovation Works, 81663 Munich, Germany (e-mail: christoph.heller@eads.net).

Harald Haas is with the University of Edinburgh, Institute for Digital Communications, the Kings Buildings, Edinburgh EH9 3JL, UK (e-mail: h.haas@ed.ac.uk).

channel is subdivided into several narrowband sub-channels. These orthogonal sub-carrier channels are used to transmit independent data streams in parallel in the frequency domain. The frequency division multiplexed channels are summed up and transformed into the time domain by using an inverse fast Fourier transformation (IFFT). The utilisation of narrowband sub-channels enables a low-complex channel equalisation: each sub-channel can be regarded as a non-frequency-selective channel which is individually equalised in the frequency domain using a single-tap zero forcing (ZF) equaliser. These properties make OFDM an ideal candidate for diffuse and scattered OWC transmission scenarios [3, 7, 11, 12]. Moreover, due to the use of fast Fourier transformation (FFT) and IFFT, OFDM enables simple and efficient signal processing implementations. For instance, compared to M-PAM, OFDM requires approximately three times less computational complexity [13].

However, a common drawback of OFDM is the fact that it requires sophisticated transceiver designs (RF or optical) which must have good linearity characteristics and large dynamic ranges. Non-linear distortion effects, *e.g.* caused by amplifiers, largely decrease the system performance [14–17]. Compared to RF communications, OWC does not require high-frequency circuit designs because the signals are transmitted in the baseband representation and directly modulate the intensity of the emitting LEDs. However, LEDs are highly non-linear due to their optical-power-versus-current characteristic. This non-linearity largely restricts the dynamic range and the transmission power of common optical transmitters as well as the overall system performance [18–21]. Moreover, the non-linearity of LEDs requires complex pre-distortion and intricate equalisation techniques [22, 23]. Consequently, conventional optical transmitter front-ends cannot provide the required linearity in a power- and cost-efficient way.

In this paper, an OWC transmitter concept is proposed which addresses the shortcomings of conventional optical transmitters. In particular the concept addresses: non-linearities, restricted dynamic range and complex system designs. The proposed transmitter employs discrete power level stepping which enables a simple and power-efficient front-end design. Sophisticated pre-distortion or intricate equalisation techniques to mitigate transmitter induced non-linearities are not required. As a result, a low-complex single-tap equalisation is sufficient. The concept can be used to implement transmitters for visible or IR light transmission as well as for line-of-sight (LOS) and diffuse propagation scenarios.

The remainder of this paper is organised as follows: In Section II, the considered system model is introduced. Section III reviews conventional transmitter front-end designs and discusses implementation issues. In Section IV, the effects of quantization on the bit error ratio (BER) performance are shown. Based on this analysis, appropriate bit resolutions are determined which provide sufficient precision. In Section V, the proposed transmitter concept is introduced which employs discrete power level stepping. Moreover, the focus is set on several realisation aspects and the implemented transmitter is described. In Section VI, the results of several transmission experiments are presented. The transmitter performance is evaluated in terms of error vector magnitude (EVM) and BER. Measurements prove the functionality of the implemented transmitter. Finally, Section VII concludes the paper.

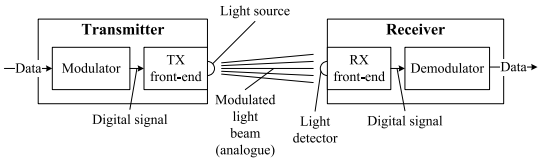

Fig. 1. Optical wireless transmission system.

II. System Model

Fig. 1 illustrates an OWC system which consists of an optical transmitter (TX) and receiver (RX). The optical transmitter comprises a modulator that transforms the incoming data stream into a signal that is to be transmitted by the light source. The output of the modulator is a digital signal. For higher order modulation techniques, such as M-PAM or OFDM, the modulator output is a bit vector representing an analogue signal value. The TX front-end transforms the bit vector into an analogue optical waveform by adequately controlling the light source. As a result, the front-end performs intensity modulation (IM) by changing the intensity of the emitted light according to the signal (data) to be sent. At the receiver side, a light detector retransforms the impinging optical waveform into an electrical signal. Commonly, this component is a photo-diode which transforms optical power into current by direct detection (DD). In this work, a silicon positive intrinsic negative (PIN) photo-diode [24] is employed. Additionally, the RX front-end contains an anti-aliasing filter, *i.e.* a low-pass filter to restrict the signal bandwidth in order to satisfy the sampling theorem, and an amplifier. After the received signal has been filtered and amplified, it is converted into a digital signal by an analogue-to-digital converter (ADC). The demodulator processes the digital signal and reconstructs the transmitted data. The remainder of this paper focuses on the TX front-end and the generation of the optical waveform.

Typically, quadrature amplitude modulation (QAM) is considered as digital modulation scheme for OFDM transmission. However, as IM/ DD based OWC requires real-valued non-negative time domain signals, QAM cannot be directly applied to optical OFDM. Therefore, the input vector $\mathbf{x}$ to the transmitter IFFT is constrained to have Hermitian symmetry. The input vector provides Hermitian symmetry if its elements fulfil $x_{L-l} = x_l^*$ $(l = 1, 2, \dots \frac{L}{2} - 1)$, where $*$ represents complex conjugation and L is the IFFT size. The complex-valued data symbols are given by x_l, with $x_0 = x_{\frac{L}{2}} = 0$. The zero sub-carrier is not modulated as it results in a direct-current (DC) bias. Hermitian symmetry of the input vector creates a real-valued time domain waveform by cancelling the imaginary components of the IFFT output. This real-valued signal can be sent by incoherent light sources.

However, the time domain signal is still bipolar. In order to provide unipolar signals which can modulate the intensity of the optical carrier, further processing is required.

To this end, the multi-carrier techniques direct-current-biased optical OFDM (DCO-OFDM), asymmetrically clipped optical OFDM (ACO-OFDM) and pulse-amplitude-modulated discrete multitone modulation (PAM-DMT) have been proposed. DCO-OFDM adds a DC offset to the waveform to be sent in order to provide non-negative time domain signals [12]. The DC offset can be added by adjusting the bias point of the transmitter LED. The DC bias has to be chosen appropriately to provide non-negativity of the time domain signals, while keeping upper and lower clipping effects to a minimum [25]. In ACO-OFDM transmission, only the odd-numbered sub-carriers are modulated, whereas the even-numbered sub-carriers are set to zero. This composition of the input vector to the transmitter IFFT generates a real-valued bipolar time domain signal. Armstrong and Lowery have shown that a hard-clipping can be applied to the entire negative signal amplitudes without affecting the data conveyed in the OFDM signal [26]. This clipping converts the bipolar signal into an unipolar waveform as all negative amplitude values are set to zero. However, as only the odd-numbered sub-carriers convey data symbols, ACO-OFDM provides half the spectral efficiency of DCO-OFDM. In contrast to DCO-OFDM and ACO-OFDM which employ complex-valued QAM symbols, PAM-DMT uses real-valued PAM symbols to modulate the sub-carriers. As proposed by Lee *et al.*, the real parts of the input vector $\mathbf{x}$ are set to zero and only the imaginary parts are pulse amplitude modulated [27]. Similar to ACO-OFDM, the negative amplitude values of the time domain signal can be hard-clipped without affecting the data symbols. Consequently, only the positive amplitude values are used to modulate the intensity of the optical carrier. As shown in [13, 27], PAM-DMT and ACO-OFDM provide similar performance for all spectral efficiencies.

Without loss of generality, DCO-OFDM is considered as transmission technique in the following. However, the transmitter concept proposed in this paper is not restricted to DCO-OFDM but can also be used with any other multi-carrier transmission scheme, such as ACO-OFDM, PAM-DMT or DMT employing adaptive bit-loading and power-loading [28], for instance. Moreover, single-carrier transmission schemes like OOK, Manchester coding [29], PAM, M-ary amplitude-shift-keying (ASK) [30] or PPM can be used as well. The comparison of different modulation techniques for OWC is beyond the scope of this paper. The reader is kindly referred to *e.g.* [13, 31, 32] for such comparison.

III. Conventional Transmitter Front-end Designs

A transmitter front-end for OWC transforms the electrical signal generated by the modulator into an optical signal which has sufficient power to enable its detection at the receiver. The block diagram of such a transmitter front-end is displayed in Fig. 2. The modulator output of common transmission techniques, such as OFDM, is a bit vector of size N. This bit vector is a binary digital representation of the signal to be transmitted. Conventional optical transmitter front-ends transform this bit vector into an analogue voltage signal by using a digital-to-analogue converter (DAC). The generated

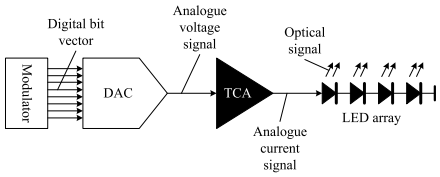

Fig. 2. Conventional transmitter front-end.

voltage signal is converted into a current signal using a transconductance amplifier (TCA). The TCA finally drives the light source. Commonly, the optical light source is a LED, either in the visible or IR light range. Only LEDs are fast enough to transform a modulated current signal into an optical signal of several MHz bandwidth. Therefore, sufficiently low rise and fall times of the LEDs are required. Moreover, arrays of several LEDs are commonly used to increase the emitted optical power. To this end, the LEDs are connected in series and are modulated by the same current signal. Laser diodes are an alternative light source. However, laser diodes are not considered as illumination devices because of their high costs and issues regarding eye safety.

The main drawback of LEDs is their optical-power-versus-current characteristic which is highly non-linear. Particularly in combination with OFDM transmission, non-linearities are a critical issue. Non-linearities directly result in a degraded signal-to-interference-plus-noise ratio (SINR), and consequently in a degraded system performance [14, 15, 17]. Therefore, OWC requires elaborated pre-distortion techniques at the transmitter or complex equalisation techniques at the receiver to compensate for the non-linear characteristic of LEDs. Without these techniques, LEDs can only be modulated in a narrow, quasi-linear operational area. Consequently, the operating point of LEDs has to be carefully chosen. However, this limited operational area largely restricts the dynamic range and the transmission power of OWC systems. Moreover, in order to enable high data rate transmission, the whole transmitter chain has to operate at several tens to hundreds of MHz. For instance in [33], a visible light transmitter system is reported which employs a DAC operating at a sampling rate of 275 Msps to provide a data rate of about 100 Mbit/s. In order to provide the required bandwidth, broadband amplifier circuits have to be used as well. However, these circuit designs result in a high parasitic electrical power consumption, which is not transformed into optical power and is therefore wasted. Additionally, these circuit designs have to provide a good linearity characteristic. Therefore, conventional optical wireless transmitters are subject to complex and elaborated front-end designs.

IV. Quantization

In the following, the effect of transmitter induced quantization on the BER performance is analysed. Fig. 3 illustrates a continuous OFDM symbol which is not quantized (dashed line) and a quantized OFDM symbol with a resolution of 5 bits (solid line). Due to the considered resolution of 5 bits, the

TABLE I
SYSTEM PARAMETERS USED FOR DCO-OFDM TRANSMISSION.

OFDM system parameters	
FFT/ IFFT size L	256
amount data sub-carriers[1]	$\frac{L}{2}-1=127$
cyclic prefix length L_{cp}	5 samples
sampling frequency f_{s}	25 Msps
modulation technique	2-, 4-, 16-QAM
data rate	12, 24, 48 Mbit/s

quantized symbol can take only 32 discrete amplitude levels, whereas the continuous OFDM symbol has a (nearly) unlimited precision (depending on the precision of the computer system, which is commonly 32 or 64 bits). As DCO-OFDM is considered within this paper, the illustrated symbols have a DC offset to provide non-negative amplitude values.

Fig. 4 shows the BER performance of 16- and 64-QAM for different bit resolutions. Note that any effects caused by channel estimation, synchronisation *etc.* are not considered in these simulations to highlight the effect of bit resolution on the BER performance. The error ratios are obtained by error counting taking the BER testing considerations given in [34, Ch. 4] into account (how many symbols have to be simulated to get accurate BER estimates). Table I shows the considered OFDM system parameters. A FFT/ IFFT size of $L=256$ and a cyclic prefix length of $L_{\text{cp}}=5$ samples is applied. Due to Hermitian symmetry, the amount of data sub-carriers is $\frac{L}{2}-1=127$. The signal to noise ratio (SNR) is defined as E_{RX}/N_0, where E_{RX} denotes the received signal energy and N_0 is the power spectral density of the noise. The noise is assumed to be the sum of ambient shot light noise and thermal noise as commonly considered in OWC [4]. Moreover, it is assumed to be independent of the transmitted symbols, and consequently it is assumed to be additive white

[1]Hermitian symmetry is considered.

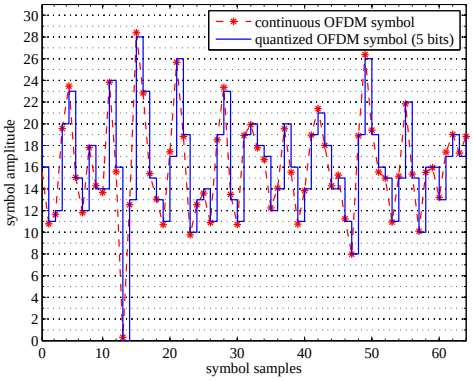

Fig. 3. Continuous OFDM symbol and quantized OFDM symbol.

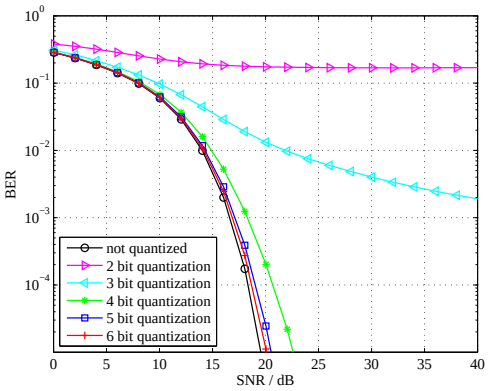

(a) 16-QAM.

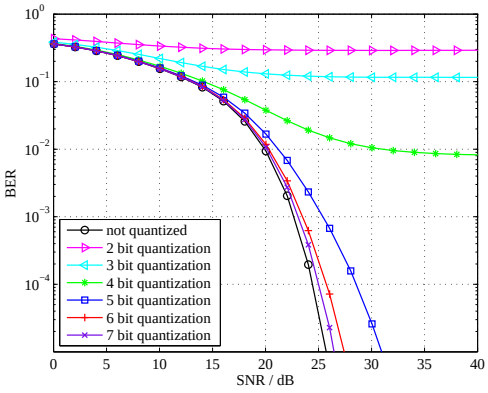

(b) 64-QAM.

Fig. 4. Effect of quantization on BER performance.

Gaussian noise (AWGN). The BER curves in Fig. 4 show that a low resolution of only 2 or 3 bits leads to an error floor due to insufficient precision and low SINR. For 16-QAM a resolution of 5 bits is sufficient as it provides only a minor SNR performance degradation (less than 1 dB) compared to 16-QAM without quantization. For 64-QAM a resolution of at least 7 bits is required to provide sufficient precision. Consequently, the simulation results show that M-level QAM transmission can operate with a reduced bit resolution without major performance degradation.

V. PROPOSED TRANSMITTER CONCEPT

The proposed transmitter concept addresses the shortcomings of conventional optical transmitter front-ends like complex circuit designs, non-linearities and low power efficiency due to the required high-speed DACs and high-bandwidth/ high-current TCAs. The architecture of the proposed optical transmitter front-end is shown in Fig. 5. The basic idea of this

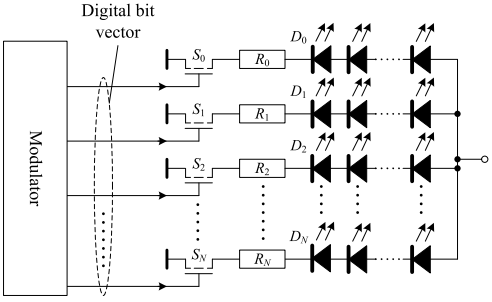

Fig. 5. Proposed optical wireless transmitter front-end architecture.

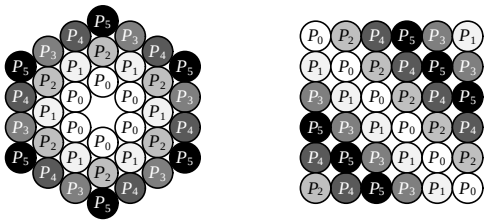

Fig. 6. Proposed LED arrangements for optical wireless transmitter front-end employing 6 LED groups with 6 LEDs per group.

concept is to omit both the DAC and the analogue current control circuit which powers the LEDs. Instead of this analogue signal shaping, an array of LEDs is used which applies discrete power scaling. The LEDs are arranged in several groups which can be switched on and off individually. Each LED group emits a specific optical intensity resulting in a discrete power level stepping. Like for conventional transmitter front-ends, the waveform to be sent is represented by a digital bit vector whose elements are binary values, *i.e.* ones and zeros. These binary values determine which LED groups are switched on or off. Consequently, the baseband modulator switches a specific combination of LED groups on or off according to the signal to be sent. Each signal sample is represented by a specific optical power level which is generated by a particular combination of activated LED groups.

As shown in Fig. 5, the transmitter circuit consists of $N+1$ groups of LEDs, D_0 to D_N. Each group D_i is set to emit a constant optical power level (intensity) P_i using a series resistor R_i. The value of R_i determines the electrical current I_i which powers the LED group D_i. Consequently, I_i determines the optical power level P_i which is emitted by D_i. Assuming $P_{\max}$ is the maximum power level that the LEDs can emit, the current I_0 driving the first group of LEDs D_0 is set accordingly to result in an emitted power level of $P_{\max}$. The remaining LED groups are driven with scaled currents to result in: $P_0 = P_{\max}$, $P_1 = P_{\max}/2$, $P_2 = P_{\max}/4, \ldots$ and $P_N = P_{\max}/2^N$. The LED group D_0 is modulated (switched on/ off) by the most significant bit of the digital bit vector generated by the baseband modulator. Group D_1 is modulated by the second most significant bit, down to group D_N which is controlled by the least significant bit of the vector. Thus, each bit of the signal vector to be sent is assigned to a specific emitter group radiating a defined optical intensity. As the discrete power levels emitted by the single LED groups constructively add up at the receiver, the proposed transmitter concept performs a digital-to-analogue conversion in the optical domain. Consequently, the circuit can be considered as a direct digital input to analogue optical output converter with a resolution of $N+1$ bits. The bit resolution can be chosen with regard to the required precision as analysed in Section IV. If a resolution of 5 bits is considered, the quantized signal waveform can take 32 discrete intensity levels. For instance, the intensity level "12" is represented by the binary sequence "$0\,1\,1\,0\,0$". If this intensity level is to be emitted, the LED groups D_1 and D_2 are activated, whereas the groups D_0, D_3 and D_4 are switched off. If DCO-OFDM is considered, the LED group D_0 represents the DC bias offset which has an optical power level of P_0. For $L \geq 64$, the OFDM time domain signal samples have approximately Gaussian distribution [12].

In order to increase the maximum transmission power and range, it is additionally proposed to combine two or more LED groups to one common group. For instance, two groups can be jointly switched on and off to commonly build group D_0. If both groups emit the maximum power level $P_{\max}$, the overall transmission power is doubled. This results in: $P_0 = 2\,P_{\max}$, $P_1 = P_{\max}$, $P_2 = P_{\max}/2, \ldots$ and $P_N = P_{\max}/2^{N-1}$. This implementation constitutes a compromise between signal precision and transmission power, respectively SNR. The combination of two LED groups provides a reduced resolution of only N bits if the same number of groups is used as above. Alternatively, the amount of LEDs per emitter group D_i can also be varied in order to create different power levels P_i.

The power levels of the individual LED groups can be adjusted using, *e.g.*, an optical power meter. This adjustment guarantees that the optical signal generated by the superposition of all groups has best linearity. Hence, the appropriate values of the series resistors R_i, respectively the currents I_i, can be determined using an optical power meter. Moreover, it is beneficial to align the LEDs in an arrangement which generates a light beam with most homogeneous emitted optical power. Two possible LED arrangements are illustrated in Fig. 6. The figures show a hexagonal (left hand side) and a diagonal (right hand side) arrangement for an implementation with 6 LED groups and 6 LEDs per group. As shown, the single LEDs belonging to a specific group, and thus emitting a specific optical power level P_i, are distributed across the LED array. For the hexagonal arrangement, the groups form inner and outer circles. For the diagonal arrangement, the single LEDs are diagonally arranged within the emitter square. It is also advisable to use LEDs with wide beam angles to ensure a broad coverage and a homogeneous illumination of the emitted light beam. The switching stages S_i (see Fig. 5) that digitally control the different LED groups are realised by fast solid state switching devices, such as transistors or gate drivers for metal-oxide-semiconductor field-effect transistors (MOSFETs). The switching speed of the stages S_i affects the achievable bandwidth of the optical transmitter. Only by fast switching speeds, a bandwidth in the range of 5 – 50 MHz or

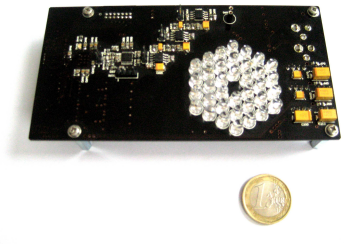

Fig. 7. Developed optical wireless transmitter front-end.

higher can be achieved. However, the bandwidth also depends on the typical rise and fall time of the LEDs. Since simple low-cost transistors are used as switching components, the proposed design enables the implementation of low-complex optical transmitters. A DAC and linear power amplifiers are not required. The OFDM signal processing can be done by an off-the-shelf field programmable gate array (FPGA) for instance, which enables flexible transceiver designs.

Fig. 7 shows the developed optical wireless transmitter front-end. The transmitter front-end has the proposed hexagonal LED arrangement. It consists of 6 LED groups. Two of these groups are combined to be jointly switched on and off in order to increase the transmission power and the SNR at the receiver. Consequently, the implemented transmitter provides a resolution of 5 bits. The emitting diodes are off-the-shelf SFH 4502 IR LEDs [35] which have a wavelength of 950 nm. These diodes have a rise and fall time of about 10 ns and a typical radiant power of 40 mW. The semiangle of the LEDs is $\pm 18°$. The overall value of raw materials of the transmitter is less than \$25. As neither heat sinks nor fans are required for cooling, the implemented transmitter has a good power efficiency. The used receiver employs a SD 445-14-21-305 PIN photo-diode [24] with a detector area of 1 cm^2. The response time of the photo-diode is about 13 ns and the responsivity at 950 nm is about 0.65 A/W. The actual receiver design is not within the scope of this paper.

VI. Transmission Experiments

In this section, the results of some transmission experiments using the implemented optical transmitter front-end are presented. Table I shows the considered OFDM system parameters. The transmitter front-end has a resolution of 5 bits which is sufficient to perform a 16-QAM transmission with appropriate precision as shown in Section IV. The switching speed f_s of the LED groups is set to 25 Msps. The achievable bit rate of DCO-OFDM employing M-QAM can be approximated by:

$$b \approx \log_2(M)\, f_\text{s}\, \frac{\frac{L}{2}-1}{L+L_\text{cp}}. \quad (1)$$

Note that this calculation does not take additional symbols into account which are required for frame synchronisation and channel estimation. These parameters depend on the specific OFDM system implementation. Considering the system parameters given in Table I, the implemented optical transmitter

TABLE II
SNR over distance for LOS and NLOS transmission.

(a) LOS transmission

distance	SNR
1.0 m	35.81 dB
2.0 m	25.77 dB
3.0 m	19.21 dB
4.0 m	14.31 dB
5.0 m	10.69 dB
6.0 m	7.86 dB
7.0 m	6.35 dB

(b) NLOS transmission

distance	SNR
1.0 m	30.75 dB
1.5 m	23.98 dB
2.0 m	20.14 dB
2.5 m	17.31 dB
3.0 m	13.78 dB
3.5 m	10.58 dB
4.0 m	8.29 dB

provides a data rate of about 12, 24 or 48 Mbit/s if 2-, 4- or 16-QAM is used. The data rate can be increased by employing higher order M-QAM. For instance, 64-QAM provides a data rate of about 72 Mbit/s. However, the application of 64-QAM requires an increased resolution of at least 7 bits as shown in Fig. 4(b). In order to further increase the data rate, higher switching speeds can also be applied if the LEDs provide sufficiently low rise and fall times. For instance, applying 64-QAM with a switching speed of $f_\text{s} = 50$ Msps provides a data rate of more than 144 Mbit/s.

The maximum optical output power (all 6 LED groups are switched on) emitted by the transmitter is $P_\text{opt} = \sum_{i=0}^{5} 6\, P_i \approx 930$ mW. The overall electrical power consumption of all LED groups is $P_\text{LED} \approx 3.218$ W, which results in a total power dissipation of $P_\text{LED} - P_\text{opt} \approx 2.288$ W. Consequently, the LEDs have a power efficiency of $P_\text{opt}/P_\text{LED} \approx 28.90\ \%$. The total electrical power consumption of the transmitter front-end is $P_\text{elec} \approx 4.956$ W if all LED groups are switched on. Therefore, the major portion of power is consumed by the LEDs resulting in a percentage of consumed power of $P_\text{LED}/P_\text{elec} \approx 64.93\ \%$. Therefore, the implemented optical transmitter has a low parasitic electrical power consumption and has an overall power efficiency of $P_\text{opt}/P_\text{elec} \approx 18.77\ \%$. For a continous DCO-OFDM transmission, the mean electrical power consumed is $\overline{P}_\text{elec} \approx 2.760$ W and the mean emitted optical power is $\overline{P}_\text{opt} \approx 441$ mW.

Table II(a) shows the SNR at the receiver for different distances between the transmitter and the receiver. The transmitter and the receiver are aligned towards each other to provide a directed LOS link. The SNR is ascertained by measuring the mean received signal energy of the OFDM symbols and by measuring the mean noise energy. The noise energy is measured in the interframe gaps between the OFDM frames since in these gaps no optical signal is emitted. Table II(b) shows the SNR for a non-line-of-sight (NLOS) transmission. Fig. 8 illustrates the measurement setup for the NLOS transmission. As shown, the transmitter and the receiver are straightly directed towards a wall. The wall is a typical office wall with white paint and non-glossy surface. This setup provides a merely diffuse transmission scenario as an opaque obstacle between the transmitter and the receiver blocks the LOS link. The distance of the transmitter, respectively of the

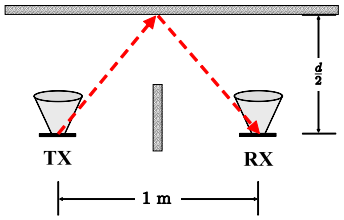

Fig. 8. NLOS transmission setup.

receiver towards the wall is $\frac{d}{2}$. This means that the entire optical path length is about d. Since uncoded wireless data transmission requires an SNR of at least 10 dB to provide reasonable BER (less than 10^{-5}) in AWGN channels [10], the implemented transmitter enables a transmission of up to 5.0 m in LOS scenarios and up to 3.5 m in NLOS scenarios. The achievable transmission distance can be increased if more powerful LEDs are used. Additionally, the amount of LEDs per emitter group can be enlarged to further increase the optical transmission power. The comparison of Table II(a) and II(b) shows that for the same transmission distance, the SNRs of the LOS and NLOS link differ by about 5.5 dB. This difference is induced by the higher transmission loss of the NLOS link due to the wall reflections.

Fig. 9 displays a received sine wave (with transmission induced noise) transmitted by the optical front-end. The transmission distance is 1 m and a LOS link is applied. As shown, the discrete power level stepping generates a quantized sine wave with discrete amplitude values. Since a resolution of 5 bits is considered, the quantized sine wave can take 32 discrete amplitude levels. Employing a larger number of LED groups results in an increased resolution, and thus provides more discrete amplitude values and smaller quantization intervals. Conventional transmitter front-ends typically employ DACs having a resolution of about 12 bits [33], whereas the effective number of bits (ENOB) is mostly smaller. Moreover, the

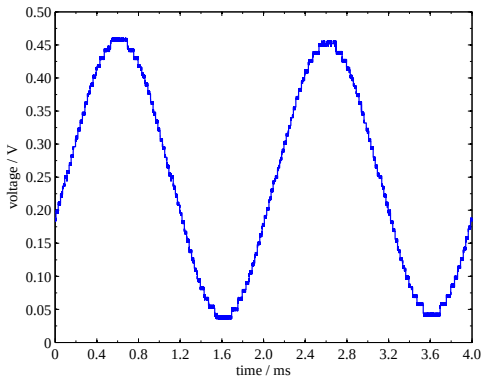

Fig. 9. Received sine wave transmitted by optical transmitter front-end employing discrete power level stepping.

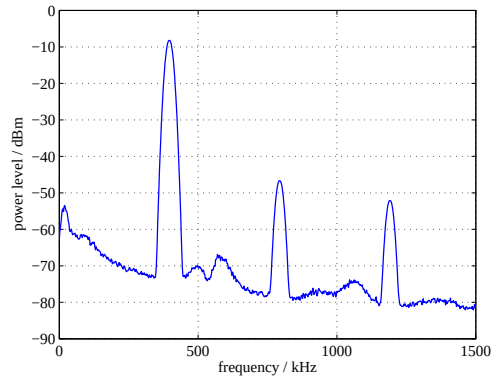

(a) Optical wireless transmission using implemented transmitter front-end.

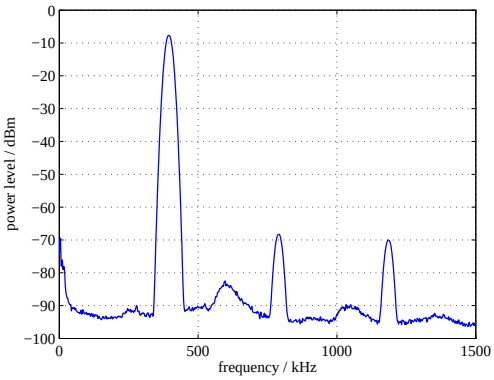

(b) Electrical transmission via cable using signal generator.

Fig. 10. Spectrum of sine wave.

received sine wave has a DC offset of about 0.2 V due to the non-negativity constraint of the emitted optical signal because of IM/ DD. Fig. 10(a) shows the spectrum of a quantized sine wave which is transmitted by the optical front-end. For means of comparison, Fig. 10(b) shows the spectrum of a sine wave which is generated by a conventional signal generator. This sine wave is electrically generated without quantization effects and is transmitted via a cable. Since a conventional signal generator is applied which provides ideal linearity characteristics, this electrical setup corresponds to an ideal conventional optical transceiver as shown in Fig. 1 and Fig. 2. Therefore, the implemented optical transmitter is compared in the following to an electrical transmission using a conventional signal generator. The electrical signal generator represents the reference performance for the implemented optical transmitter. As shown in Fig. 10, the spectra of the optically and electrically generated sine waves closely match. Besides the actual frequency of the emitted sine wave, the harmonic frequencies can also be seen. Note that both transmission methods use a

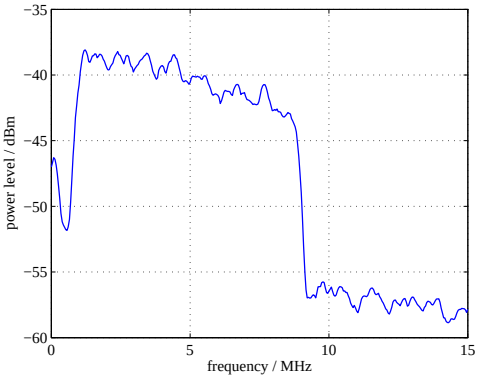

(a) Optical wireless transmission using implemented transmitter front-end.

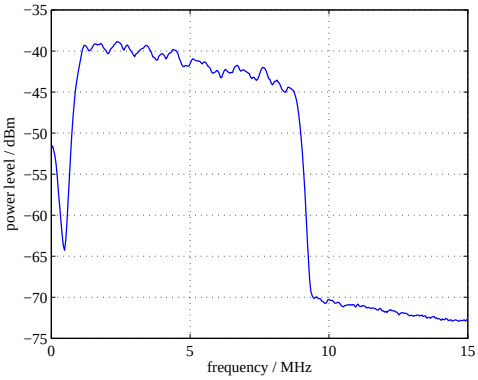

(b) Electrical transmission via cable using signal generator.

Fig. 11. Spectrum of DCO-OFDM signal. IFFT size is 256 and 16-QAM is applied.

similar power level to enable a fair comparison. Moreover, it can be seen that the noise level of the electrical transmission is lower. This is due to the fact that the electrical transmission uses a cable connection in comparison to the optical wireless transmission which undergoes ambient shot light noise. Since both spectra closely match, the implemented optical transmitter shows good linearity characteristics. Additionally, Fig. 11 shows the spectrum of a DCO-OFDM signal. An IFFT size of $L = 256$ is used and 16-QAM is applied. The spectrum of the optical wireless transmission (1 m LOS) and the spectrum electrically generated by the signal generator (transmitted via cable) closely match. Again, the optical wireless transmission undergoes a higher noise level. Fig. 12 displays the measured frequency gain of the optical transceiver (transmitter *and* receiver). A directed 1 m LOS link between the transmitter and the receiver is established. The optical transceiver has a -3 dB cut-off frequency of about 18 MHz and a -6 dB cut-off frequency of about 25 MHz.

In the following, a M-QAM DCO-OFDM transmission is

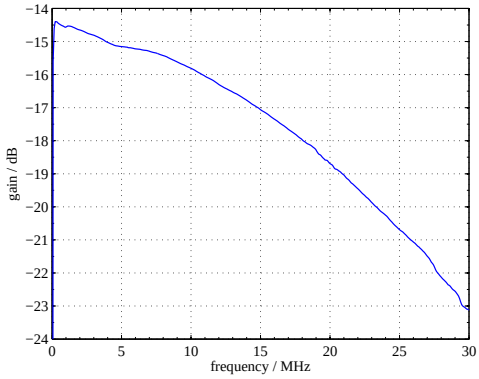

Fig. 12. Frequency gain of optical transceiver.

considered. Each transmitted OFDM frame contains a symbol used for frame detection and synchronisation. Furthermore, each frame comprises several data symbols and a dedicated symbol used for channel estimation. The estimation of the channel coefficient h_l of each OFDM sub-carrier is done by using this pilot symbol. The estimated channel coefficients $\widehat{h}_l$ are used for maximum-likelihood (ML) detection at the receiver. Therefore, for the l^{th} OFDM sub-carrier, the decoder decides for the symbol $\widehat{s}_l$ which minimises the Euclidean distance between the actual received symbol y_l and all potential symbols leading to

$$\widehat{s}_l = \underset{s_l}{\operatorname{argmin}} \left| y_l - \widehat{h}_l \, s_l \right|^2 . \tag{2}$$

The QAM symbol transmitted on the l^{th} OFDM sub-carrier is given by s_l. For an ideal transmission in a mere AWGN channel without any fading and hardware effects, the received symbol is given by $y_l = h_l \, s_l + n_l$ with $h_l = 1$. The AWGN is denoted by n_l. As a single-tap ZF channel equaliser is considered, the equalised received symbols are given by $y_l/\widehat{h}_l$. If an ideal 16-QAM DCO-OFDM transmission with 5 bit resolution and an SNR of 38 dB is simulated, the EVM is about 7.63 %. The EVM is definded as follows:

$$\begin{aligned} \text{EVM} &= \sqrt{\frac{\sum\limits_{k=1}^{K} \left| s_k - \frac{y_k}{\widehat{h}_k} \right|^2}{\sum\limits_{k=1}^{K} |s_k|^2}} \\ &= \sqrt{\frac{\sum\limits_{k=1}^{K} \left(\Im_k - \widehat{\Im}_k \right)^2 + \left(\Re_k - \widehat{\Re}_k \right)^2}{\sum\limits_{k=1}^{K} \left(\Im_k^2 + \Re_k^2 \right)}}, \end{aligned} \tag{3}$$

where $\Im_k$ and $\Re_k$ are the imaginary and the real part of the k^{th} transmitted symbol. The imaginary and the real part of the k^{th} equalised QAM symbol $y_k/\widehat{h}_k$ are represented by $\widehat{\Im}_k$ and $\widehat{\Re}_k$. The number of symbols is given by K. If an actual 16-QAM

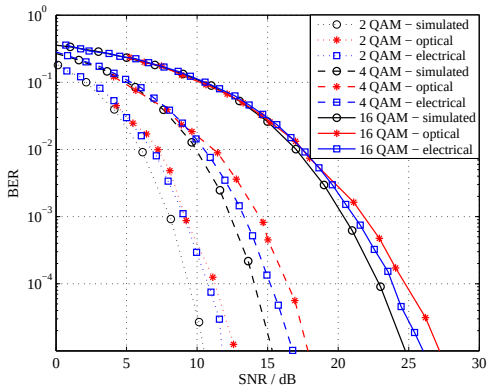

Fig. 13. Comparison of simulated BER performance and actual DCO-OFDM transmission experiments.

DCO-OFDM transmission using the optical transmitter front-end is conducted, the measured SNR is about 38 dB for a LOS transmission over a distance of 0.75 m. The measured EVM is about 8.42 %. Consequently, the transmission experiments fairly comply with the simulation results.

Fig. 13 shows the BER performance of a simulated DCO-OFDM transmission using 2-, 4- and 16-QAM. For these simulations, an ideal AWGN channel is assumed as considered above. Moreover, the BERs of an actual optical wireless transmission using the implemented transmitter are displayed. A relation between SNR and transmission distance for the optical wireless transmission is given in Table II. Additionally, the results of an electrical DCO-OFDM transmission are shown as well. The electrical transmission is done using the same (de)modulating hardware (signal generator and oscilloscope) and signal processing as for the optical transmission. However, the optical transmitter and receiver front-ends are replaced by a DAC generating analogue electrical signals. Moreover, the optical wireless link is replaced by a cable which directly connects the transmitter and the receiver. Since the electrical signal generator has ideal linearity characteristics, it can be regarded as an ideal conventional optical transceiver. As shown, the BER performance of the three scenarios is identical for low SNR values. This is due to the fact that at low SNRs, the noise is the most predominant impairment affecting the link performance. However for higher SNR values, the electrical transmission has a performance loss of about 1 dB compared to the simulation results. This is due to practical realisation issues and hardware effects like frequency offsets between the transmitter and the receiver. These effects are not considered in the mere AWGN simulations. Because of these hardware limitations, the performance of the electrical transmission represents the practical performance bound of the transmission experiments. This bound cannot be exceeded with the used setup and devices. Consequently, the performance of the wired electrical transmission system can be considered as the target performance for the optical wireless transmission. As illustrated, the implemented optical wireless transmitter shows a minor performance loss of less than 1 dB compared to the electrical transmission. This loss is due to the actual transmitter *and* receiver implementations. The receiver implementation is not within the scope of this paper but it might be optimised separately. Moreover, the optical transmission is wireless compared to the electrical transmission which is wired. This results in an additional performance degradation due to the nature of wireless transmission. Therefore, the proposed optical transmitter concept shows good performance as it closely matches the theoretical and practical error bounds.

VII. Summary & Conclusions

An optical wireless transmitter which employs discrete power level stepping has been proposed and implemented. The transmitter consists of several LED groups which can be switched on and off individually. The LED groups emit specific stepped optical intensities which constructively add up at the receiver. Therefore, the optical transmitter can be used for intensity modulated signal transmission using techniques like PAM or OFDM. The proposed transmitter concept has good linearity characteristics and is not subject to the non-linear optical-power-versus-current characteristic of LEDs compared to conventional optical wireless transmitters. Complex pre-distortion techniques are not required. The transmitter is controlled by simple digital signal modulation, *i.e.* on-off-switching of the LED groups. Thus, the implemented transmitter provides a larger dynamic range and higher optical output power compared to conventional optical front-ends which have to carefully adjust the bias point and operating area of the LEDs. Moreover, the proposed solution enables a very simple and cost-effective transmitter design without the need for DACs or complex amplifier circuits. The digital-to-analogue conversion is done in the optical domain by the superposition of the emitted discrete intensities. Additionally, the proposed transmitter concept has a better power efficiency as it does not require high-bandwidth/ high-current TCAs which waste power. Transmission experiments prove the functionality of the implemented optical transmitter as its performance closely matches the theoretical and practical error bounds. The performance of the optical transmitter is nearly similar to an electrical transmission. The latter one provides ideal linearity characteristics, and therefore corresponds to an ideal conventional optical transceiver. Nonetheless, both transmitter *and* receiver might be further optimised in future work to decrease the minor performance gap. Moreover, the bit resolution of the implemented transmitter might be further increased to enable higher order M-QAM transmission in order to provide larger data rates. A shortcoming of the proposed transmitter concept is the fact that a broken LED within the transmitter array directly affects the emitted optical waveform. However, given the high life time of LEDs of about 35000 – 50000 hours, this is unlikely to happen.

Acknowledgement

The authors acknowledge Christian Blümm, Josef Schalk and Nikolaus Schmitt for their support and technical advice.

REFERENCES

[1] GBI Research, "Visible Light Communication (VLC) - A Potential Solution to the Global Wireless Spectrum Shortage," http://www.gbiresearch.com, Sep. 2011.

[2] T. Komine and M. Nakagawa, "Fundamental Analysis for Visible–Light Communication System using LED Lights," *IEEE Transactions on Consumer Electronics*, vol. 50, no. 1, pp. 100–107, Feb. 2004.

[3] H. Elgala, R. Mesleh, and H. Haas, "Indoor Optical Wireless Communication: Potential and State-of-the-Art," *IEEE Communications Magazine*, vol. 49, no. 9, pp. 56–62, Sep. 2011.

[4] J. Kahn and J. Barry, "Wireless Infrared Communications," *Proceedings of the IEEE*, vol. 85, no. 2, pp. 265–298, Feb. 1997.

[5] J. Barry, J. Kahn, W. Krause, E. Lee, and D. Messerschmitt, "Simulation of Multipath Impulse Response for Indoor Wireless Optical Channels," *IEEE Journal on Selected Areas in Communications*, vol. 11, no. 3, pp. 367–379, Apr. 1993.

[6] F. R. Gfeller and U. Bapst, "Wireless In-House Data Communication Via Diffuse Infrared Radiation," *Proceedings of the IEEE*, vol. 67, no. 11, pp. 1474–1486, Nov. 1979.

[7] O. Gonzalez, R. Perez-Jimenez, S. Rodriguez, J. Rabadan, and A. Ayala, "OFDM Over Indoor Wireless Optical Channel," *Optoelectronics, IEE Proceedings*, vol. 152, no. 4, pp. 199–204, Aug. 2005.

[8] H. Liu and G. Li, *OFDM-Based Broadband Wireless Networks : Design and Optimization*. John Wiley & Sons Inc., 2005.

[9] J. Heiskala and J. Terry, *OFDM Wireless LANs: A Theoretical and Practical Guide*, T. Reid and D. B. Williams, Eds. Sams Publishing, 2002.

[10] A. Goldsmith, *Wireless Communications*. Cambridge University Press, 2005.

[11] M. Afgani, H. Haas, H. Elgala, and D. Knipp, "Visible Light Communication Using OFDM," in *Proc. of the 2nd International Conference on Testbeds and Research Infrastructures for the Development of Networks and Communities (TRIDENTCOM)*, Barcelona, Spain, Mar. 1–3, 2006, pp. 129–134.

[12] J. Armstrong, "OFDM for Optical Communications," *Journal of Lightwave Technology*, vol. 27, no. 3, pp. 189–204, Feb. 2009.

[13] D. Barros, S. Wilson, and J. Kahn, "Comparison of Orthogonal Frequency-Division Multiplexing and Pulse-Amplitude Modulation in Indoor Optical Wireless Links," *IEEE Transactions on Communications*, vol. 60, no. 1, pp. 153–163, Jan. 2012.

[14] E. Costa, M. Midrio, and S. Pupolin, "Impact of amplifier nonlinearities on OFDM transmission system performance," *IEEE Communications Letters*, vol. 3, no. 2, pp. 37–39, Feb. 1999.

[15] E. Costa and S. Pupolin, "M-QAM-OFDM System Performance in the Presence of a Nonlinear Amplifier and Phase Noise," *IEEE Transactions on Communications*, vol. 50, no. 3, pp. 462–472, Mar. 2002.

[16] D. Dardari, V. Tralli, and A. Vaccari, "A Theoretical Characterization of Nonlinear Distortion Effects in OFDM Systems," *IEEE Transactions on Communications*, vol. 48, no. 10, pp. 1755–1764, Oct. 2000.

[17] W. Jun and Y. Chenyang, "The influence of analog device on OFDM system," in *Proc. of International Conference on Communication Technology (ICCT)*, vol. 2, Beijing, China, Apr. 9–11, 2003, pp. 1060–1062.

[18] B. Inan, S. C. J. Lee, S. Randel, I. Neokosmidis, A. M. J. Koonen and J. W. Walewski, "Impact of LED Nonlinearity on Discrete Multitone Modulation," *IEEE/OSA Journal of Optical Communications and Networking*, vol. 1, no. 5, pp. 439–451, Oct. 2009.

[19] I. Neokosmidis, T. Kamalakis, J. W. Walewski, B. Inan, and T. Sphicopoulos, "Impact of Nonlinear LED Transfer Function on Discrete Multitone Modulation: Analytical Approach," *IEEE Journal of Lightwave Technology*, vol. 27, no. 22, pp. 4970–4978, Nov. 2009.

[20] H. Elgala, R. Mesleh, and H. Haas, "A Study of LED Nonlinearity Effects on Optical Wireless Transmission using OFDM," in *Proc. of the* 6^{th} *IEEE International Conference on Wireless and Optical Communications Networks (WOCN)*, Cairo, Egypt, Apr. 28–30, 2009.

[21] I. Stefan, H. Elgala, R. Mesleh, D. O'Brien, and H. Haas, "Optical Wireless OFDM System on FPGA: Study of LED Nonlinearity Effects," in *Proc. of the IEEE Vehicular Technology Conference (VTC)*, Budapest, Hungary, May 15–18, 2011, pp. 1–5.

[22] H. Elgala, R. Mesleh, and H. Haas, "Non-linearity Effects and Predistortion in Optical OFDM Wireless Transmission Using LEDs," *Inderscience International Journal of Ultra Wideband Communications and Systems (IJUWBCS)*, vol. 1, no. 2, pp. 143–150, 2009.

[23] A. Behravan and T. Eriksson, "PAPR and Other Measures for OFDM Systems with Nonlinearity," in *Proc. of the* 5^{th} *International Symposium on Wireless Personal Multimedia Communications*, vol. 1, Honolulu, Hawaii, USA, Oct. 27–30, 2002, pp. 149–153.

[24] Advanced Photonix Inc., "Datasheet: Red Enhanced High Performance Silicon Photodiode SD 445-14-21-305," Apr. 2006, retrieved Jun. 20, 2012 from http://www.advancedphotonix.com/ap_products/pdfs/SD445-14-21-305.pdf.

[25] S. Dimitrov, S. Sinanovic, and H. Haas, "Clipping Noise in OFDM-based Optical Wireless Communication Systems," *IEEE Transactions on Communications (IEEE TCOM)*, vol. 60, no. 4, pp. 1072–1081, Apr. 2012.

[26] J. Armstrong and A. Lowery, "Power Efficient Optical OFDM," *Electronics Letters*, vol. 42, no. 6, pp. 370–372, Mar. 16, 2006.

[27] S. C. J. Lee, S. Randel, F. Breyer, and A. M. J. Koonen, "PAM-DMT for Intensity-Modulated and Direct-Detection Optical Communication Systems," *IEEE Photonics Technology Letters*, vol. 21, no. 23, pp. 1749–1751, Dec. 2009.

[28] A. M. Khalid, G. Cossu, R. Corsini, P. Choudhury, and E. Ciaramella, "1-Gb/s Transmission Over a Phosphorescent White LED by Using Rate-Adaptive Discrete Multitone Modulation," *IEEE Photonics Journal*, vol. 4, no. 5, pp. 1465–1473, Oct. 2012.

[29] C. W. Chow, C. H. Yeh, Y. F. Liu, and P. Y. Huang, "Mitigation of Optical Background Noise in Light-Emitting Diode (LED) Optical Wireless Communication Systems," *IEEE Photonics Journal*, vol. 5, no. 1, pp. 7 900 307–7 900 307, Feb. 2013.

[30] C. H. Yeh, Y. F. Liu, C. W. Chow, Y. Liu, P. Y. Huang, and H. K. Tsang, "Investigation of 4-ASK modulation with digital filtering to increase 20 times of direct modulation speed of white-light LED visible light communication system," *OSA Optics Express*, vol. 20, no. 15, pp. 16 218–16 223, Jul. 2012.

[31] J. Armstrong and B. J. C. Schmidt, "Comparison of Asymmetrically Clipped Optical OFDM and DC-Biased Optical OFDM in AWGN," *IEEE Communications Letters*, vol. 12, no. 5, pp. 343–345, May 2008.

[32] S. Dimitrov, S. Sinanovic, and H. Haas, "Signal Shaping and Modulation for Optical Wireless Communication," *IEEE/ OSA Journal of Lightwave Technology*, vol. 30, no. 9, pp. 1319–1328, May 2012.

[33] O. Bouchet, G. Faulkner, L. Grobe, E. Gueutier, K.-D. Langer, S. Nerreter, D. O'Brien, R. Turnbull, J. Vucic, J. W. Walewski, and M. Wolf, "Deliverable D4.2b Physical Layer Design and Specification," 7^{th} *Framework Programme Information & Communication Technologies*, Feb. 2011, retrieved Jul. 18, 2012 from http://www.ict-omega.eu.

[34] D. Derickson and M. Müller, *Digital Communications: Test and Measurement*. Prentice Hall, 2008.

[35] OSRAM Opto Semiconductors GmbH, "Datasheet: SFH 4501, SFH 4502, SFH 4503 High Power Infrared Emitter," Jan. 2008, retrieved Jun. 20, 2012 from http://catalog.osram-os.com.

Optical Spatial Modulation using Colour LEDs

Thilo Fath[*‡] and Harald Haas[‡]

[*]EADS Deutschland GmbH, Innovation Works Germany, 81663 Munich, Germany, e-mail: thilo.fath@ed.ac.uk
[‡]The University of Edinburgh, Institute for Digital Communications, EH9 3JL, Edinburgh, UK, e-mail: h.haas@ed.ac.uk

***Abstract*—Spatial Modulation (SM) is a combined multiple-input-multiple-output (MIMO) and digital modulation technique. Like in any MIMO scheme, the performance of SM is related to the differentiability, *i.e.* the correlation, of the multiple channels. In this paper, we analyse the performance of optical SM for a wireless indoor environment. It is shown that the use of colour light-emitting diodes (LEDs) can improve the performance of SM by more than 10 dB. This is due to the fact that the responsivity of photo-diodes is a function of the optical wavelength. As a consequence, using LEDs with different colours induces specific optical power levels at the receiver. These distinctive power levels directly affect the channel characteristic since they reduce the channel correlation. Moreover, we analyse the computational complexity of optical SM and compare it to the complexity of other common MIMO techniques. It is found that SM requires a much lower computational complexity compared to Repetition Coding (RC) and Spatial Multiplexing (SMP).**

***Index Terms*—colour, complexity, MIMO, optical wireless communications, spatial modulation.**

I. Introduction

Optical wireless communications (OWC) is in the spotlight of ongoing research activities since it can serve as an efficient supplement to established radio frequency (RF) communications. As illumination devices are installed nearly everywhere, it is encouraging to use these installations not only for lighting but also for wireless data transmission. In order to provide sufficient illumination, recent light fixtures are typically equipped with multiple light-emitting diodes (LEDs). This property can readily be exploited to create optical multiple-input-multiple-output (MIMO) communication systems. MIMO techniques offer high data rates by providing large spectral efficiencies [1, 2]. Commonly, OWC systems use incoherent light sources in combination with intensity modulation (IM) and direct detection (DD) [3]. Off-the-shelf incoherent-light-producing LEDs are characterised by achieving only a limited bandwidth of about $30-50$ MHz in the case of infra-red (IR) light and even less for visible light. Therefore, the available bandwidth of practical OWC systems is restricted. Consequently, achieving high spectral efficiencies is of great concern for OWC systems.

Spatial Modulation (SM) is a combined MIMO and digital modulation technique, proposed in [4] and further investigated in [5] and [6] for instance. This technique provides an increased spectral efficiency by utilizing multiple transmitters while completely avoiding inter-channel interference (ICI). As the SM principle can be applied to power-signals in a straightforward manner, SM is an ideal candidate for IM/DD systems [7]. Like in any MIMO transmission, the performance of SM depends on the channel characteristics. As a consequence, its performance is degraded in scenarios with high link correlation and low differentiability of the multiple channels.

Hence, in this paper, we analyse the performance of SM applied to an indoor OWC scenario. It is found that IM/DD in combination with different optical wavelengths enhances the differentiability of the multiple channels. This is realised by the use of colour LEDs which significantly improves the bit error ratio (BER) performance of SM. Moreover, the computational complexity of optical SM is analysed and compared to the complexity of Repetition Coding (RC) and Spatial Multiplexing (SMP).

The remainder of this paper is organised as follows: in Section II, the basic system model is given. Section III introduces the setup which is used to model the optical wireless indoor scenario. In Section IV, the BER performance of SM is analysed i) for scenarios which use transmitters having the *same* optical wavelength and ii) for scenarios which use transmitters having *different* optical wavelengths. Finally, Section V concludes the paper.

II. System Model

We consider an optical wireless transmission system employing N_t transmitters, *e.g.* LEDs, and N_r photo-detectors at the receiver. The received signal vector is

$$\mathbf{y} = \mathbf{H}\,\mathbf{s} + \mathbf{n}, \tag{1}$$

where $\mathbf{n}$ is the sum of ambient shot light noise and thermal noise. It is the main noise impairment as commonly assumed in OWC [3]. Consequently, $\mathbf{n}$ is real valued additive white Gaussian noise (AWGN) with zero mean and a variance $\sigma^2 = \sigma^2_{\text{shot}} + \sigma^2_{\text{thermal}}$, where σ^2_{shot} is the shot noise variance and $\sigma^2_{\text{thermal}}$ is the thermal noise variance [3]. Thus, the noise power is given by $\sigma^2 = N_0\,B$, where N_0 is the noise power spectral density and B is the bandwidth. The transmitted signal vector is denoted by $\mathbf{s} = [s_1 \ \ldots \ s_{N_t}]^T$, where $[\cdot]^T$ is the transpose operator. The elements of $\mathbf{s}$ indicate which signal is emitted by each optical transmitter, *i.e.* s_{n_t} denotes the signal emitted by transmitter n_t. The $N_r \times N_t$ channel matrix is depicted by $\mathbf{H}$. Its elements $h_{n_r n_t}$ represent the transfer factors of the links between transmitter n_t and receiver n_r.

In SM, the conventional signal constellation diagram is extended to an additional dimension, the spatial dimension. Each transmitter of the transmitting array is assigned a unique binary sequence, the spatial symbol. A transmitter is only activated when the random spatial symbol to be transmitted

$$\mathrm{BER}_{\mathrm{SSK}} \leq \frac{1}{N_t \, \log_2(N_t)} \sum_{n_t^{(1)}=1}^{N_t} \sum_{n_t^{(2)}=1}^{N_t} \mathrm{d_H}\left(b_{n_t^{(1)}}, b_{n_t^{(2)}}\right) \mathrm{Q}\left(\sqrt{\frac{E_s}{4\,N_0} \sum_{n_r=1}^{N_r} \left| h_{n_r n_t^{(2)}} - h_{n_r n_t^{(1)}} \right|^2}\right) \tag{5}$$

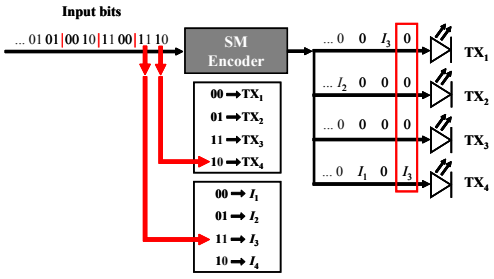

Fig. 1. Illustration of SM operation with $N_t = 4$ and $M = 4$. The first two bits in the block of four bits determine the PAM symbol and the second two bits determine the active LED.

matches the pre-allocated spatial symbol. Thus, only one transmitter is activated at any symbol duration. Therefore, only one element of the signal vector $\mathbf{s}$ to be transmitted is non-zero. The index of the non-zero element is the spatial symbol. The element is the digitally modulated signal to be sent. Without loss of generality, we assume that pulse amplitude modulation (PAM) employing rectangular pulses is used for digital signal modulation. As SM simultaneously transmits data in the signal domain and the spatial domain, it provides an enhanced spectral efficiency of $R = \log_2(N_t) + \log_2(M)$ bit/s/Hz, where M denotes the signal constellation size. Due to the distinct channel transfer factors between a particular transmitter and the receiver, the receiver is able to detect which transmitter is activated, and hence is able to detect the spatial symbol. Fig. 1 illustrates the functionality of SM for a setup with $N_t = 4$ optical emitters and a signal constellation size of $M = 4$. The bits to be transmitted are passed to the SM encoder, which maps them to the respective signal and transmitter index. In this example, the last two bits denote the index of the transmitter which emits the signal, whereas the first two bits represent the signal to be sent. For instance, the bit sequence "1 1 1 0" is represented by transmitter number 4 emitting signal I_3. In contrast to common PAM modulation, signals with intensity $I_m = 0$ cannot be used for the signal modulation of SM. In this case, no transmitter would be active and the spatial information would be lost. Therefore, the intensities of common PAM have to be modified to be suitable for SM leading to:

$$I_m^{\mathrm{SM}} = \tfrac{2\,I}{M+1}\, m \quad \text{for } m = 1 \ldots M, \tag{2}$$

where I is the mean optical power emitted. As the SM receiver has to detect which transmitter has sent the signal, its performance depends on the differentiability, *i.e.* the correlation, of the multiple channels. The pairwise error probability (PEP) of SM is the probability that the receiver mistakes the transmitted signal vector $\mathbf{s}_{m^{(1)}}$ for another vector $\mathbf{s}_{m^{(2)}}$, given knowledge of the channel matrix $\mathbf{H}$. The PEP of SM is given by [8]:

$$\begin{aligned} \mathrm{PEP}_{\mathrm{SM}} &= \mathrm{PEP}(\mathbf{s}_{m^{(1)}} \to \mathbf{s}_{m^{(2)}} | \mathbf{H}) \\ &= \mathrm{Q}\left(\sqrt{\frac{\rho^2\,T_s}{4\,N_0} \, \|\mathbf{H}\,(\mathbf{s}_{m^{(1)}} - \mathbf{s}_{m^{(2)}})\|_{\mathrm{F}}^2}\right) \\ &= \mathrm{Q}\left(\sqrt{\frac{\rho^2\,T_s}{4\,N_0} \sum_{n_r=1}^{N_r} \left| I_{m^{(2)}}^{\mathrm{SM}}\, h_{n_r n_t^{(2)}} - I_{m^{(1)}}^{\mathrm{SM}}\, h_{n_r n_t^{(1)}} \right|^2}\right), \end{aligned} \tag{3}$$

where $\mathrm{Q}(a) = \frac{1}{\sqrt{2\pi}} \int_a^{+\infty} \exp(\frac{-t^2}{2})\,\mathrm{d}t$ is the Q-function and $\|\cdot\|_{\mathrm{F}}$ denotes the Frobenius norm. The optical-to-electrical conversion coefficient is represented by ρ. Without loss of generality, ρ is assumed to be $1\,\mathrm{A}\sqrt{\Omega}/\mathrm{W}$ in the following. T_s denotes the symbol, *i.e.* the pulse, duration in seconds. The shown PEP denotes the probability that the receiver decides for intensity $I_{m^{(2)}}^{\mathrm{SM}}$ being emitted by transmitter $n_t^{(2)}$, whereas actually transmitter $n_t^{(1)}$ has emitted intensity $I_{m^{(1)}}^{\mathrm{SM}}$.

A special mode of SM is the so-called Space Shift Keying (SSK) technique. SSK conveys only information in the spatial domain. Consequently, there is no signal modulation and $M = 1$. Thus, each activated LED emits the same optical intensity, *i.e.* I. Therefore, SSK is a low complex implementation of SM and its PEP reduces to:

$$\begin{aligned} \mathrm{PEP}_{\mathrm{SSK}} &= \mathrm{PEP}(\mathbf{s}_{m^{(1)}} \to \mathbf{s}_{m^{(2)}} | \mathbf{H}) \\ &= \mathrm{Q}\left(\sqrt{\frac{\rho^2\,T_s}{4\,N_0} \, \|\mathbf{H}\,(\mathbf{s}_{m^{(1)}} - \mathbf{s}_{m^{(2)}})\|_{\mathrm{F}}^2}\right) \\ &= \mathrm{Q}\left(\sqrt{\frac{\rho^2\,T_s}{4\,N_0} \sum_{n_r=1}^{N_r} \left| I\, h_{n_r n_t^{(2)}} - I\, h_{n_r n_t^{(1)}} \right|^2}\right) \\ &= \mathrm{Q}\left(\sqrt{\frac{E_s}{4\,N_0} \sum_{n_r=1}^{N_r} \left| h_{n_r n_t^{(2)}} - h_{n_r n_t^{(1)}} \right|^2}\right), \end{aligned} \tag{4}$$

where we define $E_s = (\rho\, I)^2\, T_s$ as the mean *emitted* electrical energy of the optical signal. In IM based optical communications, the electrical energy is proportional to the square of the optical power [3]. Using this PEP and considering all N_t transmitters which can be activated, the BER of SSK can be approximated by union bound methods. The upper bound of its BER is given in (5) on top of this page, where $b_{n_t^{(1)}}$ is the bit assignment which is conveyed when transmitter $n_t^{(1)}$ is activated and $b_{n_t^{(2)}}$ is the bit assignment which is encoded when transmitter $n_t^{(2)}$ is activated. Consequently, the Hamming distance $\mathrm{d_H}\left(b_{n_t^{(1)}}, b_{n_t^{(2)}}\right)$ states the number of bit errors when erroneously decoding the bit sequence $b_{n_t^{(2)}}$ at the receiver instead of the actually transmitted sequence $b_{n_t^{(1)}}$.

TABLE I
COMPARISON OF SPECTRAL EFFICIENCIES AND COMPUTATIONAL COMPLEXITY AT RECEIVER FOR DIFFERENT MIMO TECHNIQUES.

MIMO technique	**Spectral efficiency R in bit/s/Hz**	**Number of mathematical operations at receiver**
RC	$\log_2(M)$	$2^R\,(2\,N_t\,N_r + N_r - 1)$ $= M\,(2\,N_t\,N_r + N_r - 1)$
SMP	$N_t\,\log_2(M)$	$2^R\,(2\,N_t\,N_r + N_r - 1)$ $= M^{N_t}\,(2\,N_t\,N_r + N_r - 1)$
SM	$\log_2(MN_t)$	$2^R\,(3\,N_r - 1)$ $= MN_t\,(3\,N_r - 1)$

In the following, we assume that the detection at the receiver is based on the maximum-likelihood (ML) principle. Therefore, the decoder decides for the signal vector $\widehat{\mathbf{s}}$ which minimises the Euclidean distance between the actual received signal vector $\mathbf{y}$ and all potential received signals leading to

$$\widehat{\mathbf{s}} = \underset{\mathbf{s}}{\operatorname{argmax}}\, p_{\mathbf{y}}(\mathbf{y}|\mathbf{s},\mathbf{H}) = \underset{\mathbf{s}}{\operatorname{argmin}}\, \|\mathbf{y} - \mathbf{H}\,\mathbf{s}\|_{\mathrm{F}}^2\,, \qquad (6)$$

where $p_{\mathbf{y}}$ is the probability density function of $\mathbf{y}$ conditioned on $\mathbf{s}$ and $\mathbf{H}$. Moreover, we assume perfect knowledge of the channel and ideal time synchronisation at the receiver. On the basis of this detection algorithm, we analyse the computational complexity of optical SM and compare it to the complexity of RC and SMP. Both RC and SMP are common optical MIMO techniques. RC is the simplest MIMO transmission technique as it simultaneously emits the same signal from all optical transmitters. By applying SMP, independent data streams are simultaneously emitted from all transmitters. Regarding a detailed performance comparison of these techniques, we refer to [8] as this is beyond the scope of this paper. We define the computational complexity as the total number of required mathematical operations, *i.e.* multiplications, additions and subtractions that are required for ML detection. The ascertained numbers are listed in Table I. It can be seen that RC and SMP need the same number of operations to provide equal spectral efficiency R, whereas the detection of SM is less computationally expensive. This is due to the fact that SM avoids ICI as only one transmitter is active at any symbol duration in contrast to SMP. Moreover, as SM conveys additional bits in the spatial domain, it can achieve the same spectral efficiency as RC but with a reduced signal constellation size. Thus for SM, there are less signal constellation points to be considered when performing the ML detection. For instance, if we assume a setup with $N_t = 4$ and $N_r = 4$, which provides a spectral efficiency of $R = 4$ bit/s/Hz, RC and SMP both require 560 operations, whereas SM requires only 176 operations. Fig. 2 displays the computational complexity of RC, SMP and SM for different setups and spectral efficiencies. Consequently, as SM requires a much lower computational complexity compared to common MIMO techniques, it enables the implementation of efficient and simple optical wireless MIMO receivers.

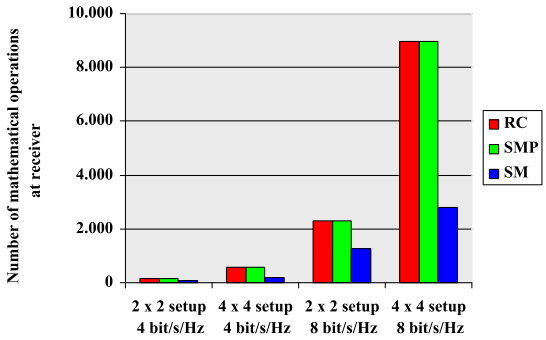

Fig. 2. Computational complexity at receiver of RC, SMP and SM for different setups and spectral efficiencies.

III. OPTICAL WIRELESS SETUP SCENARIO

In this paper, optical wireless links with line-of-sight (LOS) characteristics are considered. Fig. 3 illustrates a directed LOS link. As shown, ϕ is the angle of emergence with respect to the transmitter (TX) axis and ψ is the angle of incidence with respect to the receiver (RX) axis. Furthermore, d depicts the distance between transmitter and receiver. Using this geometric scenario, the transfer factor of an optical propagation link can be calculated according to [3] as follows:

$$h = \begin{cases} \frac{(k+1)\,A\,r}{2\,\pi\,d^2}\cos^k(\phi)\cos(\psi) & 0 \le \psi \le \Psi_{\frac{1}{2}} \\ 0 & \psi > \Psi_{\frac{1}{2}} \end{cases} \qquad (7)$$

with the order $k = \frac{-\ln(2)}{\ln\left(\cos(\Phi_{\frac{1}{2}})\right)}$ and the transmitter semiangle $\Phi_{\frac{1}{2}}$ (at half power). Furthermore, $\Psi_{\frac{1}{2}}$ denotes the field-of-view (FOV) semiangle of the receiver. The detector area of the receiver is represented by A and r is the detector responsivity, which is related to the optical wavelength.

In the following, an indoor $N_r \times N_t$ scenario within a $4.0\,\mathrm{m} \times 4.0\,\mathrm{m} \times 3.0\,\mathrm{m}$ room is considered. Specifically, different numbers of optical transmitters are considered, whereas the number of receivers (photo-diodes) is assumed to be $N_r = 4$ for each setup. Thus, a $4 \times N_t$ scenario is considered. We assume that the N_t transmitters are placed at a height of $z = 2.50$ m and are oriented downwards to point straight down from the ceiling. Moreover, the transmitters are equidistantly arranged in a circle. The circle is centred in the middle of the room and has a diameter of 0.50 m. The 4 receivers are located at a height of $z = 0.75$ m (*e.g.* height of a table) and are oriented upwards to point straight up at the ceiling. The

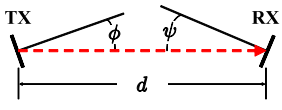

Fig. 3. Geometric scenario used for calculation of channel coefficients.

TABLE II
WAVELENGTHS OF LEDS AND CORRESPONDING RESPONSIVITY OF PHOTO-DIODES.

Wavelength of LED	Responsivity of photo-diode
462 nm (deep blue)	0.1963
467 nm (blue)	0.2019
505 nm (verde green)	0.2407
528 nm (true green)	0.2565
590 nm (yellow)	0.3343
617 nm (amber)	0.3611
625 nm (red)	0.3713
656 nm (hyper red)	0.4102

TABLE III
WAVELENGTHS OF LEDS USED IN SETUP SCENARIOS.

Wavelength of LED	Transmitter using wavelength			
	$N_t = 4$	$N_t = 8$	$N_t = 16$	$N_t = 32$
462 nm	1	1	1, 9	1, 9, 17, 25
467 nm	3	3	3, 11	3, 11, 19, 27
505 nm		5	5, 13	5, 13, 21, 29
528 nm		7	7, 15	7, 15, 23, 31
590 nm		2	2, 10	2, 10, 18, 26
617 nm		4	4, 12	4, 12, 20, 28
625 nm	4	6	6, 14	6, 14, 22, 30
656 nm	2	8	8, 16	8, 16, 24, 32

receivers are aligned in a quadratically 2×2 array which is centred in the middle of the room. The spacing of the receivers is assumed to be 0.10 m on the x- and y-axis. This receiver spacing would enable the implementation of the receiver array into typical laptop computers. Fig. 4 shows the positioning of the simulation setup within the room for the case of $N_t = 16$. The receivers are displayed as dots and the transmitters as triangles. Off-the-shelf SD 445-14-21-305 silicon photo-diodes [9], which have a detector area of about $1\,\text{cm}^2$, are considered as photo-detectors. The FOV semiangle of the photo-diodes is assumed to be $60°$. Fig. 5 shows the responsivity of the photo-diodes for different optical wavelengths. The optical transmitters are assumed to be off-the-shelf LEDs from OSRAM's Golden Dragon Plus product family [10]. These light sources have a transmitter semiangle of $85°$ and are available in different colours. Table II shows the wavelengths of the considered LEDs and the corresponding responsivity of the photo-diodes according to Fig. 5.

IV. RESULTS ON BIT ERROR RATIO PERFORMANCE

As shown in (7), the responsivity of the photo-detector affects the transfer factor of optical links. Since the responsivity is related to the wavelength of the optical transmitter, using LEDs with different wavelengths affects the differentiability of multiple optical links. Therefore, we analyse and compare the BER performance of SSK for two different scenarios: i) all optical transmitters have the same wavelength and ii) the optical transmitters have different wavelengths. Both scenarios are based on the $4 \times N_t$ setup described in Section III. For scenario ii), Table III shows the assignment of the different wavelengths to the individual transmitters. Four specific setups which have $N_t = 4, 8, 16$ and 32 optical transmitters are considered. For scenario i), all optical transmitters have a wavelength of 656 nm as this wavelength provides the highest responsivity. Therefore, this scenario provides the largest mean received electrical energy which is given by:

$$\begin{aligned} E_r &= \sum_{n_r=1}^{N_r} \left(\frac{\rho\, I}{N_t} \sum_{n_t=1}^{N_t} h_{n_r n_t} \right)^2 T_s \\ &= E_s \sum_{n_r=1}^{N_r} \left(\frac{1}{N_t} \sum_{n_t=1}^{N_t} h_{n_r n_t} \right)^2 . \end{aligned} \tag{8}$$

In the following, we evaluate the error ratios at the receiver with regard to *transmit* energy against power spectral density of the AWGN. Hence, we take into account the specific path loss of each setup caused by the alignment of the single transmitters and receivers. Consequently, we define the signal to noise ratio (SNR) as $\frac{E_s}{N_0}$. This is because considering

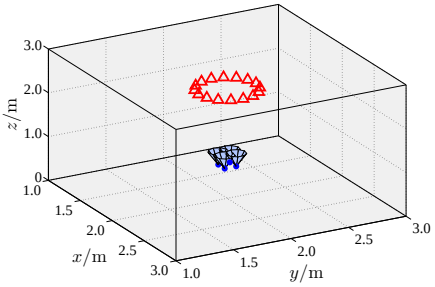

Fig. 4. Simulation setup for the case of $N_t = 16$. Downwards pointing LEDs (transmitters) are placed at ceiling height of 2.50 m, and upwards pointing photo-diodes (receivers) are placed at table height of 0.75 m.

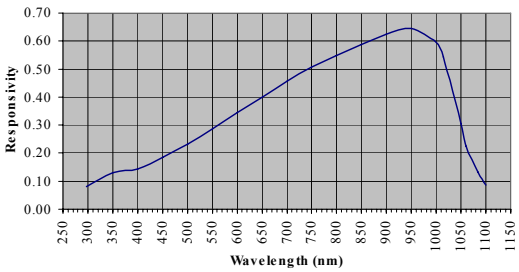

Fig. 5. Responsivity of photo-diode SD 445-14-21-305 [9].

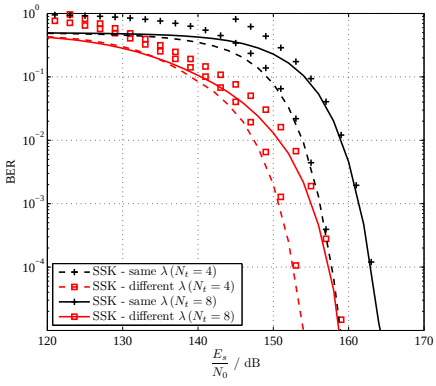

Fig. 6. Performance of SSK for 4×4 and 4×8 setup using i) same transmitter wavelength λ and ii) different transmitter wavelengths λ (lines show simulation results and markers analytical error bounds).

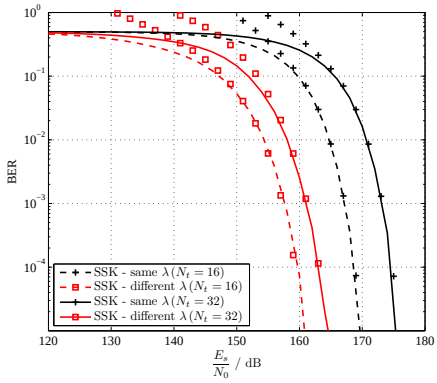

Fig. 7. Performance of SSK for 4×16 and 4×32 setup using i) same transmitter wavelength λ and ii) different transmitter wavelengths λ (lines show simulation results and markers analytical error bounds).

received energy to noise energy would disregard the difference in path loss caused by the specific responsivities. As the channel coefficients are in the region of 10^{-6}, the electrical path loss is about -120 dB. Because we defined the SNR as the ratio of *transmitted* signal energy to noise energy, the BER curves displayed in the following figures have an approximate SNR offset of about 120 dB with respect to the *received* energy to noise ratio.

Fig. 6 shows the BER of SSK for a 4×4 and 4×8 setup. It can be seen that the scenario that employs different transmitter wavelengths achieves an SNR performance gain of about 5 dB. Although using the same transmitter wavelength provides a larger received electrical energy, it results in a higher BER. This is due to the fact that using different wavelengths improves the differentiability of the multiple channels and consequently, reduces the channel correlation. As the performance of SSK is affected by the differentiability of the multiple channels, the use of colour LEDs enhances the performance of SSK. Note that the receiver does not need any knowledge about the different wavelengths because it implicitly gets this information by channel estimation which it needs to perform in any case. The wavelengths are distinguished on the basis of the specific power levels which they induce at the detector without the need for special optical filters. As shown, the theoretical upper error bounds (markers) given in (5) closely match the simulation results (lines). Fig. 7 shows the BER of SSK for a 4×16 and 4×32 setup. For these two setups, using different transmitter wavelengths achieves an even larger SNR performance gain of about 10 dB.

V. Summary & Conclusions

In this paper, we have studied the performance of SM applied to OWC in indoor environments. It has been shown that using colour LEDs with different optical wavelengths can significantly improve the performance of SM. This is due to the fact that the responsivity of common photo-diodes is a function of the optical wavelength. Thus, different wavelengths induce specific optical power levels at the receiver. These distinctive power levels improve the differentiability of the multiple channels and reduce the channel correlation. Consequently, the SM receiver can detect the activated transmitter more reliably which improves the BER performance. Moreover, we have shown that optical SM requires a much lower computational complexity compared to other common MIMO techniques like RC and SMP. Therefore, SM is a suitable transmission technique for OWC as it enables high spectral efficiencies and low-complex implementations.

References

[1] E. Telatar, "Capacity of Multi-Antenna Gaussian Channels," *European Transaction on Telecommunication*, vol. 10, no. 6, pp. 585–595, Nov. 1999.

[2] G. J. Foschini and M. J. Gans, "On Limits of Wireless Communications in a Fading Environment when Using Multiple Antennas," *Wireless Personal Communications*, vol. 6, no. 3, pp. 311–335, Mar. 1998.

[3] J. M. Kahn and J. R. Barry, "Wireless Infrared Communications," *Proceedings of the IEEE*, vol. 85, no. 2, pp. 265–298, Feb. 1997.

[4] Y. A. Chau and S. H. Yu, "Space Modulation on Wireless Fading Channels," in *Proc. of the* 54^{th} *IEEE Vehicular Technology Conference (Fall)*, Atlantic City, NJ, USA, Oct. 7–11, 2001, pp. 1668–1671.

[5] R. Mesleh, H. Haas, S. Sinanović, C. W. Ahn, and S. Yun, "Spatial Modulation," *IEEE Transactions on Vehicular Technology*, vol. 57, no. 4, pp. 2228–2241, Jul. 2008.

[6] R. Mesleh, M. Di Renzo, H. Haas, and P. M. Grant, "Trellis Coded Spatial Modulation," *IEEE Transactions on Wireless Communications*, vol. 9, no. 7, pp. 2349–2361, Jul. 2010.

[7] T. Fath, H. Haas, M. Di Renzo, and R. Mesleh, "Spatial Modulation Applied to Optical Wireless Communications in Indoor LOS Environments," in *Proc. of the IEEE Global Communications Conference*, Houston, Texas, USA, Dec. 5–9, 2011, pp. 1–5.

[8] T. Fath and H. Haas, "Performance Comparison of MIMO Techniques for Optical Wireless Communications in Indoor Environments," *IEEE Transactions on Communications*, (to appear).

[9] Advanced Photonix Inc., "Datasheet: Red Enhanced High Performance Silicon Photodiode SD 445-14-21-305," Apr. 2006, retrieved Jun. 20, 2012 from http://www.advancedphotonix.com/ap_products/pdfs/SD445-14-21-305.pdf.

[10] OSRAM Opto Semiconductors GmbH, "Datasheet: GOLDEN DRAGON Plus," Sep. 2012, retrieved Sep. 20, 2012 from http://catalog.osram-os.com.

Coloured Video Code for In-Flight Data Transmission

F. Schubert[1], T. Fath[2], H. Haas[2]

[1]EADS Innovation Works, Munich, Germany
[2]The University of Edinburgh, UK

Abstract. In this paper, a new approach for wireless data transmission between the in-flight entertainment (IFE) system of aeroplanes and mobile devices is presented. As wireless in-flight applications are subject to strict frequency and electromagnetic compatibility regulations, we propose to use optical data transmission. To this end, video streams of 2-dimensional black-and-white or coloured visual codes are displayed on the IFE screen. We present a new visual code which is captured and processed by a passenger's mobile device and which enables robust reconstruction of the transmitted data. In order to compensate for frame losses, the visual codes are coupled with a sequence-wise forward error correction (FEC) scheme. The developed system is evaluated in an Airbus A330 cabin mock-up under realistic conditions employing representative mobile devices like current low-cost and high-end smartphones. Performance evaluations show that the transmission system achieves data rates of up to 120 kbit/s per individual passenger seat.

Keywords: coloured visual codes, mobile vision, sequence-wise FEC encoding, visual transmission.

1 Introduction

We notice an increasing demand for wireless services to improve passengers' comfort during flights. General information (*e.g.* in-flight magazines, airport maps, *etc.*) and passenger specific data (*e.g.* information on connecting gates, departure time of connecting flights, *etc.*) are to be transferred to passengers' mobile devices. However, the application of wireless services within aircraft cabins imposes several constraints. As passenger specific data is to be transmitted, security and privacy aspects have to be considered. More importantly, the transmission system has to comply with high safety regulations as potential access to sensitive on-board systems has to be prevented. Conventional radio frequency (RF) communications cannot be easily employed in sensitive environments like aircraft cabins due to stringent frequency regulations. A few airlines already provide wireless local area network (WLAN) services to their passengers on some selective flights. However, these services require costly installation of dedicated hardware equipment like access points and wireless transceivers. Furthermore, the bandwidth has to be shared between all passengers (up to several hundreds of users) which simultaneously use the data transmission service.

Due to these constraints, we promote to use optical wireless transmission instead of RF-based transmission. Optical signals are not subject to frequency regulations and provide large transmission bandwidth by allowing multiple parallel data transmissions within the same area. Moreover, by applying optical transmission it is possible to reuse the existing hardware within the aircraft cabin, *i.e.* the displays of the in-flight entertainment (IFE) system and the built-in cameras of mobile devices. In detail, we propose optical wireless data transmission using a new visual code. The data to be transmitted (*e.g.* text-files or images) is encoded into several visual codes which are displayed on the screen of the IFE system like a conventional video. This sequence is captured and decoded by a mobile device. The proposed visual code is coupled with a new sequence-wise forward error correction (FEC) scheme which allows to recover capturing errors caused by frame transition effects and which enables the compensation of entirely lost video frames.

The remainder of this paper is organised as follows: In Section 2, related work is reviewed and discussed. In Section 3, the developed transmission system is presented. A description of the new visual code is given in Section 4. Transmission experiments are presented in Section 5 and evaluation results are discussed. Finally, Section 6 concludes the paper.

2 Related Work – Visual Codes for Data Transmission

Visual codes have become very popular in print media. The most common visual codes are 1-dimensional barcodes [3]. In recent years, more sophisticated 2-dimensional codes such as Data-Matrix-codes [2] or Quick Response (QR)-codes [1] have received attention. All these codes can be decoded independently of the viewpoint, work under realistic illumination conditions and allow to recover from decoding errors. However, the data rate of conventional visual codes is limited to only a few bytes, thus not allowing a practical application for in-flight communication.

In order to overcome this limitation, some research activities have focussed on spreading data across several visual codes. The multiple visual codes are displayed as a video sequence. In [6], unsynchronised 4-dimensional codes are proposed to transfer data between public displays and mobile devices. The authors combine three different 2-dimensional Data-Matrix-codes in the complementary colour channels red, green and blue to one common frame. Several of these frames are displayed in a temporal sequence resulting in a coloured visual code video. The authors propose a simple redundancy concept to enable reliable data transmission. However, the induced redundancy limits the data throughput to only 23 characters per second. In [8], the author also uses coloured visual code videos to transmit data. This system provides a low data rate of only 430 byte/s. In [9], a system called *PixNet* is proposed. The visual encoding is based on the orthogonal frequency division multiplexing (OFDM) scheme, whereas the image detection uses the conventional Data-Matrix detection algorithm. The authors report that applying OFDM encoding makes the system less sensitive to illumi-

nation variations. However to our experience, most mobile devices employ robust auto-balancing techniques which provide constant contrast. Moreover, the authors report a data rate of up to 12 Mbit/s at a distance of 10 m. However, this data rate is only achieved for a static setup using high-quality cameras and a large display. Low-cost built-in cameras as well as potential frame loss are not taken into account in their work.

3 System Overview

None of the existing systems employing visual code videos provides the simplicity and the robustness of single frame visual codes, while enabling practical data throughput. Therefore, in this paper, we present an easy to use low-cost optical transmission system which provides a data rate of several kbit/s. Fig. 1 shows the system setup. The user holds a mobile device in front of the IFE screen which is built into the front seat.

Fig. 1. Left: Setup for the transmission of passenger specific data from the central IFE server to the mobile device. Right: Typical distance between mobile device and display.

The detailed transmission process is illustrated in Fig. 2. Firstly, the data, *e.g.* text documents or images, is compressed and encrypted to provide security and privacy of the passenger specific information. Secondly, the encrypted and compressed file is FEC encoded to compensate for potential transmission errors. In a third step, the FEC encoded data is segmented into several packets. Each of these packets is visually encoded by our new visual code resulting in a sequence of several visual codes. Fourthly, this visual code sequence is displayed in a continuous loop on the IFE screen. The user can start to capture the visual codes at any time without the need for an initial synchronisation. In a fifth step, the captured visual codes are detected and processed. The visually decoded data packets are reassembled in the correct order by means of additionally encoded meta information providing the packet number. The reassembling reconstructs the originally FEC encoded data stream. In a sixth step, the FEC encoded data is decoded. Due to the induced FEC, errors which arise during the transmission and capturing process can be corrected. Finally, the FEC decoded data is decrypted and uncompressed and the reconstructed file is stored on the user device.

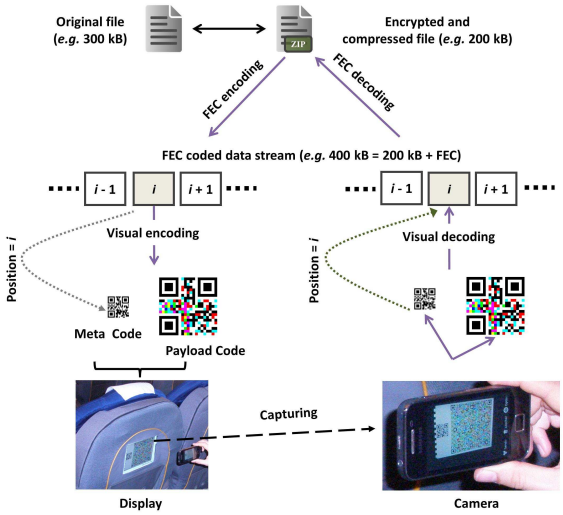

Fig. 2. Data transmission via visual code videos.

As the IFE system can display the desired content on-demand [7], the wireless data transfer can be used by each passenger simultaneously. Therefore, bandwidth needs not to be shared between passengers. Moreover, the uni-directional data transfer between display and mobile device provides a fundamental safety feature since there is no uplink connection from the user device to the sensitive on-board systems. The major benefit of the proposed transmission system is that it reuses the existing IFE equipment without the need for any additional hardware installations. The system requires only a software update of the existing IFE system and an application to be installed on the mobile device.

4 Visual Encoding and Decoding

The lack of synchronisation between IFE display and camera of the mobile device comes at the price of several effects. Since cameras often have a rolling-shutter and displays usually build up images line-wise, transition artefacts between two consecutive frames can be observed (*e.g.* two frames can partially overlap or they can overlay each other completely as shown in the centre of Fig. 3). These effects are even emphasised when low-cost cameras are used which can typically be found in smartphones - the target device of the proposed application. These cheap cameras have a small aperture, and hence require long exposure times. Long exposure times increase the chance that the camera captures a frame transition. Additionally, long exposure times cause motion blur (shown on the left hand side of Fig. 3) as hand-held cameras are never perfectly static. In order to achieve higher data rates, coloured visual codes can be applied. However, colour-

channels suffer from cross-talk (*i.e.* a blue photon does not only affect the blue channel but also the green and red channels) and show high sensitivity to bad illumination. Both effects lead to noisy images, especially in the case of low-cost sensors. On the right hand side of Fig. 3, a coloured visual code is decomposed into its three colour channels of which the blue channel is shown. One can clearly notice the higher noise level compared to pure black-and-white visual codes.

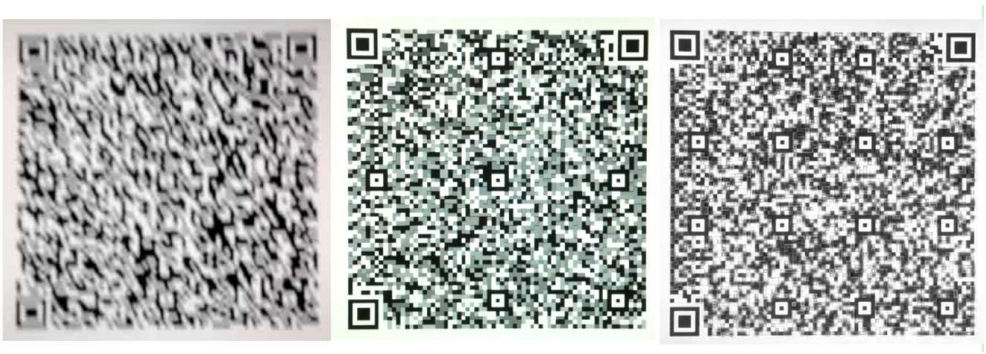

Fig. 3. Left: motion blur, Centre: transition overlay of two frames, Right: Blue colour channel.

These artefacts (*i.e.* motion blur, frame transition, pixel noise) can prevent a correct decoding of the visual code. Conventional visual codes, such as QR-codes [1], which are primarily designed for print media, have to be robust to decoding errors caused by abrasion or dirt on the printed material, for instance. Therefore, conventional visual codes have inherent FEC capabilities to compensate for such decoding errors. This FEC coding is done on a per frame basis, *i.e.* the data and the error correction codewords are contained in the same visual code. This combination allows only to correct a few decoding errors. However, in the proposed application some artefacts degrade the visual code to a much larger extent (*e.g.* by motion blur or frame transitions) so that these frames cannot be reconstructed at all. As a result, the transmitted data stream cannot be reconstructed correctly as some packets are completely lost. Consequently, the conventional frame-wise FEC encoding has to be extended to enable a recovery of completely lost frames. Therefore, a temporal sequence-wise FEC encoding of the complete data stream is proposed. This sequence-wise FEC encoding enables the recovery of lost frames. As a result, the data stream can be reconstructed correctly even if some frames are lost. Our FEC encoding scheme uses a Reed-Solomon code having a data capacity of about 52.8% and a recovery capacity of about 23.6%. This means that the data can be correctly reconstructed if up to about a quarter of the visual code sequence is completely missing. Higher, respectively lower error correction levels can also be employed if higher robustness or higher throughput is required.

In the following, the setup of our visual code is described and it is shown how the FEC encoded data stream is visually encoded. As illustrated in Fig. 2, each packet of the FEC encoded data stream is visually encoded into a single visual code. Fig. 4 shows the setup of our visual code. It consists of three parts: a

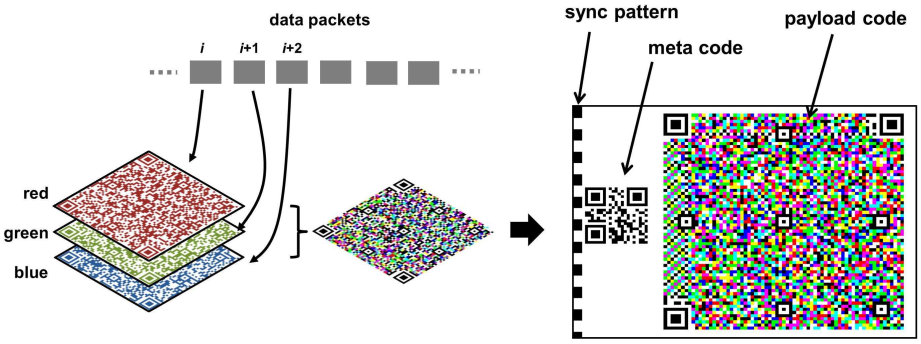

Fig. 4. Left: Three black-and-white payload codes are merged into a single coloured payload code. Right: A single visual code consists of three parts: synchronisation pattern, meta code and payload code.

synchronisation pattern, a meta code and the payload code. Each of these parts will be discussed separately:

Meta Code In order to reassemble the captured frames in the correct order, the receiver has to know the index of the visual code frame within the sequence (display and camera are not synchronised). As this meta information is required before performing the FEC decoding at the receiver side, we separate this information from the actual payload. To this end, we employ a conventional QR-code which we call meta code and which is located on the left hand side of our visual code (see Fig. 4). As there is only a small amount of meta information (*e.g.* the frame number) to be transmitted, a small QR-code having a low version number (*e.g.* version 1 – 2) is sufficient. The FEC level of the meta code is set to the highest redundancy to enable a robust detection.

Payload Code The actual data to be transmitted is encoded in the payload code, which is located on the right hand side of the visual code as shown in Fig. 4. In order to allow a viewpoint invariant capturing and decoding of the payload code, the outline of the code needs to be detected. Therefore, *finder patterns* like the ones found in conventional QR-codes are added. These patterns consist of concentric squares that are located in the corners and in the centre of the payload code. For decoding, the locations of the patterns are identified by the mobile device. We use the detector of the open source implementation *ZXing* [11]. Using the detected pixel coordinates, a homography can be calculated that rectifies the visual code employing the direct linear transform algorithm [5]. The rectification aligns the patterns of the captured camera image with the known quadratic structure of the payload code. As a result, the pixels corresponding to individual bits of the data packet can be extracted. Multiple pixels (*e.g.* 8×8) are grouped into modules which represent a single bit. The extraction is done by binarization using a threshold. This threshold is found by

calculating a histogram of the intensity values along a line-scan of the rectified payload code. The two maximum peaks of the histogram are considered as the black and white reference points. The intensity value that optimally separates both reference points in the histogram is used as threshold for the binarization. The resulting binarized pixel modules correspond to binary values, *i.e.* the actual data bits. In order to increase the data rate, we combine three black-and-white payload codes (corresponding to three consecutive data packets) to one coloured payload code. Each of the three individual payload codes is interpreted as one of the three colour channels red, green and blue as illustrated on the left hand side of Fig. 4. The decoder performs the detection of the *finder patterns* and the rectification on the coloured visual code. However, the selection of the optimal threshold and the binarization are performed for each colour channel (*i.e.* red, green and blue) separately.

Synchronisation Pattern As discussed above, the display and the camera are not synchronised. In order to ensure that the camera captures all displayed frames, the display rate of the visual codes is set to 10 – 15 frames per second (fps). This rate is half the capturing rate of the camera which is about 30 fps. Given a short image build-up time of the display of about 17 ms (60 Hz response-rate), this oversampling ensures that multiple images will be recorded for each displayed visual code. As a result, at least one visual code frame is captured without transition effects. The relation between capturing and displaying is shown in Fig. 5. For correct decoding, the captured frames which contain

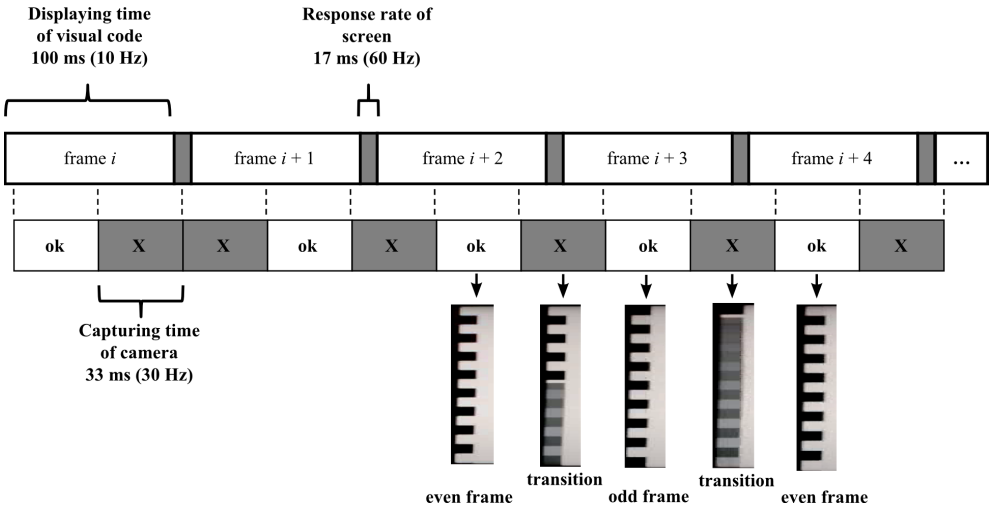

Fig. 5. The upper time-line shows how the screen displays the visual code sequence. The lower time-line shows the capturing times of the camera. At the bottom, the synchronisation patterns are depicted for frames free of artefacts ("ok") and for frames containing transition artefacts ("X").

transition effects (illustrated by "X" in Fig. 5) need to be filtered out. Additionally, due to the oversampling, more than one copy of the same visual code frame might be captured without transition effects. These frames may vary in terms of quality (*e.g.* by contrast). Hence, only the best copy should be selected for further processing. This filtering and selection process keeps the number of decoding operations to a minimum. The filtering and selection process works as follows: A black-and-white synchronisation pattern is added to the left hand side of each visual code (see Fig. 4). This pattern alternates between two versions (called even-pattern $\boldsymbol{s}_e$ and odd-pattern $\boldsymbol{s}_o$) for each frame. For each captured frame, the recorded pattern $\boldsymbol{q}$ is extracted from the rectified image. In order to determine the pattern version, synthetically constructed patterns of both versions (*i.e.* $\boldsymbol{s}_e$ and $\boldsymbol{s}_o$) are correlated with the captured pattern $\boldsymbol{q}$. The version of the pattern which provides the highest correlation score is assigned to $\boldsymbol{q}$. As a result, the recorded pattern $\boldsymbol{q}$ is classified as even- or odd-pattern. The correlation score for the even-pattern is calculated as follows:

$$r_e = \frac{\sum_i (\boldsymbol{s}_e(i) - \hat{s}_e)(\boldsymbol{q}(i) - \hat{q})}{\sqrt{\sum_i (\boldsymbol{s}_e(i) - \hat{s}_e)^2 \sum_j (\boldsymbol{q}(j) - \hat{q})^2}},$$

where the intensity values of the black-and-white pattern are linearised into the vector $\boldsymbol{s}_e$ and $\boldsymbol{q}$, respectively. The mean intensity values of the pattern are given by $\hat{s}_e$ and $\hat{q}$, respectively. The correlation score r_o for the odd-pattern is calculated in an analogous manner. While processing consecutively captured frames, the correlation scores and the captured frames are added to a buffer. This is done as long as no new pattern version is detected compared to the previous classified one. As soon as a new pattern version is detected (*e.g.* a pattern is classified as even-pattern after a series of detected odd-pattern), the frame with the highest correlation score is taken from the buffer and passed on to the decoder.

5 Transmission Experiments

In the following, the results of some transmission experiments are presented. The aim of the experiments is to find the achievable data throughput for different variations of our visual code (*i.e.* black-and-white *vs.* coloured) and for different mobile devices (*i.e.* low-end *vs.* high-end smartphone). The data to be transferred consists of typical passenger specific information. All experiments have been carried out in an Airbus A330 aircraft cabin mock-up under realistic illumination and geometric conditions (see Fig. 1). The cabin mock-up is equipped with an IFE system. The IFE display has a size of about 17 cm × 13 cm with a resolution of 1024 × 768 pixels. Fig. 1 shows the setup of the transmission experiments within the considered application scenario. The distance between the screen and the mobile device is about 20 – 30 cm. The passenger holds the mobile device in the hand during the transmission, roughly aligning it with the display.

Firstly, the transmission performance of the developed application is evaluated using a low-cost smartphone [10]. The built-in camera of this smartphone

Table 1. Performance bounds derived from transmission experiments.

User Device	Colour of Visual Code	Frame-Rate (fps)	Bit-Rate (kbit/s)
Samsung Galaxy Ace	black-and-white	10	22.40
Apple iPhone 4	black-and-white	13	54.29
Apple iPhone 4	coloured	13	120.43

has a resolution of 640×480 pixels in the video mode. In order to reduce transition artefacts, the frame rate of the IFE display has been limited to 10 fps. The transmission experiments have shown that this is the largest frame rate which ensures that each frame is captured at least once without transition effects. Moreover, only black-and-white visual codes are used due to the low quality of the camera. In this setup, each frame can contain a maximum amount of 280 bytes of actual payload data (*i.e.* without FEC overhead) ensuring that the whole data can be reconstructed correctly. Hence, at a frame rate of 10 fps, a maximum bit rate (throughput) of about $10 \cdot 280 \cdot 8 = 22.40$ kbit/s is achieved (see Table 1).

Secondly, the transmission performance is analysed if a high-end user device (an Apple iPhone 4 smartphone [4]) is used instead of a low-cost device. The built-in camera of this smartphone has a higher resolution of 1280×720 pixels in video mode. For this user device, the frame rate of the IFE display can be increased to 13 fps. This transmission rate ensures that each frame is captured at least once without transition effects. Due to the higher quality of the built-in camera, a maximum of 522 bytes of payload data can be encoded in each frame ensuring that the whole data can be reconstructed correctly. This results in a bit rate of $13 \cdot 522 \cdot 8 = 54.29$ kbit/s. This data rate exceeds the data rate of the low-cost smartphone by a factor of about 2.42.

Finally, the data rate can be additionally increased by using coloured visual codes. By using the three independent colour channels red, green and blue for parallel data transmission, the data rate can be theoretically increased by a factor of three. However as shown in Section 4, coloured visual codes suffer from optical cross-talk and colour mixing. Therefore, coloured visual codes are subject to increased error rates. In this case, a maximum of 1158 bytes of payload data can be encoded in each frame, resulting in a bit rate of about $13 \cdot 1158 \cdot 8 = 120.43$ kbit/s. Compared to the black-and-white visual code experiments, this is an increase by a factor of about 2.22.

6 Summary & Conclusions

A novel approach for wireless data transmission within an aircraft cabin has been presented. The developed system reuses the display of the IFE system to transfer passenger specific data to mobile devices. A new visual code has been introduced that is displayed as a video stream visually encoding the data to be transferred. The new visual code is coupled with a temporal FEC encoding scheme allowing robust transmission. The transmitted frames consist of a meta code, which contains supplementary information like the frame number, and

the payload code, which contains the actual information to be transmitted. In a future implementation, these two codes might be combined to one common visual code. Furthermore, a selection algorithm has been presented which uses a synchronisation pattern to detect frame transitions and to select the best captured frame for the decoding process. Transmission experiments within an aircraft cabin mock-up have demonstrated the functionality of the developed application under realistic conditions. The performance evaluation shows that a throughput of up to 120 kbit/s can be achieved with current smartphones. Further tests have shown that 30 seconds are a tolerable time which is accepted by a passenger to capture the IFE screen with a mobile device. During this time, up to 450 kB can be transmitted by a single visual code sequence. This file size is sufficient to transfer the required amount of data for the proposed application. In order to increase data rate, the black-and-white visual codes have been extended to coloured visual codes. In future work, we will evaluate the performance of visual codes with more than 8 different colours which currently result from combining only the three colour channels red, green and blue.

References

1. Information technology – Automatic identification and data capture techniques – Bar code symbology – QR Code. ISO/IEC 18004:2000(E), 2000.
2. Information technology – Automatic identification and data capture techniques – Data Matrix bar code symbology specification. ISO/IEC 16022:2006, 2006.
3. Information technology – Automatic identification and data capture techniques – EAN/UPC bar code symbology specification. ISO/IEC 15420:2009, 2009.
4. Apple Inc. Technical specification: iPhone 4, 2012. retrieved Oct. 25, 2012 from http://www.apple.com/uk/iphone/iphone-4/specs.html.
5. Richard Hartley and Andrew Zisserman. *Multiple View Geometry in Computer Vision*. Cambridge University Press, second edition, 2004.
6. Tobias Langlotz and Oliver Bimber. Unsynchronized 4d barcodes: coding and decoding time-multiplexed 2d colorcodes. In *International Conference on Advances in Visual Computing*, Lake Tahoe, NV, USA, 2007.
7. Hao Liu. Deliverable D4.1: State of Art of In-flight Entertainment Systems and Office Work Infrastructure. *Sixth Framework Programme Project: Smart Technologies for stress free Air Travel*, 2006.
8. Jeton Memeti. Data Transfer Using a Camera and a Three-Dimensional Code. Bachelor's thesis, University of Zurich, 2012.
9. Samuel David Perli, Nabeel Ahmed, and Dina Katabi. Pixnet: interference-free wireless links using lcd-camera pairs. In *International Conference on Mobile Computing and Networking*, Chicago, Illinois, USA, 2010.
10. Samsung. Technical specification: Galaxy Ace GT-S5830, May 2012. retrieved Oct. 25, 2012 from http://www.samsung.com/uk/support/model/GT-S5830OKAXEU.
11. ZXing. Multi-format 1D/2D barcode image processing library, release 1.7. Retrieved Sep. 27, 2011 from http://code.google.com/p/zxing/.

References

[1] Cisco, "Cisco Visual Networking Index: Global mobile data traffic forecast update, 2011–2016," Tech. Rep., Feb. 14, 2012.

[2] Cisco, "Cisco Visual Networking Index: Global mobile data traffic forecast update, 2012–2017," Tech. Rep., Feb. 6, 2013.

[3] V. Chandrasekhar, J. Andrews, and A. Gatherer, "Femtocell Networks: A Survey," *IEEE Communications Magazine*, vol. 46, no. 9, pp. 59–67, Sep. 2008.

[4] Electronic Communications Committee, "The European table of frequency allocations and applications in the frequency range 9 kHz to 3000 GHz," 2011, retrieved Dec. 18, 2012 from http://www.erodocdb.dk/docs/doc98/official/pdf/ERCRep025.pdf.

[5] U.S. Department of Commerce, "United States Frequency Allocations: The Radio Spectrum Chart," Aug. 2011, retrieved Dec. 18, 2012 from http://www.ntia.doc.gov/files/ntia/publications/spectrum_wall_chart_aug2011.pdf.

[6] E. Telatar, "Capacity of Multi-Antenna Gaussian Channels," *European Transactions on Telecommunications*, vol. 10, no. 6, pp. 585–595, Nov. 1999.

[7] G. J. Foschini, "Layered Space-Time Architecture for Wireless Communication in a Fading Environment when Using Multi-Element Antennas," *Bell Labs Technical Journal*, vol. 1, no. 2, pp. 41–59, 1996.

[8] G. J. Foschini and M. J. Gans, "On Limits of Wireless Communications in a Fading Environment when Using Multiple Antennas," *Wireless Personal Communications*, vol. 6, no. 3, pp. 311–335, Mar. 1998.

[9] S. M. Alamouti, "A Simple Transmit Diversity Technique for Wireless Communications," *IEEE Journal on Selected Areas in Communications*, vol. 16, no. 8, pp. 1451–1458, Oct. 1998.

[10] V. Tarokh, N. Seshadri, and A. R. Calderbank, "Space-Time Codes for High Data Rate Wireless Communication: Performance Criterion and Code Construction," *IEEE Transactions on Information Theory*, vol. 44, no. 2, pp. 744–765, Mar. 1998.

[11] Broadcom Corporation, "802.11n: Next-Generation Wireless LAN Technology," Tech. Rep., Apr. 2006, retrieved Feb. 6, 2013 from http://www.broadcom.com/collateral/wp/802_11n-WP100-R.pdf.

[12] A. Hottinen, O. Tirkkonen, and R. Wichman, *Multi-Antenna Tansceiver Techniques for 3G and Beyond*. John Wiley & Sons Ltd., 2003.

[13] M. Frodigh, S. Parkvall, C. Roobol, P. Johansson, and P. Larsson, "Future-generation wireless networks," *IEEE Personal Communications*, vol. 8, no. 5, pp. 10–17, Oct. 2001.

[14] M. Steer, "Beyond 3G," *IEEE Microwave Magazine*, vol. 8, no. 1, pp. 76–82, Feb. 2007.

[15] J. Duplicy, B. Badic, R. Balraj, R. Ghaffar, P. Horvath, F. Kaltenberger, R. Knopp, I. Z. Kovacs, H. T. Nguyen, D. Tandur, and G. Vivier, "MU-MIMO in LTE Systems," *EURASIP Journal on Wireless Communications and Networking*, no. 2011:496763, pp. 1–13, Mar. 2011.

[16] J. Lee, J. K. Han, and J. Zhang, "MIMO Technologies in 3GPP LTE and LTE-Advanced," *EURASIP Journal on Wireless Communications and Networking*, no. 2009:302092, pp. 1–10, Jul. 2009.

[17] S. Glisic, *Advanced Wireless Communications: 4G Technologies*. John Wiley & Sons Ltd., 2004.

[18] J. Mietzner, R. Schober, L. Lampe, W. H. Gerstacker, and P. A. Hoeher, "Multiple-antenna techniques for wireless communications - a comprehensive literature survey," *IEEE Communications Surveys & Tutorials*, vol. 11, no. 2, pp. 87–105, Jun. 2009.

[19] P. Wolniansky, G. Foschini, G. Golden, and R. Valenzuela, "V-BLAST: an Architecture for Realizing very High Data Rates over the Rich-Scattering Wireless Channel," in *Proc. of the URSI International Symposium on Signals, Systems, and Electronics*, Pisa, Italy, Sep. 29–Oct. 2, 1998, pp. 295–300.

[20] S. N. Diggavi, N. Al-Dhahir, A. Stamoulis, and A. R. Calderbank, "Great Expectations: The Value of Spatial Diversity in Wireless Networks," *Proc. of the IEEE*, vol. 92, no. 2, pp. 219–270, Feb. 2004.

[21] D. N. C. Tse, P. Viswanath, and L. Zheng, "Diversity-Multiplexing Tradeoff in Multiple-Access Channels," *IEEE Transactions on Information Theory*, vol. 50, no. 9, pp. 1859–1874, Sep. 2004.

[22] L. Zheng and D. N. C. Tse, "Diversity and Multiplexing: A Fundamental Tradeoff in Multiple-Antenna Channels," *IEEE Transactions on Information Theory*, vol. 49, no. 5, pp. 1073–1096, May 2003.

[23] A. Goldsmith, *Wireless Communications*. Cambridge University Press, 2005.

[24] A. J. Paulraj, R. Nabar, and D. Gore, *Introduction to Space-Time Wireless Communications*. Cambridge University Press, 2003.

[25] A. J. Paulraj and C. B. Papadias, "Space-time processing for wireless communications," *IEEE Signal Processing Magazine*, vol. 14, no. 6, pp. 49–83, Nov. 1997.

[26] V. Tarokh, H. Jafarkhani, and A. R. Calderbank, "Space-time Block Codes from Orthogonal Designs," *IEEE Transactions on Information Theory*, vol. 45, no. 5, pp. 1456–1467, Jul. 1999.

[27] V. Tarokh, H. Jafarkhani, and A. R. Calderbank, "Space-time block coding for wireless communications: performance results," *IEEE Journal on Selected Areas in Communications*, vol. 17, no. 3, pp. 451–460, Mar. 1999.

[28] M. Mouhamadou and P. Vaudon, "Smart Antenna Array Patterns Synthesis : Null Steering and Multi-user Beamforming by Phase Control," *Progress In Electromagnetics Research*, vol. 60, pp. 95–106, 2006.

[29] D. Love, R. Heath, and T. Strohmer, "Grassmannian Beamforming for Multiple-Input Multiple-Output Wireless Systems," in *Proc. of the IEEE International Conference on Communications*, Anchorage, Alaska, USA, May 11–15, 2003, pp. 2618–2622.

[30] K. Mukkavilli, A. Sabharwal, E. Erkip, and B. Aazhang, "On Beamforming with Finite Rate Feedback in Multiple-Antenna Systems," *IEEE Transactions on Information Theory*, vol. 49, no. 10, pp. 2562–2579, Oct. 2003.

[31] T. Yoo and A. Goldsmith, "On the Optimality of Multiantenna Broadcast Scheduling Using Zero-Forcing Beamforming," *IEEE Journal on Selected Areas in Communications*, vol. 24, no. 3, pp. 528–541, Mar. 2006.

[32] J. Winters, J. Salz, and R. Gitlin, "The Impact of Antenna Diversity on the Capacity of Wireless Communication Systems," *IEEE Transactions on Communications*, vol. 42, no. 234, pp. 1740–1751, Feb./Mar./Apr. 1994.

[33] H. Zhuang, L. Dai, S. Zhou, and Y. Yao, "Low Complexity Per-Antenna Rate and Power Control Approach for Closed-Loop V-BLAST," *IEEE Transactions on Communications*, vol. 51, no. 11, pp. 1783–1787, Nov. 2003.

[34] J. N. Laneman, D. N. C. Tse, and G. W. Wornell, "Cooperative Diversity in Wireless Networks: Efficient Protocols and Outage Behavior," *IEEE Transactions on Information Theory*, vol. 50, no. 12, pp. 3062–3080, Dec. 2004.

[35] X. He, T. Luo, and G. Yue, "Optimized distributed MIMO for cooperative relay networks," *IEEE Communications Letters*, vol. 14, no. 1, pp. 9–11, Jan. 2010.

[36] R. C. Meitzler, W. Schneider, and R. Conde, "IRCOMM: spacecraft free-space optical bus development," in *Proc. of the IEEE Aerospace Conference*, Big Sky, Montana, USA, Mar. 5–12, 2005, pp. 1583–1588.

[37] F. R. Gfeller and U. Bapst, "Wireless In-House Data Communication Via Diffuse Infrared Radiation," *Proc. of the IEEE*, vol. 67, no. 11, pp. 1474–1486, Nov. 1979.

[38] L. Hanzo, H. Haas, S. Imre, D. O'Brien, M. Rupp, and L. Gyongyosi, "Wireless Myths, Realities and Futures: From 3G/4G to Optical and Quantum Wireless," *Proc. of the IEEE*, vol. 100, pp. 1853–1888, May 2012.

[39] G. W. Marsh and J. M. Kahn, "Performance Evaluation of Experimental 50-Mb/s Diffuse Infrared Wireless Link using on-off Keying with Decision-Feedback Equalization," *IEEE Transactions on Communications*, vol. 44, no. 11, pp. 1496–1504, Nov. 1996.

[40] J. B. Carruther and J. M. Kahn, "Angle Diversity for Nondirected Wireless Infrared Communication," *IEEE Transactions on Communications*, vol. 48, no. 6, pp. 960–969, Jun. 2000.

[41] Infrared Data Association (IrDA), retrieved Oct. 27, 2013 from http://www.irda.org.

[42] M. Afgani, H. Haas, H. Elgala, and D. Knipp, "Visible Light Communication Using OFDM," in *Proc. of the* 2^{nd} *International Conference on Testbeds and Research Infrastructures for the Development of Networks and Communities*, Barcelona, Spain, Mar. 1–3, 2006, pp. 129–134.

[43] K. D. Langer, J. Vucic, C. Kottke, L. F. del Rosal, S. Nerreter, and J. W. Walewski, "Advances and prospects in high-speed information broadcast using phosphorescent white-light LEDs," in *Proc. of the* 11^{th} *International Conference on Transparent Optical Networks*, Island of São Miguel, Azores, Portugal, Jun. 28–Jul. 2, 2009, pp. 1–6.

[44] H. Haas, "Wireless Data from Every Light Bulb," Technology, Entertainment, Design (TED) website, Aug. 2011, retrieved Mar. 24, 2013 from http://www.ted.com/talks/harald_haas_wireless_data_from_every_light_bulb.html.

[45] Y. Tanaka, T. Komine, S. Haruyama, and M. Nakagawa, "Indoor Visible Communication Utilizing Plural White LEDs as Lighting," in *Proc. of the IEEE International Symposium on Personal, Indoor and Mobile Radio Communications*, San Diego, California, USA, Sep. 30–Oct. 3, 2001, pp. 81–85.

[46] T. Komine and M. Nakagawa, "Fundamental Analysis for Visible-Light Communication System using LED Lights," *IEEE Transactions on Consumer Electronics*, vol. 50, no. 1, pp. 100–107, Feb. 2004.

[47] J. Grubor, S. Randel, K. D. Langer, and J. W. Walewski, "Bandwidth Efficient Indoor Optical Wireless Communications with White Light Emitting Diodes," in *Proc. of the* 6^{th} *International Symposium on Communication Systems, Networks and Digital Signal Processing*, Graz, Austria, Jun. 23–25, 2008, pp. 165–169.

[48] K. D. Langer, J. Grubor, O. Bouchet, M. El Tabach, J. W. Walewski, S. Randel, M. Franke, S. Nerreter, D. O'Brien, G. Faulkner, I. Neokosmidis, G. Ntogari, and M. Wolf, "Optical Wireless Communications for Broadband Access in Home Area Networks," in *Proc. of the* 10^{th} *Anniversary International Conference on Transparent Optical Networks*, Athens, Greece, Jun. 22–26, 2008, pp. 149–154.

[49] H. Elgala, R. Mesleh, and H. Haas, "Indoor Broadcasting via White LEDs and OFDM," *IEEE Transactions on Consumer Electronics*, vol. 55, no. 3, pp. 1127–1134, Aug. 2009.

[50] Visible Light Communications Consortium (VLCC), retrieved Oct. 27, 2013 from http://www.vlcc.net.

[51] Japan Electronics and Information Technology Industries Association (JEITA), *Visible Light Communication System Standard*, CP-1221, Std., 2007.

[52] Japan Electronics and Information Technology Industries Association (JEITA), *Visible Light ID System Standard*, CP-1222, Std., 2007.

[53] IEEE 802.15.7 Visible Light Communication Task Group, retrieved Oct. 27, 2013 from http://www.ieee802.org/15/pub/TG7.html.

[54] Institute of Electrical and Electronics Engineers (IEEE), *IEEE Standard for Local and Metropolitan Area Networks–Part 15.7: Short-Range Wireless Optical Communication Using Visible Light*, IEEE Std 802.15.7-2011, Std., Sep. 2011.

[55] Home Gigabit Access (OMEGA) project, retrieved Oct. 27, 2013 from http://www.ict-omega.eu.

[56] Data Light (D-Light) project, retrieved Oct. 27, 2013 from http://www.visiblelightcomm.com/about-2.

[57] S. Hranilovic, *Wireless Optical Communication Systems*. Springer, 1996.

[58] J. M. Kahn and J. R. Barry, "Wireless Infrared Communications," *Proc. of the IEEE*, vol. 85, no. 2, pp. 265–298, Feb. 1997.

[59] GBI Research, "Visible Light Communication (VLC) - A Potential Solution to the Global Wireless Spectrum Shortage," Tech. Rep., 2011.

[60] H. Elgala, R. Mesleh, and H. Haas, "Indoor Optical Wireless Communication: Potential and State-of-the-Art," *IEEE Communications Magazine*, vol. 49, no. 9, pp. 56–62, Sep. 2011.

[61] D. O'Brien, H. L. Minh, L. Zeng, G. Faulkner, K. Lee, D. Jung, Y. Oh, and E. T. Won, "Indoor visible light communications: challenges and prospects," in *Proc. of the SPIE, Free-Space Laser Communications VIII*, vol. 7091, 709106, San Diego, California, USA, Aug. 10, 2008.

[62] R. Mesleh, H. Elgala, and H. Haas, "Optical Spatial Modulation," *IEEE/OSA Journal of Optical Communications and Networking*, vol. 3, no. 3, pp. 234–244, Mar. 2011.

[63] A. C. Boucouvalas, "IEC 825-1 Eye Safety Classification of Some Consumer Electronic Products," in *Proc. of the IEE Colloquium on Optical Free Space Communication Links*, London, UK, Feb. 19, 1996, pp. 13/1–13/6.

[64] International Electrotechnical Commission, *Photobiological safety of lamps and lamp systems*, IEC 62471:2006, Std., 2006.

[65] International Electrotechnical Commission, *Safety of laser products Part 1: Equipment classification, requirements and users guide*, IEC 60825-1:2007, Std., 2007.

[66] D. K. Borah, A. C. Boucouvalas, C. C. Davis, S. Hranilovic, and K. Yiannopoulos, "A review of communication-oriented optical wireless systems," *EURASIP Journal on Wireless Communications and Networking*, no. 2012:91, pp. 1–28, Mar. 2012.

[67] T. Ohtsuki, "Multiple–Subcarrier Modulation in Optical Wireless Communications," *IEEE Communications Magazine*, vol. 41, no. 3, pp. 74–79, Mar. 2003.

[68] O. Gonzalez, R. Perez-Jimenez, S. Rodriguez, J. Rabadan, and A. Ayala, "OFDM Over Indoor Wireless Optical Channel," *IEE Proceedings Optoelectronics*, vol. 152, no. 4, pp. 199–204, Aug. 2005.

[69] J. Armstrong and A. Lowery, "Power Efficient Optical OFDM," *IET Electronics Letters*, vol. 42, no. 6, pp. 370–372, Mar. 2006.

[70] J. Armstrong and B. J. C. Schmidt, "Comparison of Asymmetrically Clipped Optical OFDM and DC-Biased Optical OFDM in AWGN," *IEEE Communications Letters*, vol. 12, no. 5, pp. 343–345, May 2008.

[71] J. Armstrong, "OFDM for Optical Communications," *IEEE/OSA Journal of Lightwave Technology*, vol. 27, no. 3, pp. 189–204, Feb. 2009.

[72] S. Dimitrov, S. Sinanovic, and H. Haas, "Clipping Noise in OFDM-based Optical Wireless Communication Systems," *IEEE Transactions on Communications*, vol. 60, no. 4, pp. 1072–1081, Apr. 2012.

[73] S. Dimitrov, S. Sinanovic, and H. Haas, "Signal Shaping and Modulation for Optical Wireless Communication," *IEEE/OSA Journal of Lightwave Technology*, vol. 30, no. 9, pp. 1319–1328, May 2012.

[74] H. Liu and G. Li, *OFDM-Based Broadband Wireless Networks : Design and Optimization*. John Wiley & Sons Ltd., 2005.

[75] J. Heiskala and J. Terry, *OFDM Wireless LANs: A Theoretical and Practical Guide*. Sams Publishing, 2002.

[76] D. J. F. Barros, S. K. Wilson, and J. M. Kahn, "Comparison of Orthogonal Frequency-Division Multiplexing and Pulse-Amplitude Modulation in Indoor Optical Wireless Links," *IEEE Transactions on Communications*, vol. 60, no. 1, pp. 153–163, Jan. 2012.

[77] J. G. Proakis, *Digital Communications*. McGraw-Hill Higher Education, 2000.

[78] S. C. J. Lee, S. Randel, F. Breyer, and A. M. J. Koonen, "PAM-DMT for Intensity-Modulated and Direct-Detection Optical Communication Systems," *IEEE Photonics Technology Letters*, vol. 21, no. 23, pp. 1749–1751, Dec. 2009.

[79] S. G. Wilson, M. Brandt-Pearce, Q. Cao, and M. Baedke, "Optical Repetition MIMO Transmission with Multipulse PPM," *IEEE Journal on Selected Areas in Communications*, vol. 23, no. 9, pp. 1901–1910, Sep. 2005.

[80] S. M. Navidpour, M. Uysal, and M. Kavehrad, "BER Performance of Free-Space Optical Transmission with Spatial Diversity," *IEEE Transactions on Wireless Communications*, vol. 6, no. 8, pp. 2813–2819, Aug. 2007.

[81] T. Tsiftsis, H. Sandalidis, G. Karagiannidis, and M. Uysal, "Optical Wireless Links With Spatial Diversity Over Strong Atmospheric Turbulence Channels," *IEEE Transactions on Wireless Communications*, vol. 8, no. 2, pp. 951–957, Feb. 2009.

[82] G. Yun and M. Kavehrad, "Indoor Infrared Wireless Communications Using Spot Diffusing and Fly-Eye Receivers," *The Canadian Journal of Electrical and Computer Engineering*, vol. 18, no. 4, pp. 151–157, Oct. 1993.

[83] S. Jivkova and M. Kavehrad, "Multispot diffusing configuration for wireless infrared access," *IEEE Transactions on Communications*, vol. 48, no. 6, pp. 970–978, Jun. 2000.

[84] S. Jivkova, B. Hristov, and M. Kavehrad, "Power-efficient multispot-diffuse multiple-input-multiple-output approach to broad-band optical wireless communications," *IEEE Transactions on Vehicular Technology*, vol. 53, no. 3, pp. 882–889, May 2004.

[85] P. Djahani and J. M. Kahn, "Analysis of Infrared Wireless Links Employing Multibeam Transmitters and Imaging Diversity Receivers," *IEEE Transactions on Communications*, vol. 48, no. 12, pp. 2077–2088, Dec. 2000.

[86] G. Ntogari, T. Kamalakis, and T. Sphicopoulos, "Performance analysis of space time block coding techniques for indoor optical wireless systems," *IEEE Journal on Selected Areas in Communications*, vol. 27, no. 9, pp. 1545–1552, Dec. 2009.

[87] M. Garfield, C. Liang, T. Kurzweg, and K. Dandekar, "MIMO space-time coding for diffuse optical communication," *Microwave and Optical Technology Letters*, vol. 48, no. 6, pp. 1108–1110, Jun. 2006.

[88] M. K. Simon and V. A. Vilnrotter, "Alamouti-Type Space-Time Coding for Free-Space Optical Communication With Direct Detection," *IEEE Transactions on Wireless Communications*, vol. 4, no. 1, pp. 35–39, Jan. 2005.

[89] E. Bayaki and R. Schober, "On space-time coding for free-space optical systems," *IEEE Transactions on Communications*, vol. 58, no. 1, pp. 58–62, Jan. 2010.

[90] M. Safari and M. Uysal, "Do We Really Need OSTBCs for Free-Space Optical Communication with Direct Detection?" *IEEE Transactions on Wireless Communications*, vol. 7, no. 11, pp. 4445–4448, Nov. 2008.

[91] D. O'Brien, S. Quasem, S. Zikic, and G. Faulkner, "Multiple Input Multiple Output Systems for Optical Wireless; Challenges and Possibilities," in *Proc. of the SPIE, Free-Space Laser Communications VI*, vol. 6304, 630416, San Diego, California, USA, Aug. 13, 2006.

[92] D. Takase and T. Ohtsuki, "Optical Wireless MIMO Communications (OMIMO)," in *Proc. of the IEEE Global Communications Conference*, Dallas, Texas, USA, Nov. 29–Dec. 3, 2004, pp. 928–932.

[93] D. Takase and T. Ohtsuki, "Performance Analysis of Optical Wireless MIMO With Optical Beat Interference," in *Proc. of the IEEE International Conference on Communications*, Seoul, Korea, May 16–20, 2005, pp. 954–958.

[94] L. Zeng, D. O'Brien, H. L. Minh, G. Faulkner, K. Lee, D. Jung, Y. Oh, and E. T. Won, "High Data Rate Multiple Input Multiple Output (MIMO) Optical Wireless Communications using White LED Lighting," *IEEE Journal on Selected Areas in Communications*, vol. 27, no. 9, pp. 1654–1662, Dec. 2009.

[95] D. O'Brien, "Multi-Input Multi-Output (MIMO) indoor optical wireless communications," in *Conference Record of the Asilomar Conference on Signals, Systems and Computers*, Pacific Grove, California, USA, Nov. 1–4, 2009, pp. 1636–1639.

[96] K. Dambul, D. O'Brien, and G. Faulkner, "Indoor Optical Wireless MIMO System With an Imaging Receiver," *IEEE Photonics Technology Letters*, vol. 23, no. 2, pp. 97–99, Jan. 2011.

[97] A. Azhar, T. Tran, and D. O'Brien, "A Gigabit/s Indoor Wireless Transmission Using MIMO-OFDM Visible-Light Communications," *IEEE Photonics Technology Letters*, vol. 25, no. 2, pp. 171–174, Jan. 2013.

[98] Y. A. Chau and S. H. Yu, "Space Modulation on Wireless Fading Channels," in *Proc. of the IEEE Vehicular Technology Conference (Fall)*, Atlantic City, New Jersey, USA, Oct. 7–11, 2001, pp. 1668–1671.

[99] R. Mesleh, H. Haas, S. Sinanovic, C. W. Ahn, and S. Yun, "Spatial Modulation," *IEEE Transactions on Vehicular Technology*, vol. 57, no. 4, pp. 2228–2241, Jul. 2008.

[100] J. Jeganathan, A. Ghrayeb, and L. Szczecinski, "Spatial Modulation: Optimal Detection and Performance Analysis," *IEEE Communications Letters*, vol. 12, no. 8, pp. 545–547, Aug. 2008.

[101] R. Mesleh, M. Di Renzo, H. Haas, and P. M. Grant, "Trellis Coded Spatial Modulation," *IEEE Transactions on Wireless Communications*, vol. 9, no. 7, pp. 2349–2361, Jul. 2010.

[102] R. Mesleh, R. Mehmood, H. Elgala, and H. Haas, "Indoor MIMO Optical Wireless Communication Using Spatial Modulation," in *Proc. of the IEEE International Conference on Communications*, Cape Town, South Africa, May 22–27, 2010, pp. 1–5.

[103] E. Basar, U. Aygolu, E. Panayirci, and V. H. Poor, "Space-Time Block Coded Spatial Modulation," *IEEE Transactions on Communications*, vol. 59, no. 3, pp. 823–832, Mar. 2011.

[104] R. Mesleh, H. Haas, C. W. Ahn, and S. Yun, "Spatial Modulation – A New Low Complexity Spectral Efficiency Enhancing Technique," in *Proc. of the* 1^{st} *International Conference on Communications and Networking in China*, Beijing, China, Oct. 25–27, 2006, pp. 1–5.

[105] R. Mesleh, "Spatial Modulation: A Spatial Multiplexing Technique for Efficient Wireless Data Transmission," Ph.D. dissertation, Jacobs University, Bremen, Germany, Jun. 2007.

[106] A. Younis, M. Di Renzo, R. Mesleh, and H. Haas, "Sphere Decoding for Spatial Modulation," in *Proc. of the IEEE International Conference on Communications*, Kyoto, Japan, Jun. 5–9, 2011, pp. 1–6.

[107] M. Di Renzo and H. Haas, "On the Performance of Space Shift Keying MIMO Systems Over Correlated Rician Fading Channels," in *Proc. of the ITG International Workshop on Smart Antennas*, Bremen, Germany, Feb. 23–24, 2010, pp. 72–79.

[108] M. Di Renzo and H. Haas, "Performance analysis of Spatial Modulation," in *Proc. of the* 5^{th} *International Conference on Communications and Networking in China*, Beijing, China, Aug. 25–27, 2010, pp. 1–7.

[109] J. Jeganathan, A. Ghrayeb, L. Szczecinski, and A. Ceron, "Space Shift Keying Modulation for MIMO Channels," *IEEE Transactions on Wireless Communications*, vol. 8, no. 7, pp. 3692–3703, Jul. 2009.

[110] R. Mesleh, H. Haas, C. W. Ahn, and S. Yun, "Spatial Modulation – OFDM," in *Proc. of the International OFDM Workshop*, Hamburg, Germany, Aug. 30–31, 2006, pp. 288–292.

[111] S. U. Hwang, S. Jeon, S. Lee, and J. Seo, "Soft-Output ML Detector for Spatial Modulation OFDM Systems," *IEICE Electronics Express*, vol. 6, no. 19, pp. 1426–1431, Oct. 2009.

[112] Tottori SANYO Electric Co., Ltd., "Datasheet: RED LASER DIODE DL-6147-040," May 2005, retrieved Sep. 8, 2011 from http://combinlasers.com/1sanyo/dl-6147-040.pdf.

[113] OSRAM Opto Semiconductors GmbH, "Datasheet: BPX 61 Silicon PIN Photodiode," Mar. 2007, retrieved Sep. 8, 2011 from http://catalog.osram-os.com.

[114] R. Mesleh, I. Stefan, H. Haas, and P. M. Grant, "On the Performance of Trellis Coded Spatial Modulation," in *Proc. of the ITG International Workshop on Smart Antennas*, Berlin, Germany, Feb. 16–19, 2009, pp. 235–242.

[115] O. Bouchet, G. Faulkner, L. Grobe, E. Gueutier, K. D. Langer, S. Nerreter, D. O'Brien, R. Turnbull, J. Vucic, J. W. Walewski, and M. Wolf, "Deliverable D4.2b: Physical Layer Design and Specification," 7^{th} *Framework Programme Information & Communication Technologies*, Feb. 2011, retrieved Jul. 18, 2012 from http://www.ict-omega.eu.

[116] D. O'Brien, G. Faulkner, H. L. Minh, O. Bouchet, M. El Tabach, M. Wolf, J. W. Walewski, S. Randel, S. Nerreter, M. Franke, K. D. Langer, J. Grubor, and T. Kamalakis, "Home access networks using optical wireless transmission," in *Proc. of the IEEE International Symposium on Personal, Indoor and Mobile Radio Communications*, Cannes, France, Sep. 15–18, 2008, pp. 1–5.

[117] The MathWorks Inc., "Floating-Point Numbers," Oct. 2013, retrieved Oct. 26, 2013 from http://www.mathworks.de/de/help/matlab/matlab_prog/floating-point-numbers.html.

[118] Advanced Photonix Inc., "Datasheet: Red Enhanced High Performance Silicon Photodiode SD 445-14-21-305," Apr. 2006, retrieved Jun. 20, 2012 from http://www.advancedphotonix.com/ap_products/pdfs/SD445-14-21-305.pdf.

[119] OSRAM Opto Semiconductors GmbH, "Datasheet: GOLDEN DRAGON Plus," Sep. 2012, retrieved Sep. 20, 2012 from http://catalog.osram-os.com.

[120] J. R. Barry, J. M. Kahn, W. J. Krause, E. A. Lee, and D. G. Messerschmitt, "Simulation of Multipath Impulse Response for Indoor Wireless Optical Channels," *IEEE Journal on Selected Areas in Communications*, vol. 11, no. 3, pp. 367–379, Apr. 1993.

[121] E. Costa, M. Midrio, and S. Pupolin, "Impact of amplifier nonlinearities on OFDM transmission system performance," *IEEE Communications Letters*, vol. 3, no. 2, pp. 37–39, Feb. 1999.

[122] E. Costa and S. Pupolin, "M-QAM-OFDM System Performance in the Presence of a Nonlinear Amplifier and Phase Noise," *IEEE Transactions on Communications*, vol. 50, no. 3, pp. 462–472, Mar. 2002.

[123] D. Dardari, V. Tralli, and A. Vaccari, "A Theoretical Characterization of Nonlinear Distortion Effects in OFDM Systems," *IEEE Transactions on Communications*, vol. 48, no. 10, pp. 1755–1764, Oct. 2000.

[124] W. Jun and Y. Chenyang, "The influence of analog device on OFDM system," in *Proc. of the International Conference on Communication Technology*, Beijing, China, Apr. 9–11, 2003, pp. 1060–1062.

[125] B. Inan, S. C. J. Lee, S. Randel, I. Neokosmidis, A. M. J. Koonen and J. W. Walewski, "Impact of LED Nonlinearity on Discrete Multitone Modulation," *IEEE/OSA Journal of Optical Communications and Networking*, vol. 1, no. 5, pp. 439–451, Oct. 2009.

[126] I. Neokosmidis, T. Kamalakis, J. W. Walewski, B. Inan, and T. Sphicopoulos, "Impact of Nonlinear LED Transfer Function on Discrete Multitone Modulation: Analytical Approach," *IEEE/OSA Journal of Lightwave Technology*, vol. 27, no. 22, pp. 4970–4978, Nov. 2009.

[127] H. Elgala, R. Mesleh, and H. Haas, "A Study of LED Nonlinearity Effects on Optical Wireless Transmission using OFDM," in *Proc. of the IEEE International Conference on Wireless and Optical Communications Networks*, Cairo, Egypt, Apr. 28–30, 2009, pp. 1–5.

[128] I. Stefan, H. Elgala, R. Mesleh, D. O'Brien, and H. Haas, "Optical Wireless OFDM System on FPGA: Study of LED Nonlinearity Effects," in *Proc. of the IEEE Vehicular Technology Conference (Spring)*, Budapest, Hungary, May 15–18, 2011, pp. 1–5.

[129] I. Stefan, H. Elgala, and H. Haas, "Study of Dimming and LED Nonlinearity for ACO-OFDM Based VLC Systems," in *Proc. of the IEEE Wireless Communications and Networking Conference*, Paris, France, Apr. 1–4, 2012, pp. 990–994.

[130] H. Elgala, R. Mesleh, and H. Haas, "Non-linearity Effects and Predistortion in Optical OFDM Wireless Transmission Using LEDs," *Inderscience International Journal of Ultra Wideband Communications and Systems*, vol. 1, no. 2, pp. 143–150, 2009.

[131] A. Behravan and T. Eriksson, "PAPR and Other Measures for OFDM Systems with Nonlinearity," in *Proc. of the* 5^{th} *International Symposium on Wireless Personal Multimedia Communications*, Honolulu, Hawaii, USA, Oct. 27–30, 2002, pp. 149–153.

[132] OSRAM Opto Semiconductors GmbH, "Datasheet: SFH 4501, SFH 4502, SFH 4503 High Power Infrared Emitter," Jan. 2008, retrieved Jun. 20, 2012 from http://catalog.osram-os.com.

[133] Lufthansa, "Lufthansa FlyNet: limitless communication on long-haul flights," 2013, retrieved Oct. 27, 2013 from http://www.lufthansa.com/online/portal/lh/de/info_and_services/on_board?nodeid=3108158&l=en&cid=18002.

[134] American Airlines, "Wi-Fi in the Sky," 2013, retrieved Oct. 27, 2013 from http://www.aa.com/i18n/urls/entertainmentOnDemand.jsp.

[135] N. Schmitt, "Wireless optical NLOS Communication in Aircraft Cabin for In-flight Entertainment Distribution," in *Proc. of the ESA* 1^{st} *Optical Wireless Onboard Communications Workshop*, Noordwijk, Netherlands, Sep. 29–30, 2004.

[136] N. Schmitt, T. Pistner, C. Vassilopoulos, D. Marinos, A. Boucouvalas, M. Nikolitsa, C. Aidinis, and G. Metaxas, "Diffuse Wireless Optical Link for Aircraft Intra-cabin Passenger Communication," in *Proc. of the* 5^{th} *International Symposium on Communication Systems, Networks and Digital Signal Processing*, Patras, Greece, Jul. 19–21, 2006, pp. 1–4.

[137] D. O'Brien, G. Faulkner, S. Zikic, and N. Schmitt, "High Data-Rate Optical Wireless Communications in Passenger Aircraft: Measurements and Simulations," in *Proc. of the* 6^{th} *International Symposium on Communication Systems, Networks and Digital Signal Processing*, Graz, Austria, Jul. 23–25, 2008, pp. 68–71.

[138] S. Dimitrov, R. Mesleh, H. Haas, M. Cappitelli, M. Olbert, and E. Bassow, "On the SIR of a Cellular Infrared Optical Wireless System for an Aircraft," *IEEE Journal on Selected Areas in Communications*, vol. 27, no. 9, pp. 1623–1638, Dec. 2009.

[139] International Standards Organisation, *Information technology – Automatic identification and data capture techniques – EAN/UPC bar code symbology specification*, ISO/IEC 15420:2009, Std., Dec. 2009.

[140] International Standards Organisation, *Information technology – Automatic identification and data capture techniques – Data Matrix bar code symbology specification*, ISO/IEC 16022:2006, Std., Sep. 2006.

[141] Y. P. Wang and A. Ye, "Maxicode data extraction using spatial domain features," *United States Patent 5637849*, Jun. 1997.

[142] A. Longacre, Jr. and R. Hussey, "Two Dimensional Data Encoding Structure and Symbology for use with Optical Readers," *United States Patent 5591956*, Jan. 1997.

[143] International Standards Organisation, *Information technology – Automatic identification and data capture techniques – Bar code symbology – QR Code*, ISO/IEC 18004:2000(E), Std., Jun. 2000.

[144] Microsoft, "Tag Implementation Guide," Dec. 2011, retrieved Oct. 4, 2012 from http://tag.microsoft.com/home.aspx.

[145] A. Mohan, G. Woo, S. Hiura, Q. Smithwick, and R. Raskar, "Bokode: imperceptible visual tags for camera based interaction from a distance," *ACM Transactions on Graphics*, vol. 28, no. 3, pp. 98:1–98:8, Jul. 2009.

[146] H. Kato and K. Tan, "2d barcodes for mobile phones," in *Proc. of the* 2^{nd} *International Conference on Mobile Technology, Applications and Systems*, Guangzhou, China, Nov. 15–17, 2005, pp. 1–8.

[147] T. Langlotz and O. Bimber, "Unsynchronized 4d barcodes: coding and decoding time-multiplexed 2d colorcodes," in *Proc. of the* 3^{rd} *International Conference on Advances in Visual Computing*, Lake Tahoe, Nevada, USA, Nov. 26–28, 2007, pp. 363–374.

[148] J. Memeti, "Data Transfer Using a Camera and a Three-Dimensional Code," Bachelor's thesis, University of Zurich, Zurich, Switzerland, Apr. 2012.

[149] Samsung, "Technical specification: Galaxy S II," 2012, retrieved Oct. 29, 2012 from http://www.samsung.com/uk/consumer/mobile-devices/smartphones/android/GT-I9100LKAXEU.

[150] S. Hranilovic and F. Kschischang, "Short-range wireless optical communication using pixelated transmitters and imaging receivers," in *Proc. of the IEEE International Conference on Communications*, Paris, France, Jun. 20–24, 2004, pp. 891–895.

[151] S. D. Perli, N. Ahmed, and D. Katabi, "Pixnet: interference-free wireless links using lcd-camera pairs," in *Proc. of the* 16^{th} *Annual International Conference on Mobile Computing and Networking*, Chicago, Illinois, USA, Sep. 20–24, 2010, pp. 137–148.

[152] Rockwell Collins, "Inflight Entertainment System," 2012, retrieved Oct. 31, 2012 from http://www.rockwellcollins.com/Products_and_Systems/Cabin/Inflight_Entertainment_Systems.aspx.

[153] Panasonic Avionics, "In-Flight Entertainment Products," 2012, retrieved Oct. 31, 2012 from http://www.mascorp.com/Products/Products.aspx.

[154] Thales Group, "In-Flight Entertainment Solutions - IFE," 2012, retrieved Oct. 31, 2012 from http://www.thalesgroup.com/Portfolio/Aerospace/Aerospace_Product_IFE%_Products.

[155] H. Liu, "Deliverable D4.1: State of Art of In-flight Entertainment Systems and Office Work Infrastructure," 6^{th} *Framework Programme Project: Smart tEchnologies for stress free Air Travel*, Dec. 2006, retrieved Feb. 6, 2013 from http://www.seat.id.tue.nl/publications/D4-1-State%20of%20the%20Art%20Report.pdf.

[156] Kentaro Fukuchi, "libqrencode - QR Code encoding library, release 3.1.1," Feb. 2010, retrieved Sep. 12, 2011 from http://fukuchi.org/works/qrencode/index.html.

[157] ZXing, "Multi-format 1D/2D barcode image processing library, release 1.7," Jun. 2011, retrieved Sep. 27, 2011 from http://code.google.com/p/zxing.

[158] Samsung, "Technical specification: Galaxy Ace GT-S5830," May 2012, retrieved Oct. 25, 2012 from http://www.samsung.com/uk/support/model/GT-S5830OKAXEU.

[159] Apple Inc., "Technical specification: iPhone 4," 2012, retrieved Oct. 25, 2012 from http://www.apple.com/uk/iphone/iphone-4/specs.html.

[160] J. Jalden and B. Ottersten, "On the complexity of sphere decoding in digital communications," *IEEE Transactions on Signal Processing*, vol. 53, no. 4, pp. 1474–1484, Apr. 2005.

[161] B. Hassibi and H. Vikalo, "On the Sphere-Decoding Algorithm I. Expected Complexity," *IEEE Transactions on Signal Processing*, vol. 53, no. 8, pp. 2806–2818, Aug. 2005.